Susceptibility of ruminant livestock to experimental infection with SARS-CoV-2 and HPAIV H5N1

by

Konner Robert Cool

B.S., Kansas State University, 2017
M.S., Kansas State University, 2020

AN ABSTRACT OF A DISSERTATION

submitted in partial fulfillment of the requirements for the degree

DOCTOR OF PHILOSOPHY

Department of Diagnostic Medicine/Pathobiology
College of Veterinary Medicine

KANSAS STATE UNIVERSITY
Manhattan, Kansas

2025

Abstract

Emerging RNA viruses represent a constant and expanding threat to global public health, agriculture, and biosecurity. The recent panzootics of severe acute respiratory syndrome coronavirus 2 (SARS-CoV-2) and highly pathogenic avian influenza virus (HPAIV) H5N1 clade 2.3.4.4b illustrate how host-generalist viruses can infect a broad range of wildlife, companion, and food production animal species, sometimes sustaining transmission and spillover to humans. These events underscore the critical need to understand host susceptibility and potential transmission pathways early in an outbreak.

The experiments described here were designed to investigate the susceptibility and transmission potential of ruminant hosts to SARS-CoV-2 and HPAIV H5N1 through controlled experimental infection studies. The objectives were to assess infection outcomes, viral shedding, within host virus competition, host adaptation, and potential animal-to-animal transmission following experimental exposure to each of these pathogens. The resulting data clarified the role of ruminant species in the respective pathogen ecology, reduced the uncertainty about undetected virus maintenance, and informed targeted surveillance and outbreak response. Collectively, these findings advanced our understanding of host range, intraspecies transmission, and the potential for these emerging zoonotic RNA viruses to establish new animal reservoirs.

Susceptibility of ruminant livestock to experimental infection with SARS-CoV-2 and HPAIV H5N1

by

Konner Robert Cool

B.S., Kansas State University, 2017
M.S., Kansas State University, 2020

A DISSERTATION

submitted in partial fulfillment of the requirements for the degree

DOCTOR OF PHILOSOPHY

Department of Diagnostic Medicine/Pathobiology
College of Veterinary Medicine

KANSAS STATE UNIVERSITY
Manhattan, Kansas

2025

Approved by:

Major Professor
Prof. Jürgen A. Richt, D.V.M., Ph.D.

Copyright

Abstract

Emerging RNA viruses represent a constant and expanding threat to global public health, agriculture, and biosecurity. The recent panzootics of severe acute respiratory syndrome coronavirus 2 (SARS-CoV-2) and highly pathogenic avian influenza virus (HPAIV) H5N1 clade 2.3.4.4b illustrate how host-generalist viruses can infect a broad range of wildlife, companion, and food production animal species, sometimes sustaining transmission and spillover to humans. These events underscore the critical need to understand host susceptibility and potential transmission pathways early in an outbreak.

The experiments described here were designed to investigate the susceptibility and transmission potential of ruminant hosts to SARS-CoV-2 and HPAIV H5N1 through controlled experimental infection studies. The objectives were to assess infection outcomes, viral shedding, within host virus competition, host adaptation, and potential animal-to-animal transmission following experimental exposure to each of these pathogens. The resulting data clarified the role of ruminant species in the respective pathogen ecology, reduced the uncertainty about undetected virus maintenance, and informed targeted surveillance and outbreak response. Collectively, these findings advanced our understanding of host range, intraspecies transmission, and the potential for these emerging zoonotic RNA viruses to establish new animal reservoirs.

Table of Contents

List of Figures

List of Tables

Dedication

This work is dedicated to all of those who set me on this path, to be curious and appreciate the small things.

To my wife, Emily,

your steadfast support, unwavering love, patience, and encouragement

To our sweet Everly,

your laughter has been the brightest part of every day.

You reminded me that joy can always be found, even in the middle of chaos.

To my parents, Kari and Kent,

your support throughout my education laid the foundation for everything I have achieved.

Thank you for showing me the value of kindness, curiosity, perseverance, and hard work.

"The greatest enemy of knowledge is not ignorance –it is the illusion of knowledge"

Q -Daniel Boorstin (*1984*)

Acknowledgements

I would like to express my deepest gratitude to my mentor, Dr. Richt – you set the bar high, and we are all better for it. My time with this team will always be held very close; the friendships, the education, the mind-set; These years were well spent - enlightening and fruitful. The opportunities and responsibilities that I have been afforded here will serve we well as I begin to carve my own path. Thank you.

Dr.'s Willson, Pogranichniy, and Gaudreault – The dream team. Thank you for taking a genuine interest and investment into my development. Your mentorship in the lab, in the animal room, and in literature have given me so many tools to be successful. It has truly been a privilege to work so closely with each of you.

Dr. Trujillo and Dr. Morozov – It has been such a privilege to work alongside each of you – to constantly be learning from you, and sometimes with you, as we take one challenging study after another. Thank you for your mentorship, and your trust, and the many laughs along the way. We sure have gotten a lot of work done and honestly had a pretty good time doing it.

My fellow graduate students, Daniel, Dashka, Taeyong, Chester - Thanks for taking me in and showing me the ropes. I've always admired your skills as Veterinarians and am fortunate have some of that knowledge transferred to me. I knew I was in the right place from day 1.

Finally, the team members, technicians, post-docs that have come and gone and those that are here today – nothing we do in this lab can be done without a team mentality and positive attitude you all carry.

Preface

The 21st century has been a constant reminder of how closely our world is interconnected. It seems that emerging diseases are less often affecting only wildlife or human health in isolation—they ripple through agriculture, trade, food security, and even the stability of national economies. H5N1 has already devastated the global poultry industry more than once, and its recent spread into dairy cattle has forced us to confront a new, uncomfortable question: What happens when a virus begins to move through the very species that anchor our food systems? Poultry, cattle, swine—together, these sectors supply most of the world's animal protein. A serious outbreak in any one of them is disruptive; simultaneous pressure across all three would be unprecedented but does not seem far from reality.

At the same time, SARS-CoV-2 has taken a very different path. Emerging also from a wildlife reservoir, but in a very different scenario– in an isolated region and under uncommon circumstances. After moving explosively through humans, it spilled over into wildlife, becoming firmly established in white-tailed deer across North America. This demonstrated, again, how quickly a virus that is well adapted to one animal species (here: humans) can jump into a new species. And once a virus settles into wildlife, it has a much broader ecological impact. New lineages can emerge; old ones displaced; virus evolution continues outside of our direct line of sight in multi-host ecological transmission cycles that we are just beginning to understand. In regions where wildlife farming and exotic animal trade is common, the interface between humans, wild species, and domestic animals forms an especially efficient network for viral exchange. SARS-related coronaviruses emerging from wildlife markets might become more common - three high consequence CoVs have emerged in the last quarter century - an active, ongoing risk.

Together, these examples illustrate how pathogen emergence is shaped by human behavior, land use, and our dependence on ever increasing livestock production. But they also highlight how much remains unknown, especially regarding ruminant susceptibility to zoonotic pathogens. For years, cattle, sheep, and goats were considered unlikely hosts for either influenza A viruses or human coronaviruses (HCoVs). That view has slowly shifted. The discovery of HPAIV H5N1 in dairy cows—and the detection of SARS-CoV-2 antibodies in cattle, sheep, and goats, alongside widespread infection in white-tailed deer—has broadened the landscape of concern. Each unexpected host species expands the ecological space in which these viruses can circulate and genetically evolve.

This dissertation examines this human-animal intersection. By studying the susceptibility of ruminant livestock to experimental infection with SARS-CoV-2 and HPAIV H5N1, it addresses a critical gap in our understanding of how these viruses may behave in animal species that are fundamental to global food security. If either virus were to establish sustained infection or efficient transmission in ruminants, the implications for food production, disease control, and public health would be profound. Understanding these risks is essential for preparing and protecting both animal and human populations.

Chapter 1 - Introduction

Modern Landscape of Emerging Infectious Disease

Emerging infectious diseases (EIDs) have become increasingly visible and prominent in our daily lives over the last century, reshaping public health, global economics, and agricultural stability (2, 3). Although EIDs are caused by a wide range of pathogens, zoonotic RNA viruses remain the predominant drivers of recent epidemics and pandemics, owing to their high mutation rates, genomic plasticity, broad host ranges, and capacity for ecological disruption (4, 5). The persistent rise in zoonotic risk is a reflection of how tightly interconnected human, animal, and environmental health have become—a reality captured by the modern One Health framework (6). As agricultural systems expand, wildlife habitats contract, and global trade intensifies, this overlapping interconnectedness increases the opportunities for cross-species transmission, creating unprecedented conditions for viral spillover and sustained circulation.

Humans and Wildlife Interface

Historically, EIDs were episodic and regionally constrained, but the last four decades have demonstrated a shift toward more frequent, geographically widespread events. Many of the most consequential EIDs—SARS, MERS, pandemic H1N1, COVID-19, and the ongoing panzootic spread of HPAIV H5N1—have disproportionately affected either humans, animals, or both (2, 7). These viruses do not simply cause morbidity and mortality; they alter agricultural output, disrupt trade, shift food security dynamics, and produce cascading economic effects. For example, the global impact of COVID-19 extended far beyond human disease, affecting supply chains, animal production, and wildlife health simultaneously (8, 9). Similarly, the H5N1 panzootic has generated severe losses in poultry, threatened wildlife populations, and, more recently, demonstrated a troubling capacity to infect livestock—particularly dairy cattle—at an

unprecedented scale (10, 11). These events highlight an increasingly complex landscape where animal and human health crises are deeply entangled.

Zoonotic RNA Viruses

RNA viruses account for the majority of documented EIDs due to intrinsic biological traits. Their error-prone polymerases generate rapid genetic diversity, enabling adaptation to new hosts and immune environments (5). Recombination and reassortment—particularly among coronaviruses and segmented orthomyxoviruses—facilitate the emergence of novel viral genotypes with altered pathogenicity, transmissibility, or tissue tropism (12, 13). Importantly, many zoonotic RNA viruses are host generalists, capable of infecting diverse taxa or quickly adapting to new species. SARS-CoV-2's rapid expansion into companion animals, wildlife, and livestock underscores this capacity (14-17). Similarly, HPAIV H5N1 clade 2.3.4.4b—once predominantly avian—has expanded into carnivores, marine mammals, and now cattle, demonstrating remarkable ecological flexibility (10, 18-20). These characteristics explain why zoonotic RNA viruses continue to dominate spillover events and underscore the necessity for integrated surveillance and collaboration across animal sectors.

Drivers of EID Emergence:

There are several variables that must converge for cross-species transmission events to occur. Many of these fall under three categories and are considered the primary forces that drive EID emergence: *i)* viral evolutionary events, *ii)* host susceptibility and availability, and *iii)* changes in environment or ecological circumstances brought about by anthropogenic pressures.

Virus Factors

Viruses, particularly RNA viruses, have several mechanisms that generate diversity and facilitate host switching. Replication of RNA viruses often occurs with low fidelity and is absent

of proof reading, resulting in a high rate of nucleotide substitution errors. The recombination potential for many RNA viruses provides more dramatic mutations and greater diversity along longer segments of the genome. Such events could change the structure of viral surface proteins or mechanisms of immune evasion, each having potential to alter host tropism (21, 22). For example, the SARS-CoV-2 spike protein is more commonly affected by both point mutations and recombination, facilitating receptor switching and affinity enhancement (5, 13). For viruses with segmented genomes, such as influenza viruses, co-infected cells present opportunities for reassortment events that produce novel subtypes capable of infecting new species or evading host immunity (23).

Host Ecology

Host factors include receptor compatibility (binding affinity) with viral surface proteins, host immune response and prior exposure, health status at the time of exposure, presence of cellular machinery for viral replication, and finally - ecological behavior and interactions that overlap with reservoir hosts or virus contaminated environments. Comparative analyses of various host Angiotensin converting enzyme-2 (ACE2) receptors predicted susceptibility across broad vertebrate lineages prior to confirmation of SARS-CoV-2 infection in species such as mink, deer, and cattle (21, 24-30). Similarly, the distribution of avian- and human-like influenza receptors in bovine mammary tissue helps explain susceptibility of cattle to H5N1 (31, 32).

Anthropogenic Forces

Anthropogenic activities are perhaps the most significant factor that shape spillover risk and contribute to the accelerated emergence of new EIDs. Agricultural intensification, habitat fragmentation, wildlife-livestock interfaces, global travel, live-animal trade, climate-induced migration, and the encroachment of human populations into wildlife habitats collectively

increase contact opportunities between different host species (33-36). The dramatic changes in environmental and ecological conditions have eroded many of the natural barriers that separated wildlife from dense populations of humans and domestic animals and increase the probability that viruses will encounter new ecological niches or immunologically naïve populations.

Host-generalists - Coronavirus and Orthomyxovirus

Virus species within family *Coronaviridae* and *Orthomyxoviridae* possess the evolutionary processes that embody host-generalist viruses and constantly circulate within and between host populations in distant geographical regions; the genetic and ecological diversity that shape EID emergence and persistence. Coronaviruses possess large RNA genomes with high recombination potential that facilitate rapid adaptive evolution and host switching, as illustrated by the repeated emergence of *Betacoronaviruses* from SARS-related coronaviruses (SARSr-CoVs) that have a reservoir in southeast Asian bats (7, 37, 38). Orthomyxoviruses, by contrast, generate antigenically distinct subtypes primarily through reassortment that occurs during co-infection, an important mechanism for highly pathogenic avian influenza H5Nx strains (39, 40). Both families demonstrate an ability to acquire mutations that broaden host range, enhance transmissibility, or increase virulence, making them persistent threats to humans, livestock, and wildlife.

The transmission of SARS-CoV-2 and HPAIV H5N1 into livestock species has been a surprise to most and emerged as a major concern for establishment of new reservoir species and pathogen endemicity. SARS-CoV-2 has infected a wide range of domesticated and wild species, including deer, cattle, mink, and companion animals (15, 25, 41-45). More recently, HPAIV H5N1 clade 2.3.4.4b infection was confirmed in dairy cattle in the United States, with sustained transmission among dairy herds, and multiple spillover events from wild avian species; a series

of events and disease without precedent in influenza ecology (10, 46, 47). These developments epitomize the threats and unpredictable nature of host-generalist virus species, and their capacity to embed themselves in new hosts and cause abrupt disruptions to agriculture.

Livestock and Agricultural Systems in EID Emergence

Livestock production systems have been a corridor for EIDs and also a critical component for early detection and control of zoonotic viruses . Livestock populations are maintained at high density and nearly ubiquitous throughout the world – encroaching closer into rural regions where wildlife populations have largely been isolated from the rest of the world. In these new ecological systems, cattle, swine, small ruminants, and poultry are largely naive and could become new reservoirs for EIDs and conduit for EID exposure in humans or the livestock could succumb to disease and negatively impact food security in these regions that are undergoing population growth, threating food security (8). Livestock diseases produce direct economic losses such as productivity and output slumps, trade restrictions set in and potentially subjected to depopulation to contain outbreaks. Indirect consequences would also be seen throughout labor markets that support large supply chains.

Sustained transmission of SARS-CoV-2 between farmed mink in Europe and white-tailed deer in the United States (U.S.) are an example of the risks that is posed to farm hands, hunters and unsuspecting persons that come into close contact. This has also become true for dairy workers, more than 40 of which have been confirmed infected with bovine HPAIV H5N1.The ease at which these two viruses cross-species barriers, into a third host in short periods of time, demonstrates how livestock and wildlife interface zones act as high-risk conduits for viral evolution and spillover (10, 48). Importantly, infections in livestock may have atypical manifestation or not display any clinical signs (e.g. H5N1 in dairy cattle) and circulate

unrecognized for several weeks or months or longer. The delayed diagnosis hinders intervention strategies to interrupt transmission and complicates containment of outbreaks. Agricultural systems therefore represent both vulnerable targets and critical surveillance platforms for mitigating spillovers and protecting human and animal health.

Severe Acute Respiratory Syndrome Coronavirus-2

History

Twentieth Century: Coronavirus Discovery and Convictions

Throughout the 20th century Coronaviruses (CoV; order *Nidovirales,* family *Coronaviridae*) were largely regarded as significant disease-causing agents for domestic pigs and poultry, presenting with respiratory and gastrointestinal infections and subsequent economic losses (49). Human coronaviruses HCoV-229E and HCoV-OC43 were isolated in the 1960's but generally manifested as mild upper respiratory tract infections.

Twenty-First Century: Acute Awakening

In 2002 an outbreak of severe pneumonia in Hong Kong instantly flipped the 20th century dogma and ignited a new era of zoonotic CoV research. The etiological agent was identified as a novel coronavirus, designated severe acute respiratory syndrome coronavirus (SARS-CoV, genus *Betacoronavirus*) (50). The first lethal human CoV had emerged and quickly spread across 4 continents, ultimately claiming nearly 800 lives with a 10% case fatality rate (51, 52).

In the following years, evidence compiled from field investigations (epidemiological and wildlife surveillance) identified bats of the *Rhinolophus* species as the likely reservoir for SARS-CoV (37, 53). However, transmission to humans occurred via an intermediate host, likely the masked palm civets (*Paguma larvoto)* or Chinese ferret badgers *(Melogale moschata)* that were

being sold in live animal markets where the index SARS-CoV cases occurred. This also shed light on the wildlife trade and farming industry that had quietly expanded to near-industrial level scale across larger geographic regions in SE Asia and taken hold in international markets.

SARS-CoV had made known the clear and present danger that had been lurking in the isolated wildlife of desolate forests. The expansion of agricultural lands and urban environments began to encroach into ecosystems full of foreign hosts and the pathogens they harbor, providing a new corridor into dense populations of naïve hosts.

In 2012 it became clear that SARS-CoV would not be the last lethal CoV to emerge. Sporadic cases of severe, and sometimes fatal, respiratory infections around the Arabian Peninsula were identified as another novel *Betacoronavirus*, later named Middle East respiratory syndrome (MERS-CoV) (50, 53). There are several ecological and epidemiological factors that are distinctly different from SARS-CoV. Both are believed to have originated from bats, considered an ancestral reservoir for many *Betacoronaviruses*, but MERS is also maintained in dromedary camels (*Camelus dromedarius)* which are the primary source of exposure in humans (54, 55). Under these circumstances and frequent interaction between humans and camels in this region, spillovers of MERS occur several times per year and remain endemic in this region. Alternatively, humans do not have the same level of exposure to racoon dogs, pangolins, or bats, and additional spillovers have not been reported for SARS-CoV. The abundance and frequency of interaction with reservoir hots are critical determinants for the risk of spillovers and how long outbreaks may last; SARS-CoV has not been reported since 2003, only circulating for one year before totally disappearing from humans (53). MERS, on the other hand, has had opportunities to continue to spillover from camels and is still associated with human-to-human transmission, primarily in hospital settings.

The third major zoonotic coronavirus spillover event to occur in less than two decades was reported in Wuhan, China in December of 2019. The initial outbreak of SARS-CoV-2 in Wuhan, China, was characterized by clusters of severe pneumonia of unknown etiology. Within weeks, a novel *Betacoronavirus* (subgenus *Sarbecovirus*) was identified as the etiological agent and was shown to transmit efficiently from human-to-human, largely through respiratory droplets, aerosols, and contaminated surfaces (33, 56, 57). By the time SARS-CoV-2 was recognized as a novel pathogen, international spread was already underway, aided by heavy global travel and dense population centers. In February of 2020 the first confirmed case of SARS-CoV-2 infection in animals was reported (58). The reverse zoonoses and occasional bidirectional transmission between humans and animals is an area of active research to further our understanding of how these events contribute to SARS-CoV-2 evolution.

The emergence of SARS-CoV-2 in late 2019, and the ensuing COVID-19 pandemic, will be remembered as one of the most consequential public-health crises in recorded history, its scale comparable only to the 1918 influenza pandemic. Unlike 1918, the world today is densely populated and more globally interconnected. Access to rapid international travel accelerated viral dissemination, and advanced medical infrastructure simultaneously enabled the most rapid diagnostic, vaccine, and therapeutic development effort ever undertaken.

Betacoronaviruses **and the Precedents for SARS-CoV-2**

Molecular clock analyses reveal that many human coronaviruses (HCoVs) represent relatively recent cross-species transmission events. For example, HCoV-OC43 likely emerged from a bovine coronavirus spillover around the late 19th century (12) while HCoV-229E and HKU1 appear to have originated from bat and rodent reservoirs, respectively (37). These

repeated host-jumping events demonstrate that coronaviruses have a propensity to move between taxonomic groups and acquire mutations for host-adaptation.

The emergence of SARS-CoV (2002–2003), MERS-CoV (2012), and SARS-CoV-2 (2019) demonstrates a pattern of *Betacoronaviruses* periodically spilling over into humans from wildlife reservoirs (de Wit et al., 2016). Each virus was introduced to humans through distinct ecological pathways and intermediate hosts, civets for SARS-CoV, dromedary camels for MERS-CoV, and each sustained human-to-human transmission driven by respiratory transmission. SARS-CoV-2, however, proved to be exceptionally more efficient and rapidly disseminated around the globe, in part due to high viral loads during presymptomatic virus shedding and mass international movements of people, creating pockets local infection that quickly transformed into a pandemic within weeks (Harvey et al., 2021).

SARS-CoVs continue to circulate widely in bat species, harboring diverse spike proteins and accessory genes that increase their spillover potential (4, 36). Comparative receptor analyses performed early in the pandemic predicted a broad potential host range for SARS-CoV-2 due to host receptor ACE2 compatibility across many mammals, including ruminants and wildlife species, foreshadowing the widespread cross-species infections to come (59).

Virology and Etiology of *Betacoronavirus*

Taxonomic Classification

Coronaviruses (order *Nidovirales*, family *Coronaviridae*) are enveloped, single-stranded, positive-sense RNA viruses known to infect a broad range of vertebrates, including mammals, birds, amphibians, and bony fish. The namesake for this family is derived from the distinctive crown-like morphology, or 'corona', attributed to the glycoproteins protruding from the exterior

surface of the viral envelope. Current taxonomy recognizes three subfamilies: *Letovirinae*, *Pitovirinae*, and *Orthocoronavirinae*, the latter comprised of four genera—*Alpha*-, *Beta*-, *Gamma*-, and *Deltacoronavirus*. The most consequential group for human and animal health is genus *Betacoronavirus*, including species SARS-CoV, MERS-CoV, and SARS-CoV-2.

Genome Organization and Products

The large 29.9kb positive-sense, single-stranded RNA genome of SARS-CoV-2 encodes 29 proteins: 16 nonstructural proteins (snp1-16), four structural proteins (spike, envelope, membrane, and nucleocapsid), and 9 accessory proteins. Mature virions measure ~80–120 nm and possess a lipid envelope with spike (S) glycoproteins protruding through the surface that mediate receptor binding and fusion (Hoffmann et al., 2020). The function of the four structural proteins that form the virion are as follows: Spike (S) is a fusion protein with S1 (receptor-binding domain; RBD) and S2 (fusion machinery), Envelope (E) proteins are small and involved in assembly and inflammasome activation, the Membrane (M) protein functions to interact with S and N package and assemble the virion, the Nucleocapsid (N) forms a complex with RNA and packages the ~29.9 kb genome within the virion and has functions for host immune modulation (60).

The genome also encodes non-structural proteins (nsp1–16) that form the replication complex and other replication activities like proofreading, unique for RNA viruses. Other non-structural proteins have innate immune antagonism functions. The accessory proteins (ORF3a, ORF6, ORF7a/b, ORF8, ORF10) also contribute to various aspects of virulence and host adaptation; the activity of each appears to vary between host species.

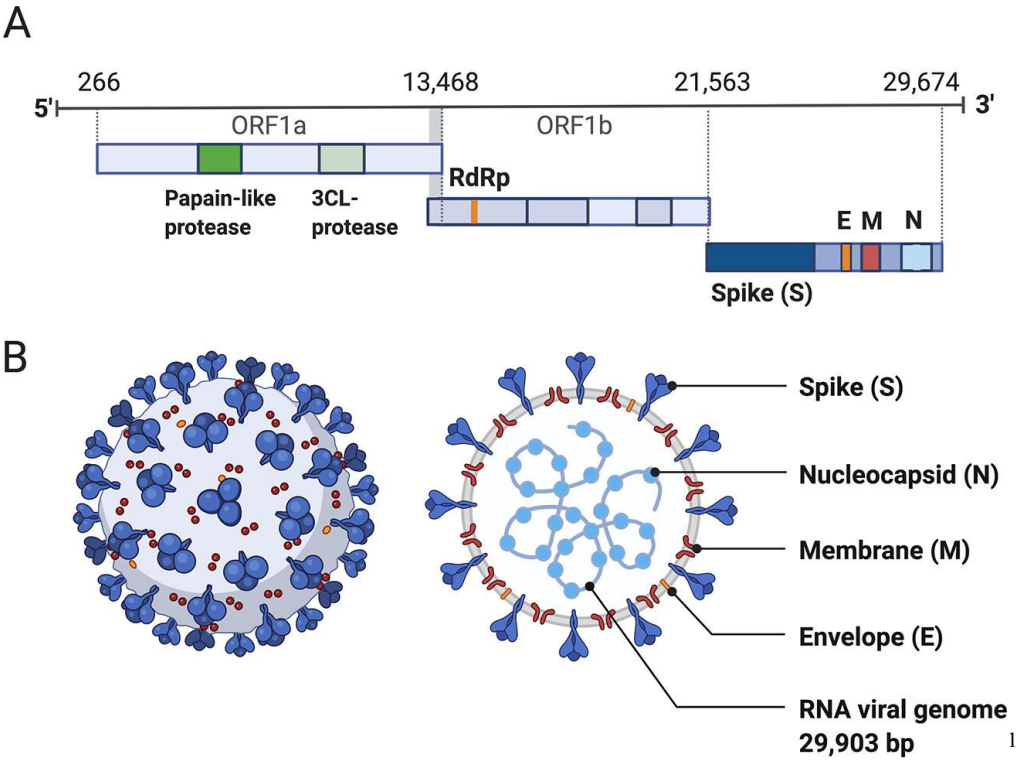

Figure 1.1 Structure of SARS-CoV-2 capsid and genome

The genome organization (A) and physical structure of SARS-CoV-2 virion (B) (1)

Replication Cycle

The viral life cycle is initiated when the S1 (RBD) binds to host ACE2 receptors, followed by TMPRSS2-mediated cleavage or endosomal activation of S2 (61). Following entry, the genomic RNA acts directly as template mRNA to produce polyproteins pp1a and pp1ab, which are cleaved into replication-transcription complex components. Nested sub-genomic

---

Rando Halie, M. *et al.* Pathogenesis, Symptomatology, and Transmission of SARS-CoV-2 through Analysis of Viral Genomics and Structure. *mSystems* **6**, 10.1128/msystems.00095-00021 (2021). https://doi.org:10.1128/msystems.00095-21 [1]

RNAs are produced via discontinuous transcription. Virions assemble in the ER-Golgi intermediate compartment and exit the cell via vesicular pathways.

Mechanisms of Mutation, Recombination, and Variant Evolution

Although coronaviruses possess a proofreading exonuclease (nsp14), SARS-CoV-2 accumulates mutations rapidly due to the rate and scale of replication. Key evolutionary mechanisms for SARS-CoV-2 include: *i)* point mutations, such as N501Y, resulting in changes to receptor binding, *ii)* recombination between co-infecting lineages, permitting exchange of genome encoding the spike protein and regulatory elements (Graham & Baric, 2010), and *iii)* Insertion/deletion events affecting accessory genes associated with immune modulation. There are also host-driven selective pressures that have been found associated with rodents, mink, deer, and likely others, producing lineage-specific adaptations (Kuchipudi et al., 2022).

These mechanisms are central to the emergence of recognized variants of concern (VOCs), Alpha, Beta, Gamma, Delta, Omicron, each possessing distinct adaptive changes and fitness advantages to displace the prior dominant lineage in circulation, or other aspects of transmission, host immunity, or ecological transitions (Harvey et al., 2021). Several VOCs arose in contexts of persistent infection or animal reservoirs, highlighting the role of long-term replication in single hosts and the role of host-adaptation in generating virus diversity.

Etiology

SARS-CoV-2 has a complex evolutionary landscape that is shaped by high mutation rates, extensive recombination, a diverse *sarbecovirus* reservoir in bats, and strong selective pressures acting on the spike. Its large virus genome, broad host receptor ACE2 compatibility, cell entry pathways, and capacity for rapid lineage diversification underpin its pandemic potential and drive ongoing spillover and spillback events across wildlife, companion animals,

and select livestock. These features collectively define SARS-CoV-2 as a highly adaptable zoonotic RNA virus whose continued evolution will remain relevant to both public health and veterinary systems.

Epidemiology

Humans drive SARS-CoV-2 Transmission

SARS-CoV-2 epidemiology is defined by efficient respiratory transmission, high viral loads, and substantial asymptomatic carriage. Humans remain the primary driver sustaining global circulation. Variants emerged sequentially in waves—each shaped by immune pressure, control measures, and introductions—making SARS-CoV-2 one of the most rapidly evolving viruses ever documented at population scale.

By the time nCoV-19 was identified as the etiological agent causing severe pneumonia in Wuhan, clusters of new cases had begun to appear across the region and rapidly disseminate further across the globe. Based on previous experiences with SARS and MERS, and data accruing in real-time, SARS-CoV-2 was likely being transmitted through respiratory routes and occurring human-to-human. Molecular diagnostic tests were quickly developed and deployed, and countries began reporting cases on a regular basis to the World Health Organization (WHO). By the end of the first month, more than 8,000 cases and 170 deaths had been confirmed across 18 countries (52) .

This information was used to develop and initiate response and mitigation measures, focused first on isolating those that are infected and quarantine of close contacts. Eventually the policies were expanded and extended more broadly to the public, including social distancing, wearing masks, and mandatory diagnostic screenings before travel. These policies likely reduced the mortality, particularly for the most vulnerable populations including elderly or those with

certain co-morbidities. Travel restrictions were limited in their effectiveness, as infected individuals still in the incubation period would not be detected or restricted from travel.

Several factors contributed to the persistent community spread. Asymptomatic infections, common in school-aged children and young adults, were unaware of their infections and unknowing shedding virus and infecting others. To curb the spread, more strict policies were implemented at the community level. Generally, these 'lock-down' policies required that non-essential businesses close and non-essential workers remain at home. These policies would remain in place until vaccines became available. The vaccines were effective in preventing severe disease, but breakthrough infections became more common when new variants would emerge. Globally, the impact of the social policies, travel restrictions, and vaccinations became apparent when new variants remained geographically isolated to the origin of emergence, rather than circulating broadly and replacing prior dominant variants in circulation. As of September 28, 2025 the WHO COVID19 dashboard has reported a total of 778,741,845 human cases and 7,102,636 deaths (62).

In February 2020, prior to the official declaration of a global pandemic by the WHO, the first confirmed detection of SARS-CoV-2 in animals was reported. A domestic canine in Hong Kong was confirmed to be infected after its owner was diagnosed with COVID-19 a few days prior, suggesting that human-to-animal transmission (spillback) was possible.

Reverse Zoonoses

As SARS-CoV-2 became more prevalent in humans, so did the incidence of reverse zoonotic transmission (spillback) events, confirmed in a growing number of domestic and captive animals including big cats (tigers and lions, and others of the *Felidae* family) in zoological collections (14, 63, 64). Additional resources were soon allocated to expand

surveillance operations in animal species, particularly those in close contact with humans, or animal species suspected of being susceptible based on homology of the host receptor ACE2. The list of species confirmed to have been exposed to or infected with SARS-CoV-2 expanded to include mink, white-tailed deer, non-human primates, and several rodent species, among others. Throughout the pandemic there were no less than 775 outbreaks in animals across 36 countries (65, 66). This is likely a gross underestimate as resources were primarily allocated to human testing, particularly during peak periods of transmission which would likely correlate with peak incidence in animals (67).

Evidence for natural infection with SARS-CoV-2 was reported in 29 species, many of which had little involvement in the larger epidemiological context (WOAH, USDA). However, bidirectional transmission was observed to occur between humans and hamsters, farmed mink, white-tailed deer, and domestic cats. These spillovers were revealed after probe failures became commonly observed while testing human clinical specimens with multi-plex RT-qPCR assay. Specific mutations were revealed after bioinformatic analysis which aligned with variants that were circulating in farmed mink populations. Follow up investigations confirmed epidemiological links between infected humans and mink farms (17, 68). The result of this was mass culling of mink to reduce the threat of vaccine breakthrough infections, as vaccines just became available. Other well documented cases of bidirectional transmission occurred in the international shipments of infected hamsters and North American white-tailed deer (69-71).

White-Tailed Deer Reservoir

Perhaps the most striking development was the established reservoir of SARS-CoV-2 in white-tailed deer. This was a significant development in the ecology and evolution of SARS-CoV-2 as white-tailed deer are the most abundant and geographically widespread ruminant

species in North America with a population estimated to be >30 million and stretches coast to coast through most of the United States and Southern Canada. Although not fully domesticated, they are considered an alternative livestock species, and more than 4,000 deer farms have been established throughout the United States.

It is not fully understood currently how SARS-CoV-2 has been introduced into the deer population, but a substantial amount of evidence supports that SARS-CoV-2 is repeatedly introduced, over several years, and in several distant regions of North America.

As early as 2021, upwards of 40% of wild white-tailed deer were seropositive for SARS-CoV-2 antibodies in Ohio, Pennsylvania, and other US states. Data that has been acquired by or reported to USDA-APHIS is included in the online SARS-CoV-2 tracking portal, currently showing that 37 states have confirmed cases in deer (65). More intricate analysis has been conducted using viral RNA collected from wild deer populations. These studies have detected nearly all VOC in white tailed deer and provide additional evidence that multiple introductions of SARS-CoV-2 into white-tailed deer have occurred (44, 45, 72-74). It was shown that these variants maintain circulation in wild populations long after they had faded from human circulation. Further, deer adapted strains have been identified in human clinical samples in Ontario, Canada; evidence that transmission chains from human-to-deer-to-human have occurred naturally, but currently appear to be rare (69, 74, 75). These events emphasize the risks associated with wildlife reservoirs and the potential for divergent viral evolution outside human populations(64).

There are abundant opportunities for reverse-zoonoses to occur on deer farms, where humans are in close contact with dense populations of deer, and the mesh fencing surrounding the herd allows for contact with wild deer populations or other intermediate hosts. Other

possibilities exist in urban environments where deer come into contact contaminated surfaces (food, compost, garbage) or through other means of direct or indirect contact when humans hand feed or leave pans of food/water for wild deer. There are many questions that remain to be answered in this regard.

Livestock exposure and Ruminant Susceptibility

Experimental infections in cattle, sheep, and goats show low-level susceptibility but limited shedding, yet serological and sporadic natural infections demonstrate that ruminants are not completely refractory (15, 24, 30, 76-82). While cattle did not appear to sustain efficient transmission, their close proximity to humans and wildlife, large population size, and global distribution warrant continued surveillance. Experimental infections conducted in cattle using Delta and Omicron VOCs showed higher levels of replication and distribution throughout tissues than a similar study conducted early in the pandemic using ancestral lineages (29, 83).

There are a limited number of targeted surveillance studies that fully described in the primary literature, which were conducted in Italy, Germany, and the US. Generally, cows, sheep, goats, and other ruminants are reported to have low incidence of SARS-CoV-2 exposure or infection (24, 76, 77, 82). However, this data represents a minute fraction of the ruminant population in each country. This is not to insinuate that the data is irrelevant, but to suggest that more data would be required in order to make definitive conclusions about host susceptibility. Aside from a larger sample size, other variables must be considered, such as host genome variability (herd/region/global), environmental conditions, and various agricultural/husbandry practices. Cross-species transmission events are thought to be rare, largely due to the plethora of variables and specific conditions that need present to facilitate such events. Thus, populations of identical species that exist in different geographical regions or that are managed though different

methods are important components that might contribute to the success and/or frequency of cross-species transmission and the inferred susceptibility to SARS-CoV-2. A relevant example of this would be the high incidence of SARS-CoV-2 found in North American deer, but not in other regions. Some of these studies also included molecular detection methods, indicating active infection and potential transmission pathways to human caretakers (84, 85).

Several efforts have been made to curtail the threat of transmission between humans and animals. Extensive guidance and updates were published by the World Organization for Animal Health (86-89), including "guidance on working with farmed animals of species susceptible to infection with SARS-CoV-2". These reports are excellent examples of how rapidly the relationship between humans and animals was unfolding and the focused efforts that were allocated/dedicated to address these developments.

There has been an unprecedented amount of epidemiological data collected from humans and other mammals to track the spread and evolution of SARS-CoV-2 (90). The maintenance and dissemination of SARS-CoV-2 was primarily driven by human-to-human transmission. The genomic data and metadata have provided invaluable tools for in-depth analysis of virus transmission and evolution over time (91, 92). The epidemiological significance and associated influence that resulted from the extensive cross-species transmission of SARS-CoV-2 is not fully understood .

Control Measures: Vaccines and Therapeutics

Vaccines

Rapid development of mRNA, adenoviral vector, and protein-subunit vaccines transformed the pandemic trajectory. Vaccines reduced disease severity and transmission in humans, ultimately constrain viral evolution through lower number of infections. Subunit

vaccines were also developed for cats, a species that co-habitats with humans and highly susceptible to SARS-CoV-2 (93-95). Vaccine efficacy was reduced when new variants emerged and dominated; early vaccines provided more protection against ancestral lineages and the Alpha variant, and provided reduced protection against Delta and early Omicron variants (96). Breakthrough infections increased with immune-evasive variants like Omicron, demonstrating the complex interplay between vaccine-induced immunity, viral antigenic drift, and waning immunity (97). Nonetheless, vaccines remain the cornerstone of SARS-CoV-2 control and saved countless lives, particularly the elderly and the immunocompromised. Fortunately, mRNA vaccine platforms can be reformulated more easily than seasonal influenza vaccines to protect against new lineages in circulation.

Antivirals and Therapeutics

Therapeutic development and deployment occurred in paralleled timeline with vaccines. Antivirals (e.g., remdesivir, nirmatrelvir/ritonavir), monoclonal antibodies, and immunomodulatory therapies became available for treatment of severe disease; all were important tools to combat infection in those with co-morbidities. As with vaccines, the continuous evolution of SARS-CoV-2 threatens the success of countermeasures and requires ongoing genomic surveillance and flexible therapeutic design. This is particularly true for monoclonal antibodies that displayed diminishing effectiveness as variants evolved.

Perspective: Lessons, Advancements, and Ongoing Challenges

SARS-CoV-2 fundamentally reshaped biomedical research, accelerating vaccine technologies, genomic epidemiology, and real-time surveillance tools. The pandemic also illuminated substantial vulnerabilities: inconsistent messaging and guidance from authorities,

underinvestment in surveillance in some regions, political polarization, and public distrust in scientific institutions.

At the human–animal interface, SARS-CoV-2 offered a sobering preview of how zoonotic viruses can establish new reservoirs, circulate and diversify unnoticed for long periods, and spill back into humans with unpredictable consequences. For livestock and wildlife sectors, the pandemic emphasized the importance of integrated surveillance, experimental infection studies, and characterization of species susceptibility—not only to anticipate threats but to guide agricultural decision-making, protect workers, and maintain global food systems (16).

Highly Pathogenic Avian Influenza Virus (H5N1), Clade 2.3.4.4b

History

The influence that virus species of the family O*rthomyxoviridae* have had on humans and animals is present in many of the strategies and approaches we have today in addressing virus ecology, biosecurity, and surveillance networks. The focus here will be on Influenza A viruses, as they have been the progenitor for the most consequential human pandemics and maintain relevance today, as highly pathogenic avian influenza expands its host tropism into mammalian species (98-100). The historical and contemporary context demonstrates the incredible diversity and rapid fluctuations in influenza virus ecology and transmission dynamics, and the purpose for maintaining a prominent position on the list of “high-risk” pathogens of pandemic potential (101).

Influenza A viruses: Ecology and Evolution

Influenza viruses belong to the family *Orthomyxoviridae*, a diverse group of segmented, negative-sense RNA viruses that circulate widely in avian, mammalian, and occasionally reptilian hosts. Among these, influenza A viruses (IAVs) are the host-generalists and most zoonotically relevant. The segmented genome possesses eight negative sense, single-stranded RNA segments that are capable of reassortment when two viruses co-infect the same cell; a powerful evolutionary mechanism that allows exchange of entire gene segments and dramatic shifts in antigenic profiles (40)This capacity for genetic exchange has shaped the emergence of pandemic strains and remains the defining evolutionary engine of avian influenza.

Wild aquatic birds, particularly *Anseriformes* and *Charadriiformes*, constitute the primary reservoir for IAVs of nearly all subtypes with minimal disease associated with infection (8)Viral maintenance in these species involves fecal–oral and environmental transmission in wetlands and migration corridors, introducing and exchanging subtypes during migration.

Influenza A Subtypes and Host Associations

Influenza A viruses are classified by their hemagglutinin (H1–H18) and neuraminidase (N1–N11) surface proteins. Specific combinations are historically associated with particular host species; H1, H2, and H3 circulate in humans; H3, H7, and H10 spill into horses; H1, H3, and H5–H9 infect swine; while wild birds harbor nearly the full antigenic spectrum (23). Avian H5Nx lineages, especially those containing a polybasic cleavage site that expands cellular tropism, have repeatedly generated highly pathogenic avian influenza (HPAI) phenotypes that are devastating to domestic poultry populations.

Emergence of Goose/Guangdong Lineage and Clade Evolution

The progenitor for the current HPAIV H5N1 panzootic traces to the 1996 emergence of the A/goose/Guangdong (Gs/GD) lineage in China. Since then, H5 viruses have diversified into multiple clades. The most promiscuous of these is clade 2.3.4.4, exhibiting especially high evolutionary flexibility and expansive tropism into mammalian hosts. This clade repeatedly reassorts with neuraminidase (NA) segments circulating locally, producing H5N2, H5N6, H5N8, H5N5, and most recently H5N1 variants that comprise the globally prevalent panzootic strains (39, 102)

Clade 2.3.4.4b and Global Dissemination

Beginning around 2020–2021, clade 2.3.4.4b H5N1 expanded rapidly across Eurasia, Africa, and the Americas. Transatlantic movement via migratory waterfowl was documented in 2021, and subsequent surveillance confirmed rapid establishment in North American flyways (103, 104). By 2022–2024, this lineage had caused unprecedented mortality events in seabirds, marine mammals, raptors, seals, and terrestrial carnivores, with confirmed mammal-to-mammal transmission in mink and elephant seals (18, 105).The broad ecological interactions, mammalian spillover frequency, and continued reassortment events underscore that clade 2.3.4.4b viruses have reached a level of fitness and prowess unmatched by previous HPAIV H5N1 waves (106).

Introduction of H5N1 2.3.4.4b into North America

The introduction of this lineage into North America led to widespread detection in wild birds, backyard flocks, commercial poultry, and numerous mammalian species, including foxes, skunks, bears, and marine mammals (20, 100, 107). The scale of wildlife infection represents a large shift in HPAIV ecology, with viral persistence occurring year-round in some regions.

Detection in Dairy Cattle: A Historic Shift

In 2024, clade 2.3.4.4b H5N1 was detected in U.S. dairy cattle, the first time that it is known to occur with sustained infection in a major ruminant livestock species (10, 108, 109). The unique host tropism also presented unique sites of viral replication, specifically in the mammary tissue, and high titer virus shedding in milk likely the primary contributor to inter- and intra-herd transmission (110). Experimental infections reproduced clinical signs and viral tropism in cows and calves (111, 112)), providing direct evidence that cattle can support replication and onward spread.

This discovery represents one of the most surprising and potentially consequential developments in the history of influenza. The movement of a traditionally avian-adapted virus into a globally distributed livestock species with immense economic footprint warrants intensive investigation and rapid implementation of control measures.

Virology and Etiology of Influenza A Viruses

Taxonomy, Classification, Nomenclature

Influenza viruses comprise four of the seven genera within the family *Orthomyxoviridae*: *Alpha-, Beta-, Gamma-, and Deltainfluenzavirus.* All virus species have a segmented, negative-sense, single-stranded RNA genome, packaged within a viral envelope, containing either seven (*Gamma* and *Delta)* or eight (*Alpha* and *Beta)* segments.

Genome Organization and Products

There are 11 essential proteins translated from the viral RNA segments of Influenza A (IAV) and B (IBV), encoding structural proteins (PB2, PB1, PA), nucleoprotein (NP), matrix proteins (M1, M2), and surface glycoproteins, hemagglutinin (HA) and neuraminidase (NA) as well as non-structural proteins (NS1, NS2). Additional accessory proteins are present/produced

by some, but not all, species and/or subtypes via splicing and alternative open reading frames (M and NS; PB1-F2 and PB1-N40). The protein products from each segment and a brief description of their function are as follows:

1. PB2 – polymerase cap-binding; a determinant of mammalian adaptation
2. PB1 – polymerase catalytic subunit
3. PA – endonuclease; host modulatory functions
4. HA (Hemagglutinin) – receptor binding and fusion
5. NP (Nucleoprotein) – genome encapsidation
6. NA (Neuraminidase) – receptor cleavage, virion release
7. M (M1/M2) – matrix protein and ion channel
8. NS (NS1/NEP) – innate immune suppression, nuclear export

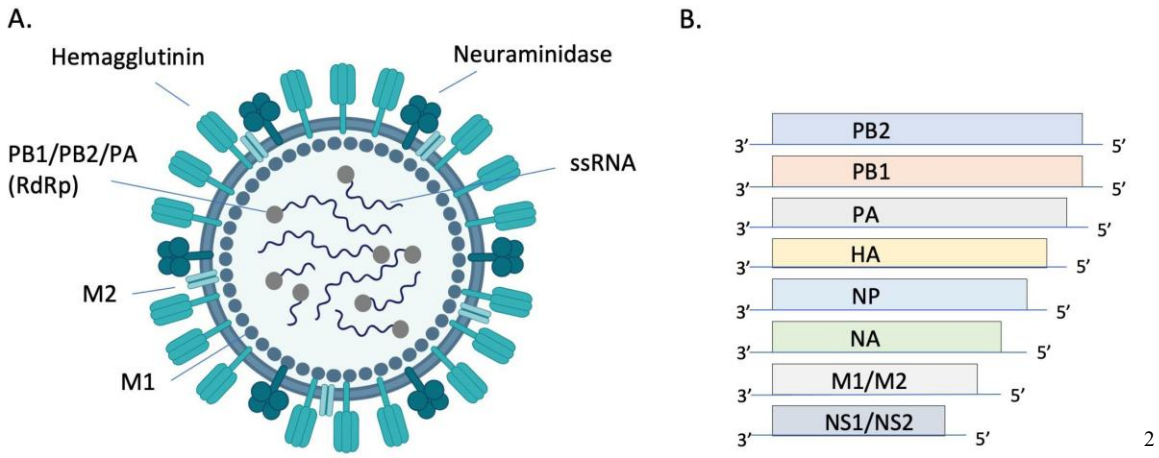

Figure 1.2 Structure and genomic organization of influenza A virus.
The virion (A) and the eight genome segments (B) (113)

[2] Kirk, N. M., Liang, Y. & Ly, H. Comparative Pathology of Animal Models for Influenza A Virus Infection. *Pathogens* **13** (2024).

Another important note regarding recombination is that each segment can reassort independently, creating “genotype mosaics” that can have profound influence on virulence, tropism, and transmissibility (98).

HA Structure, Receptor Binding, and Determinants of Host Range

The receptor specificity is a critical component of HPAIV H5N1 tropism. The HA protein binds α2,3-linked sialic acids receptors that are found predominantly in avian gastrointestinal tissues. In mammals, however, α2,3 receptors are restricted to the lower respiratory tract, whereas α2,6 receptors dominate the upper airways. This inaccessibility of H5's preferred receptor typically prevents H5N1 infection or transmission in humans and livestock (32).

However, recent clade 2.3.4.4b isolates from dairy cattle demonstrate the plasticity of H5N1 features, such as enhanced cleavage activation at α2,6 receptors due to the multibasic cleavage sites present on H5 HA (114, 115). There are also new mutations associated with mammalian adaptation that have become fixed (e.g., PB2 E627K, D701N) and unexpected tissue tropism in the mammary gland in cattle (10, 116, 117). These changes indicate an evolving viral phenotype capable of replicating in tissues not traditionally known to be permissive to avian influenza viruses. In poultry, systemic spread occurs when HA acquires the multibasic cleavage site, enabling activation by ubiquitous furin-like proteases, infection is systemic and highly lethality in chickens (118).

Replication Cycle and Pathogenesis

Replication begins with HA-mediated attachment and endosomal entry, followed by fusion and nuclear import of ribonucleoproteins. Replication and transcription occur in the

nucleus, where the viral polymerase interacts with host mRNAs. The NS1 protein or other immunomodulatory proteins antagonizes innate immune responses, enabling early replication. Virions assemble at the plasma membrane, with NA facilitating release and preventing self-aggregation.

Mechanisms of Evolution: Mutation, Reassortment, and Mammalian Adaptation

H5N1 evolution is dominated four key mechanisms involving: *i)* Reassortment which produces novel subtypes and polymerase constellations, *ii)* Polymerase adaptations — enabling efficient replication in mammalian cells, *iii)* Mutations in HA that modify receptor specificity and affinity, producing diverse antigenic phenotypes, and *iv)* insertion/deletion events that are common amongst RNA viruses (119). RNA virus replication in general is error prone due to the lack of proof-reading capabilities of the RNA-dependent-RNA polymerase, which can influence virulence, tropism, environmental stability, or other features, depending on the site of point mutations and any frame shifts that might result.

The current panzootic clade 2.3.4.4b has generated dozens of genotypes, several showing increased mammalian virulence, neurotropism, and capacity for efficient replication in the mammary gland of cattle (10, 46)

Epidemiology

IAV's are endemic to all regions, with epidemic surges occurring in regular spatiotemporal patterns (seasonally). Avian species serve as the natural reservoirs for most IAV subtypes (H1-H16, H19; N1-N9) while only a subset is generally found circulating within swine (H1, H2, H5; N1, 2,) and humans (H1, 2, 3, 5, 7, 9; N1, 2, 3, 6, 9); although subtypes are not exclusive/restricted to these species.

While humans are frequently infected with seasonal strains, vaccines are effective and reformulated every year. Humans do not play a role in the epidemiology of HPAIV H5N1, at least not in terms of human-to-human transmission. However, it is possible that human activities (husbandry; movement of cows/birds) could facilitate the spread of HPAIV H5N1 in cattle or other species. The production and distribution of contaminated dairy products have also caused disease and mortality in domestic felids(120).

Global Spread and Panzootic Dynamics

Clade 2.3.4.4b H5N1 now behaves as a panzootic lineage, affecting all inhabited continents except Australia. Unlike prior outbreaks characterized by episodic poultry die-offs, the current virus has established persistent circulation in wild birds, with seasonal amplification at migratory staging sites (121)

High environmental stability, long-distance migratory movements, and widespread carnivore scavenging contribute to the virus's resilience and distribution.

Poultry and Economic Impact

Poultry outbreaks have resulted in hundreds of millions of birds culled globally, surpassing all previous HPAI losses. Economic impacts extend beyond direct mortality to include trade restrictions, supply chain disruptions, and long-term market instability.

Mammalian Infections and Transmission Pathways

Spillover into mammals has occurred at unprecedented frequency. Red foxes, skunks, bears, mink, seals, sea lions, and mustelids have shown natural infection, with multiple events of neurotropism and high case fatality (100, 107, 122). Importantly, mink outbreaks in Spain demonstrated sustained mammal-to-mammal transmission (123) and elephant seals and sea lions exhibited large mortality events consistent with efficient spread (100, 105). These events

collectively raise concerns about the virus gaining human-adaptive traits through serial passage in mammals.

Outbreak in United States Dairy Cattle, 2024

The detection of H5N1 in U.S. dairy cattle represented a paradigm shift for influenza A virus ecology and further exacerbating the concerns for mammalian adaptation. Some of the key epidemiologic insights from this outbreak are that inter-farm spread was happening often, likely associated with the movement of infected cattle (110) The primary route of shedding is through the milk, as viral replication is primarily confined to the udder (mammary tissue) (10) The high titer shedding in milk and the mass quantity of milk produced generates a massive amount of environmental contamination including milking equipment and wastewater (124). Infected dairy parlors have subsequently become a source for further cross-species transmission to mammals in proximity such as cats (98). This constellation of findings and the results of experimental infections confirm that cattle function as an amplifying host in dairy-intensive regions, although the broader implications for viral evolution remain uncertain. This outbreak has resulted in contaminated consumer products, including raw milk, cheese, or other dairy products, which has caused concern for further spread and assessment of food supply, and reassessment of the U.S. cattle infrastructure.

Spillover into Humans

In previous outbreaks, as well as this one, there have been occasional cases of H5N1 confirmed in humans, generally associated with poultry and poultry workers during the culling of impacted poultry operations. Similarly, human infections have been confirmed in over 40 dairy workers, although no sustained human-to-human transmission has been reported (125). Serological surveys have also found that veterinarians who have had contact with cattle were

seropositive for H5-specific antibodies, although they had never had any symptoms. This raises concern that spillover into humans is occurring unnoticed and human-adapted H5N1 strains could recombine with seasonal influenza to produce new subtypes with pandemic potential.

Control Strategies

In the United States, outbreaks of HPAI in poultry operations are considered a mandatory reportable disease and demands quarantine of the facility and culling of the population. This prevents spread from one operation to the next, but introductions from wild birds continue to occur. This same strategy was used when H5N1 was detected in mink farms.

The global influenza surveillance network has been critical to stay ahead of seasonal influenza and update vaccines each year. This has been an incredibly successful international effort and instillment of One Health approaches for mitigating disease (126).

Dairy cattle

In response to the outbreak in dairy cattle, several government agencies including the USDA, CDC, and FDA worked to coordinate a response that would cover all aspects of the zoonotic disease outbreak in a major food production system, like dairy cows. This involved increasing the capacity for HPAIV specific diagnostic testing, which needed new assays developed and validated. Federal authority, however, was not able to demand access to dairy herds or require testing unless the cows were being transported. State veterinary agencies coordinated surveillance, worker safety recommendations, and epidemiologic tracing. It was only when a state veterinarian would report outbreaks and invite USDA into the state to assist with investigations and outbreak response that they could do more thorough field investigations and sampling. However, information from these reports has been scarce.

Listed below are a few of the other control measures that were implemented by the Federal agencies to try and limit the spread of HPAIV H5N1 in dairy cattle:

- Mandatory reporting of affected herds
- Movement restrictions and testing requirements
- Biosecurity reinforcement at farms and milk collection points
- Diagnostic expansion through NAHLN laboratories
- USDA guidance for producers (USDA, 2024)

Ultimately, this outbreak revealed several vulnerabilities, including gaps in surveillance and testing, in part due to the voluntary status of these programs and variable willingness to participate. This has resulted in inconsistent reporting across jurisdictions.

Perspective

The emergence of H5N1 in cattle represents one of the most consequential events in modern veterinary virology. It expands the ecological niche of HPAIV into a high-density livestock species positioned at the center of global food production. This seemingly lowers the threshold for future outbreaks in mammalian species and potentially novel HPAIV subtypes emerging in human populations. However, this has provided a unique opportunity to observe natural processes of viral evolution under sustained replication in a mammalian host. It has been observed that some fixed mutations are present in the PB2 region that are associated with mammalian adaptation, but potentially more bovine adapted lineages could appear. There is also a minor risk of reassortment with endemic bovine influenza viruses like influenza D or C, and unknown consequences if that were to happen. Most concerning is the zoonotic spillover that has occurred at human: bovine interface, a new occupational hazard for dairy workers and more opportunities for reassortment with human seasonal influenza strains.

In a broader context, clade 2.3.4.4b illustrates the increasing permeability of species boundaries for RNA viruses in a world shaped by intensive agriculture, globalized supply chains, and ecological disturbance.

Concluding Chapter Summary

Emerging infectious diseases driven by zoonotic RNA viruses continue to reshape global public health and agricultural industries, revealing the profound biological and economic consequences of viral spillover. SARS-CoV-2 and HPAIV H5N1 clade 2.3.4.4b, though belonging to entirely different viral families, converge at the genomic plasticity of: single-stranded RNA viruses have rapidly adapted and evolved through exposures to ecological disturbance, host diversity, evolutionary mechanisms, and agricultural interfaces with remarkable efficiency. Their capacity to cross species barriers, adapt rapidly through mutation or genetic exchange, and persist across wildlife and domestic animal populations is exemplary of how interconnected human and animal health is, and how thin the boundary has become over time.

SARS-CoV-2 demonstrated this permeability early in the COVID-19 pandemic. Human-to-animal transmission occurred across a wide range of household, farmed, and free-living species, most notably mink and white-tailed deer. These spillover events provided real-time illustrations of viral evolution outside the human population, including the emergence of deer-adapted lineages capable of spilling back into humans (44, 69, 127). Such findings redefined the concept of a "reservoir"—from a passive wildlife host to an active participant in viral diversification and a persistent source for direct spillover into human populations.

HPAIV H5N1 clade 2.3.4.4b reveals some of the same concepts but with distinct differences in the scale and consequences. Previously restricted to avian species, it has now

caused widespread mortality in marine mammals and livestock and established persistent circulation across continents. The discovery of efficient replication in mammary tissue, high viral loads in milk, and inter-farm transmission represents a paradigm shift in influenza ecology (10, 110). This event expands the ecological niche of HPAIV, alters its evolutionary landscape, and raises questions about consequences for food security, viral reassortment, and zoonotic risk.

Together, SARS-CoV-2 and HPAIV H5N1 clade 2.3.4.4b highlight a central theme of emerging virology: host boundaries are fluid, particularly in environments shaped by intensive agriculture, wildlife-livestock interfaces, and globalized trade. Livestock systems—by virtue of their scale, distribution, and biological connectivity—are uniquely positioned at this intersection. Their infections carry implications not only for animal health but for public health, food security, and international commerce. This review highlights the need for experimental infection studies, targeted surveillance, and genomic monitoring to characterize susceptibility and evolution of these promiscuous pathogens in ruminants, an area where substantial knowledge gaps remain. Understanding how emerging viruses interact with cattle, sheep, white-tailed deer, and other livestock or peridomestic species is essential for estimating future spillover potential, proactively adjusting biosecurity practices to reduce future spillover events, and in helping to mitigate potential economic impacts. As agricultural landscapes evolve and viruses continue to adapt, integrated approaches drawing from veterinary medicine, virology, ecology, and One Health principles will be required to safeguard both animal and human populations.

Chapter 2 - Infection and transmission of ancestral SARS-CoV-2 and its alpha variant in pregnant white-tailed deer[3]

Abstract

SARS-CoV-2 was first reported circulating in human populations in December 2019 and has since become a global pandemic. Recent history involving SARS-like coronavirus outbreaks have demonstrated the significant role of intermediate hosts in viral maintenance and transmission. Evidence of SARS-CoV-2 natural infection and experimental infections of a wide variety of animal species has been demonstrated, and *in silico* and *in vitro* studies have indicated that deer are susceptible to SARS-CoV-2 infection. White-tailed deer (WTD) are amongst the most abundant and geographically widespread wild ruminant species in the US. Recently, WTD fawns were shown to be susceptible to SARS-CoV-2. In the present study, we investigated the susceptibility and transmission of SARS-CoV-2 in adult WTD. In addition, we examined the competition of two SARS-CoV-2 isolates, representatives of the ancestral lineage A and the alpha variant of concern (VOC) B.1.1.7 through co-infection of WTD. Next-generation sequencing was used to determine the presence and transmission of each strain in the co-infected and contact sentinel animals. Our results demonstrate that adult WTD are highly susceptible to SARS-CoV-2 infection and can transmit the virus through direct contact as well as vertically from doe to fetus. Additionally, we determined that the alpha VOC B.1.1.7 isolate of SARS-CoV-2 outcompetes the ancestral lineage A isolate in WTD, as demonstrated by the genome of

---

[3] Reprinted with permission from " Infection and transmission of ancestral SARS-CoV-2 and its alpha variant in pregnant white-tailed deer" by Cool, K. *et al., 2022. Emerging Microbes & Infections* **11**, 95-112.

the virus shed from nasal and oral cavities from principal infected and contact animals, and from virus present in tissues of principal infected deer, fetuses and contact animals

Introduction

The family *Coronaviridae* is comprised of enveloped, single-stranded, positive-sense RNA viruses, and include four genera *Alpha-, Beta- Gamma- and Delta-coronaviruses*. *Betacoronaviruses* have been the subject of intensive research since the emergence of severe acute respiratory syndrome coronavirus (SARS-CoV) in 2002, Middle East respiratory syndrome coronavirus (MERS-CoV) in 2012, and most recently SARS-CoV-2 in 2019. In order to determine the origins of SARS-CoV-2, surveillance efforts have mainly focused on bat populations since they were identified as the reservoir species for SARS-CoV-like and MERS-CoV-like viruses (37). Intermediate hosts such as civet cats (*Paguma larvata)* for SARS-CoV or camels (*Camelus dromedaries)* for MERS-CoV have also been identified as an important vehicle for virus spillover into human populations and have shown to play a significant role in pathogen establishment and continued animal-to-human transmission (7, 128).

The World Organization for Animal Health (WOAH; formerly OIE) has reported the natural infection of SARS-CoV-2 in at least 10 animal species across continents including the Americas, Europe, Africa and Asia: domestic cats and dogs, tigers, lions, cougar, snow leopard, puma, mink, ferrets, gorilla, and otter (https://www.aphis.usda.gov/aphis/dashboards/tableau/sars-dashboard). In the United States alone, USDA-APHIS has reported 217 incidences of natural SARS-CoV-2 infections amongst 9 different species (www.aphis.usda.gov). Experimental infection of SARS-CoV-2 in animal models has identified cats, ferrets, mink, Syrian golden hamsters, non-human primates, tree shrews, and deer mice as highly susceptible to SARS-CoV-2 infection (43, 129-136). Dogs,

cattle, and Egyptian fruit bats have shown moderate susceptibility while non-transgenic mice (with the exception of variants containing the N501Y polymorphism in their S gene), poultry, and pigs are not readily susceptible to SARS-CoV-2 infection (58, 137-140). It is important to determine susceptible host species for SARS-CoV-2 in order to better understand the ecology of this virus and to identify potential reservoir species which may be sources of spillover into human populations (16). Additionally, the emergence and sustained transmission of SARS-CoV-2 variants of concern (VOC) has important implications in virus evolution and pathogenesis (141). It is therefore necessary to investigate the transmission efficiency and pathogenesis of SARS-CoV-2 VOCs in susceptible species.

A recent publication by Palmer and coworkers (142) describes susceptibility of white-tailed deer (*Odocoileus virginianus*) fawns to the SARS-CoV-2 tiger isolate TGR/NY/20 (142). Recent surveillance studies have also shown SARS-CoV-2 antibodies in wild white-tailed deer (143). The work presented here expands upon the previous findings by describing SARS-CoV-2 infection in pregnant adult deer, as well as horizontal and vertical transmission of the virus. Furthermore, we investigated the competition of two SARS-CoV-2 isolates in deer, representatives of the ancestral lineage A (SARS-CoV-2/human/USA/WA1/2020) and the alpha VOC B.1.1.7 (SARS-CoV-2/human/USA/CA_CDC_5574/2020), and determined the relative abundance of each strain after replication and transmission by next generation sequencing. The results of this study confirm that adult white-tailed deer are highly susceptible to SARS-CoV-2 infection and shed virus in sufficient quantities through oral and nasal cavities to infect naïve contact sentinel deer. Furthermore, our results illustrate the *in vivo* competition of two lineages of SARS-CoV-2 through analysis of excreted virus and the virus presence in tissues collected

postmortem. Importantly, this is the first study which provides evidence for vertical transmission of SARS-CoV-2 from doe to fetus.

Materials and methods

Cells and virus isolation/titrations

Vero E6 cells (ATCC; Manassas, VA) and Vero E6 cells stably expressing transmembrane serine protease 2 (Vero-E6/TMPRSS2)(144) were obtained from Creative Biogene (Shirley, NY) via Kyeong-Ok Chang at KSU and used for virus propagation and titration. Cells were cultured in Dulbecco's Modified Eagle's Medium (DMEM, Corning, New York, N.Y, USA), supplemented with 5% fetal bovine serum (FBS, R&D Systems, Minneapolis, MN, USA) and antibiotics/antimycotics (ThermoFisher Scientific, Waltham, MA, USA), and maintained at 37 °C under a 5% CO_2 atmosphere. The addition of the selection antibiotic, G418, to cell culture medium was used to maintain TMPRSS2 expression but was not used during virus cultivation or assays. The SARS-CoV-2/human/USA/WA1/2020 lineage A (referred to as lineage A WA1; BEI item #: NR-52281) and SARS-CoV-2/human/USA/CA_CDC_5574/2020 lineage B.1.1.7 (alpha VOC B.1.1.7; NR-54011) strains were acquired from BEI Resources (Manassas, VA, USA). A passage 2 plaque-purified stock of lineage A WA1 and a passage 1 of the alpha VOC B.1.1.7 stock were used for this study. Virus stocks were sequenced by next generation sequencing (NGS) using the Illumina MiSeq and the consensus sequences were found to be homologous to the original strains obtained from BEI (GISAID accession numbers: EPI_ISL_404895 (WA-CDC-WA1/2020) and EPI_ISL_751801 (CA_CDC_5574/2020).

To determine infectious virus titers of virus stocks and study samples, 10-fold serial dilutions were performed on Vero-E6/TMPRSS2 cells. The presence of cytopathic effects (CPE) after 96 hours incubation at 37 °C was used to calculate the 50% tissue culture infective dose

($TCID_{50}$)/ml using the Spearman-Kaerber method (145). Selected swab and tissue homogenate samples were tested for viable virus by culture on Vero E6/TMPRRS2 cells. Virus isolation was performed by culturing 400 µL of filtered (0.2 µm; MidSci, St. Louis, MO) sample on Vero E6 cells and monitoring for CPE for up to 5 days post inoculation. Virus isolation attempts were primarily performed on samples with $\geq 10^6$ RNA copy number per mL, as this was our approximate limit of detection (LOD) for viable virus using this method.

Susceptibility of cervid cells to SARS-CoV-2

The SARS-CoV-2 USA-WA1/2020 strain was passaged 3 times in Vero-E6 cells to establish a stock virus for infection experiments. Primary white-tailed (*Odocoileus virginianus*), mule deer (*Odocoileus hemionus)* and elk (*Cervus canadensis*) lung cells (provided by USDA ARS-ABADRU) were infected at approximately 0.1 MOI. Infected cell supernatants were collected at 0, 2, 4, 6 or 8 days post infection (DPI) and stored at -80°C until further analysis. Cell lines were tested in at least two independent infection experiments. Cell supernatants were titrated on Vero E6 cells to determine $TCID_{50}$/mL.

Ethics statement

All animal studies and experiments were approved and performed under the Kansas State University (KSU) Institutional Biosafety Committee (IBC, Protocol #1460) and the Institutional Animal Care and Use Committee (IACUC, Protocol #4468) in compliance with the Animal Welfare Act. All animal and laboratory work were performed in biosafety level-3+ and −3Ag laboratories and facilities in the Biosecurity Research Institute at KSU in Manhattan, KS, USA.

Virus challenge of animals

Six female white-tailed deer (WTD), approximately 2 years of age, were acquired from a Kansas deer farm (Muddy Creek Whitetails, KS) and acclimated for ten days in BSL-3Ag

biocontainment with feed and water *ad libitum* prior to experimental procedures. On day of challenge, four principal infected deer were inoculated with a 1:1 titer ratio of lineage A WA1 and the alpha VOC B.1.1.7 strains (**Supplementary Figure 2.1**). A 2 ml dose of $1x10^6$ $TCID_{50}$ per animal was administered through intra-nasal (IN) and oral (PO) routes simultaneously. The remaining two non-infected deer were placed up-current of the room directional airflow from the principal infected deer, separated by an 8-foot tall, solid partition wall. At 1 day-post-challenge (DPC), the two naïve deer were co-mingled with the principal infected animals as contact sentinels for the duration of the study. Two principal infected deer were euthanized and *postmortem* examination performed at 4 DPC. *Postmortem* examination of the remaining two principal infected and two sentinels was performed at 18 DPC (**Table 2.1**). Five of the six deer were pregnant; the number of fetuses per deer are indicated in **Table 2.1**. Four naïve white-tailed deer from a previous study evaluating a baculovirus-expressed subunit vaccine for the protection from epizootic hemorrhagic disease (EHD) caused by an orbivirus, performed in 2017 (146), were used as controls for serology and histopathology (**Table 2.1 and Supplementary Figure 2.1**).

Table 2.1 Animals and treatment assignments

Animal ID#	Treatment	Necropsy	No. of fetuses
108	Principal infected	4 DPC	0
905	Principal infected	4 DPC	3
106	Principal infected	18 DPC	3 (mummified)
919	Principal infected	18 DPC	3
49	Sentinel introduced 1 DPC	18 DPC	2
50	Sentinel introduced 1 DPC	18 DPC	1
1755, 1756, 1760, 1763	Vaccinated/sham vaccinated and EHDV challenged deer [23] served as controls	2017	0

DPC = day post challenge

Clinical evaluations and sample collection

Deer were observed daily for clinical signs. Clinical observations focused on activity level (response to human observer), neurological signs, respiratory rate, and presence of gastrointestinal distress. Rectal temperature, nasal, oropharyngeal, and rectal swabs were collected from sedated animals at 0, 1, 3, 5, 7, 10, 14 and 18 DPC. Swabs were placed in 2mL of viral transport medium (DMEM, Corning; combined with 1% antibiotic-antimycotic, ThermoFisher), vortexed, and aliquoted directly into cryovials and RNA stabilization/lysis Buffer RLT (Qiagen, Germantown, MD, USA). EDTA blood and serum were collected prior to challenge and on days 3, 7, 10, 14, and 18 DPC. Full *postmortem* examinations were performed, and gross changes recorded. A comprehensive set of tissues were collected in either 10% neutral-buffered formalin (Fisher Scientific, Waltham, MA, USA), or as fresh tissues directly stored at -80°C. Tissues were collected from the upper respiratory tract (URT) and lower respiratory tract (LRT), central nervous system (brain and cerebral spinal fluid [CSF]), gastrointestinal tract (GIT) as well as accessory organs. The lungs were removed *in toto* including the trachea, and the main bronchi were collected at the level of the bifurcation and at the entry point into the lung lobe. Lung lobes were evaluated based on gross pathology and collected and sampled separately. Bronchoalveolar lavage fluid (BALF), nasal wash and urine were also collected during *postmortem* examination. Fetal tissues including lung, liver, spleen, kidney as well as placenta were also collected. Fresh frozen tissue homogenates were prepared as described previously (43). All clinical samples (swabs, nasal washes, BALF, CSF, urine) and tissue homogenates were stored at -80°C until further analysis.

RNA extraction and reverse transcription quantitative PCR (RT-qPCR)

SARS-CoV-2 specific RNA was detected and quantified using a quantitative reverse transcription real time – PCR (RT-qPCR) assay specific for the N2 segment as previously described (43). Briefly, nucleic acid extractions were performed by combining equal amounts of Lysis Buffer RLT (Qiagen, Germantown, MD, USA) with supernatant from clinical samples (swabs, nasal washes, BALF, CSF, urine), tissue homogenates in DMEM (20% W/V), EDTA blood or body fluids. Sample lysates were vortexed and 200 µL was used for extraction using a magnetic bead based extraction kit (GeneReach USA, Lexington, MA) and the Taco™ mini nucleic acid extraction system (GeneReach) as previously described (43). Extraction positive controls (IDT, IA, USA; 2019-nCoV_N_Positive Control), diluted 1:100 in RLT lysis buffer, and negative controls were included throughout this process.

Quantification of SARS-CoV-2 RNA was accomplished using an RT-qPCR protocol established by the CDC for detection of SARS-CoV-2 nucleoprotein (N)-specific RNA (https://www.fda.gov/media/134922/download). Our lab has validated this protocol using the N2 SARS-CoV-2 primer and probe sets (CDC assays for RT-PCR SARS-CoV-2 coronavirus detection | IDT (idtdna.com)) in combination with the qScript XLT One-Step RT-qPCR Tough Mix (Quanta Biosciences, Beverly, MA, USA), as previously described (43). Quantification of RNA copy number (CN) was based on a reference standard curve method using a 10-point standard curve of quantitated viral RNA (USA-WA1/2020; lineage A). This RT-qPCR assay was also validated to the detection of the USA/CA_CDC_5545/2020 alpha VOC B.1.1.7 strain. Each sample was run in duplicate wells and all 96-well plates contained duplicate wells of quantitated PCR positive control (IDT, IA, USA; 2019-nCoV_N_Positive Control, diluted 1:100) and four non-template control wells. A positive Ct cut-off of 38 cycles was used when both wells were

positive. The cut-off of 38 cycles is based on our validation of this assay and is consistent with CDC guidelines which use the same assay. The standard curve of SARS-CoV-2 RNA has a limit of detection at 38 Cycles (single copy/uL). Samples with one of two wells positive at or under CT of 38 were considered suspect-positive. Data are presented as the mean of the calculated N gene CN per mL of liquid sample or per mg of 20% tissue homogenate.

Next-Generation Sequencing

RNA extracted from cell culture supernatant (virus stocks), clinical swab/tissue homogenates, and clinical samples were sequenced by next generation sequencing (NGS) using an Illumina NextSeq platform (Illumina Inc.) to determine the genetic composition (% lineage) of viral RNA in each sample. SARS-CoV-2 viral RNA was amplified using the ARTIC-V3 RT-PCR protocol [Josh Quick 2020. nCoV-2019 sequencing protocol v2 (GunIt). Protocols.io https://gx.doi.org/10.17504/protocols.io.bdp7i5rn]. Library preparation of amplified SARS-CoV-2 DNA for sequencing was performed using a Nextera XT library prep kit (Illumina Inc.) following the manufacturer's protocol. The libraries were sequenced on the Illumina NextSeq using 150 bp paired end reads with a mid-output kit. Reads were demultiplexed and parsed into individual sample files that were imported into CLC Workbench version 7.5 (Qiagen) for analysis. Reads were trimmed to remove ambiguous nucleotides at the 5' terminus and filtered to remove short and low-quality reads. The consensus sequences of viral stocks used for challenge material preparation were found to be homologous to the original strains obtained from BEI (GISAID accession numbers: EPI_ISL_404895 (WA-CDC-WA1/2020) and EPI_ISL_751801 (CA_CDC_5574/2020). To determine an accurate relative percentage of each SARS-CoV-2 lineage in each sample, BLAST databases were first generated from individual trimmed and filtered sample reads. Subsequently, two 40-nucleotide long sequences were generated for each

strain at locations that include the following gene mutations: Spike (S) A570D, S D614G, S H1118H, S ΔH69V70, S N501Y, S P681H, S 982A, S T716I, S ΔY145, Membrane (M) V70, Nucleoprotein (N) D3L, N R203KG204R, N 235F, and non-structural NS3 T223I, NS8 Q27stop, NS8 R52I, NS8 Y73C, NSP3 A890D, NSP3 I1412T, NSP3 T183I, NSP6 ΔS106G107F108, NSP12 P323L, NSP13 A454V and NSP13 K460R. A word size of 40 was used for the BLAST analysis to exclude reads where the target mutation fell at the end of a read or reads that partially covered the target sequence. The two sequences for each of the locations listed above, corresponding to either lineage A (USA-WA1/2020) or alpha VOC B.1.1.7 (USA/CA_CDC_5574/2020), were subjected to BLAST mapping analysis against individual sample read databases to determine the relative amount of each strain in the samples. The relative amount of each strain present was determined by calculating the percent of reads that hit each of the twenty-three target mutations. The percentages for all mutations were averaged to determine the relative amount of each strain in the sample. Samples with incomplete or low coverage across the genome were excluded from analysis. Average depth of read coverage ranged from 554 up to 48315 with 9312 as the median coverage per sample (**Supplementary Figure 2.2**).

Virus neutralizing antibodies

Virus neutralizing antibodies in sera were determined using microneutralization assay as previously described (43). Briefly, heat inactivated (56°C/ 30 min) serum samples were subjected to 2-fold serial dilutions starting at 1:20 and tested in duplicate. Then, 100 $TCID_{50}$ of SARS-CoV-2 virus in 100 µL DMEM culture media was added 1:1 to 100 µL of the sera dilutions and incubated for 1 hour at 37ºC. The mixture was subsequently cultured on Vero-E6/TMPRSS2 cells in 96-well plates. The neutralizing antibody titer was recorded as the highest

serum dilution at which at least 50% of wells showed virus neutralization based on the absence of CPE observed under a microscope at 72 h post infection. Sera collected on -3 DPC were pooled prior to testing.

Detection of antibodies by indirect ELISA

Indirect ELISAs were used to detect SARS-CoV-2 antibodies in sera with nucleocapsid (N) and the receptor-binding domain (RBD) recombinant viral proteins, both produced in-house (43). Briefly, wells were coated with 100 ng of the respective protein in 100 µL per well coating buffer (Carbonate–bicarbonate buffer, catalogue number C3041, Sigma-Aldrich, St. Louis, MO, USA). Following an overnight incubation at 4 ºC, plates were washed three times with phosphate buffered saline (PBS-Tween 20 [pH=7.4]; catalogue number 524653, Millipore Sigma), blocked with 200 µL per well casein blocking buffer (Sigma-Aldrich, catalogue number B6429) and incubated for 1 hour at room temperature (RT). Plates were subsequently washed three times with PBS-Tween-20 (PBS-T). Serum samples were diluted 1:400 in casein blocking buffer, then 100 µL per well was added to ELISA plates and incubated for 1 hour at RT. Following three washes with PBS-T, 100 µL of HRP-labelled Rabbit Anti-Deer IgG (H+L) secondary antibody (95058-328, VWR, Batavia, IL, USA) diluted 1:1000 (100ng/mL) was added to each well and incubated for 1 hour at RT. Plates were then washed five times with PBS-T and 100 µL of TMB ELISA Substrate Solution (Abcam, catalogue number ab171525, Cambridge, MA, USA) was added to all wells of the plate and incubated for 5 minutes before the reaction was stopped. The OD of the ELISA plates were read at 450 nm on an ELx808 BioTek plate reader (BioTek, Winooski, VT, USA). The cut-off for a sample being called positive was determined as follows: Average OD of negative serum + 3X standard deviation. Everything above this cut-off was considered positive. Indirect ELISA was used to

detect Bovine Coronavirus (BCoV) antibodies in sera with Spike (S) recombinant viral protein (LSBio, LS-G64076-20, Seattle, WA, USA) using the methods described above.

Histopathology

Tissue samples from the respiratory tract (nasal cavity [rostral, middle and deep turbinates following decalcification with Immunocal™ Decalcifier (StatLab, McKinney, TX, for 4-7 days at room temperature), trachea, and lungs as well as various other extrapulmonary tissues (liver, spleen, kidneys, heart, pancreas, gastrointestinal tract [stomach, small intestine including Peyer's patches and colon], cerebrum [including olfactory bulb], tonsils and numerous lymph nodes were routinely processed and embedded in paraffin. Four-micron tissue sections were stained with hematoxylin and eosin following standard procedures. Two independent veterinary pathologists (blinded to the treatment groups) examined the slides and morphological descriptions were provided. Tissues from naïve white-tailed deer from a previous study (146) were used as negative controls for histopathological analysis including immunohistochemistry.

SARS-CoV-2-specific immunohistochemistry (IHC)

IHC was performed as previously described (43) on four-micron sections of formalin-fixed paraffin-embedded tissue mounted on positively charged Superfrost® Plus slides and subjected to IHC using a SARS-CoV-2-specific anti-nucleocapsid rabbit polyclonal antibody (3A, developed by our laboratory) with the method previously described (147). Lung sections from a SARS-CoV-2-infected hamster were used as positive assay controls.

Results

Susceptibility of cervid primary lung cells to SARS-CoV-2

Primary lung cells isolated from white-tailed deer (*Odocoileus virginianus*), mule deer (*Odocoileus hemionus*) and elk (*Cervus canadensis*) were tested for susceptibility to SARS-

CoV-2 and viral growth kinetics. SARS-CoV-2 lineage A WA1 strain was found to replicate in both, white-tailed deer and mule deer lung cells but not in elk lung cells (**Figure 2.1A**), and replication resulted in cell death (**Figure 2.1B**). Similar kinetics were observed at 2 and 4 DPI for both the white-tailed deer and mule deer cells. Virus titers declined by 6 DPC in white-tailed deer lung cells, while titers in mule deer lung cultures remained elevated even at 8 DPC. Elk lung cell input virus rapidly declined by day 2 and virus was not detectable by 8 DPC. These results suggest that besides white-tailed deer, mule deer species may be susceptible to SARS-CoV-2 and could serve as a potential reservoir species.

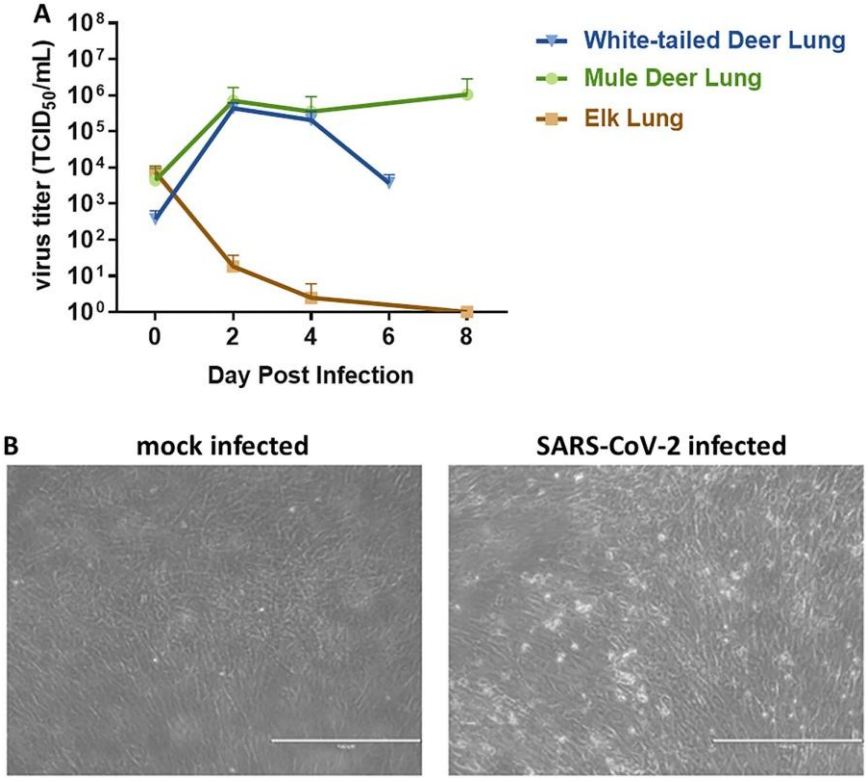

Figure 2.1 SARS-CoV-2 replication in various cervid lung cells

SARS-CoV-2 replication in various cervid lung cells. (A) Primary lung cells were infected with the SARS-CoV-2 USA-WA1/2020 at 0.1 MOI and cell supernatants collected at 0, 2, 4, 6 or 8 days post infection (DPI). Cell supernatants were titrated on Vero E6 cells to determine virus titres. Mean titres of at least two independent infection experiments per cell line are shown. (B) Cytopathic effect observed at 6 DPI with SARS-CoV-2 but not in mock infected white-tailed deer primary lung cells at the same time point DPI.

SARS-CoV-2-infected adult white-tailed deer remain subclinical

Four deer were inoculated with an approximate 1:1 titer ratio of the lineage A WA1 and alpha VOC B.1.1.7 strains (**Supplementary Figure 2.1**) with $1x10^6$ $TCID_{50}$ per animal administered through IN and PO routes simultaneously. Clinical signs were recorded daily, including respiratory rate, posture, and activity levels. Rectal temperatures were recorded on days of sample collection. No major clinical signs were observed throughout the course of this study. Ocular discharge was noted in the principal infected animal #106 from 5 to 10 DPC and nasal discharge was noted on 7 DPC in principal infected animal #919. Rectal temperatures of principal and sentinel deer remained within normal range (99-105°F), although there was a slight elevation in body temperature of principal infected deer from 0 to 3 DPC, and at 1 to 3 DPC in the sentinels (**Supplementary Figure 2.3**). Soft stool was observed in one deer (#905) for the duration of the study; this was not considered as a result from SARS-CoV-2 infection as this was also observed prior to challenge.

SARS-CoV-2 RNA/virus shedding

SARS-CoV-2 RNA shedding was determined by evaluating nasal, oral and rectal swabs of principal infected (**Figure 2.2A**) and sentinel deer (**Figure 2.2B**) for the presence of SARS-CoV-2 specific RNA by RT-qPCR. Viral RNA was detected in nasal swabs from all principal infected animals (n=4) from 1 to 10 DPC (**Figure 2.2A**), and the sentinel contact deer (n=2) starting at 3 DPC (2 days post comingling) up to 10 DPC (**Figure 2.2B**). All deer had SARS-CoV-2 RNA detected in oral swabs at some time point post infection/contact, although less frequently and at lower levels compared to nasal swabs. Viral RNA from oral swabs was detected from 1 to 7 DPC in at least one of the principal infected deer. Oral swabs from at least one sentinel deer were detectable at 3 and 5 DPC (2 to 4 days post comingling), and both

sentinels were positive at 7 DPC. Rectal swabs had low levels of viral RNA detected at 5 and 7 DPC in two principal infected animals, and in only one sentinel deer at 5 DPC. Infectious virus could be isolated from nasal swabs of at least one of the principal infected deer at 1, 3 and 4 DPC, and from one sentinel at 7 DPC (**Table 2.2**). Infectious virus was isolated from oral swabs from one principal infected animal at 3 DPC and from one sentinel at 5 DPC (**Table 2.2**). In addition, virus was also isolated from a single rectal swab at 5 DPC from a principal infected deer.

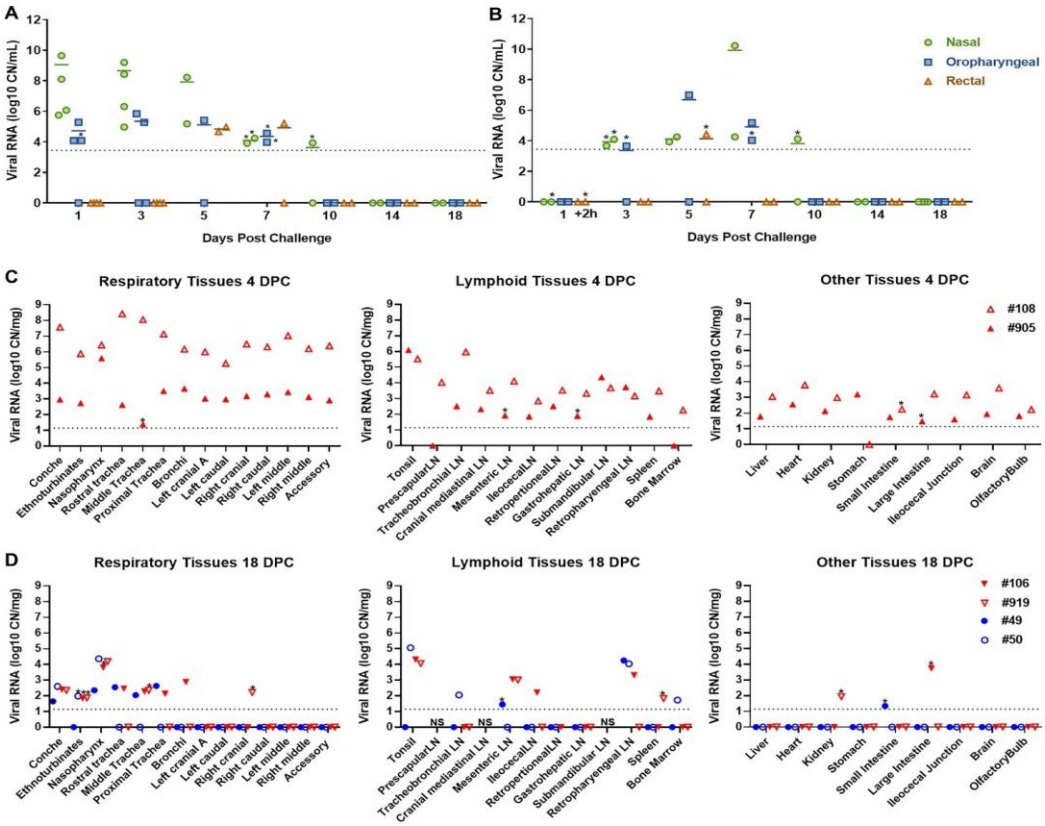

Figure 2.2 Viral shedding and viral RNA detected in tissues of SARS-CoV-2-infected white-tailed deer

RT-qPCR was performed on nasal, oropharyngeal, and rectal swabs collected from principal infected (A) and sentinel deer (B), and various tissues of deer euthanized at 4 (C) and 18 (D) days post challenge (DPC) to detect the presence of SARS-CoV-2 specific RNA. Mean ($n = 2$) viral RNA copy number (CN) per mL (A and B) or per mg (C and D) based on the SARS-CoV-2 nucleocapsid gene are plotted for individual animals. Asterisks (*) indicate samples with 1 out of 2 RT-qPCR reactions below the limit of detection, which is indicated by the dotted lines.

Table 2.2 Virus isolation from swabs and tissues.

Sample type	DPC	Animal number	Virus titre ($TCID_{50}$/mL)
Nasal Swab	1	#106, 905, 919	NEG
Nasal Swab	1	#108	1.00E+02
Nasal Swab	3	#106	9.98E+02
Nasal Swab	3	#108, 905, 919	NEG
Nasal Swab	4	#108, 905	9.98E+02, NEG
Nasal Swab	5	#106, 919	NEG
Nasal Swab	7	#49	3.15E+02
Oral Swab	1	#905	NEG
Oral Swab	3	#106, 108	5.00E+00, NEG
Oral Swab	4	#108, 905	NEG
Oral Swab	5	#50, 106	5.00E+00, NEG
Oral Swab	7	#49, 50	NEG
Rectal Swab	5	#49, 919	NEG
Rectal Swab	5	#106	3.15+02
Rectal Swab	7	#919	NEG
Nasopharynx	4	#108, 905	NEG
Conchae	4	#108	NEG
Ethnoturbinates	4	#108	NEG
Trachea	4	#108, 905	3.15E+02, NEG
Bronchi	4	#108, 905	3.15E+02, NEG
Lung	4	#108, 905	NEG
Tonsil	4	#108, 905	NEG
Lymph nodes[a]	4	#108, 905	NEG
Stomach	4	#905	NEG
Spleen	4	#108	NEG
Heart	4	#108	NEG
Brain	4	#108	NEG
CSF	4	#108	NEG
BALF	4	#108, 905	3.15E+03, NEG
Nasal Wash	4	#108, 905	3.15E+02, NEG
Nasopharynx	18	#50, 106, 919	NEG
Conchae	18	#50	NEG
Ethnoturbinates	18	#50	NEG
Tonsil	18	#50, 106, 919	NEG
Lymph nodes[a]	18	#49, 50, 106	NEG
Large intestine	18	#106	NEG
Bone Marrow	18	#50	NEG

In general, samples with $>10^6$ RNA copy number were subjected to virus isolation

[a]*Multiple different types of lymph nodes were tested.*

Evaluation of deer during the acute stage of infection (4 DPC)

To evaluate the acute stage of infection, two of the principal infected deer (#108 and #905) were humanely euthanized and examined at 4 DPC. SARS-CoV-2 RNA was detected throughout the upper and lower respiratory tract tissues of both deer necropsied at 4 DPC (**Figure 2.2C**). The highest levels of SARS-CoV-2 RNA were detected in the nasal cavity, trachea, bronchi, and all lung lobe sections. There was a distinct difference in viral RNA load observed in the respiratory tract tissues between the two deer at 4 DPC; one deer (#905) revealed consistently lower quantities of SARS-CoV-2 RNA throughout upper and lower respiratory tissues than the other deer (#108). Nasal washes and BALF from both animals were also positive for SARS-CoV-2 RNA at 4 DPC. Infectious virus was isolated from the nasal wash, BALF, trachea and bronchi of deer #108, but not from any tissues tested for deer #905 (**Table 2.2**).

Histological evaluations and IHC for the presence of SARS-CoV-2 antigen in the upper and lower respiratory tract tissues, tonsils and select lymph nodes collected at 4 DPC were performed (**Figure 2.3A-L**). In the respiratory tract, histological changes were more pronounced in deer #108 compared to #905, and a mild to moderate multifocal lymphohistiocytic and neutrophilic rhinitis (**Figure 2.3A**), erosive to suppurative tracheitis (**Figure 2.3C**) and erosive bronchitis with mixed peribronchiolitis were noted (**Figure 2.3D, E, F**). Specifically, there was marked attenuation of the respiratory epithelium lining the trachea and a main bronchus with loss of cilia, individual cell degeneration and necrosis, neutrophil transmigration, and accumulation of cellular debris in the lumen (**Figure 2.3C, D**). The subjacent edematous lamina propria was infiltrated by neutrophils, lymphocytes and histiocytes; and respiratory epithelial cells frequently contained intracytoplasmic viral antigen, also abundant in the superficial exudate (**Figure 2.3I, J**). In the remaining pulmonary parenchyma, bronchioles and blood vessels were delineated by

perivascular and peribronchiolar lymphocytes, histiocytes and few neutrophils, but viral antigen was generally not detected (**Figure 2.3E, K**). Rarely, sloughed and necrotic epithelial cells and few degenerate leukocytes lodged at the termini of respiratory bronchioles and containing intracytoplasmic viral antigen were observed (**Figure 2.3F, L**). In deer #905, the inflammatory component was mild and predominantly lymphocytic with no viral antigen detected in the respiratory tract. Along the rostral turbinates of both animals (#905 and 108), the lamina propria was infiltrated by lymphocytes, histiocytes and fewer neutrophils that transmigrated through the lining nasal epithelium and encircled subjacent nasal glands. In contrast, the deep turbinates including the olfactory neuroepithelium, olfactory nerve fascicles and olfactory bulb were unremarkable (**Figure 2.3B**). No viral antigen was detected within the segments of the nasal passages that were evaluated (**Figure 2.3G, H)**. A mild erosive tonsilitis with a small focus of intraepithelial SARS-CoV-2 antigen was also noted in deer #108 at 4 DPC (**Supplementary Figure 4**). No other significant histologic alterations were found in other tissues examined from the adult deer. Fetal lungs occasionally contained intrabronchial/intrabronchiolar foci of squamous cell proliferation; however, no viral antigen was detected here or within the placenta.

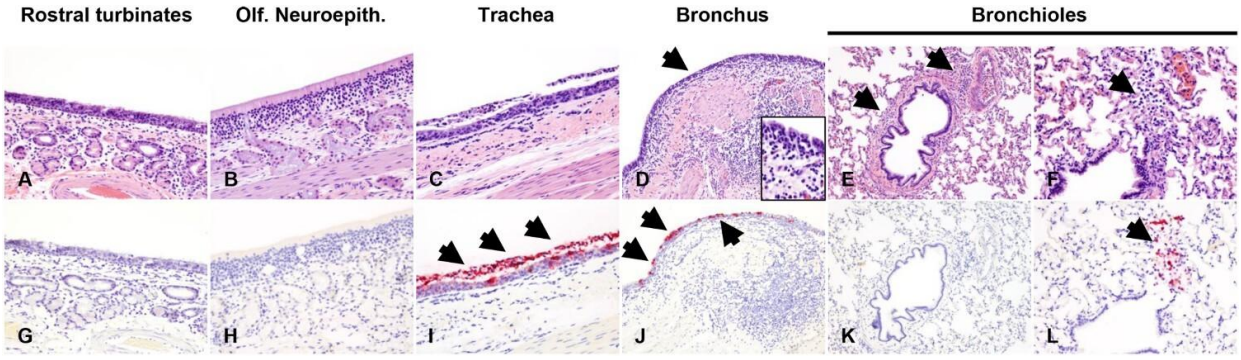

Figure 2.3 Histological lesions and SARS-CoV-2 antigen distribution in the upper and lower respiratory tract of principal infected white-tailed deer at 4 DPC.

Histological lesions and SARS-CoV-2 antigen distribution in the upper and lower respiratory tract of principal infected white-tailed deer at 4 DPC. Rostral turbinates (A and G), olfactory neuroepithelium (B and H), trachea (C and I), bronchus (D and J) and bronchioles (E, F, K and L). At 4 DPC, in the rostral turbinates, neutrophilic rhinitis with epithelial transmigration and mixed lymphocytic and histiocytic infiltration of the subjacent lamina propria and around nasal glands were observed (A) but no viral antigen was detected (G). The olfactory neuroepithelium was histologically unremarkable (B) with no viral antigen detected (H). In the trachea, there was marked attenuation of the respiratory epithelium with loss of cilia, individual cell degeneration and necrosis, neutrophil transmigration, and accumulation of cellular debris in the lumen (C). Frequently, respiratory epithelial cells of the trachea contained intracytoplasmic viral antigen indicated by the red staining (arrows), which was also abundant in the superficial exudate (I). The bronchial mucosa was characterized by segmental attenuation of the lining respiratory epithelium with loss of cilia, degeneration/necrosis of individual epithelial cells and neutrophil and lymphocyte transmigration, and a mixed lymphocytic and histiocytic infiltrate in the edematous lamina propria (D, arrows and inset). The bronchial epithelium lining affected segments frequently contained viral antigen stained red (J, arrows). In the pulmonary parenchyma, bronchioles and blood vessels were delimited by perivascular and peribronchiolar lymphocytes, histiocytes and few neutrophils (E, arrows). Viral antigen was generally not detected (K). In bronchioles, rarely sloughed and necrotic epithelial cells and few degenerate leukocytes lodged within alveolar ducts (F, arrow) contained intracytoplasmic viral antigen indicated by the red staining (L, arrow). H&E and Fast Red, 100× total magnification.

Evaluation of deer during the convalescent stage of infection (18 DPC)

Postmortem examination of the remaining four deer, consisting of two principal infected animals and two contact sentinels, was performed on 18 DPC. SARS-CoV-2 RNA was detected in the upper respiratory tract tissues (nasal cavity and trachea) of the principal infected and sentinel deer at 18 DPC (**Figure 2.2D**). One of the principal infected animals had viral RNA in

the bronchi. The lung lobes were negative for viral RNA in all deer except for the right cranial lung lobe from one of the principal infected deer (#919) that was considered as suspect. No viral RNA was detected from nasal wash or BALF collections from any of the deer at 18 DPC. Infectious virus was not detected in different tissues from one sentinel animal (#50) or in the nasopharynx of one principal infected animal (#919; **Table 2.2**).

Histologic examination at 18 DPC of principal infected deer #106 and #919 (**Figure 2.4A-E**) showed minimal changes in the lungs, with scattered peribronchiolar/perivascular cuffs of lymphocytes and plasma cells (**Figure 2.4E**). Principal infected deer #919 showed evidence of chronic suppurative bronchopneumonia restricted to one lung lobe, but the overall histological changes suggest a possible underlying bacterial component (data not shown). Minimal mononuclear inflammation was noted in the trachea. Similarly, deer #106 had minimal changes in the trachea with rare mononuclear inflammatory aggregates within the lamina propria and extending into the lining respiratory epithelium (**Figure 2.4C**). No viral antigen was detected by IHC in any of the respiratory tissues of principal infected deer at 18 DPC (**Figure 2.4F-J**). The sentinel contact animals (#49 and #50; **Figure 2.4K-O**) showed predominantly histological alterations along the trachea, with mild to moderate lymphoplasmacytic and erosive tracheitis characterized by multifocal segments of epithelial attenuation, necrosis and loss with occasional areas of epithelial hyperplasia, intense lymphoplasmacytic and neutrophilic inflammation along the superficial lamina propria, and luminal necrotic cell debris (**Figure 2.4M**). While the changes in the lungs were mostly characterized by minimal peribronchiolar lymphocytic cuffing (**Figure 2.4O**), deer #49 had a localized area of subacute to chronic suppurative bronchopneumonia with evident intralesional bacteria, likely representing a secondary opportunistic infection. Moderate lymphoplasmacytic pharyngitis with occasional attenuation and loss of surface epithelium and

lymphoid follicle formation, and marked tonsillar lymphoid hyperplasia were also noted (data not shown). No other significant histologic alterations were identified in principal or sentinel animals, including their fetuses. Viral antigen was neither detected in the respiratory tract tissues (**Figure 2.4P-T**) nor in placenta nor fetal tissues derived from sentinel animals. A summary of the histological and immunohistochemical findings in the respiratory tract of SARS-CoV-2-infected white-tailed deer can be found in **Supplementary Table 2.2**.

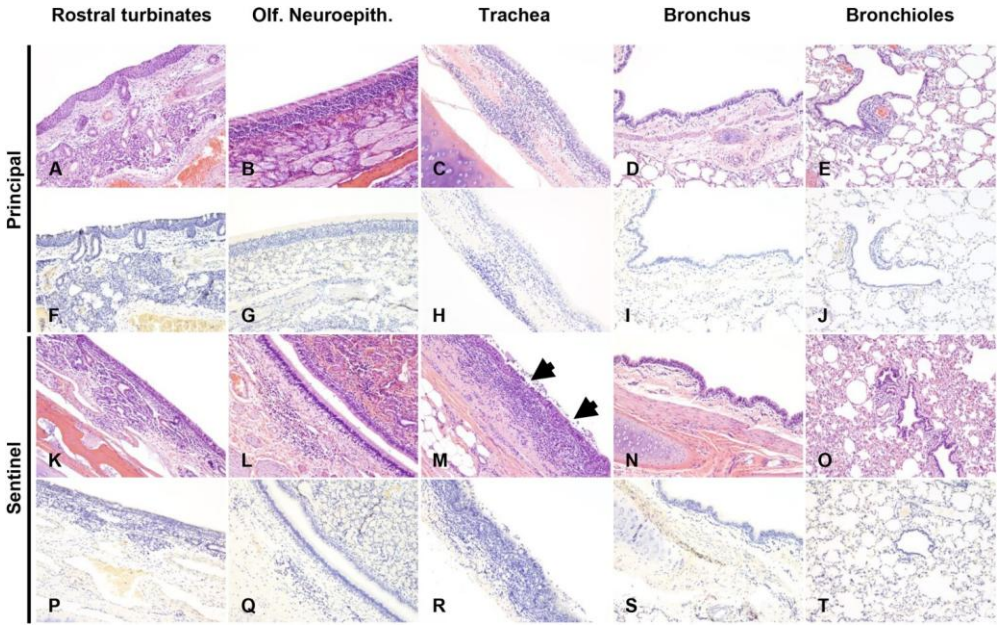

Figure 2.4 Histological lesions and SARS-CoV-2 antigen distribution in the upper and lower respiratory tract of principal infected and sentinel white-tailed deer at 18 DPC

Histological lesions and SARS-CoV-2 antigen distribution in the upper and lower respiratory tract of principal infected and sentinel white-tailed deer at 18 DPC. Rostral turbinates (A, F, K, P), olfactory neuroepithelium (B, G, L, Q), trachea (C, H, M, R), bronchus (D, I, N, S) and bronchioles (E, J, O, T). In principal infected deer, few lymphocytes were noted in the lamina propria of the rostral turbinates (A). The olfactory neuroepithelium was histologically unremarkable (B), and the tracheal and bronchial lamina propria were occasionally infiltrated by either dispersed or aggregates of mononuclear cells (C, D), which also encircled few bronchioles and pulmonary vessels (E). In sentinel deer, the lamina propria of rostral turbinates and sporadically subjacent to the olfactory neuroepithelium were infiltrated by mild numbers of lymphocytes and plasma cells (K, L). There was segmental erosive tracheitis with epithelial attenuation and necrosis, and intense lymphoplasmacytic and neutrophilic inflammation (M, arrows). Few mononuclear cells were noted delimiting bronchi, bronchioles and pulmonary vessels (N, O). No viral antigen was detected in respiratory tract tissues of principal infected (F–J) and sentinel (P–T) deer at 18 DPC. H&E and Fast Red, 100× total magnification.

Presence of SARS-CoV-2 RNA in non-respiratory organs and tissues during the acute and convalescent stage of infection

At 4 DPC, tissues collected from the two principal infected deer demonstrate a systemic presence of viral RNA (**Figure 2.2C**). Both deer had especially high levels of viral RNA detected in the tonsil. Lymph nodes from both animals, which included the cranial mediastinal, retropharyngeal, submandibular, tracheobronchial, prescapular, mesenteric, ileocecal, retroperitoneal, and gastrohepatic, were all positive for SARS-CoV-2 RNA at 4 DPC. Other tissues consisting of spleen, liver, heart, kidney, bone marrow, stomach, ileocecal junction and brain were also all positive for viral RNA in both animals at 4 DPC. Small and large intestine and olfactory bulb tissues were collected from the two principal infected deer at 4 DPC, and these tissues were RT-qPCR positive in one of the two animals whereas the other one was considered suspect. CSF obtained from deer #108 was also positive for SARS-CoV-2 RNA at 4 DPC.

At 18 DPC, SARS-CoV-2 RNA was detected at relatively high levels in the tonsil of both principal infected and one sentinel animal (**Figure 2.2D**). Several lymph nodes were also positive for viral RNA at 18 DPC, although fewer compared to 4 DPC, and included the mesenteric, ileocecal and retropharyngeal lymph nodes from principal infected deer, and the tracheobronchial, retropharyngeal and a suspect positive mesenteric lymph node from the sentinels. At 18 DPC, SARS-CoV-2 RNA was not detected in the liver, heart, stomach, brain or olfactory bulb. The spleen, kidney and large intestine of at least one principal infected deer, and the small intestine of one sentinel were suspect positive for viral RNA at 18 DPC. No viral RNA was detected in the CSF or urine from any deer at 18 DPC. In addition, no infectious virus was

isolated in samples collected from one principal infected (#919) and one sentinel (#50) at 18 DPC **(Table 2.2)**.

SARS-CoV-2-specific markers present in deer fetuses

Fetal tissues were collected from 5 pregnant deer consisting of 12 fetuses in total – one animal (#108) was not pregnant (**Table 2.2.1**). The uteri were removed *in toto* and the amniotic sac was left intact until all other tissues had been cleared from the table, the necropsy area cleaned, and new, sterile, instruments were used for the fetus dissection. The fetuses were approximately 2.5 months into gestation based on crown to rump measurements. Full tissue sample sets, consisting of spleen, liver, kidney, lungs, and placenta were collected when possible (from 6 out of the 12 fetuses). Two of the three fetuses from deer #905 collected at 4 DPC, had detectable amounts of SARS-CoV-2 RNA in at least one of the tissues collected: one fetus was RNA positive in the lungs, liver, spleen, and placenta while the other fetus had viral RNA detected only in the spleen (**Supplementary Table 2.2.1**). At 18 DPC, partial tissue sample sets were collected from the nine fetuses present in the four remaining pregnant deer (**Table 2.1**); they were all negative for SARS-CoV-2 RNA (**Supplementary Table 2.1**). The three fetuses from deer #106 were found mummified, two viable fetuses each were obtained from deer #919 and #49, whereas the remaining two fetuses analyzed at 18 DPC appeared to be non-viable. This indicates that more than 50% (5/9) of the fetuses collected on 18 DPC were non-viable based on gross and histological evidence of autolysis or tissue degradation in the absence of hemorrhage and/or inflammation. Only the uterus of deer #108 which was not pregnant was positive for SARS-CoV-2 RNA at 4 DPC. The two RNA-positive fetuses from doe #905 were negative for the presence of SARS-CoV-2 antigen by IHC, which is not surprising given the low levels of RNA present and the reduced sensitivity of IHC compared to RT-qPCR.

Serology

SARS-CoV-2-specific and neutralizing serum antibodies were evaluated for control, principal infected and sentinel deer (**Figure 5**). Some of the control sera which includes pre-challenge sera (-3 DPC) were weak positive in the ELISA for the SARS-CoV-2 nucleocapsid protein N. The principal infected animals and the sentinels remained weak positive over the 18-day course of the study (**Figure 5A**); only one principal infected deer developed substantial N-specific antibodies at 7, 14 and 18 DPC. Similarly, some of the control sera were weak positive in the ELISA for the SARS-CoV-2 RBD antigen. The two principal infected animals remaining after 4 DPC were clearly positive at 7 DPC with subsequent lower OD levels observed at 14 and 18 DPC, whereas the sentinel deer remained weak positive or even negative for RBD-specific antibodies over the 18-day course of the study (**Figure 5B**). The presence of virus neutralizing antibodies in the sera was tested in a classical virus neutralization assay. Some of the control sera had borderline levels of reactivity in the virus neutralization assay. However, at 7 DPC, significant levels of neutralizing antibody titers were observed in sera of principal infected deer, and similarly in the sera of sentinel deer at 10 DPC (**Figure 5C**). At 14 and 18 DPC, both the principal infected and sentinel deer had similar titers (approximately 1:1280) of neutralizing antibodies (**Figure 5C**). No significant differences in neutralizing antibody titers were observed between the two strains. Finally, sera from the principal infected and sentinel deer were tested for the presence of bovine coronavirus S-specific antibodies by an indirect ELISA. Although the OD value was slightly higher in some of the principal infected animals, all were at near negative bovine control sera levels (**Figure 5D**). No SARS-CoV-2 RNA was detected in any of the blood collections from animals over the course of the study.

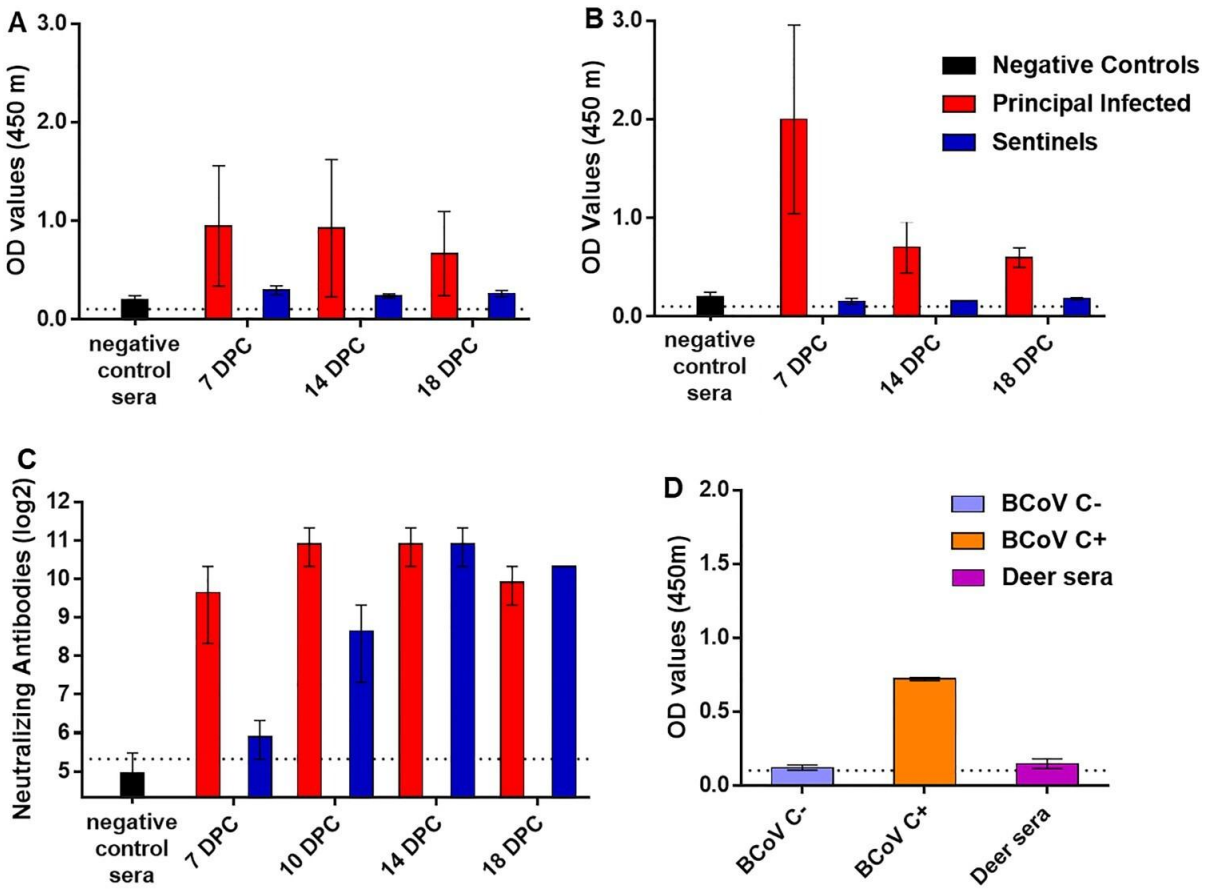

Figure 2.5 Serology of SARS-CoV-2 infected deer

Serology of SARS-CoV-2 infected deer. Detection of SARS-CoV-2 nucleocapsid protein (A), and the receptor binding domain (B) by indirect ELISA tests. The cut-off was determined by averaging the OD of negative serum + 3X the standard deviation as indicated by the dotted line. All samples with resulting OD values above this cut-off were considered positive. (C) Virus neutralizing antibodies detected in serum are shown as log2 of the reciprocal of the neutralization serum dilution. The cut-off of 1:40 is indicated by the dotted line. A–C: Negative controls were pooled deer sera ($n = 4$) collected from deer enrolled in a previous epizootic hemorrhagic disease virus vaccine study [Citation23] and pre-challenge sera (-3 DPC) from the six deer enrolled in this study. (D) Sera from principal infected ($n = 4$) and sentinel deer ($n = 2$) were tested against the bovine coronavirus (BCoV) spike protein using an indirect ELISA; both, positive (C+) and negative (C−) bovine control sera were included. The cut-off was determined by averaging the OD of negative serum + 3X the standard deviation as indicated by the dotted line. A-D: Mean with standard error are shown.

Competition between SARS-CoV-2 strains in co-infected white-tailed deer

To evaluate the *in vivo* competition between the ancestral lineage A (SARS-CoV-2/human/USA/WA1/2020) and the alpha VOC (SARS-CoV-2/human/USA/CA-5574/2020)

strains, cDNA products of SARS-CoV-2 RNA extracted from swabs and tissue homogenates were sequenced on the Illumina NextSeq platform. While the intent was to use a 1:1 titer ratio of the two strains, we were limited in our ability to obtain an exact 1:1 ratio since our only means to quantify virus was through virus titrations. Subsequently, sequencing analysis showed the inoculum used for infection was 60% alpha VOC B.1.1.7 and 40% lineage A WA1. Nasal swabs collected at 1 DPC revealed the proportion of lineage A strain ranged from 0.7-40.0% and of alpha VOC B.1.17 strain from 60.0-99.3% in the 4 principal infected deer **(Table 2.3, Supplementary Figure 5)**. In contrast, one of the oral swabs from a principal infected deer (#905) at 1 DPC showed 51.0% lineage A WA1 and 49.0% VOC B.1.1.7, while the other swab contained 5.4% lineage A and 94.6% VOC B.1.1.7. By 3 DPC, the composition of all nasal and most oral swabs was entirely alpha VOC B.1.1.7, with the exception of a 4 DPC oral swab collected from deer #905 that showed 2.9% lineage A and 97.1% VOC B.1.1.7. Swab and tissue samples collected from sentinel deer were also dominated by the alpha VOC B.1.1.7 strain. The B.1.1.7 strain was also dominant in tissues collected from the two primary challenged deer at 4 DPC, with the highest lineage A percentage (20.9%) found in the nasopharynx of deer #905 (**Table 2.3, Supplementary Figure 5**). Virus genome analysis was only possible in a few tissues collected from principal (nasopharynx and tonsil) and sentinel (retropharyngeal lymph node) deer at 18 DPC; the results revealed a > 95% presence of alpha VOC B.1.1.7 genomic sequences. These results indicate a competitive advantage of the alpha VOC B.1.1.7 isolate over the lineage A WA1 isolate.

Table 2.3 SARS-CoV-2 competition in deer co-infected with two strains determined by next generation sequencing

Sample	4 DPC				18 DPC							
	#108		#905		#106		#919		#49		#50	
	%WA1	%B.1.1.7	%WA1	%B.1.1.7	%WA1	%B.1.1.7	%WA1	%B.1.1.7	%WA1	%B.1.1.7	%WA1	%B.1.1.7
Nasal Swab 0 DPC	ND	ND	ND	ND	ND	ND	ND	ND	ND	ND	ND	ND
Nasal Swab 1 DPC	1.70	98.30	40	60	0.70	99.30	15.80	84.20	ND	ND	ND	ND
Nasal Swab 3 DPC	0	100.00	0	100.00	0	100.00	0	100.00	LMR	LMR	NT	NT
Nasal Swab 4 DPC	0	100.00	0	100.00	NT	NT	NT	NT	NT	NT	NT	NT
Nasal Swab 5 DPC	NT	NT	NT	NT	0	100.00	LMR	LMR	LMR	LMR	LMR	LMR
Nasal Swab 7 DPC	NT	NT	NT	NT	LMR	LMR	LMR	LMR	0	100.00	LMR	LMR
Nasal Swab 10 DPC	NT	NT	NT	NT	ND	ND	NT	NT	LMR	LMR	ND	ND
Oral Swab 0 DPC	ND	ND	ND	ND	ND	ND	ND	ND	ND	ND	ND	ND
Oral Swab 1 DPC	5.40	94.60	51	49	LMR	LMR	ND	ND	ND	ND	ND	ND
Oral Swab 3 DPC	0	100.00	ND	ND	0	100.00	ND	ND	LMR	LMR	ND	ND
Oral Swab 4 DPC	0	100.00	2.90	97.10	NT	NT	NT	NT	NT	NT	NT	NT
Oral Swab 5 DPC	NT	NT	NT	NT	0	100.00	ND	ND	ND	ND	0	100.00
Oral Swab 7 DPC	NT	NT	NT	NT	ND	ND	NT	NT	0	100.00	NT	NT
Oral Swab 10 DPC	NT	NT	NT	NT	ND	ND	ND	ND	ND	ND	ND	ND
Rectal Swab 0 DPC	ND	ND	ND	ND	ND	ND	ND	ND	ND	ND	ND	ND
Rectal Swab 1 DPC	ND	ND	ND	ND	ND	ND	ND	ND	ND	ND	LMR	LMR
Rectal Swab 3 DPC	ND	ND	ND	ND	ND	ND	ND	ND	ND	ND	ND	ND
Rectal Swab 4 DPC	ND	ND	ND	ND	NT	NT	NT	NT	NT	NT	NT	NT
Rectal Swab 5 DPC	NT	NT	NT	NT	NT	NT	NT	NT	NT	NT	ND	ND

Rectal Swab 7 DPC	NT	NT	NT	NT	ND	ND	NT	NT	ND	ND	ND	ND
Rectal Swab 10 DPC	NT	NT	NT	NT	ND	ND	ND	ND	ND	ND	ND	ND
Nasal Wash	0	100.00	ND	ND	ND	ND	ND	ND	ND	ND	ND	ND
BALF	0	100.00	1.30	98.70	ND	ND	ND	ND	ND	ND	ND	ND
Conchae	0	100.00	LMR	LMR	NT	NT	NT	NT	NT	NT	NT	NT
Ethnoturbinates	0	100.00	0	100.00	NT	NT	NT	NT	ND	ND	NT	NT
Nasopharynx	3.90	96.10	20.90	79.10	4.10	95.90	13.80	86.20	NT	NT	LMR	LMR
Trachea, rostal	0	100.00	0	100.00	NT	NT	ND	ND	NT	NT	ND	ND
Trachea, middle	0	100.00	NT	NT	NT	NT	NT	NT	NT	NT	ND	ND
Trachea, distal	0	100.00	0	100.00	NT	NT	ND	ND	NT	NT	ND	ND
Bronchi	0	100.00	0	100.00	NT	NT	ND	ND	ND	ND	ND	ND
Lung, left cranial A	0	100.00	0	100.00	ND	ND	ND	ND	ND	ND	ND	ND
Lung, left cranial B	NT	NT	NT	NT	ND	ND	ND	ND	ND	ND	ND	ND
Lung, left caudal	NT	NT	NT	NT	ND	ND	ND	ND	ND	ND	ND	ND
Lung, right cranial	0	100.00	0	100.00	ND	ND	NT	NT	ND	ND	ND	ND
Lung, right caudal	0	100.00	0	100.00	ND	ND	ND	ND	ND	ND	ND	ND
Lung, right middle	NT	NT	NT	NT	ND	ND	ND	ND	ND	ND	ND	ND
Accessory	0	100.00	0	100.00	ND	ND	ND	ND	ND	ND	ND	ND
Tonsil	0	100.00	LMR	LMR	1.20	98.80	NT	NT	ND	ND	LMR	LMR
Prescapular LN	NT	NT	ND	ND	ND	ND	ND	ND	ND	ND	NT	NT
Tracheobronchial LN	0	100.00	LMR	LMR	ND	ND	ND	ND	ND	ND	NT	NT
Cranial mediastinal LN	NT	NT	NT	NT	ND	ND	ND	ND	ND	ND	ND	ND
Mesenteric LN	1	99	NT	NT	NT	NT	NT	NT	NT	NT	ND	ND
Ileocecal LN	NT	NT	NT	NT	NT	NT	ND	ND	ND	ND	ND	ND

Retropertioneal LN	NT	NT	0.90	99.10	ND	ND	ND	ND	ND	ND	ND	ND
Gastrohepatic LN	NT	NT	NT	NT	ND	ND	ND	ND	ND	ND	ND	ND
Submandibular LN	NT	NT	LMR	LMR	ND	ND	ND	ND	ND	ND	ND	ND
Retropharyengeal LN	0.20	99.80	NT	NT	NT	NT	ND	ND	0.30	99.70	LMR	LMR
Spleen	0	100.00	LMR	LMR	ND	ND	NT	NT	ND	ND	ND	ND
Liver	NT	NT	NT	NT	ND	ND	ND	ND	ND	ND	ND	ND
Heart	0	100.00	0	100.00	ND	ND	ND	ND	ND	ND	ND	ND
Kidney	3.50	96.50	0	100.00	ND	ND	NT	NT	ND	ND	ND	ND
Bone Marrow	NT	NT	ND	ND	ND	ND	ND	ND	ND	ND	NT	NT
Stomach	ND	ND	NT	NT	ND	ND	ND	ND	ND	ND	ND	ND
Small Intestine	NT	NT	LMR	LMR	ND	ND	ND	ND	NT	NT	ND	ND
Large Intestine	0	100.00	NT	NT	NT	NT	ND	ND	ND	ND	ND	ND
Ileocecal Junction	NT	NT	NT	NT	ND	ND	ND	ND	ND	ND	ND	ND
Brain	2.90	97.10	LMR	LMR	ND	ND	ND	ND	ND	ND	ND	ND
Olfactory Bulb	NT	NT	NT	NT	ND	ND	ND	ND	ND	ND	ND	ND

WA1 = USA-WA1/2020 lineage A strain; B.1.1.7 = USA/CA-5574/2020 strain alpha VOC; LN = lymph node; NT = not tested; ND = not detected; LMR = low mapped reads #106, 108, 905 and 919: principal infected animals; #49 and 50: sentinel animals.

Discussion

Zoonotic diseases reportedly account for approximately 60% of emerging infectious disease (EID) events over the last century (2). Increased interaction with wild animal populations is a critical factor associated with increased occurrence of zoonotic EIDs. In the last twenty years, three virus species from the genus *Betacoronavirus*, family *Coronaviridae,* have spilled over from wild animal populations into humans, resulting in outbreaks of respiratory disease and global economic losses (5, 9, 14). The emergence, global dissemination, and rapid evolution of SARS-CoV-2 has had global impacts on public health and economic stability. The emergence of variant strains, in part due to the exceptional spread of the virus and secondary zoonotic transmissions, has caused additional waves of SARS-CoV-2 infection and re-infection, highlighting the need for enhanced mitigation strategies (128, 141, 148-150). To design more comprehensive surveillance efforts, it is necessary to identify susceptible animal hosts which may contribute as secondary reservoirs to the continued animal-animal and animal-human transmission of SARS-CoV-2 (14, 16). Maintenance of SARS-CoV-2 in wild animal populations would create additional challenges in surveillance and control of this virus. Human interaction with infected wild animal populations could provide avenues for un-checked spillover back into human populations and spontaneous resurgence of SARS-CoV-2 infections with new animal-adapted SARS-CoV-2 variants, as already experienced with mink (128).

White-tailed deer (*Odocoileus virginianus*) are the second most abundant, densely populated, and geographically widespread wild ruminant species in the United States. Furthermore, commercially farmed deer is a growing industry in the US. Human interaction with white-tailed deer have resulted in the occurrence of infectious diseases such as brucellosis or tuberculosis in human populations in the past (151). Recently, white-tailed deer fawns were

demonstrated to be susceptible to experimental SARS-CoV-2 infection (142). Also, it was recently reported that sero-surveillance studies conducted in 2021 show that 40% of wild white-tailed deer tested across the midwestern US were positive for SARS-CoV-2 neutralizing antibodies (143). Although it is unclear at this time if these results are caused by SARS-CoV-2 exposure or cross-reactivity of a yet unidentified closely related coronavirus infection in deer (143). Surprisingly, antibodies were detected in one sample as early as 2019, and several from January to March of 2020 in that survey, but not in sera collected in years prior to 2019 (143). In the present study, we investigated the susceptibility of approximately 2-year-old, adult white-tailed deer to SARS-CoV-2 infection and the potential for direct transmission to naïve contact sentinel deer. Furthermore, our data is the first to date to provide evidence of vertical transmission of SARS-CoV-2 from mother to fetus. In addition, this study examined the competition of two SARS-CoV-2 isolates, representatives of the ancestral lineage A (SARS-CoV-2/human/USA/WA1/2020; lineage A WA1) and the alpha VOC B.1.1.7 (SARS-CoV-2/human/USA/CA-5574/2020; VOC B.1.1.7) by co-infection of white-tailed deer. We also demonstrated *in vitro* virus replication in primary lung cells derived from white-tailed deer, mule deer and elk, which suggests that besides white-tailed deer, mule deer may also be susceptible to SARS-CoV-2. Elk primary lung cells were refractory to SARS-CoV-2 infection with the lineage A WA1 strain.

The recently published study by Palmer and coworkers (142) showed infection and transmission of the SARS-CoV-2 tiger isolate TGR/NY/20 at a dose of $5 \times 10^{6.3}$ $TCID_{50}$ in 6-week-old fawns, with prolonged viral RNA shedding detected in nasal swabs over the course of the 21-day study. Here, we used a lower infectious dose (1×10^{6} $TCID_{50}$) in 2-year-old adult deer. Our data indicate that adult deer shed SARS-CoV-2 virus and RNA for a lesser period of

time, which could be due to difference in challenge dose, differences in virus isolates, route of administration (IN and PO vs. IN only) or the effects of a more rapid immune response in adult deer. Both studies show lower levels of intermittent virus/RNA shedding detected from oral and rectal swabs through 7 DPC, compared to nasal swabs which were RNA positive for all animals up to 10 DPC in our study. Similarly, as described by Palmer and coworkers (142) in fawns, we observed efficient transmission of virus to co-housed naïve adult deer, as demonstrated by isolation of SARS-CoV-2 virus from contact sentinels on days 4- and 6-days post comingling (i.e., 5 and 7 DPC) as well as consistent viral RNA detection in swabs and tissues. While our results show that transmission could occur after co-mingling naïve deer with infected deer, further studies are needed to address specifically aerosol versus direct versus indirect/environmental routes of transmission.

In the present study, high copy numbers of viral RNA were detected in many clinical samples and tissues derived from the principal infected and sentinel deer, however virus isolation was infrequent. SARS-CoV-2 RNA can be trafficked through many tissues in infected individuals, presumably through the lymphatic system via monocytes/macrophages and dendritic cells. Organs such as lymph nodes might be a "sink" for viral RNA or virus infected cells, but not necessarily sites of active SARS-CoV-2 replication. Additionally, the quantification of our CN/mL could be overestimated given it is based on a DNA plasmid which contains the N gene segment which has higher replication efficiency (since it skips the RT step) than an RNA (IVT RNA) standard. Furthermore, infection with the alpha VOC B.1.1.7 has been associated with an abundant production of the nucleocapsid N protein, creating prominent levels of N-specific mRNA which could explain why an N-gene targeting RT-qPCR assay (CDC N2 RT-qPCR assay) might over-estimate viable virus quantities (152, 153). Weak reactivity was observed with

some of the pre-challenged deer sera by our *in-house* SARS-CoV-2 N and RBD ELISAs, as well as using an ELISA specific for the bovine coronavirus S protein. Using our in-house ELISA test, antibody titers against the RDB of the spike protein decreased over time. The RBD ELISA was developed for the detection of the WA1/2020 isolate. Since the alpha VOC isolate has mutations in the RBD region, the ELISA could have reduced sensitivity against it. This could explain why antibody titers against the RBD are higher at the beginning of the study, when the ancestral WA1/2020 isolate was present and decreases later in the infection when the alpha B.1.1.7. variant was prevalent. Also, some of the deer in our study had borderline levels of SARS-CoV-2 neutralizing antibodies present at pre-challenge. Since these were low levels of antibodies, and all the deer in this study were highly susceptible to SARS-CoV-2 infection, we consider it unlikely that the animals were previously infected with SARS-CoV-2. Nevertheless, we cannot exclude the possibility that the deer were exposed to an unknown deer *Betacoronavirus* with some level of antigenic cross reactivity to SARS-CoV-2, since deer coronaviruses similar to bovine coronaviruses have been previously described (154); further investigation would be required to ascertain whether this is the case.

Tissues which were collected *postmortem* at 4 DPC and 18 DPC demonstrate widespread distribution of SARS-CoV-2 RNA in the upper respiratory and lymphatic tissues. To evaluate the acute stage of infection, two deer - one pregnant, one not pregnant - were sacrificed at 4 DPC. There was a pronounced difference of viral RNA load (copy number [CN]/mg) in respiratory tissues between these two deer, which may represent different levels of susceptibility between pregnant (low viral loads) and non-pregnant (high viral loads) animals.

Histological evaluations in the upper and lower respiratory tract tissues collected at 4 DPC revealed pathological changes described as rhinitis, marked attenuation of the respiratory

epithelium of the trachea, bronchitis, and in some cases bronchiolitis. No interstitial pneumonia was observed. IHC analyses for the presence of SARS-CoV-2 antigen in the respiratory tract at 4 DPC revealed that viral antigen was not detected in the nasal passages, but in the trachea, the bronchi and occasionally in terminal bronchioles. It is suspected that the detection of antigen in only one (#108) of two animals may be due to genetic differences between the respective deer or a susceptibility characteristic of pregnant (#905) versus non-pregnant (#108) deer. In contrast, the histologic examination of principal infected deer euthanized at 18 DPC showed minimal changes in the lungs with no viral antigen detected along the respiratory tract; in the case of sentinel animals, no viral antigen was associated with the histological changes present in the trachea. These findings are not unexpected since none of the deer had obvious clinical signs of disease. As shown previously, cats experimentally infected with SARS-CoV-2 displayed mild to moderate histopathological changes (rhinitis, tracheal and bronchial adenitis) accompanied by viral RNA and antigen at 4 and 7 DPC. However, by 21 DPC histological changes were unremarkable and no detectable viral RNA or antigen was observed (43, 95).

Sequence analysis preformed on the NextSeq Illumina platform revealed a competitive advantage of the alpha VOC B.1.1.7 (SARS-CoV-2/human/USA/CA-5574/2020) isolate over the lineage A WA1 (SARS-CoV-2/human/USA/WA1/2020) isolate. This data confirms what others have recently reported *in vivo* in ferrets, hamsters, and transgenic ACE2 mice models (141, 155). It is suggested that a component of this competitive advantage is associated with an Aspto Gly substitution at amino acid position 614 (D614G), which alters the interaction of the spike (S) glycoprotein with the hACE2 receptor (156, 157). The D614G substitution has been shown to enhance the affinity of S to bind hACE2 when compared to the parental D614 strain (141). Moreover, the N501Y substitution and perhaps even some other S substitutions, might further

increase affinity for the ACE2 receptor (13, 158). Additionally, recent data suggests that infection with B.1.1.7 antagonizes innate immunity early in infection by upregulating gene segments which effectively decrease host IFNβ expression and secretion (152). This allows for un-interrupted viral replication until subsequent changes in transcriptional regulation of SARS-CoV-2 reverse this effect, inducing an inflammatory response which leads to the presentation of typical clinical symptoms and at the same time promotes virus transmission. This sequence of events may partially explain why alpha VOC B.1.1.7 demonstrates higher replication and transmission efficiency than lineage A (152).

Animal coronaviruses are not commonly associated with reproductive problems, except avian coronaviruses (159, 160). A feline alphacoronavirus which is responsible for feline infectious peritonitis, can be transmitted vertically with major consequences on post-partum kittens resulting in a mortality up to 100% following birth of infected kittens (161). In the present study, we identified SARS-CoV-2 genetic markers in two fetuses of one principal infected deer euthanized at 4 DPC as evidenced by viral RNA detected from multiple fetal tissues. Interestingly, we only detected viral RNA in the uterus of the deer which was not pregnant, but also had higher viral RNA levels detected systemically in tissues compared to the pregnant doe necropsied at the same time point 4 DPC. We did not detect viral RNA in fetal tissues derived from nine fetuses of does necropsied at 18 DPC, and more than 50% (5/9) of the fetuses collected at this time point were found to be unviable. However, it is difficult to draw conclusively the full effects of SARS-CoV-2 infection in pregnant deer given the small number of animals, the short duration of this study and the absence of control pregnant non-infected animals.

It is well known that pregnancy can increase the risk of illness caused by viral infections like influenza as well as enhance complications due to other underlying medical conditions such as diabetes. The effects of SARS-CoV-2 infection on pregnant women, the pregnancy, the fetus, and *postpartum* are still not fully understood. Several retrospective studies have shown pregnancy to be associated with higher risk of severe illness caused by COVID-19 as well as increased admissions to intensive care and neonatal units; also increased numbers of preterm births (under 37 weeks) have been observed during the course of the pandemic (162-166). Still births and neonatal death appear to be relatively low for mothers independent whether they are infected or not with SARS-CoV-2 (163). Importantly, in utero SARS-CoV-2 vertical transmission from mother to fetus, while rare, seems possible (167, 168).

Recent large-scale SARS-CoV-2 surveillance efforts in animal and humans have found evidence of reverse-zoonosis (human-animal) resulting in natural infections in companion animals, farmed mink, primates and large cat species in several countries. The source of infection in these incidences are likely infected pet-owners and animal care workers on farms and at zoos. Additionally, SARS-CoV-2 has demonstrated its ability to rapidly mutate and cross back into human populations, giving rise to new variants of interest or concern (128, 169). International and government organizations like WHO and the CDC continue to state that the chance of transmission of SARS-CoV-2 from animals to humans remains low. While interactions between deer and humans may be rather limited, processing of infected game or carcasses could pose a potential risk. Furthermore, certain circumstances where known susceptible animal species frequently interact with humans should be monitored. These situations exemplify the critical need to evaluate potential host species for SARS-CoV-2 which may act as reservoirs for future, secondary zoonotic events. Furthermore, this work demonstrates the need

for more intensive, focused surveillance efforts on high-risk animal populations, as well as farm, wildlife and zoo workers, in order to identify new animal derived SARS-CoV-2 variants which may evade current mitigation strategies.

Acknowledgments:

We thank the staff of KSU Biosecurity Research Institute, the histology laboratory at the Kansas State Veterinary Diagnostic Laboratory (KSVDL), members of the Histology and Immunohistochemistry sections at the Louisiana Animal Disease Diagnostic Laboratory (LADDL), the Comparative Medicine Group staff at Kansas State University and technical support from Emily Gilbert-Esparza, Yonghai Li, and Jingwen Peng of KSU, and Dane Jasperson and Jeana Owens from USDA. The SARS-CoV-2 strains USA/CA-5574/2020 and USA/WA1/2020 were obtained through BEI Resources (catalog # NR-52281 and #54011). We also thank Dr. Kyeong-Ok Chang for the Vero E6/TMPRSS2 cells used in these studies.

Disclosure statement

Mention of trade names or commercial products in this publication is solely for the purpose of providing specific information and does not imply recommendation or endorsement by the U.S. Department of Agriculture. USDA is an equal opportunity provider and employer. The J.A.R laboratory received support from Tonix Pharmaceuticals, Xing Technologies and Zoetis, outside of the reported work. J.A.R. is inventor on patents and patent applications on the use of antivirals and vaccines for the treatment and prevention of virus infections, owned by Kansas State University, KS, or the Icahn School of Medicine at Mount Sinai, New York. The A.G.-S. laboratory has received research support from Pfizer, Senhwa Biosciences, Kenall Manufacturing, Avimex, Johnson & Johnson, Dynavax, 7Hills Pharma, Pharmamar, ImmunityBio, Accurius, Nanocomposix, Hexamer, N-fold LLC, and Merck, outside of the

reported work. A.G.-S. has consulting agreements for the following companies involving cash and/or stock: Vivaldi Biosciences, Contrafect, 7Hills Pharma, Avimex, Vaxalto, Pagoda, Accurius, Esperovax, Farmak, Applied Biological Laboratories and Pfizer, outside of the reported work. A.G.-S. is inventor on patents and patent applications on the use of antivirals and vaccines for the treatment and prevention of virus infections, owned by the Icahn School of Medicine at Mount Sinai, New York.

Funding

Funding for this study was partially provided through grants from the National Bio and Agro-Defense Facility (NBAF) Transition Fund from the State of Kansas (JAR), the AMP Core of the Center of Emerging and Zoonotic Infectious Diseases (CEZID) from National Institute of General Medical Sciences (NIGMS) under award number P20GM130448 (JAR, IM), the NIAID Centers of Excellence for Influenza Research and Surveillance under contract number HHSN 272201400006C (JAR), the United States Department of Agriculture (USDA)-NIFA (A1711 Program) under award number 2020-67015-33157, the German Federal Ministry of Health (BMG) COVID-19 Research and development funding to WHO R&D Blueprint (JAR), the NIAID supported Center of Excellence for Influenza Research and Response (CEIRR, contract number 75N93021C00016 to JAR), and the USDA Animal Plant Health Inspection Service's National Bio- and Agro-defense Facility Scientist Training Program (KC, CM). This study was also partially supported by the Louisiana State University, School of Veterinary Medicine start-up fund under award number PG 002165 (UBRB), the USDA-Agricultural Research Service (WCW), by the Center for Research for Influenza Pathogenesis (CRIP), a NIAID supported Center of Excellence for Influenza Research and Surveillance (CEIRS, contract # HHSN272201400008C to AG-S), and the Center for Research for Influenza Pathogenesis and

Transmission (CRIPT), a NIAID supported Center of Excellence for Influenza Research and Response (CEIRR, contract # 75N93019R00028 to AG-S), and by the generous support of the JPB Foundation, the Open Philanthropy Project (research grant 2020-215611 [5384]) and anonymous donors to AG-S.

Supplemental Material

Supplemental data for this article can be accessed https://doi.org/10.1080/22221751.2021.2012528

Chapter 3 - Susceptibility of sheep to experimental co-infection with the ancestral lineage of SARS-CoV-2 and its alpha variant[4]

Abstract

Severe acute respiratory syndrome coronavirus 2 (SARS-CoV-2) is responsible for a global pandemic that has had significant impacts on human health and economies worldwide. SARS-CoV-2 is highly transmissible and the cause of coronavirus disease 2019 in humans. A wide range of animal species have also been shown to be susceptible to SARS-CoV-2 by experimental and/or natural infections. Sheep are a commonly farmed domestic ruminant that have not been thoroughly investigated for their susceptibility to SARS-CoV-2. Therefore, we performed *in vitro* and *in vivo* studies which consisted of infection of ruminant-derived cells and experimental challenge of sheep to investigate their susceptibility to SARS-CoV-2. Our results showed that sheep-derived kidney cells support SARS-CoV-2 replication. Furthermore, experimental challenge of sheep demonstrated limited infection with viral RNA shed in nasal and oral swabs at 1-day post challenge (DPC); viral RNA was also detected in the respiratory tract and lymphoid tissues at 4 and 8 DPC. Sero-reactivity was observed in some of the principal infected sheep but not the contact sentinels, indicating that transmission to co-mingled naïve sheep was not highly efficient; however, viral RNA was detected in some of the respiratory tract tissues of sentinel animals at 21 DPC. Furthermore, we used challenge inoculum consisting of a

[4] Reprinted with permission from "Susceptibility of sheep to experimental co-infection with the ancestral lineage of SARS-CoV-2 and its alpha variant" by Gaudreault, N. N., Cool, K., et al. 2022. *Emerging Microbes & Infections*, *11*(1), 662–675. https://doi.org/10.1080/22221751.2022.2037397

mixture of two SARS-CoV-2 isolates, representatives of the ancestral lineage A and the B.1.1.7-like alpha variant of concern, to study competition of the two virus strains. Our results indicate that sheep show low susceptibility to SARS-CoV-2 infection, and that the alpha variant outcompeted the lineage A strain

Introduction

Severe acute respiratory syndrome coronavirus 2 (SARS-CoV-2) continues to significantly impact human health and the economies of countries around the world. Since its identification in December 2019, the virus has rapidly spread and evolved resulting in the emergence of multiple variants. Several variants of concern (VOCs) have been shown to be more infectious/transmissible in humans and at the same time reduce the efficacy of currently available vaccines (96, 97, 170). Furthermore, SARS-CoV-2 is a zoonotic virus with a wide-range of susceptible animal species which could serve as secondary reservoirs to perpetuate viral evolution and produce novel variants (15, 64, 128). As of 31 October 2021, the OIE reports that more than 598 natural infections have been identified in 14 different animal species including companion animals such as: cats and dogs; zoo animals including large cats, otter and gorillas; and farmed or wild animals, including mink and white-tailed deer (www.oie.int); (14). Experimental infections have demonstrated non-human primates, hamsters, ferrets, cats, and deer to be readily susceptible species, while dogs, pigs and cattle appear to have limited susceptibility, and avian species such as chickens and ducks are resistant to infection (129, 132, 137-140, 142, 171-173). Rabbits, raccoon dogs, fruit bats, several wild mice species, and skunks have also been shown to be susceptible after experimental infection with SARS-CoV-2 (25, 139, 174, 175). Mice are not susceptible to the ancestral lineage A strains but to the alpha, beta and gamma VOCs with the 501Y mutation in the Spike protein (176, 177).

Transmission of SARS-CoV-2 occurs via respiratory droplets/aerosols and direct contact with infected individuals or indirect via contaminated fomites. Host factors which contribute to transmission include duration of infection, intensity of shedding, and host behavior and population density. Interactions regularly occur between infected humans and animals, infected animals with other animals, and their environments, complicating the epidemiology of SARS-CoV-2. Natural SARS-CoV-2 infection in farmed mink has demonstrated the significant economic and public health repercussions that can result when variants emerge from an animal reservoir (128, 178). Cross-species maintenance of SARS-CoV-2 makes control of the virus exponentially more complicated. Identification of susceptible hosts and respective biosurveillance is critical to mitigate future secondary zoonotic events. Furthermore, the absence or limited manifestation of clinical symptoms presented by some of the highly susceptible species, such as cats, ferrets or wild-tailed deer, likely contributes to many unnoticed and underreported zoonotic and reverse-zoonotic events.

Sheep are economically important domestic ruminants, commonly farmed worldwide. Sheep are often maintained in large flocks, and frequently interact with humans during standard farming activities, sheering, milking, slaughter for meat, at petting-zoos; sheep also potentially have contact with other susceptible animal species such as mice, cats and deer. However, to date there has been very limited data on the susceptibility of sheep to SARS-CoV-2. An *in silico* study modeling the interactions between species-specific ACE2 receptors and the SARS-CoV-2 spike protein (27) indicates that sheep are potentially susceptible to SARS-CoV-2. In agreement with that study, replication of SARS-CoV-2 in sheep-derived respiratory tissues was demonstrated in an *ex vivo* infection study (28). A recent *in vivo* study with experimentally infected sheep (n=4) found no virus nor viral RNA in swabs or tissues, but some sheep did

develop low neutralizing antibodies suggesting possible limited infection (41). However, a limited serological survey of sheep in close contact with humans pre- and post-pandemic at a veterinary campus in Spain discovered no detectable SARS-CoV-2 antibodies, suggesting sheep might not be readily susceptible (179).

In this study, we investigated the susceptibility of sheep (*Ovis aries*) both *in vitro* and *in vivo* to SARS-CoV-2. First, ruminant-derived cell cultures were infected and viral growth kinetics determined. Secondly, we challenged eight sheep and studied virus transmission by co-mingling two naïve sentinel sheep at 1-day post challenge (DPC). *Postmortem* evaluations and tissues collections were performed at 4, 8 and 21 DPC to determine SARS-CoV-2 infection and disease progression. Clinical (swabs) and serological samples were collected over the course of the study to monitor viral shedding and seroconversion, respectively. In addition, sheep were inoculated with a mixture of two SARS-CoV-2 strains, representatives of the ancestral lineage A strain and the B.1.1.7-like alpha variant of concern (VOC) to study the competition of the two viruses. The results of this study are important for understanding the role of sheep in the ecology of SARS-CoV-2.

Materials and methods

Cells and virus isolation/titrations

Vero E6 cells (ATCC; Manassas, VA) and Vero E6 cells stably expressing transmembrane serine protease 2 (Vero-E6/TMPRSS2) (144) were obtained from Creative Biogene (Shirley, NY) via Kyeong-Ok Chang at KSU and used for virus propagation and titration. Cells were cultured in Dulbecco's Modified Eagle's Medium (DMEM, Corning, New York, N.Y, USA), supplemented with 10% fetal bovine serum (FBS, R&D Systems, Minneapolis, MN, USA) and antibiotics/antimycotics (ThermoFisher Scientific, Waltham, MA,

USA), and maintained at 37 °C under a 5% CO_2 atmosphere. The addition of the selection antibiotic, G418, to cell culture medium was used to maintain TMPRSS2 expression but was not used during virus cultivation or assays. The SARS-CoV-2/human/USA/WA1/2020 lineage A (referred to as lineage A WA1; BEI item #: NR-52281) and SARS-CoV-2/human/USA/CA_CDC_5574/2020 lineage B.1.1.7 (alpha VOC B.1.1.7; NR-54011) strains were acquired from BEI Resources (Manassas, VA, USA). A passage 2 plaque-purified stock of lineage A WA1 and a passage 1 of the alpha VOC B.1.1.7 stock were used for this study. Virus stocks were sequenced by next generation sequencing (NGS) using the Illumina MiSeq and the consensus sequences were found to be homologous to the original strains obtained from BEI (GISAID accession numbers: EPI_ISL_404895 (WA-CDC-WA1/2020) and EPI_ISL_751801 (CA_CDC_5574/2020).

To determine infectious virus titers of virus stocks and study samples, 10-fold serial dilutions were performed on Vero-E6/TMPRSS2 cells. The presence of cytopathic effects (CPE) after 96 hours incubation at 37 °C was used to calculate the 50% tissue culture infective dose ($TCID_{50}$)/ml using the Spearman-Kaerber method (145). Virus isolation attempts were only performed on samples with $\geq 10^3$ RNA copy number per mL, as this was our approximate limit of detection (LOD) for viable virus using this method. Virus isolation was performed by culturing 100 µl of filtered (0.2 µm; MidSci, St. Louis, MO) sample /well in duplicate on Vero E6/TMPRRS2 cells and monitoring for CPE for up to 5 days post inoculation.

Susceptibility of ovine and bovine cells to SARS-CoV-2

The SARS-CoV-2 USA-WA1/2020 strain was passaged 3 times in Vero-E6 cells to establish a stock virus for infection experiments. Primary ovine kidney and American pronghorn lung cells (provided by USDA ARS-ABADRU), and bovine fetal fibroblast, Madin-Darby ovine

kidney and Madin-Darby bovine cell lines (ATCC; Manassas, VA) were infected at approximately 0.1 multiplicity of infection (MOI). Infected cell supernatants were collected at 0, 2, 4, 6 or 8 days post infection (DPI) and stored at -80ºC until further analysis. Cell lines were tested in at least two independent infection experiments. Cell supernatants were titrated on Vero E6 cells to determine SARS-CoV-2 replication kinetics by virus titers ($TCID_{50}$/mL).

Ethics statement

All animal studies and experiments were approved and performed under the Kansas State University (KSU) Institutional Biosafety Committee (IBC, Protocol #1460) and the Institutional Animal Care and Use Committee (IACUC, Protocol #4508.2) in compliance with the Animal Welfare Act. All animal and laboratory work were performed in biosafety level-3+ and −3Ag laboratories and facilities in the Biosecurity Research Institute at KSU in Manhattan, KS, USA.

Virus challenge of animals

Ten male sheep, approximately 6 months of age, were acquired from Frisco Farms (Ewing, IL) and acclimated for ten days in BSL-3Ag biocontainment with feed and water *ad libitum* prior to experimental procedures. On day of challenge, eight principal infected sheep were inoculated with a 1:10 titer ratio of lineage A WA1 and the alpha VOC B.1.1.7 strains (**Figure 3.1**). A 2 ml dose of $1x10^6$ $TCID_{50}$ per animal was administered through intra-nasal (IN) and oral (PO) routes simultaneously. The remaining two non-infected sheep were separated and held in a dedicated clean room. At 1 day-post-challenge (DPC), the two naïve sheep were co-mingled with the principal infected animals as contact sentinels for the duration of the study. A subset of the principal infected sheep were euthanized and *postmortem* examination was performed at 4 (n=3) and 8 (n=3) DPC. *Postmortem* examination of the remaining two principal infected and two sentinel sheep was performed at 21 DPC (**Table 3.1**).

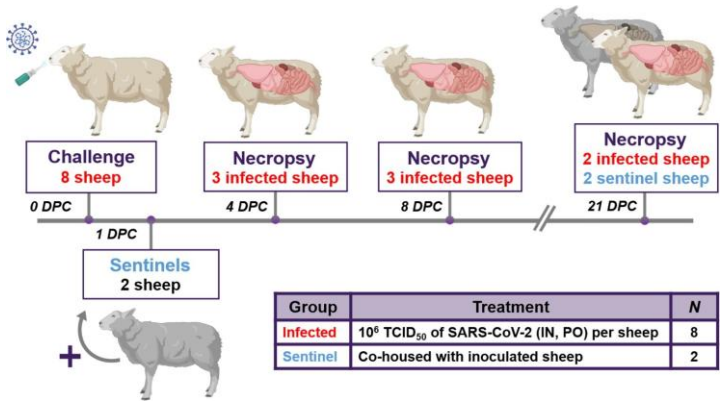

Figure 3.1 Experimental Design

Note: Eight sheep were inoculated with a mixture of SARS-CoV-2/human/USA/WA1/2020 lineage A (referred to as lineage A WA1; BEI item #: NR-52281) and SARS-CoV-2/human/USA/CA_CDC_5574/2020 lineage B.1.1.7 (alpha VOC B.1.1.7; BEI item #: NR-54011) acquired from BEI Resources (Manassas, VA, USA). A 2 mL dose of 1×10^6 $TCID_{50}$ per animal was administered IN and PO. At 1-day post challenge (DPC), two sentinel sheep were co-mingled with the eight principal infected animals to study virus transmission. Daily clinical observations and body temperatures were performed. Nasal/oropharyngeal/rectal swabs, blood/serum and faeces were collected at 0, 1, 3, 5, 7, 10, 14 17 and 21 DPC. Postmortem examinations were performed at 4 (3 principal), 8 (3 principal) and 21 DPC (2 principal + 2 sentinels). BioRender.com was used to create figure illustrations.

Table 3.1 Animal treatment assignment.

Treatment	Necropsy	Sheep ID#
Principal infected	4 DPC	712
		713
		714
	8 DPC	715
		716
		717
	21 DPC	718
		719
1 DPC contact sentinel	21 DPC	710
		711

DPC = days post challenge.

Clinical evaluations and sample collection

Sheep were observed daily for clinical signs. Clinical observations focused on activity level (response to human observer), neurological signs, respiratory rate, and presence of

gastrointestinal distress. Rectal temperature, nasal, oropharyngeal, and rectal swabs were collected from animals at 0, 1, 3, 5, 7, 10, 14, 17 and 21 DPC. Swabs were placed in 2mL of viral transport medium (DMEM, Corning; combined with 1% antibiotic-antimycotic, ThermoFisher), vortexed, and aliquoted directly into cryovials and RNA stabilization/lysis Buffer RLT (Qiagen, Germantown, MD, USA). EDTA blood and serum were collected prior to challenge and on days 3, 7, 10, 14, 17, and 21 DPC. Full *postmortem* examinations were performed, and gross changes recorded. A comprehensive set of tissues were collected in either 10% neutral-buffered formalin (Fisher Scientific, Waltham, MA, USA), or as fresh tissues directly stored at -80°C. Tissues were collected from the upper respiratory tract (URT) and lower respiratory tract (LRT), central nervous system (brain and cerebral spinal fluid [CSF]), gastrointestinal tract (GIT) as well as accessory organs. The lungs were removed *in toto* including the trachea, and the main bronchi were collected at the level of the bifurcation and at the entry point into the lung lobe. Lung lobes were evaluated based on gross pathology and collected and sampled separately. Nasal wash and bronchoalveolar lavage fluid (BALF) were also collected during *postmortem* examination. Fresh frozen tissue homogenates were prepared as described previously (43). All clinical samples (swabs, nasal washes, BALF, CSF) and tissue homogenates were stored at -80°C until further analysis.

RNA extraction and reverse transcription quantitative PCR (RT-qPCR)

SARS-CoV-2 specific RNA was detected and quantified using a quantitative reverse transcription real time – PCR (RT-qPCR) assay specific for the N2 segment as previously described (43). Briefly, nucleic acid extractions were performed by combining equal amounts of Lysis Buffer RLT (Qiagen, Germantown, MD, USA) with supernatant from clinical samples (swabs, nasal washes, BALF, CSF), tissue homogenates in DMEM (20% W/V), EDTA blood or

body fluids. Sample lysates were vortexed and 200 µL was used for extraction using a magnetic bead-based extraction kit (GeneReach USA, Lexington, MA) and the Taco™ mini nucleic acid extraction system (GeneReach) as previously described (43). Extraction positive controls (IDT, IA, USA; 2019-nCoV_N_Positive Control), diluted 1:100 in RLT lysis buffer, and negative controls were included throughout this process.

Quantification of SARS-CoV-2 RNA was accomplished using an RT-qPCR protocol established by the CDC for detection of SARS-CoV-2 nucleoprotein (N)-specific RNA (https://www.fda.gov/media/134922/download). Our lab has validated this protocol using the N2 SARS-CoV-2 primer and probe sets (CDC assays for RT-PCR SARS-CoV-2 coronavirus detection, IDT, idtdna.com) in combination with the qScript XLT One-Step RT-qPCR Tough Mix (Quanta Biosciences, Beverly, MA, USA), as previously described (43). Quantification of RNA copy number (CN) was based on a reference standard curve method using a 5-point standard curve of quantitated plasmid DNA containing the N-gene segment (IDT, IA, USA; 2019-nCoV_N_Positive Control). The equation from this standard curve was used to extrapolate CN values from a 10-point standard curve of viral RNA extracted from a USA/CA_CDC_5574/2020 cell culture supernatant. This 10-point standard curve of viral RNA was used as reference for CN quantification from unknown samples to more accurately quantify Ct values at the extremity of quantification. Each sample was run in duplicate wells and all 96-well plates contained duplicate wells of quantitated PCR positive control (IDT, IA, USA; 2019-nCoV_N_Positive Control, diluted 1:100) and four non-template control wells. A positive Ct cut-off of 38 cycles was used when both wells were positive, as this represented a single copy number/µL and the LOD for this assay. Samples with one of two wells positive at or under CT of 38 were considered suspect-positive. Data are presented as the mean of the calculated N gene CN

per mL of liquid sample or per mg of 20% tissue homogenate. The LOD for swab samples was $2.61x10^3$ CN/mL, and $1.23x10^1$ CN/mg for tissue homogenate samples.

Next-Generation Sequencing

RNA extracted from cell culture supernatant (virus stocks), clinical swab/tissue homogenates, and clinical samples were sequenced by next generation sequencing (NGS) using an Illumina NextSeq platform (Illumina Inc.) to determine the genetic composition (% lineage) of viral RNA in each sample. SARS-CoV-2 viral RNA was amplified using the ARTIC-V3 RT-PCR protocol [Josh Quick 2020. nCoV-2019 sequencing protocol v2 (GunIt). Protocols.io https://gx.doi.org/10.17504/protocols.io.bdp7i5rn]. Library preparation of amplified SARS-CoV-2 DNA for sequencing was performed using a Nextera XT library prep kit (Illumina Inc.) following the manufacturer's protocol. The libraries were sequenced on the Illumina NextSeq using 150 bp paired end reads with a mid-output kit. Reads were demultiplexed and parsed into individual sample files that were imported into CLC Workbench version 7.5 (Qiagen) for analysis. Reads were trimmed to remove ambiguous nucleotides at the 5' terminus and filtered to remove short and low-quality reads. The consensus sequences of viral stocks used for challenge material preparation were found to be homologous to the original strains obtained from BEI (GISAID accession numbers: EPI_ISL_404895 (WA-CDC-WA1/2020) and EPI_ISL_751801 (CA_CDC_5574/2020). To determine an accurate relative percentage of each SARS-CoV-2 lineage in each sample, BLAST databases were first generated from individual trimmed and filtered sample reads. Subsequently, two 40-nucleotide long sequences were generated for each strain at locations that include the following gene mutations: Spike (S) A570D, S D614G, S H1118H, S ΔH69V70, S N501Y, S P681H, S 982A, S T716I, S ΔY145, Membrane (M) V70, Nucleoprotein (N) D3L, N R203KG204R, N 235F, and non-structural NS3 T223I, NS8 Q27stop,

NS8 R52I, NS8 Y73C, NSP3 A890D, NSP3 I1412T, NSP3 T183I, NSP6 ΔS106G107F108, NSP12 P323L, NSP13 A454V and NSP13 K460R. A word size of 40 was used for the BLAST analysis to exclude reads where the target mutation fell at the end of a read or reads that partially covered the target sequence. The two sequences for each of the locations listed above, corresponding to either lineage A (USA-WA1/2020) or alpha B.1.1.7 VOC (USA/CA_CDC_5574/2020), were subjected to BLAST mapping analysis against individual sample read databases to determine the relative amount of each strain in the samples. The relative amount of each strain present was determined by calculating the percent of reads that hit each of the twenty-three target mutations. The percentages for all mutations were averaged to determine the relative amount of each strain in the sample. Samples with incomplete or low coverage across the genome were excluded from analysis.

Virus neutralizing antibodies

Virus neutralizing antibodies in sera were determined using microneutralization assay as previously described (43). Briefly, heat inactivated (56°C/30 min) serum samples were subjected to 2-fold serial dilutions starting at 1:20 and tested in duplicate. Then, 100 $TCID_{50}$ of SARS-CoV-2 virus in 100 µL DMEM culture media was added 1:1 to 100 µL of the sera dilutions and incubated for 1 hour at 37°C. The mixture was subsequently cultured on Vero-E6/TMPRSS2 cells in 96-well plates. The neutralizing antibody titer was recorded as the highest serum dilution at which at least 50% of wells showed virus neutralization based on the absence of CPE observed under a microscope at 72 h post infection.

Detection of antibodies by indirect ELISA

Indirect ELISAs were used to detect SARS-CoV-2 antibodies in sera with nucleocapsid (N) and the receptor-binding domain (RBD) recombinant viral proteins, both produced in-house

(43). Briefly, wells were coated with 100 ng of the respective protein in 100 µL per well coating buffer (Carbonate–bicarbonate buffer; Sigma-Aldrich, St. Louis, MO, USA). Following an overnight incubation at 4ºC, plates were washed three times with phosphate buffered saline (PBS-Tween 20 [pH=7.4]; Millipore Sigma), blocked with 200 µL per well casein blocking buffer (Sigma-Aldrich) and incubated for 1 hour at room temperature (RT). Plates were subsequently washed three times with PBS-Tween-20 (PBS-T). Serum samples were diluted 1:400 in casein blocking buffer, then 100 µL per well was added to ELISA plates and incubated for 1 hour at RT. Following three washes with PBS-T, 100 µL of HRP-labelled Rabbit Anti-Sheep IgG (H+L) secondary antibody (VWR, Batavia, IL, USA) diluted 1:1000 (100ng/mL) was added to each well and incubated for 1 hour at RT. Plates were then washed five times with PBS-T and 100 µL of TMB ELISA Substrate Solution (Abcam, Cambridge, MA, USA) was added to all wells of the plate and incubated for 5 minutes before the reaction was stopped. The OD of the ELISA plates were read at 450 nm on an ELx808 BioTek plate reader (BioTek, Winooski, VT, USA). The cut-off for a sample being called positive was determined as follows: Average OD of negative serum + 3X standard deviation. Everything above this cut-off was considered positive. Indirect ELISA was used to detect bovine coronavirus (BCoV) antibodies in sera with Spike (S) recombinant viral protein (LSBio, Seattle, WA, USA) using the methods described above.

Histopathology

Tissue samples from the respiratory tract (nasal cavity [rostral, middle and deep turbinates following decalcification with Immunocal™ Decalcifier (StatLab, McKinney, TX, for 4-7 days at room temperature), trachea, and lungs as well as various other extrapulmonary tissues (liver, spleen, kidneys, heart, pancreas, gastrointestinal tract [stomach, small intestine including Peyer's patches and colon], cerebrum [including olfactory bulb], tonsils and numerous lymph

nodes) were routinely processed and embedded in paraffin. Four-micron tissue sections were stained with hematoxylin and eosin following standard procedures. Two independent veterinary pathologists (blinded to the treatment groups) examined the slides and morphological descriptions were provided.

SARS-CoV-2 specific immunohistochemistry (IHC)

IHC was performed as previously described (43) on four-micron sections of formalin-fixed paraffin-embedded tissue mounted on positively charged Superfrost® Plus slides and subjected to IHC using a SARS-CoV-2-specific anti-nucleocapsid rabbit polyclonal antibody (3A, developed by our laboratory) with the method previously described (147). Lung sections from a SARS-CoV-2-infected hamster were used as positive assay controls.

Results

SARS-CoV-2 replication in ruminant-derived cell lines

Ruminant cell cultures derived from cattle (*Bos taurus*), sheep (*Ovis aries*), and pronghorn (*Antilocapra americana*) were tested for susceptibility to SARS-CoV-2 and viral growth kinetics (**Figure 3.2**). SARS-CoV-2 lineage A WA1 strain was found to replicate in both, primary and immortalized sheep kidney cell cultures with virus titers increasing over the course of 6 to 8 days post infection (DPI). SARS-CoV-2 did not replicate in the primary pronghorn lung cell cultures, or in the two immortalized bovine cell lines, a bovine kidney and a bovine fetal fibroblast cell; instead reduction of virus titer was observed by 2 DPI to 6 DPI (**Figure 3.2**). These results indicate that sheep may be susceptible to SARS-CoV-2 infection, while cattle and American pronghorn likely are not.

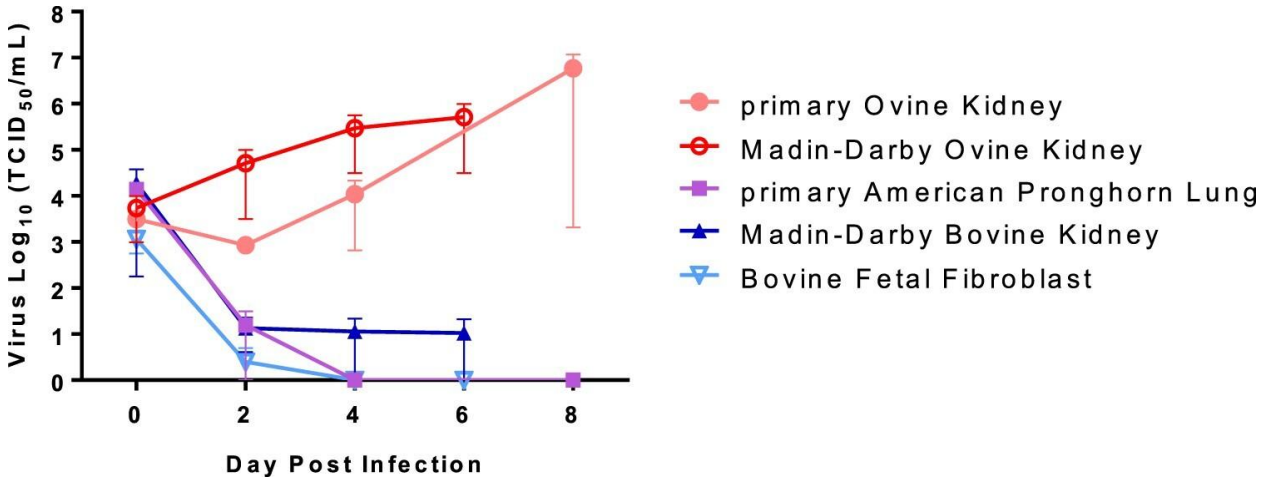

Figure 3.2 SARS-CoV-2 replication in ruminant-derived cell cultures

Primary ovine kidney cells, Madin-Darby ovine kidney cells, primary American pronghorn lung cells, bovine fetal fibroblasts (BFF) and Madin-Darby bovine cells were infected with SARS-CoV-2 USA-WA1/2020 at 0.1 MOI and cell supernatants collected at 0, 2, 4, 6 or 8 days post infection (DPI). Cell supernatants were titrated on Vero E6 cells to determine virus titres. Mean titres and SEM of at least two independent infection experiments per cell line are shown.

Sheep remain subclinical following challenge with SARS-CoV-2

Eight sheep were infected through IN and PO routes simultaneously with 1 x10^6 $TCID_{50}$ per animal of a 1:10 titer ratio of the lineage A WA1 and the B.1.1.7-like alpha VOC strains. One day later, 2 sentinel sheep were co-mingled with the principal infected animals (**Figure 3.1**). Average daily rectal temperatures of all ten sheep showed that they did not become febrile after challenge or during the 21-day study (**Supplementary Figure 3.1**). In addition, no obvious clinical signs were observed in any of the principal infected or sentinel sheep. No weight loss, lethargy, diarrhea, inappetence, or respiratory distress was observed during the study.

SARS-CoV-2 shedding from infected sheep

Nasal, oropharyngeal, and rectal swabs were collected over the course of the 21-day study and tested for the presence of SARS-CoV-2 RNA (**Figure 3.3**) and infectious virus (**Supplementary Tabel 3.1**). Viral RNA was detected in the nasal swab samples from 7 (ID#s

713-719) of the 8 principal infected sheep at 1 DPC, and only in one principal animal (#715) at 3 DPC. One oropharyngeal swab from a principal infected animal (#719) was also positive at 1 DPC. No other nasal or oropharyngeal swabs, and none of the rectal swab samples, collected up to 21 DPC were positive for viral RNA. Swab samples positive by RT-qPCR were also tested for the presence of infectious virus on susceptible VeroE6/TMPRSS2 cells, but no infectious virus was isolated. Nasal, oropharyngeal, and rectal swabs from the two sentinel sheep remained PCR negative over the course of 20 days of co-mingling with the principal infected animals.

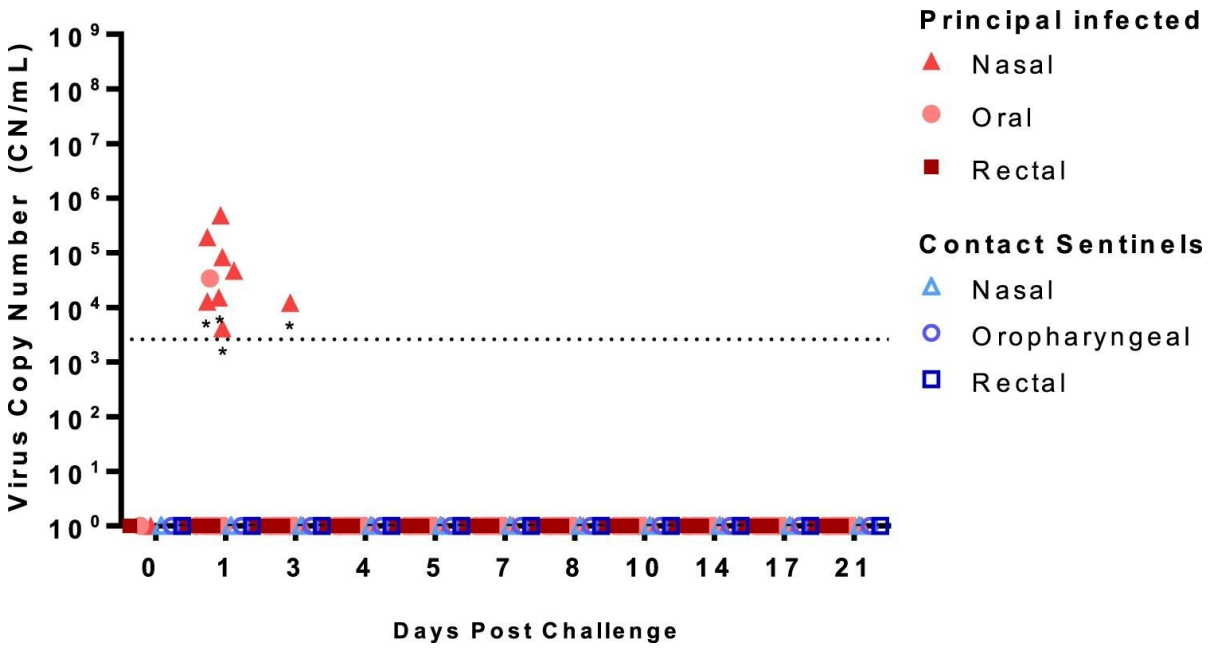

Figure 3.3 Viral RNA shedding of SARS-CoV-2 infected sheep

RT-qPCR was performed on nasal, oropharyngeal, and rectal swabs collected from principal infected (solid red symbols) and sentinel sheep (open blue symbols) on the indicated days post-challenge (DPC). Mean (n = 2) viral RNA copy number (CN) per mL based on the SARS-CoV-2 nucleocapsid gene are plotted for individual animals. Asterisks (*) indicate samples with one out of two RT-qPCR reactions above the limit of detection, which is indicated by the dotted line.

SARS-CoV-2 RNA detection in tissues of infected sheep

Tissues were collected from sheep euthanized at 4, 8, and 21 DPC (**Table 3.1**). SARS-CoV-2 RNA was detected in the respiratory tract tissues of all three principal infected sheep euthanized at 4 DPC, with the highest viral RNA loads detected in the trachea followed by the nasopharynx (**Figure 3.4A**). At 8 DPC, viral RNA was detected in some of the respiratory tissues of the three principal infected sheep, and similarly as found on 4 DPC, the nasopharynx and trachea had the highest RNA levels (**Figure 3.4B**). At 21 DPC, viral RNA was detected in the nasopharynx of both principal infected sheep euthanized at this time point, as well as in the conchae and ethmoturbinates of one principal infected animal (#718) (**Figure 3.4C**). On day 21 DPC, both sentinel sheep had viral RNA present in the conchae, and one sentinel animal (#710) also had detectable viral RNA in the trachea and bronchi (**Figure 3.4C).**

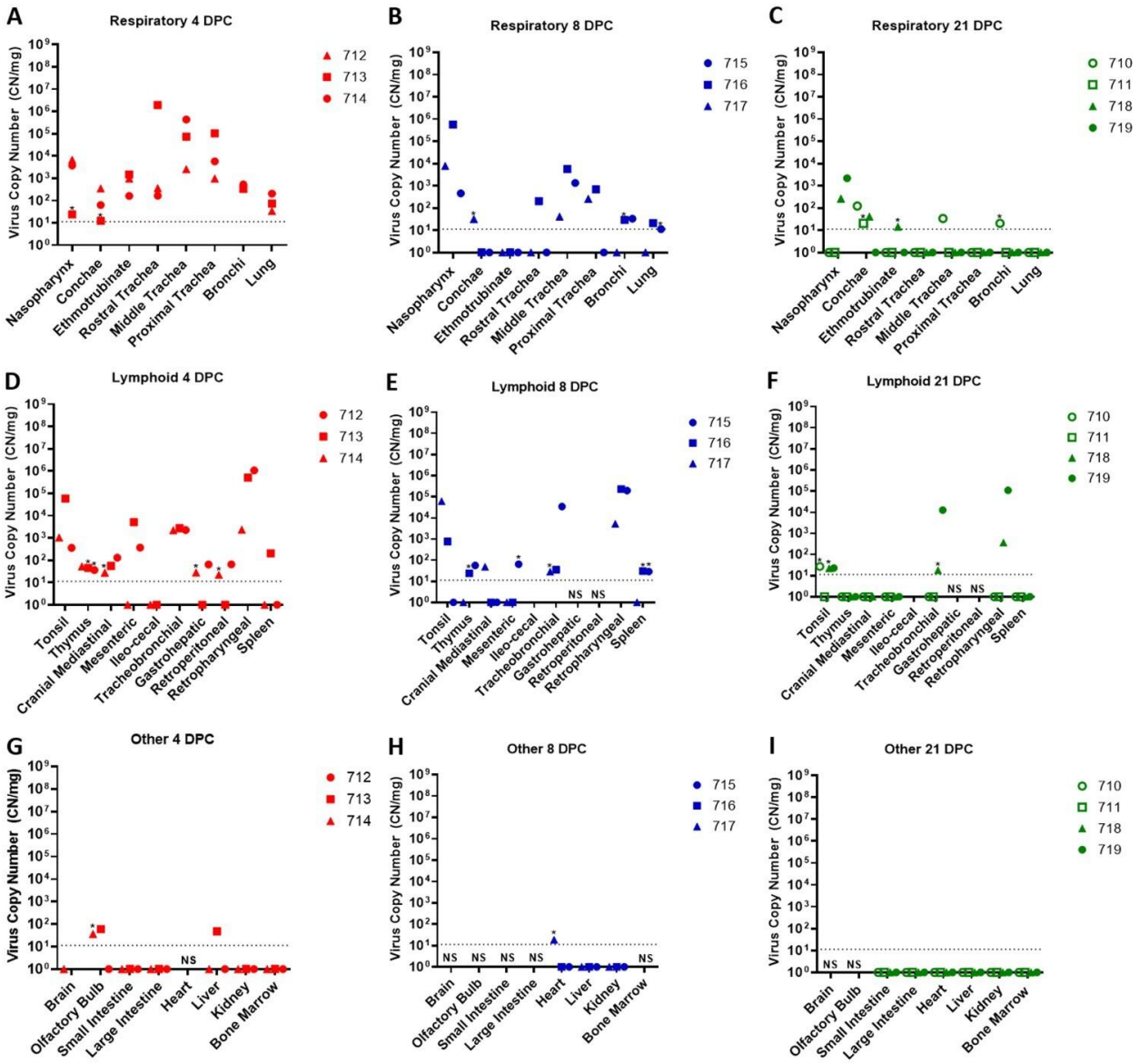

Figure 3.4 Viral RNA detected in tissues of SARS-CoV-2 infected sheep

RT-qPCR was performed on respiratory (A–C), lymphoid (D–F) and other (G–I) tissues of sheep euthanized at 4 (A,D,G), 8 (B,E,H), and 21 (C,F,I) days post challenge (DPC) to detect the presence of SARS-CoV-2-specific RNA. Mean (n = 2) viral RNA copy number (CN) per mg of tissue based on the SARS-CoV-2 nucleocapsid gene are plotted for individual animals. Asterisks (*) indicate samples with one out of two RT-qPCR reactions above the limit of detection, which is indicated by the dotted line. NS = no sample. Solid symbols indicate principal animals necropsied at 4, 8, and 21DPC; open symbols indicate sentinel animals necropsied at 21 DPC.

SARS-CoV-2 RNA was also detected in the lymphoid tissues. At 4 DPC, the tonsil, thymus and several lymph nodes (cranial mediastinal, gastro-hepatic, retroperitoneal,

retropharyngeal) from all three principal sheep euthanized on that day were RT-PCR positive (**Figure 3.4D**). The spleen, and the mesenteric, ileocecal and tracheobronchial lymph nodes of at least 1 or 2 out of the 3 principal sheep were also RNA positive at 4 DPC. At 8 DPC, viral RNA was detected in the lymphoid tissues of only some of the three principal sheep (**Figure 3.4E**). At 21 DPC, both principal infected sheep had detectable viral RNA in the tonsil and in the retropharyngeal and tracheobronchial lymph nodes; the tonsil of one sentinel (#710) was also RNA positive (**Figure 3.4F**). The lymphoid tissues with the highest viral RNA levels at 4, 8, and 21 DPC were the tonsil, and the retropharyngeal and tracheobronchial lymph nodes.

Other tissues such as the brain (only #714), olfactory bulb, small and large intestine, heart, liver, kidney and bone marrow were also collected at necropsy and tested for presence of SARS-CoV-2-specific RNA. At 4 DPC, the olfactory bulb of two of the three principal animals and the liver of animal #713 were RNA positive, whereas the small and large intestine, kidney, and bone marrow were negative (**Figure 3.4G**). At 8 DPC, the heart of sheep #717 was considered a suspect RNA positive, and the liver and kidney of all three principal sheep were negative (**Figure 3.4H**). At 21 DPC, the olfactory bulb, small and large intestine, heart, liver, kidney, and bone marrow from both principal and sentinel sheep were all negative for the presence of viral RNA (**Figure 3.4I**). In addition, whole blood was collected during the 21-day study, but no viral RNA was detected in the blood of any of the sheep enrolled in the study (data not shown).

Nasal washes, BALF, and CSF collected from sheep at necropsy were also tested for the presence of viral RNA. SARS-CoV-2 RNA was detected in the nasal washes of all principal infected sheep at 4 DPC (**Supplementary Table 3.2**). Viral RNA was detected in the BALF of two out of the three principal sheep at 4 DPC (#713, 714) and in one animal at 8 DPC (#716).

Nasal washes and BALF collected from principal and sentinel sheep at 21 DPC were all negative. No viral RNA was detected in the CSF of any of the sheep at any time point.

Virus isolation was attempted on samples that were RT-qPCR positive having at least 10^3 RNA copy number/mL (**Supplementary Table 3.1**). Viable virus was detected in proximal and rostral trachea samples ($5x10^0$ $TCID_{50}$/ml each) collected from principal infected sheep #713 at 4 DPC. No other samples had detectable viable virus.

Serology

Indirect ELISA tests were used to detect SARS-CoV-2 antibodies against the recombinant N and the spike RBD antigens. Sera collected from principal infected sheep had detectable antibodies to N (**Figure 3.5A**) and RBD (**Figure 3.5B**) at 10, 14, 17 and 21 DPC. Sentinels did not develop antibodies to N or RBD above the assay cutoff. Only one of the principal infected sheep (#719) developed a low level of neutralizing antibodies with a 1:20 titer, detectable at 10 and 21 DPC (**Figure 3.5C**). Sera collected from sheep prior to SARS-CoV-2 challenge was also tested for reactivity against the bovine coronavirus spike antigen by indirect ELISA and were found to be negative (**Figure 3.5D**).

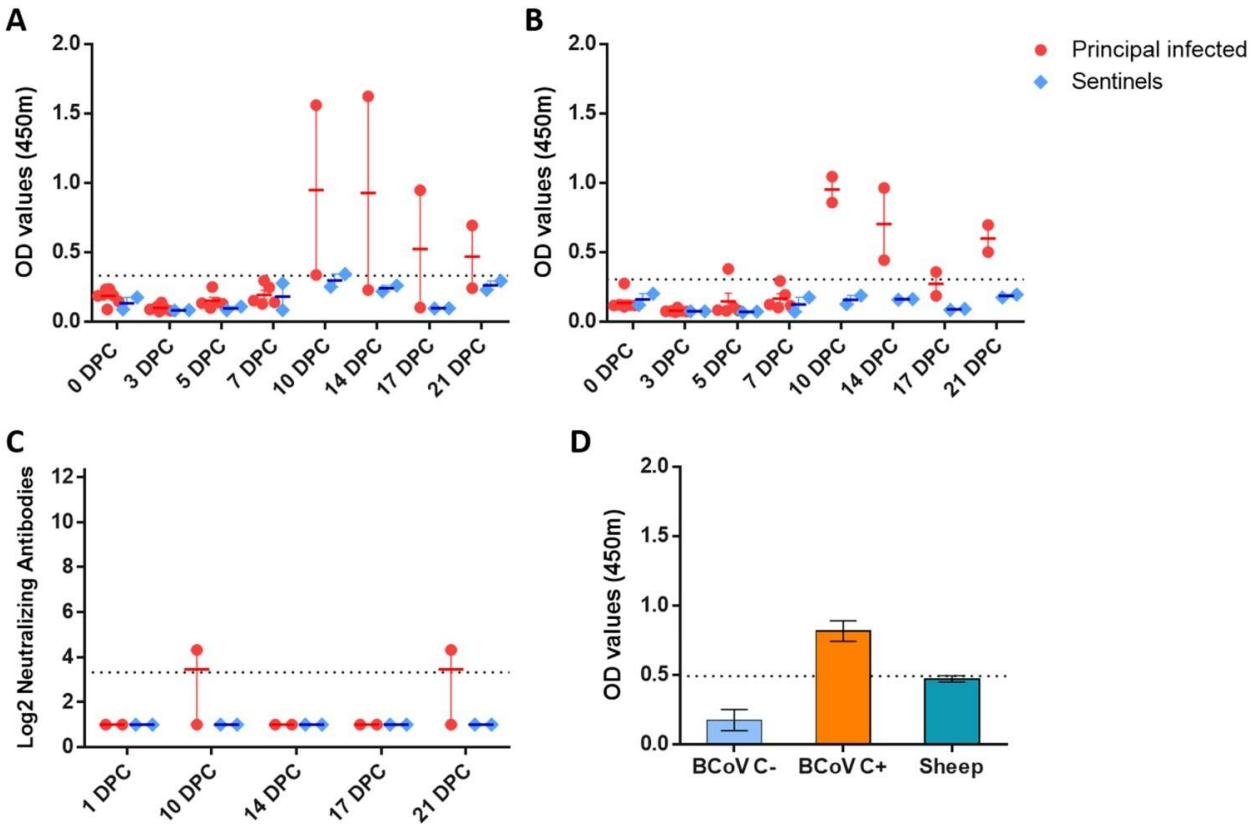

Figure 3.5 Serology of SARS-CoV-2 infected sheep

Detection of antibodies directed against the SARS-CoV-2 nucleocapsid protein (A), and the receptor binding domain (B) by indirect ELISA tests. The cut-off was determined by averaging the OD of negative serum + 3X the standard deviation as indicated by the dotted line. All samples with resulting OD values above this cut-off were considered positive. (C) Virus neutralizing antibodies detected in serum are shown as log2 of the reciprocal of the neutralization serum dilution. Sera were tested starting at a dilution of 1:20 with a 1:10 cut-off indicated by the dotted line. (D) Sera from principal infected (n = 8) and sentinel sheep (n = 2) were tested against the bovine coronavirus (BCoV) spike protein using an indirect ELISA; both, positive (C+) and negative (C−) bovine control sera were included. The cut-off was determined by averaging the OD of negative serum + 3X the standard deviation as indicated by the dotted line. A–D: Mean with SEM are shown.

Pathology

Postmortem pathological evaluations of sheep were performed at 4, 8, and 21 DPC (**Table 3.1**). Overall, no significant gross lesions were observed. Prominent respiratory tract-associated lymphoid tissue was noted in the upper and lower respiratory tract of all infected sheep at 4 and 8 DPC as well as mock-infected controls (**Figures 6**). These lymphoid aggregates

were subjectively more frequent and prominent at 8 DPC compared to 4 DPC. No other changes were noted in nasal turbinates or lungs at 4 DPC, and no viral antigen was detected in these organs (**Figure 3.6 A, B, E and F**). In addition to the prominent lymphoid aggregates, moderate tracheitis was observed in animals #713 and #714 at 4 DPC, with evidence of lymphocytic transmigration and few scattered necrotic epithelial cells (**Figure 3.6C**). Viral antigen was detected in the trachea of sheep #713, and was solely localized to lymphoid aggregates in the lamina propria and, based on the morphology of the immunopositive cells, these likely represent macrophages/dendritic cells (i.e., antigen presenting cells) (**Figure 3.6D**). Lymph nodes associated with the respiratory tract, tonsils, and third eyelids were characterized by severe lymphoid hyperplasia with traces of viral antigen detected in few cells resembling macrophages/dendritic cells, within a few lymphoid aggregates of the pharyngeal region of animals #712 and #713 euthanized on 4 DPC. Overall, viral antigen appeared associated with lymphoid aggregates, with limited antigen positivity observed primarily in phagocytic cells. No viral antigen was detected within the respiratory epithelium, associated glands, or pulmonary pneumocytes.

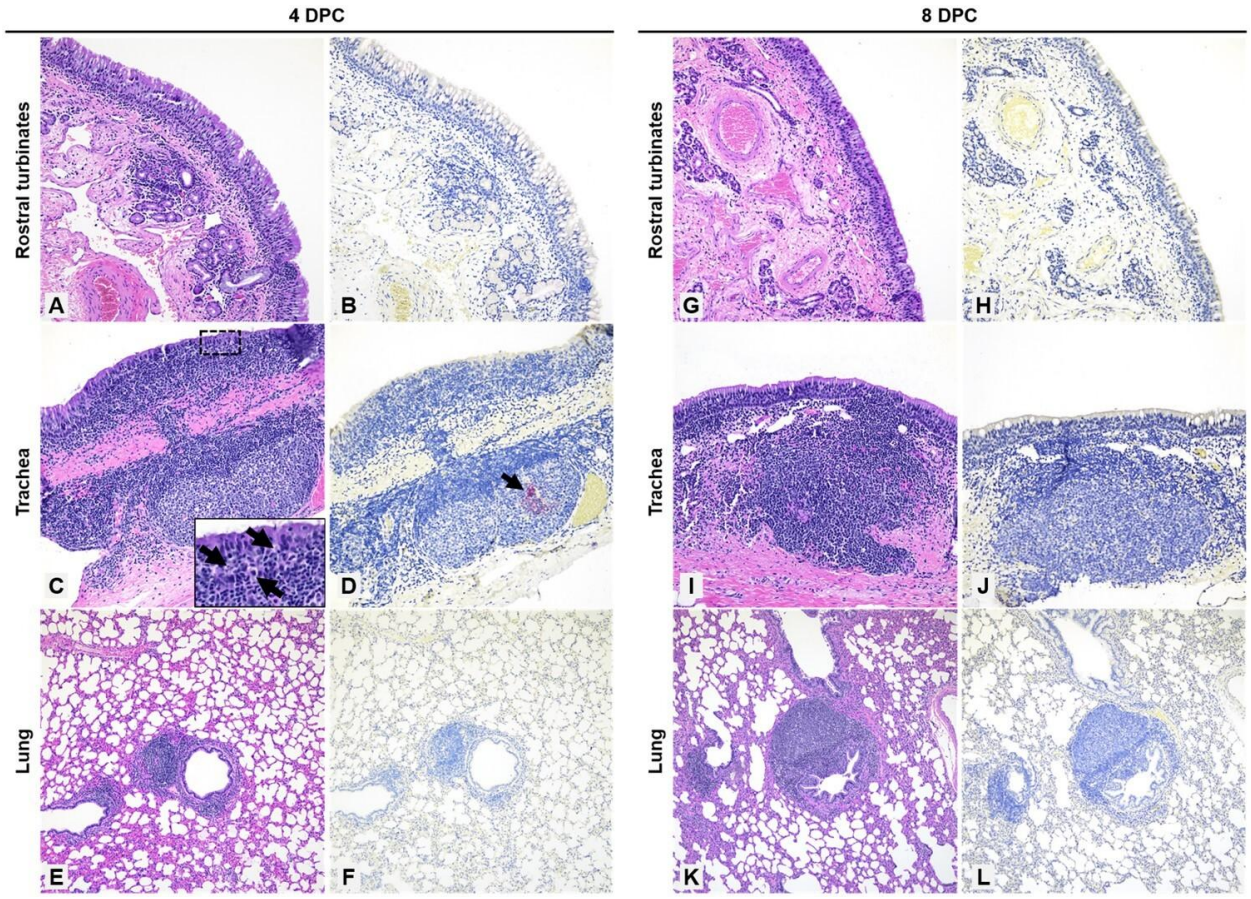

Figure 3.6 Histopathology and SARS-CoV-2 antigen distribution in the upper and lower respiratory tract of infected sheep at 4 and 8 DPC

Rostral turbinates (A and B), trachea (C and D), and lung (E and F) at 4 DPC. Minimal changes were noted in the rostral turbinates, with mild, dispersed and aggregates of lymphocytes. No viral antigen was detected (B). In the trachea, there were multifocal prominent aggregates of lymphocytes and plasma cells in the lamina propria and extending/transmigrating through the lining epithelium, with few individual cell degeneration and necrosis (C and inset [arrows]). Sporadic lymphoid aggregates showed viral antigen (D, arrow). In the pulmonary parenchyma, bronchioles and blood vessels were delimited by hyperplastic bronchus-associated lymphoid tissue (BALT) (E), no viral antigen was detected (F). Rostral turbinates (G and H), trachea (I and J), and lung (K and L) at 8 DPC. Rostral turbinates were within normal limits and no viral antigen was detected (G and H). The tracheal lamina propria had multiple prominent and dense lymphoid aggregates (I) but no evidence of viral antigen (J) or epithelial alterations. In the pulmonary parenchyma, bronchioles and blood vessels were frequently delimited by prominent BALT (K), no viral antigen was detected (L) H&E and Fast Red, 200× total magnification (A–D; G–J) and 100× total magnification (E and F; K and L).

No significant histologic changes were noted in the respiratory tract at 8 DPC other than the hyperplastic respiratory tract-associated lymphoid tissue (**Figure 3.6G-L**). In a single animal

(#716), there was moderate lymphocytic tracheitis with minimal adenitis, transmigration of lymphocytes along the lining epithelium, and occasionally necrotic epithelial cells. No viral antigen was detected in the respiratory tract (nasal passages, trachea, and lungs) or associated lymphoid tissue at 8 DPC.

SARS-CoV-2 competition in co-infected sheep

To study the competition of two SARS-CoV-2 strains, the sheep challenge inoculum was prepared as a mixture of two SARS-CoV-2 isolates which were representative of the ancestral lineage A and the B.1.1.7-like alpha VOC. Next generation sequencing (NGS) was used to determine the percent presence of each strain in various swab and tissue samples collected from each sheep. The intention was to use a 1:1 titer ratio of each strain to inoculate sheep; however, back-titration showed that the actual ratio was closer to 1:10 of the WA1 lineage A to the B.1.1.7-like alpha VOC. The overall results indicate that the SARS-CoV-2 alpha variant outcompeted the ancestral lineage A strain in sheep (**Table 3.2**). NGS analysis consisted of 1 DPC nasal swabs, and various respiratory and lymphoid tissues collected at 4, 8 and 21 DPC. Analysis of the 1 DPC nasal swab samples of principal infected sheep #715 and #719 showed 100% presence of the B.1.7-like alpha VOC. The alpha VOC was found at 99.7-100%, compared to 0.0-0.3% of the ancestral lineage A strain in respiratory tissues (ethmoturbinates, nasopharynx, and trachea) of principal infected sheep #712, 713, and 714 analyzed at 4 DPC. At 8 DPC, the alpha VOC was found at 99.1-100% compared to 0.0-0.9% of the ancestral lineage A strain in the nasopharynx and trachea of principal infected sheep #715, 716, and 718. In the tonsil, the B.1.1.7-like alpha VOC was present at 76.4-100% in all three of the principal infected sheep euthanized at 4 DPC, and at 98.6-99.9% in 2 out of 3principal infected sheep at 8 DPC. This indicates that there was some replication of the lineage A strain in at least some of the

tissues, especially the tonsil, of some of the sheep. However, all SARS-CoV-2 positive tissues showed a majority presence of the alpha VOC strain. No sequencing data is available for samples collected from principal infected or sentinel sheep at 21 DPC, due to low RNA copy numbers in the tissues.

Table 3.2 SARS-CoV-2 competition in sheep co-infected with two strains determined by next-generation sequencing

Sample	4 DPC						8 DPC						21 DPC					
	#712		#713		#714		#715		#716		#717		#710		#718		#719	
	%WA1	%B.1.1.7	%WA1	%B.1.1.7	%WA1	%B.1.1.7	%WA1	%B.1.1.7	%WA1	%B.1.1.7	%WA1	%B.1.1.7	%WA1	%B.1.1.7	%WA1	%B.1.1.7	%WA1	%B.1.1.7
Nasal Wash	LMR	LMR	LMR	LMR	LMR	LMR	ND	ND	ND	ND	ND	ND	ND	ND	ND	ND	ND	ND
Conchae	NT	NT	NT	NT	NT	NT	ND	ND	ND	ND	NT	NT	LMR	LMR	NT	NT	ND	ND
Ethmoturbinates	0.00%	100.00%	0.00%	100.00%	LMR	LMR	ND	ND	ND	ND	ND	ND	ND	ND	NT	NT	ND	ND
Nasopharynx	0.30%	99.70%	NT	NT	0.10%	99.90%	0.00%	100.00%	0.00%	100.00%	0.90%	99.10%	ND	ND	LMR	LMR	LMR	LMR
Trachea, rostral	NT	NT	NT	NT	NT	NT	ND	ND	NT	NT	ND	ND	ND	ND	ND	ND	ND	ND
Trachea, middle	0.00%	100.00%	0.10%	99.90%	0.00%	100.00%	0.00%	100.00%	0.10%	99.90%	NT	NT	NT	NT	ND	ND	ND	ND
Trachea, distal	NT	NT	NT	NT	NT	NT	ND	ND	NT	NT	0.00%	100.00%	ND	ND	ND	ND	ND	ND
Tonsil	23.60%	76.40%	0.00%	100.00%	1.70%	98.30%	ND	ND	0.10%	99.90%	1.40%	98.60%	NT	NT	NT	NT	NT	NT
Retropharyngeal Lymph Node	0%	100%	1%	99%	0%	100%	0%	100%	0%	100%	0%	100%	NT	NT	LMR	LMR	0%	100%
1 DPC Nasal Swab	ND	ND	NT	NT	NT	NT	0.00%	100.00%	NT	NT	LMR	LMR	ND	ND	NT	NT	0.00%	100.00%

WA1 = USA-WA1/2020 strain; B.1.1.7-like = USA/CA-5574/2020 strain; DPC = day post challenge; NT = not tested; ND = not detected; LMR = low mapped reads;
[C]hallenge inoculum contained 8% WA1 and 92% B.1.1.7 virus; [S]amples from sentinel sheep #711 did not contain sufficient level of viral RNA for NGS analysis.

Discussion

The emergence, rapid evolution, and persistence of SARS-CoV-2 has been an unwelcome reminder of our co-existence with, and vulnerability to, formidable microorganisms. It has been shown that emerging infectious diseases (EID) of humans frequently arise from the human-animal interface, i.e. are zoonotic pathogens (8, 180). Some EID's resolve themselves in dead-end hosts while other pathogens, such as SARS-CoV-2, adapt quickly to new hosts and maintain transmission cycles in susceptible populations. The public health implications of SARS-CoV-2 do not start or stop with humans. Similar to SARS-CoV, which emerged in 2002, SARS-CoV-2 utilizes the ACE2 receptor to bind to and enter host cells. Provided the high conservation of ACE2 receptors amongst mammalian species, many animal species are potentially susceptible to SARS-CoV-2 infection (27). Therefore, a holistic, *One-Health* approach is necessary to fully understand and properly mitigate further escalation of the SARS-CoV-2 pandemic and its impacts.

So far, the susceptibility and epidemiological role of domestic ruminant species has been largely understudied. Sheep are a valuable agricultural species and are in close contact with potential SARS-CoV-2 reservoir species including humans, cats, deer, mustelids and rodents. Current data regarding their susceptibility is inconclusive. In order to address this gap, we investigated the susceptibility of sheep to SARS-CoV-2 by *in vitro* infection of sheep- and other ruminant-derived cell cultures and by *in vivo* challenge of sheep with SARS-CoV-2. In addition, we introduced two sentinel sheep to evaluate the potential of transmission of the virus from principal infected animals to naïve sheep. Furthermore, we co-infected sheep with the ancestral lineage A and the B.1.1.7-like alpha VOC SARS-CoV-2 strains in order to study virus strain competition in the animal host.

Our results of SARS-CoV-2 infected ruminant-derived cell cultures showed that sheep primary kidney cells and an immortal sheep kidney cell line supported SARS-CoV-2 infection and replication, while the pronghorn and bovine cell cultures used in this study did not (**Figure 3.2**). These results are consistent with several previous *in silico*, *in vitro* and *in vivo* studies (27, 28, 61, 138). As we have not monitored levels of ACE2 on the cell surface of these cell lines, we cannot exclude that lack of SARS-CoV-2 infection in pronghorn and bovine cell cultures is due to lack of expression of the host ACE2 receptor in these cell lines. However, the pronghorn cells were lung cells and, therefore, should express ACE2; and the bovine cells were fetal fibroblast and kidney cells, with the latter cells usually expressing ACE2. It should be noted, that computational modeling studies by Damas et al. (27) predicted the ACE2 molecule of cattle (*Bos taurus*), sheep (*Ovis aries*) and pronghorn sheep (*Antilocapra americana*) to have a medium binding score with the RBD region of the SARS-CoV-2 spike protein, identifying these ruminant species as potential susceptible hosts. Furthermore, results from a study with SARS-CoV-2 infection of tracheal and lung organ cultures from sheep and cattle *ex vivo* showed that both were capable of supporting viral replication (28). Together these studies and ours suggest that sheep seem to have low susceptibility toSARS-CoV-2 infection. However, a serological survey in Spain of sheep in frequent contact with humans during the pandemic did not provide evidence to support infection of sheep with SARS-CoV-2 (179). Another very recent study of ancestral SARS-CoV-2 experimental infected sheep found no virus nor viral RNA was detected from swabs or tissues, but some animals did develop low neutralizing antibodies on day 28 post infection (41). In that study, experimental infection of goats, cattle, alpacas and a horse with SARS-CoV-2 was also performed; results showed that viral RNA was detected in a portion of

the cattle (1/3) and goats (2/3), as well as low levels of neutralizing antibodies in some goats (41). All animals challenged in that study remained subclinical up to 28 DPC.

Our results showing that the Madin-Darby bovine kidney (MDBK) cells and bovine fetal fibroblasts do not support SARS-CoV-2 infection are consistent with a study by Hoffman and colleagues (61) that utilized a Spike-based pseudovirus system that demonstrated MDBKs do not support SARS-CoV-2 cell entry. Furthermore, a study in cattle showed that only 2 out of 6 experimentally challenged animals became infected and that transmission of the virus did not occur to co-housed naïve animals (138). Collectively these studies indicate that susceptibility of cattle to SARS-CoV-2 infection is low.

In this study, we determined susceptibility and transmission in experimentally challenged sheep. Challenge route, dose, and experimental design used in this study were in line with other SARS-CoV-2 infection studies in animals (6). Following infection of highly susceptible species such as cats or white-tailed deer, viral shedding can be observed for up to a week or more while the animals remain asymptomatic (11, 12, 13, 14, 30). In the current study, sheep remained subclinical throughout the 21-day long study, and the duration of SARS-CoV-2 RNA shedding in clinical samples was rather short and primarily from the nasal cavity. At 1 DPC viral RNA was detected in nasal swabs of seven out of eight principal infected sheep. It cannot be ruled out that this was artifact or residual from the challenge inoculum. However, one principal infected sheep (#715) had a RT-qPCR positive nasal swab at 3 DPC and virus was isolated and viral antigen detected in the trachea of sheep #713 at 4 DPC. These findings are indicative of limited virus replication. Viral RNA detected in the oral swabs was limited to only 1 animal at 1 DPC, and no viral RNA was detected from rectal swabs from any sheep during the 21-day study.

Similar to observations from other experimental infection studies of susceptible species with SARS-CoV-2, viral RNA was frequently detected in the respiratory and lymphoid tissues at 4 and 8 DPC, and less frequently at 21 DPC. Low levels of viral RNA were also detected in the olfactory bulb, liver and heart in a few animals up to 8 DPC. Nasopharynx, trachea, tonsil, and tracheobronchial and retropharyngeal lymph node tissues had the highest viral RNA levels. In addition, viable virus was isolated from the trachea of one of the challenged animals at 4 DPC, evident of active SARS-CoV-2 infection. The prominent lymphoid hyperplasia along the respiratory tract was a feature common to both infected and mock-infected animals. Even though this response seems to be most prominent at 8 DPC, its background presence in mock-infected animals precludes establishment of a direct association with SARS-CoV-2 infection. Few animals at 4 DPC showed mild to moderate tracheitis with evidence of epithelial alterations, however, viral antigen was not detected in the respiratory epithelium and solely localized to phagocytic cells within lymphoid aggregates (#713). Overall, viral antigen appeared associated with lymphoid aggregates, with limited antigen positivity observed primarily in phagocytic cells. Alternatively, SARS-CoV-2 antigen might have been acquired by phagocytosis of viral proteins rather than by limited infection. This observation explains the lack of significant virus shedding and effective transmission to co-mingling animals. Together our results indicate that sheep can be experimentally infected with SARS-CoV-2 resulting in a limited infection primarily associated with the upper respiratory tract and regional lymphoid tissues. Domestic sheep showed low susceptibility to SARS-CoV-2 infection and limited ability to transmit to contact animals.

The two contact sentinel sheep did not shed viral RNA nor seroconverted during the 21-day long study, but low levels of viral RNA were detected at 21 DPC in the trachea, bronchi and

tonsil of one sentinel sheep, and the conchae of both sentinel animals. This suggests that transmission could occur but was not very effective in order to result in detectable virus shedding or a robust immune response in the contact sentinel sheep, i.e. a productive SARS-CoV-2 infection was not established in the sentinel animals. While viral shedding from principal infected animals did not appear to be sufficient to cause a productive infection in naïve contact sheep in our study, transmission to other highly susceptible species such as humans or other animals could be of potential concern.

Finally, the virus competition results from co-challenge of sheep demonstrated co-infection by both SARS-CoV-2 strains and confirmed the competitive advantage of the SARS-CoV-2 B.1.1.7-like alpha VOC over the ancestral lineage A strain in sheep. However, the input ratio of the two virus strains was unintentionally biased toward the alpha VOC (10x), therefore limited conclusions can be drawn from this particular experiment. Nonetheless, these results confirm the ability of the SARS-CoV-2 alpha VOC to infect sheep and its increased replicative capacity in general.

In conclusion, our results demonstrate that experimental challenge of sheep with SARS-CoV-2 results in a limited subclinical infection, and while transmission to naïve co-mingled sheep appeared to occur, it did not lead to highly productive infection; therefore, domestic sheep are unlikely to be amplifying hosts for SARS-CoV-2. Based on our results and the currently available published data, further investigations into SARS-CoV-2 infection in sheep and other ruminant species are warranted. The identification of additional susceptible hosts provides critical information for SARS-CoV-2 epidemiology, in order to establish surveillance protocols, and to improve our mitigation strategies and preventative measures at the human-animal interface.

Acknowledgments

We thank the staff of KSU Biosecurity Research Institute, the histology laboratory at the Kansas State Veterinary Diagnostic Laboratory (KSVDL), members of the Histology and Immunohistochemistry sections at the Louisiana Animal Disease Diagnostic Laboratory (LADDL), the Comparative Medicine Group staff at Kansas State University and technical support from Emily Gilbert-Esparza, Yonghai Li and Cassidy Keating of KSU, and Jeana Owens and Dane Jasperson from USDA ARS. The SARS-CoV-2 strains USA/CA-5574/2020 and USA/WA1/2020 were obtained through BEI Resources (catalog # NR-52281 and #54011). We also thank Dr. Kyeong-Ok Chang for the Vero E6/TMPRSS2 cells used in these studies.

Disclosure statement

Mention of trade names or commercial products in this publication is solely for the purpose of providing specific information and does not imply recommendation or endorsement by the U.S. Department of Agriculture. USDA is an equal opportunity provider and employer. The JAR laboratory received support from Tonix Pharmaceuticals, Xing Technologies and Zoetis, outside of the reported work. JAR is inventor on patents and patent applications on the use of antivirals and vaccines for the treatment and prevention of virus infections, owned by Kansas State University, KS, or the Icahn School of Medicine at Mount Sinai, New York. The AG-S laboratory has received research support from Pfizer, Senhwa Biosciences, Kenall Manufacturing, Avimex, Johnson & Johnson, Dynavax, 7Hills Pharma, Pharmamar, ImmunityBio, Accurius, Nanocomposix, Hexamer, N-fold LLC, Model Medicines, Atea Pharma, and Merck, outside of the reported work. AG-S has consulting agreements for the following companies involving cash and/or stock: Vivaldi Biosciences, Contrafect, 7Hills Pharma, Avimex, Vaxalto, Pagoda, Accurius, Esperovax, Farmak, Applied Biological Laboratories,

Pharmamar and Pfizer, outside of the reported work. AG-S is inventor on patents and patent applications on the use of antivirals and vaccines for the treatment and prevention of virus infections, owned by the Icahn School of Medicine at Mount Sinai, New York.

Funding

Funding for this study was partially provided through grants from the National Bio and Agro-Defense Facility (NBAF) Transition Fund from the State of Kansas (JAR), the AMP Core of the Center of Emerging and Zoonotic Infectious Diseases (CEZID) from National Institute of General Medical Sciences (NIGMS) under award number P20GM130448 (JAR, IM), the German Federal Ministry of Health (BMG) COVID-19 Research and development funding to WHO R&D Blueprint (JAR), the NIAID supported Center of Excellence for Influenza Research and Response (CEIRR, contract number 75N93021C00016 to JAR), and the USDA Animal Plant Health Inspection Service's National Bio- and Agro-defense Facility Scientist Training Program (KC, CM). This study was also partially supported by the Louisiana State University, School of Veterinary Medicine start-up fund under award number PG 002165 (UBRB), the USDA-Agricultural Research Service (DM, WCW), the Center for Research for Influenza Pathogenesis and Transmission (CRIPT), a NIAID supported Center of Excellence for Influenza Research and Response (CEIRR, contract # 75N93019R00028 to AG-S), and by the generous support of the JPB Foundation, the Open Philanthropy Project (research grant 2020-215611 [5384]) and anonymous donors to AG-S.

Supplemental Material

Supplemental data for this article can be accessed at https://doi.org/10.1080/22221751.2022.2037397

Chapter 4 - Experimental co-infection of calves with SARS-CoV-2 Delta and Omicron variants of concern[5]

Abstract

Since emerging in late 2019, severe acute respiratory syndrome coronavirus 2 (SARS-CoV-2) has repeatedly crossed the species barrier with natural infections reported in various domestic and wild animal species. The emergence and global spread of SARS-CoV-2 variants of concern (VOCs) has expanded the range of susceptible host species. Previous experimental infection studies in cattle using Wuhan-like SARS-CoV-2 isolates suggested that cattle were not likely amplifying hosts for SARS-CoV-2. However, SARS-CoV-2 sero- and RNA-positive cattle have since been identified in Europe, India, and Africa. Here, we investigated the susceptibility and transmission of the Delta and Omicron SARS-CoV-2 VOCs in cattle. Eight Holstein calves were co-infected orally and intranasally with a mixed inoculum of SARS-CoV-2 VOCs Delta and Omicron BA.2. Twenty-four hours post-challenge, two sentinel calves were introduced to evaluate virus transmission. The co-infection resulted in a high proportion of calves shedding SARS-CoV-2 RNA at 1- and 2-days post-challenge (DPC). Extensive tissue distribution of SARS-CoV-2 RNA was observed at 3 and 7 DPC and infectious virus was recovered from two calves at 3 DPC. Next-generation sequencing revealed that only the SARS-CoV-2 Delta variant was detected in clinical samples or tissues. Similar to previous experimental infection studies in

---

[5] [5] Reprinted with permission from " Experimental co-infection of calves with SARS-CoV-2 Delta and Omicron variants of concern" by Cool, K*. *et al., 2023. Emerging Microbes & Infections* 13(1). https://doi.org/10.1080/22221751.2023.2281356

cattle, we observed only limited seroconversion and no clear evidence of transmission to sentinel calves. Together, our findings suggest that cattle are more permissive to infection with SARS-CoV-2 Delta than Omicron BA.2 and Wuhan-like isolates but, in the absence of horizontal transmission, are not likely to be reservoir hosts for currently circulating SARS-CoV-2 variants.

Introduction

Severe acute respiratory syndrome coronavirus 2 (SARS-CoV-2) has been circulating in the human population since its emergence in 2019. SARS-CoV-2 has repeatedly spilled back from humans into animals, occasionally establishing sustained transmission in felids, hamsters, mustelids, and white-tailed deer, and developing host-adapted mutations (15, 17, 74, 181-183). Epidemiological investigations of these outbreaks have revealed subsequent secondary spillover events where host-adapted variants were found present in humans. This has led to mass culling of mink and hamsters, resulting in economic losses and trade restrictions (68, 184). The threat of additional animal reservoirs being established has prompted increased surveillance efforts in companion, farmed, and wild animal populations. To date, nearly 700 outbreaks in 26 species have been reported by the WOAH (185).

Several *in silico* and *in vitro* methods have been applied to evaluate animal species for their susceptibility to SARS-CoV-2, however these predictions do not always translate when tested *in vivo* (28, 59, 78, 186-189). The emergence of SARS-CoV-2 variants of concern (VOCs) has made it necessary to re-evaluate the host-pathogen interaction, since many species have not been evaluated *in vivo* for their susceptibility to SARS-CoV-2 VOCs (190-192). VOCs are characterized by mutations in the Spike (S) protein, particularly in the Receptor Binding Domain (RBD), and are associated with enhanced transmissibility, changes in pathogenicity, evasion of pre-existing immunity from previous infections or vaccination, and/or decreased effectiveness of

vaccines, therapies, and/or diagnostics (141, 193). Changes in host range have also been described for SARS-CoV-2 VOCs, most notably in mice, that can be infected by alpha, beta, gamma and Omicron VOCs, but not by the ancestral or delta VOC (191-194). The expansion of host range is largely attributed to key amino acid substitutions in the RBD of the S protein. These substitutions alter the binding affinity between SARS-CoV-2 Spike protein and the host ACE-2 protein, which serves as at least one of the cellular receptors for SARS-CoV-2.

Cattle (*Bos taurus*) have been evaluated for their susceptibility to Wuhan-like SARS-CoV-2 isolates using various methods, including *in silico* predictions, receptor binding/affinity assays, replication kinetics in primary cell cultures and tissue explants, as well as by *in vivo* experimental infection (28, 29, 78, 79, 138, 187, 195). Together, this data suggested that cattle were unlikely to support sufficient viral replication to contribute or sustain transmission of SARS-CoV-2 within cattle herds. However, seropositive cattle have since been identified in Italy and Germany, and SARS-CoV-2 RNA has been isolated from cattle in India and Nigeria, all coinciding with the Delta wave of SARS-CoV-2 transmission in humans, warranting further investigation into the susceptibility of this species to SARS-CoV-2 VOCs (48, 63, 77, 196).

Here, we present our findings on the susceptibility and transmission of SARS-CoV-2 VOCs in calves after co-infection with the Delta and Omicron BA.2 VOCs. Our analysis includes clinical evaluations, viral RNA shedding and RNA distribution in respiratory and other tissues, virus isolation, pathological findings, and virus-specific antibody responses. Furthermore, RNA isolated from clinical and tissue samples was analyzed by next generation sequencing to examine the potential virus evolution and competition of these two VOCs *in vivo.*

Materials and Methods

Ethics statement

All animal studies and experiments were approved and performed under the Kansas State University (KSU) Institutional Biosafety Committee (IBC, Protocol #1460) and the Institutional Animal Care and Use Committee (IACUC, Protocol #4508) in compliance with the Animal Welfare Act. All animal and laboratory work were performed in biosafety level-3+ and −3Ag laboratories and facilities in the Biosecurity Research Institute (BRI) at KSU in Manhattan, KS, USA.

Cells and virus propagation

Vero E6 cells stably expressing transmembrane serine protease 2 (Vero-E6/TMPRSS2; (197) obtained from Creative Biogene (Shirley, NY) via Kyeong-Ok Chang at KSU were used for SARS-CoV-2/Omicron BA.2 VOC propagation, titration, and isolation. Cells were cultured in Dulbecco's Modified Eagle's Medium (DMEM, Corning, New York, N.Y, USA), supplemented with 10% fetal bovine serum (FBS, R&D Systems, Minneapolis, MN, USA) and antibiotics/antimycotics (ThermoFisher Scientific, Waltham, MA, USA), and maintained at 37°C under 5% CO_2 atmosphere. To maintain TMPRSS2 expression, a selection antibiotic, G418, was added to cell culture medium at 0.5mg/mL but was not used during virus cultivation or assays. The SARS-CoV-2/Delta (hCoV-19/USA/NYMSHPSP-PV29995/2021; lineage B.1.617.2, clade GK) VOC is a clinical isolate provided by the Mount Sinai Pathogen Surveillance program (directed by Drs. van Bakel, Sordillo and Simon). Delta virus stock was propagated in a single passage on Calu3 cells. The SARS-CoV-2 Omicron BA.2 strain (Lineage B.1.1.529, BA.2; clade GRA) was acquired from BEI Resources (NR-56520; Manassas, VA, USA). Virus stock was produced by a single passage on Vero-E6/TMPRSS2 cells.

To determine infectious titers of virus stocks and inoculum, 10-fold serial dilutions were performed using Vero-E6/TMPRSS2 cells on 96-well cell culture plates. Cells were observed under a light microscope for the presence or absence of cytopathic effect (CPE) after at least 96 hours of incubation at 37°C under 5% CO_2 atmosphere. Tissue culture infective dose 50% ($TCID_{50}$)/mL was calculated using the Spearman-Kaerber method (198).

Virus challenge of animals

Ten male Holstein calves, approximately 4 months old, were purchased and transported from a South Dakota feedlot to KSU and held outdoors for an acclimation period of 2 weeks prior to challenge with SARS-CoV-2. Prior vaccinations included Nalsalgen, Virashield 6, Covexin 8, and Endovac, animals also received Draxxin and Ivermectin. Upon arrival, cattle were examined by a KSU veterinarian. Several calves had enlarged prescapular lymph nodes (#673, 88, T7477), likely associated with recent vaccinations. Additionally, a mild cough was noted in calf #678 and mild respiratory signs in calf HT9.

After the acclimation period, all calves were transported to one large BSL-3Ag room at the BRI. A 50/50 mixture of SARS-CoV-2 Delta and Omicron BA.2 VOCs was administered to eight calves intra-nasally (IN), using a MAD Nasal™ atomization device (Teleflex, Morrisville, NC, USA), and orally (PO), administered with a micropipette, simultaneously for a total volume of 4mL containing $1x10^6$ $TCID_{50}$ ($2.5x10^5$ $TCID_{50}$/mL; $0.5x10^6$ $TCID_{50}$ for each VOC). These 8 calves are considered the principal-infected animals. Two sentinel calves were isolated in a separate pen, physically distant and up-current of directional airflow from the challenged animals. The sentinel calves were introduced to the eight principal-infected calves after sampling at 1 DPC, approximately 24 hours post-challenge (**Figure 4.1**).

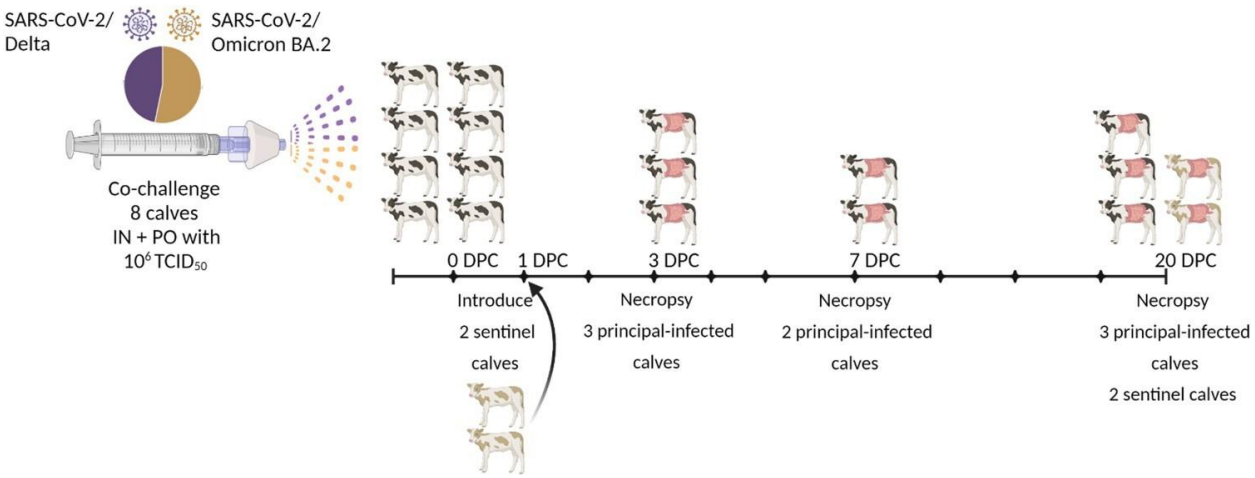

Figure 4.1 Experimental Design

Experimental design. Eight male Holstein calves, approximately 4 months old, were administered a 50/50 mixture of SARS-CoV-2 Delta (B.1.617.2, clade GK) and Omicron BA.2 (lineage B.1.1.529; clade GRA) intranasally (IN) using a MAD Nasal™ atomization device (Teleflex, Morrisville, NC, USA), and orally (PO) by a micropipette, with a total dose of 1×10^6 $TCID_{50}$ in 4 mL (2.5×10^5 $TCID_{50}$/mL). Two sentinel calves were isolated in a separate pen, physically distant and up-current of directional airflow from the challenged animals. The sentinel calves were co-mingled with the eight principal-infected calves after sampling at 1 DPC, 24 h post-challenge. Whole blood (EDTA) was collected on −1, 3, 7, 10, 14, 18, and 20 days post-challenge (DPC). Serum was collected on −1, 3 (calves HT1, HT8, 678 only), 7, 10, 14, 18, and 20 DPC. Nasal, oral, and rectal swabs were collected on −1, 1 through 5, 7, 10, 14, 18, and 20 DPC. Calves were humanely euthanized and postmortem examinations were performed at 3 (n = 3 principal-infected), 7 (n = 2 principal-infected), and 20 DPC (n = 5; 3 principal-infected, and 2 sentinels).

Clinical evaluations and sample collection

Calves were observed daily and evaluated for clinical symptoms including respiratory distress, gastrointestinal irregularities, appetite, activity levels, and elevated body temperatures. Nasal, oral, and rectal swabs were collected on days -1, 1 through 5, 7, 10, 14, 18, and 20 post-challenge. Samples were collected with FLOQSwabs® (Copan Diagnostics, Murrieta, CA) in 1mL DMEM supplemented with 1% antibiotics/antimycotics (ThermoFisher Scientific, Waltham, MA, USA), placed directly on ice, and transported to the BSL-3+ lab for processing.

Whole blood (EDTA) was collected on days -1, 3, 7, 10, 14, 18, and 20 post-challenge. Serum was collected on days -1, 3 (# HT1, HT8, 678 only), 7, 10, 14, 18, and 20.

At 3 days post challenge (3 DPC) three principal-infected calves were euthanized (HT1, HT8, 678) and full postmortem examinations were performed. Two additional principal-infected calves (# 673 and T7478) were euthanized, and postmortem examinations performed at 7 DPC. The remaining 5 calves (3 principal-infected and 2 sentinels) were euthanized, and postmortem examinations performed at the end of the study (20 DPC). During postmortem examination, the head including the entire upper respiratory tract and central nervous system (brain), trachea and lower respiratory tract, lymphatic and cardiovascular systems, gastrointestinal (GI) tract and urogenital system, and integument were grossly evaluated. Lungs were evaluated for gross alterations such as edema, congestion, discoloration, atelectasis, and consolidation/pneumonia. Cerebrospinal fluid (CSF) was collected by syringe and needle via the atlanto-occipital (C0-C1) joint, and bronchoalveolar lavage fluid (BALF), nasal wash and urine were collected and stored at -80°C until processed for virus isolation/RNA detection. Tissue samples from the respiratory tract, nasal turbinate (rostral and deep), trachea at multiple levels, all lung lobes, gastrointestinal tract and visceral organs (spleen, kidney, liver, heart), tonsils and lymph nodes (retropharyngeal, mandibular, tracheo-bronchial and mesenteric), brain including olfactory bulb, and bone marrow were collected and either fixed in 10% neutral-buffered formalin (Fisher Scientific, Waltham, MA, USA) for histopathologic examination or frozen for reverse transcriptase quantitative PCR (RT-qPCR) and virus isolation.

RNA extraction and reverse transcriptase quantitative PCR (RT-qPCR)

To detect SARS-CoV-2 specific RNA, nucleic acids were extracted from swab samples, whole blood, and tissue homogenates using a magnetic bead based total nucleic acid extraction

system and quantified using the N2 primer/probe set from the CDC 2019-novel coronavirus real-time RT-PCR diagnostic panel as described previously (26). Briefly, swabs in DMEM or 20% weight:volume tissue homogenates in DMEM were combined in equal amounts with RNA stabilization/lysis Buffer RLT (Qiagen, Germantown, MD, USA) and vortexed. Sample lysates were transferred into Taco extraction plates (GeneReach, USA) loaded with GeneReach reagents and extracted following the manufacturer's instructions with minor modifications as previously described (26). Additionally, an exogenous internal positive control was added to the extraction to monitor extraction efficiency and consistency, and downstream inhibition of the RT-qPCR reaction (199).

Following extraction, duplicate RT-qPCR reactions were set up as follows: 5µL of eluent was combined with qScript XLT One-Step RT-qPCR Tough Mix (Quanta BioSsciences, Beverly, MA, USA) and N2 targeted primers/probes (CDC 2019-novel coronavirus real-time RT-PCR diagnostic panel) and run as 20µL reactions on a 96-well PCR plate (BioRad, Hercules, CA, USA). RT-qPCR reactions were carried out on a CFX96 Real-Time thermocycler (BioRad, Hercules, CA, USA) using a 20-minute reverse transcription step and a 45 cycle PCR. A quantitated PCR positive control (IDT, IA, USA; 2019-nCoV_N_Positive Control, diluted 1:100) and four non-template control (NTC) samples were included on every plate. A reference standard curve method using a 10-point standard curve of quantitated viral RNA (USA-WA1/2020 isolate) was used to quantify RNA copy number. A positive Ct cut-off of 38 cycles was used. Data are presented as the mean of the calculated N gene copy number per mL of liquid sample or per gram of a 20% tissue homogenate.

Next-generation sequencing

Virus stocks were sequenced by next generation sequencing (NGS) using the Illumina NextSeq platform (Illumina, San Diego, CA, USA). The consensus sequence of the SARS-CoV-2 Delta variant (B.1.617.2) was found to have 100% sequence similarity to the reference sequence in GISAID (accession number: EPI_ISL_2290769). The Omicron BA.2 virus stock sequence was obtained by mapping reads to the reference sequence for SARS-CoV-2 Omicron BA.2 on GISAID (accession number: EPI_ISL_8643930), followed by extraction of the consensus sequence. One mutation in ORF1ab (NSP6) was present at 54% (A3694V).

Data generated from NGS on the Illumina NextSeq platform (Illumina) was used in conjunction with the VirStrain (200) analysis package to determine the genetic composition (% lineage) of SARS-CoV-2 RNA present in virus stocks, clinical swab samples, and tissue homogenates. SARS-CoV-2 DNA amplicons were generated from viral RNA using the Midnight V.6 protocol (dx.doi.org/10.17504/protocols.io.bwyppfvn), a tiled primer amplification protocol. Library preparation of amplified SARS-CoV-2 DNA for sequencing was performed using a Nextera XT library prep kit (Illumina) following the manufacturer's protocol. The libraries were sequenced on the Illumina NextSeq using 150 bp paired end reads with a mid-output kit. Reads were demultiplexed and parsed into individual sample files that were imported into CLC Genomic Workbench version 21 (Qiagen) for analysis. Reads were trimmed to remove primer sequences and filtered to remove any short and low-quality reads (Q-score < 25). FASTQ files of the filtered and trimmed reads were exported for downstream analysis (**Supplementary Table 3**). Reads were then analyzed on VirStrain (Version 1.12) to determine SARS-CoV-2 lineage/strain. The genome sequences from the virus stocks used for animal challenge were used to construct the reference database for VirStrain lineage assignment used for this study. The

VirStrain software was used to build a library of sample sequence SNPs based on the inoculum used as the reference sequences.

Virus isolation

Samples taken from calves post-challenge with Ct values <30 were subjected to a single passage on Vero-E6/TMPRSS2 cells and subsequent indirect immunofluorescence assay (IFA) using SARS-CoV-2-specific monoclonal antibodies to confirm the absence/presence of infectious virus. Virus isolation was performed on 24-well cell culture plates seeded at a density of $1x10^5$ cells/well with low passage Vero-E6/TMPRSS2 cells 24 hours prior to infection. Tissue homogenates were diluted 1:10 in DMEM, syringe filtered through a 0.22µm filter, and 150µL was added per well in 12 replicates. Diluted homogenates were incubated on cells for 1 hour at 37°C under 5% CO_2 atmosphere, then removed, washed with phosphate buffered saline (PBS), and replaced with 500µL of fresh DMEM supplemented with 5% FBS and 1% antibiotics/antimycotics. Plates were then incubated as described above and observed daily for CPE. After 72 hours, the media was removed, and wells were washed with 1x PBS and then fixed with cold 100% methanol and incubated at -20°C for 10 minutes. Plates were then washed three times with 1x PBS. A mixture of SARS-CoV-2 N- and RBD-specific monoclonal antibodies, produced in-house, were diluted 1:5 in 1x PBS + 1% BSA, added to the wells and incubated at room temperature for 1 hour. Following three washes with 1x PBS + Tween-20 (0.05%), Alexa Flour™ 488 Goat anti-mouse IgG (ThermoFisher Scientific, Waltham, MA, USA) secondary antibody was diluted 1:1000 in 1x PBS + 1% BSA and added to all wells and incubated for 1 hour at room temperature. All wells were then washed and dried and observed with an EVOS fluorescent microscope (ThermoFisher Scientific, Waltham, MA, USA). Mock-

infected and SARS-CoV-2-infected Vero-E6/TMPRSS2 cells were used as negative and positive controls, respectively.

Virus neutralizing antibodies

A microneutralization assay was used to determine SARS-CoV-2 virus neutralizing antibody titers from cattle sera as previously described (43). Briefly, cattle serum was diluted 1:4 and heat-inactivated at 56°C for 30 minutes while shaking. In duplicate wells, 100µL of serum was combined with 100µL of culture media and subjected to 2-fold serial dilutions starting at 1:8 through 1:1024. Separately, SARS-CoV-2 Delta and Omicron BA.2 virus stocks were diluted to 1000 $TCID_{50}$/mL and 100µl added to 100µl of the sera dilutions and incubated for 1 hour at 37°C. Following incubation, 200µl of the virus/serum mixture was transferred to 96-well cell culture plates seeded at approximately $2x10^5$ cells/mL with low passage Vero-E6/TMPRSS2 cells. Serum with known SARS-CoV-2 neutralizing antibody titer was used as a positive control. Virus only and media only wells were also included. The highest serum dilution at which at least 50% of wells showed virus neutralization (NT_{50}) based on the appearance of CPE observed under a light microscope at 96-hours was recorded as the final neutralizing antibody titer.

In a similar manner, serum samples were assayed for neutralizing antibodies against the bovine coronavirus (BCV) Mebus strain (GenBank: U00735.2). Since CPE is not clearly visible with this virus, IFA was used to visualize the presence or absence of neutralizing activity. The IFA procedure was performed as described above for SARS-CoV-2, with the substitution of a BCV specific primary antibody, Z3A5, a monoclonal antibody that targets the spike protein subunit of BCV, kindly provided by Roman Pogranichniy of KSU.

Detection of antibodies by ELISA

Indirect ELISAs using in-house recombinant SARS-CoV-2/Delta receptor-binding domain (RBD) of the spike protein and SARS-CoV-2/Wuhan nucleocapsid (N) proteins were used to detect SARS-CoV-2 specific antibodies in cattle sera, as described previously (201). Briefly, wells were coated with 100ng of the RBD or N proteins in 100µL per well coating buffer and incubated overnight at 4°C. Plates were washed twice with PBS-T (0.5% Tween-20 in PBS), blocked with 200µL per well casein blocking buffer (Sigma-Aldrich) and incubated for 1 hour at room temperature followed by a wash with PBS-T. Serum was diluted 1:400 in casein blocking buffer and 100µL was added to the ELISA plate and incubated for 1 hour at room temperature. Wells were then washed three times with PBS-T. An HRP-labelled goat anti-bovine IgG (H+L) secondary antibody was diluted 1:10,000 and 100µL was added to each well and incubated 1 hour at room temperature. Following five washes with PBS-T, 100µL of TMB ELISA Substrate Solution (Abcam, Cambridge, MA, USA) was added to all wells. After incubation at room temperature for 5 minutes, the reaction was stopped with 100µL of stop solution. The Optical density (OD) of the ELISA plates was read at 450nm on an ELx808 BioTek plate reader (BioTek, Winooski, VT, USA). Bovine serum collected in 2014 was used as negative control to determine the positive cut-off value for these assays. The cut-off value was defined by the average OD of the negative serum + 3X standard deviation. Everything above this cut-off was considered positive.

Further analysis of cattle serum was carried out using the commercial ID-Vet ID Screen SARS-CoV-2 Double Antigen Multi-Species Test Kit (Innovative Diagnostics), targeting the N protein, per manufacturer's instructions.

Histopathology (H&E)

After 7 days in 10% neutral buffered formalin, tissues were transferred to 70% ethanol (ThermoFisher) prior to trimming for paraffin embedding. Bony tissues from the respiratory tract (i.e. nasal cavity, rostral, middle and deep turbinates) were decalcified with Immunocal™ Decalcifier (StatLab, McKinney, TX), diluted 1:2 in nanopure water, for 5 days at room temperature with agitation prior to trimming and paraffin embedding. Tissues were routinely processed and stained with hematoxylin and eosin following standard procedures at the Kansas State Veterinary Diagnostic Laboratory (KSVDL). Veterinary pathologists (unbiased to the treatment groups) examined the slides and provided pathological descriptions. Tissues from naïve calves were used as negative controls for histopathological analysis including immunohistochemistry (IHC) and RNAscope® *in situ* hybridization (ISH), performed at the Louisiana Animal Disease Diagnostic Laboratory (LADDL).

SARS-CoV-2 specific immunohistochemistry (IHC)

IHC was performed as previously described (26) on four-micron sections of formalin-fixed paraffin-embedded tissue mounted on positively charged Superfrost® Plus slides and subjected to IHC using a SARS-CoV-2-specific anti-nucleocapsid rabbit polyclonal antibody. Lung sections from a SARS-CoV-2-infected hamster were used as positive assay controls.

SARS-CoV-2-specific RNAscope® in situ hybridization (RNAscope® ISH)

For RNAscope® ISH, an anti-sense probe targeting the spike protein gene (S; nucleotide sequence: 21,563–25,384) of SARS-CoV-2, USA-WA1/2020 isolate (GenBank accession number MN985325.1) was used as previously described (Advanced Cell Diagnostics [ACD], Newark, CA, USA). Five-micron sections of FFPE tissue were mounted on positively charged Superfrost® Plus Slides (VWR, Radnor, PA). The RNAscope® ISH assay was performed using

the RNAscope 2.5 LS Duplex Reagent Kit (Advanced Cell Diagnostics, Newark, CA) on the automated BOND RXm platform (Leica Biosystems, Buffalo Grove, IL) with modifications for single-plex detection. Tissue sections were subjected to automated baking and deparaffinization followed by heat-induced epitope retrieval (HIER) using a ready-to-use EDTA-based solution (pH 9.0; Leica Biosystems) at 95 °C for 15 min. Subsequently, tissue sections were treated with a ready-to-use protease (RNAscope® 2.5 LS Protease) for 15 min at 40 °C followed by a ready-to-use hydrogen peroxide solution for 10 min at room temperature. Slides were then incubated with the SARS-CoV-2 S-specific probe mixture for 2 h at 40 °C. The signal was amplified using amplifiers 1 through 3 (AMP1 through AMP3) followed by AMP8 through AMP10 as recommended by the manufacturer. The signal was subsequently detected by incubating with 3,3'-diaminobenzidine (DAB) for 20 minutes and the BOND DAB Enhancer (Leica Biosystems) for an additional 20 minutes at room temperature. Slides were counterstained with a ready-to-use hematoxylin for 5 min, followed by a ready to use bluing solution for 2 minutes. Slides were finally rinsed in deionized water, dried in a 60 °C oven for 30 min, and mounted with Ecomount® (Biocare, Concord, CA, USA). Lung tissue from a SARS-CoV-2-infected Syrian hamster was used as a positive assay control.

Results

Clinical evaluations and detection of common bovine pathogens

Prior to the challenge with SARS-CoV-2, calves were examined by a veterinarian. One calf, HT9, was suspected to have mild respiratory signs, and elevated body temperature, cough, and nasal discharge were noted. Coughing was also noted in calf 678 during the acclimation period. Therefore, nasal swabs collected at -1 DPC, were submitted to the KSVDL for the Bovine Respiratory Bacterial and Viral Panel PCR testing (**Supplementary Table 1**). The

results revealed that all calves were negative for bovine coronavirus but were positive for influenza D virus (IDV), *Mannheimia haemolytica*, and *Pasteurella multocida*. Provided this information, RNA extracted from respiratory and lymphoid tissues at 3 DPC was pooled and tested via RT-qPCR for the presence of IDV. RNA from both SARS-CoV-2 and IDV were detected in the nasal turbinate and trachea/bronchi of calf HT1 and the mandibular lymph node of calves HT1 and 678 (**Supplementary Table 2**); animal 678 was showing respiratory signs before SARS-CoV-2 challenge.

Following SARS-CoV-2 challenge, health checks and rectal temperatures were recorded daily. Coughing was documented in calf HT6 at 4 and 14 DPC, and coughing and nasal discharge were noted in calf HT9 at 5 and 18 DPC. Rectal temperatures did not exceed 103.4°F during the study period in any of the animals enrolled in the study (data not shown).

Detection of SARS-CoV-2 RNA in clinical samples and tissues

Clinical samples, including nasal, oral, and rectal swabs, and whole blood were tested for the presence of SARS-CoV-2 RNA by RT-qPCR assay (**Figure 4.2A**). Samples which were collected prior to challenge (-1 DPC) were negative for SARS-CoV-2 RNA. Six of the eight challenged calves shed SARS-CoV-2 RNA during the first 2 DPC (**Figure 4.2A**). At 1 DPC, three out of eight challenged calves (673, 678, 88) had SARS-CoV-2 RNA present in nasal swabs; all oral swabs and rectal swabs were negative. At 2 DPC, three different calves (HT1, HT9, HT6), all in the primary challenge group, had SARS-CoV-2 RNA detected in nasal swabs. One calf (HT1) had SARS-CoV-2 RNA also detected in an oral swab at 2 DPC. Whole blood and all swabs collected after 2 DPC (3, 4, 5, 7, 10, 14, 18, 20 DPC) were negative for the presence of SARS-CoV-2 RNA. No SARS-CoV-2 RNA was detected in swabs or blood collected from sentinel calves (n=2; T7477 and HT2) at any time point.

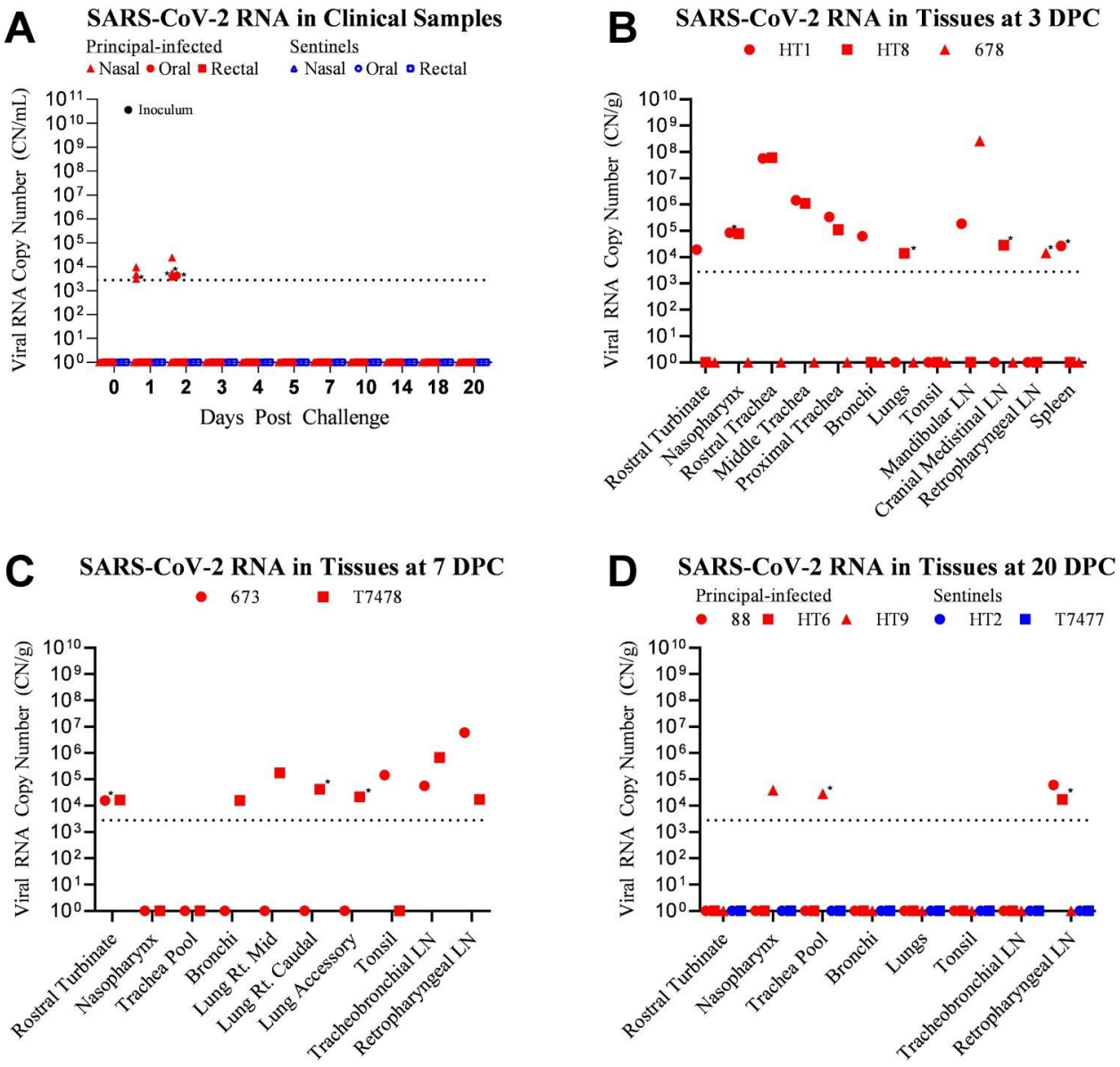

Figure 4.2 Detection of SARS-CoV-2 RNA in clinical samples and tissues

Detection of SARS-CoV-2 RNA in clinical samples and tissues. RT-qPCR was performed on nasal, oral, and rectal swabs collected from principal-infected and sentinel calves (A), and on various tissues homogenates of calves euthanized at 3 (B), 7 (C), and 20 (D) days post-challenge (DPC) to detect the presence of SARS-CoV-2 specific RNA. Mean (n = 2) viral RNA copy number (CN) per mL (A) or per gram of tissue (B, C, D) is reported based on the detection of SARS-CoV-2 nucleocapsid gene in individual animals. Only a subset of tissues which were collected and tested are represented in this figure. Asterisks (*) indicate samples with one of two RT-qPCR reactions positive. The limit of detection for this RT-qPCR assay is indicated by the dotted lines.

Three calves from the principal-infected group (HT1, HT8, 678) were euthanized at 3 DPC, and another two calves (673, T7478) from this group were euthanized at 7 DPC to evaluate SARS-CoV-2 distribution in tissues and pathological alterations during different stages of infection. At 3 DPC, SARS-CoV-2 RNA was present in upper respiratory tissues of two calves (HT1 and HT8) (**Figure 4.2B**). The spleen, mandibular, cranial mediastinal, and retropharyngeal lymph nodes were also occasionally positive for SARS-CoV-2 RNA at 3 DPC. At 7 DPC, SARS-CoV-2 RNA was present in the nasal turbinate, tracheobronchial, and retropharyngeal lymph nodes of both calves 673 and T7478 (**Figure 4.2C**). The tonsil of calf 673 was also positive at 7 DPC. Additionally, three lung lobes (right middle, right caudal, and accessory) and the bronchi of calf T7478 had SARS-CoV-2 RNA present at 7 DPC.

The five remaining calves (three principal-infected animals and two sentinels) were euthanized at 20 DPC. Of the principal-infected group, two calves (88, HT6) had SARS-CoV-2 RNA present in the retropharyngeal lymph node (**Figure 4.2D**). The nasopharynx and trachea of principal-infected calf HT9 were also positive for SARS-CoV-2 RNA at 20 DPC. There was no SARS-CoV-2 RNA detected in any tissues of the two sentinel calves (HT2, T7477) evaluated at 20 DPC.

Competition between SARS-CoV-2 Delta and Omicron BA.2 VOCs in co-infected calves

Calves were challenged with a 50/50 mixture of SARS-CoV-2 Delta and Omicron BA.2 VOCs. To evaluate the *in vivo* competition between these two strains, next generation sequencing (NGS) was used in conjunction with the VirStrain software package to identify the proportion of each virus strain present in the inoculum as well as clinical samples, and tissues which contained SARS-CoV-2 RNA (**Figure 4.3**). The inoculum contained 53.2% Omicron

BA.2 VOC and 46.8% Delta VOC. Of the seven nasal/oral swabs which were positive on 1 and 2 DPC, only one nasal swab at 2 DPC from calf HT9 had sufficient sequencing coverage and depth to provide reliable results; the nasal swab of calf HT9 at 2 DPC was 100% Delta VOC (**Supplementary Table 3**). Trachea samples collected at 3 DPC from calves HT1 and HT8 were also analyzed by NGS and found to be 100% Delta VOC (**Figure 4.3**). Additionally, one retropharyngeal lymph node collected at 7 DPC from calf 673 was also found to be 100% Delta VOC.

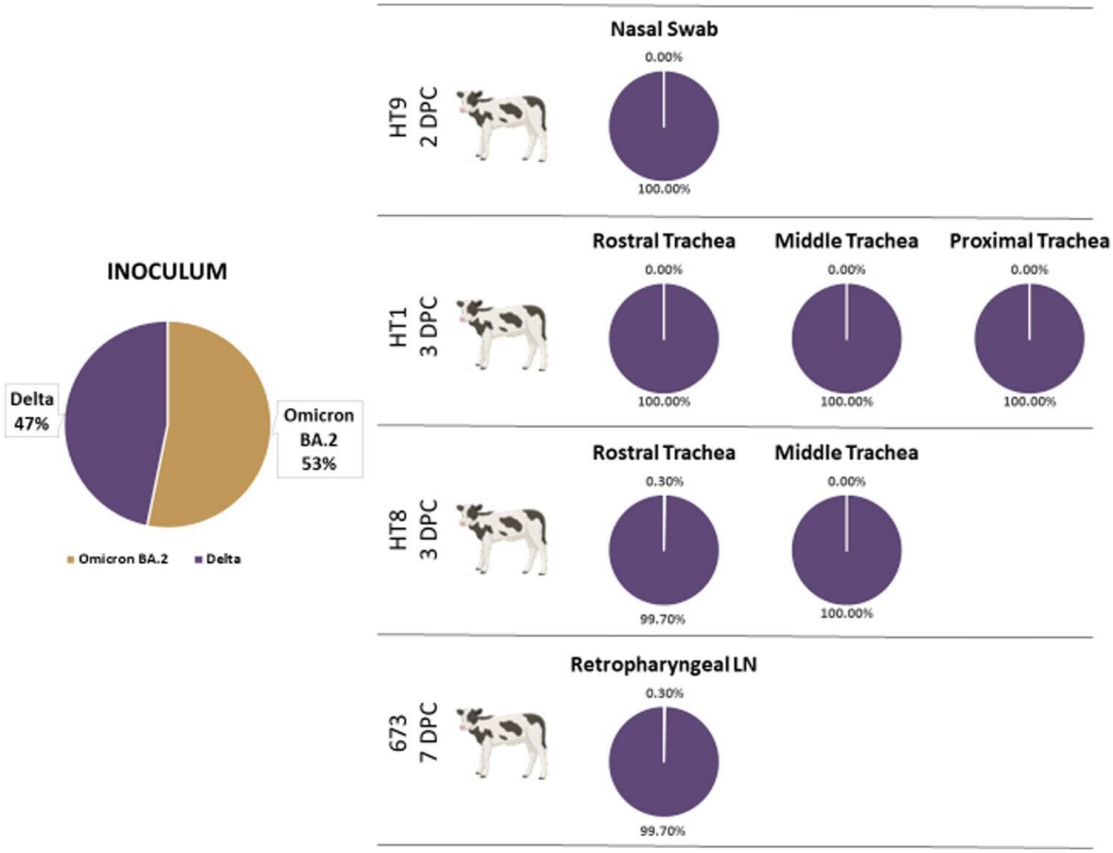

Figure 4.3 Identification of SARS-CoV-2 variants of concern in nasal swab and tissues

. Identification of SARS-CoV-2 variants of concern in nasal swab and tissues. Next-generation sequencing was used to determine the percent composition of the SARS-CoV-2 variants of concern Delta and Omicron BA.2, present in the inoculum, swab samples and tissues collected from the co-infected calves. Reads were analyzed using the VirStrain (Version 1.12) software package to determine the genetic composition (% of each lineage) of SARS-CoV-2 RNA present in samples. The genome sequences from the virus stocks used in our challenge experiment were used to construct the reference database for VirStrain lineage assignment

Isolation of virus from tissues.

The presence of SARS-CoV-2 RNA in clinical samples and tissues collected from the calves warranted further evaluation for the presence of infectious virus. Samples with Ct values < 30 were selected as candidate samples for virus isolation. This included tissue homogenates produced from the rostral trachea sections of calves HT1 and HT8 at 3 DPC, the mandibular lymph node from calf 678 at 3 DPC, and the retropharyngeal lymph node from calf 673 at 7 DPC. Homogenates were divided among 12 replicate wells for each sample. Of the twelve replicates, two wells of the rostral trachea from calf HT1 showed CPE, and three wells of the mandibular lymph node from calf 678 showed CPE after a single passage on Vero-E6/TMPRSS2 cells. All wells were fixed and subjected to IFA for confirmation of SARS-CoV-2 antigen presence (**Supplementary Figure 4.1**). The wells with CPE were IFA positive; none of the wells without CPE, or negative control wells, were fluorescence positive, suggesting there was no SARS-CoV-2 replication in the wells without CPE. NGS analysis of the virus isolated from the rostral trachea of calf HT1 showed no changes in the RBD region of the S gene sequence compared to the sequence of the SARS-CoV-2 Delta inoculum. The sequence obtained from the mandibular lymph node of calf 678 had insufficient coverage to make a detailed assessment.

ELISAs

Indirect ELISAs, developed *in-house*, targeting SARS-CoV-2/Delta RBD and SARS-CoV-2/Wuhan N were used to screen cattle serum for SARS-CoV-2-specific antibodies. All serum was negative for antibodies against the SARS-CoV-2 RBD and N protein prior to challenge. SARS-CoV-2/Delta RBD-specific antibodies were detected at 14 and 20 DPC in calf HT9 (**Figure 4.4A**). Surprisingly, ELISA-antibodies against the SARS-CoV-2 N protein were not detected in any cattle during the study period of 20 days, although calf HT9 had elevated OD

readings at 14 DPC, however it was below the positive cut-off value (**Figure 4.4B**). These results were confirmed with the ID-Vet ID Screen SARS-CoV-2 Double Antigen Multi-Species Test Kit (Innovative Diagnostics) targeting the SARS-CoV-2 N protein (data not shown). The sentinel calves did not produce ELISA-positive RBD- or N-specific antibodies during the study period.

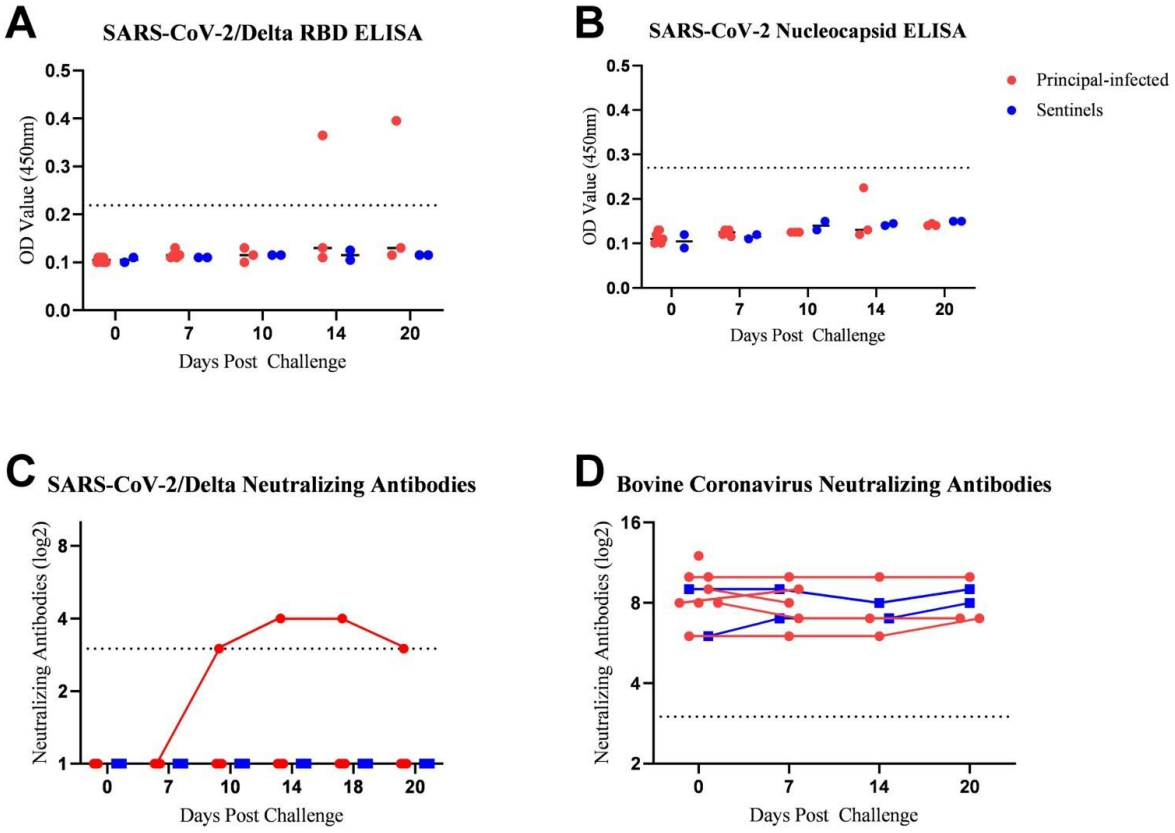

Figure 4.4 Serology of SARS-CoV-2 infected calves

Serology of SARS-CoV-2 infected calves. Indirect ELISAs using in-house produced recombinant SARS-CoV-2/Delta receptor-binding domain (RBD) of the spike protein (A) and SARS-CoV-2/Wuhan-like nucleocapsid (N) protein (B), for detection of SARS-CoV-2 specific antibodies in cattle sera (Bold et al. 2022). The cut-off (dotted line) was determined by the average OD value of negative serum samples (n = 12) collected from cattle in 2014 + 3X the standard deviation. Serum was also tested for the presence of SARS-CoV-2 neutralizing antibodies using a classic virus neutralization assay employing the Delta VOC (C) or Omicron BA.2 VOC (data not shown) with serum dilutions starting at 1:8 (dotted line). Data is represented as log2 of the reciprocal of the dilution where one of two replicates exhibited 100% neutralization of the input virus (1000 TCID50/mL). Likewise, serum was tested for the presence of neutralizing antibodies for bovine coronavirus (D) using the Mebus strain of Bovine Coronavirus

Virus neutralizing antibodies

Serum was evaluated for the presence of neutralizing antibodies against both SARS-CoV-2 Delta and Omicron BA.2, as well as bovine coronavirus. No SARS-CoV-2 neutralizing antibodies were present prior to challenge. At 10 DPC, one of three remaining principal-infected calves, animal HT9, had developed neutralizing antibodies against SARS-CoV-2 Delta, but not Omicron BA.2; the neutralizing titer was maintained until the termination of the study at 20 DPC (**Figure 4.4C**). The sentinel calves did not produce neutralizing antibodies against either SARS-CoV-2 VOC during the study period. These results were confirmed using a commercial SARS-CoV-2 surrogate virus neutralization test kit (GenScript; data not shown). All calves (principal infected and sentinels) had neutralizing antibody titers against bovine coronavirus prior to challenge, which persisted through the study period, although no significant increase was observed during the study period (**Figure 4.4D**).

Gross pathology

On postmortem examination at 3 DPC, the only significant gross lesions observed were present in the lung of principal-infected calf HT1 and consisted of mild multifocal consolidation of the right cranial and right and left middle lung lobes, affecting less than 5% of the total lung parenchyma. No significant gross lesions were observed for either of the calves euthanized at 7 DPC. At 20 DPC, one principal challenged calf, animal HT9, had mild to moderate multifocal consolidation of the right cranial lobe affecting less than 5% of the total lung parenchyma; no significant gross lesions were observed for the other two principal-infected or the two sentinel calves.

Histopathology

Histological evaluation was performed on tissue sections from all organs collected during postmortem examination at 3, 7 and 20 DPC for all animals in the study. IHC for viral antigen and RNAscope® ISH for viral RNA was performed on selected tissues (nasal turbinates, nasopharynx, trachea, lung and selected lymph nodes) from all animals at 3, 7 and 20 DPC. Histological lesions were characterized by mild to moderate, multifocal, non-suppurative inflammation with mild to severe lymphoid hyperplasia in the upper respiratory tract including the nasal turbinates, oropharynx, trachea, and bronchi. Representative histological lesions at 3, 7, and 20 DPC are provided in **Figure 4.5**, **Figure 6**, and **Supplementary Figure 4.2**, respectively. Histological changes in calves HT1 and 678 at 3 DPC and calves T47478 and 673 at 7 DPC were the most prominent and represent active inflammatory lesions. Overall, lymphoid hyperplasia was present in the form of dense aggregates of lymphocytes, plasma cells, and macrophages commonly arranged as immature follicular structures in the submucosa at 3 DPC throughout the respiratory tract, becoming more organized and mature and occurring among, and extending deeper up to, the submucosal glands by 7 DPC. Turbinate sections and nearly all tracheal sections had mild to moderate segmental inflammation in the respiratory epithelium and submucosa that was most prominent at 3 and 7 DPC (**Figures 4.5 and 4.66**). Inflammation was observed predominantly within the superficial submucosa, as loose aggregates or dense sheets of mononuclear cells. Submucosal edema was infrequent, occurring segmentally in regions where inflammatory cells infiltrated the epithelium. Cellular infiltrates in the respiratory epithelium were observed as individual or small clusters of primarily mononuclear cells. Neutrophilic infiltrates were infrequent and observed scattered in the respiratory epithelium and subjacent submucosa commonly in foci where epithelial changes and submucosa edema were noted. The

epithelial changes were characterized by mild to moderate attenuation of the epithelium with disorganization and thinning and flattening of the epithelium with occasional segmental loss of cilia (**Figure 4.5, Figure 6A and inserts**). Epithelial necrosis, when present, was observed as shrunken or vacuolated cells with karyorrectic and pyknotic nuclei. Occasionally, inflammation and cellular degradation was observed in the glandular epithelium. Similar inflammation, albeit less severe, was observed in sections of the nasal turbinates and ethmoturbinates (**Figures 4.5 and 4.6; panels C and D)**. Cellular debris and inflammatory cells were infrequently found in small clusters and as individual cells within the airway lumen and commonly attached to the cilia (**Figure 4.6B and insert, and 4.6C).**

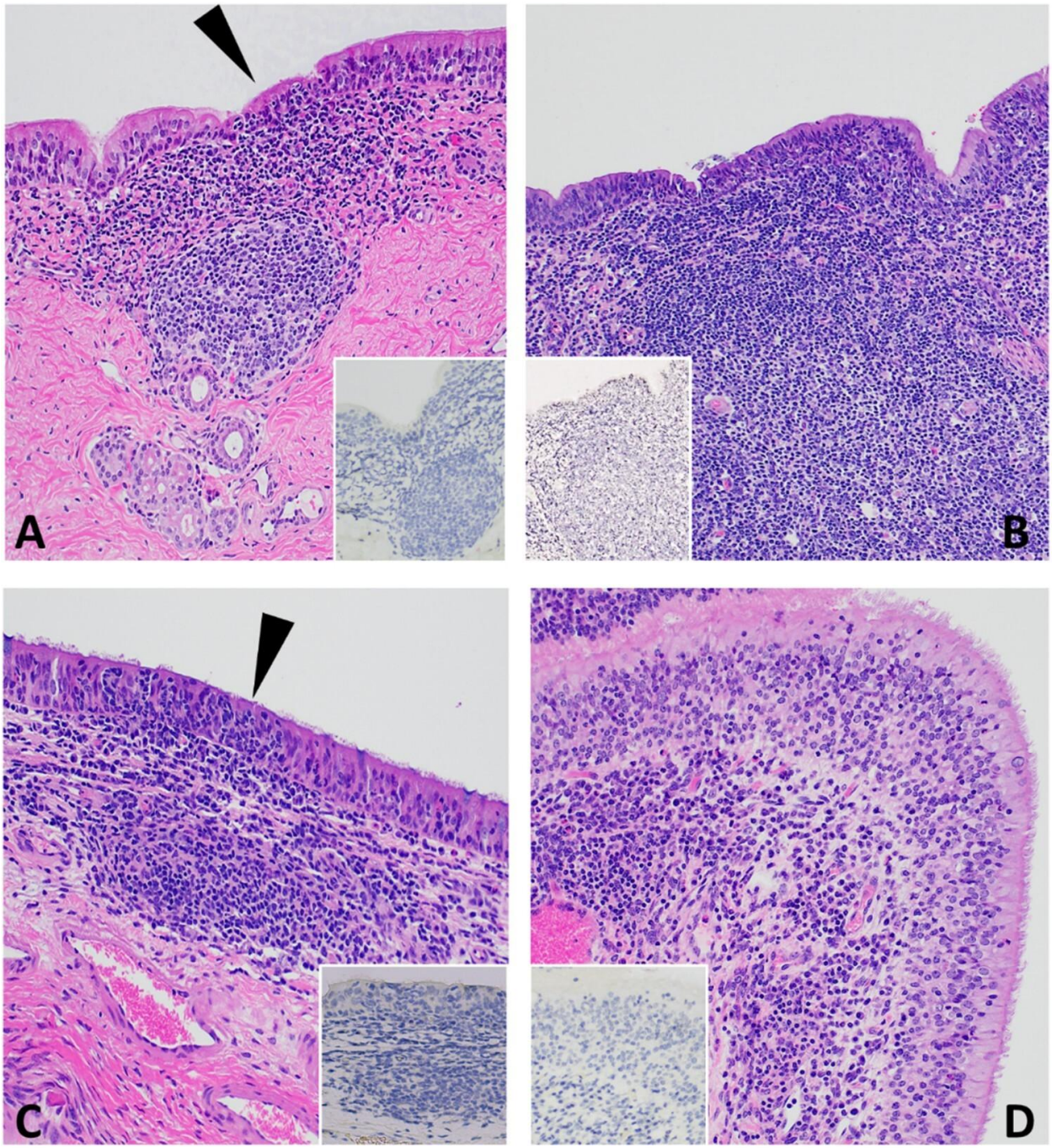

Figure 4.5 Histopathology of 3 DPC respiratory tissues from calf HT1

Histopathology of 3 DPC respiratory tissues from calf HT1. At 3 DPC, (A) in the trachea, there was mild and segmental attenuation of the respiratory epithelium with loss of cilia, lymphocyte and/or neutrophil transmigration through the epithelium, individual cellular degeneration and necrosis, and occasional accumulation of cellular debris on the epithelial surface (arrowhead). Dense sheets of mononuclear inflammatory cells expanded into the lamina propria and commonly follicular aggregates of lymphocytes, plasma cells and macrophages arranged into

loose aggregates or partially organized follicular structures; SARS-CoV-2 antigen was not detected by IHC (insert). (B) Similar segmental attenuation of the respiratory epithelium was noted in the bronchi with cellular degeneration/necrosis of individual epithelial cells, lymphocytic and neutrophilic transmigration. Loose infiltrates of lymphocytes and a lesser number of neutrophils were observed in the superficial mucosa and mixed lymphocytic and histiocytic infiltrates, many arranged in follicular aggregates expanding into the superficial and deep lamina propria; SARS-CoV-2 viral antigen was not detected (insert). (C) The rostral turbinates were characterized by lymphoplasmacytic or neutrophilic rhinitis with epithelial transmigration of inflammatory cells (arrowhead) and segmental loss of cilia. Mixed lymphocytic and histiocytic inflammation multifocally expanded the subjacent lamina propria and the interstitium separating submucosal glands. IHC for SARS-CoV-2 viral antigen was negative (insert). (D) The olfactory mucosa contained similar lymphoplasmacytic or histiocytic inflammation within the lamina propria and the interstitum separating submucosal glands; SARS-CoV-2 viral antigen was not detected (insert). H&E and Fast Red, 40× total magnification

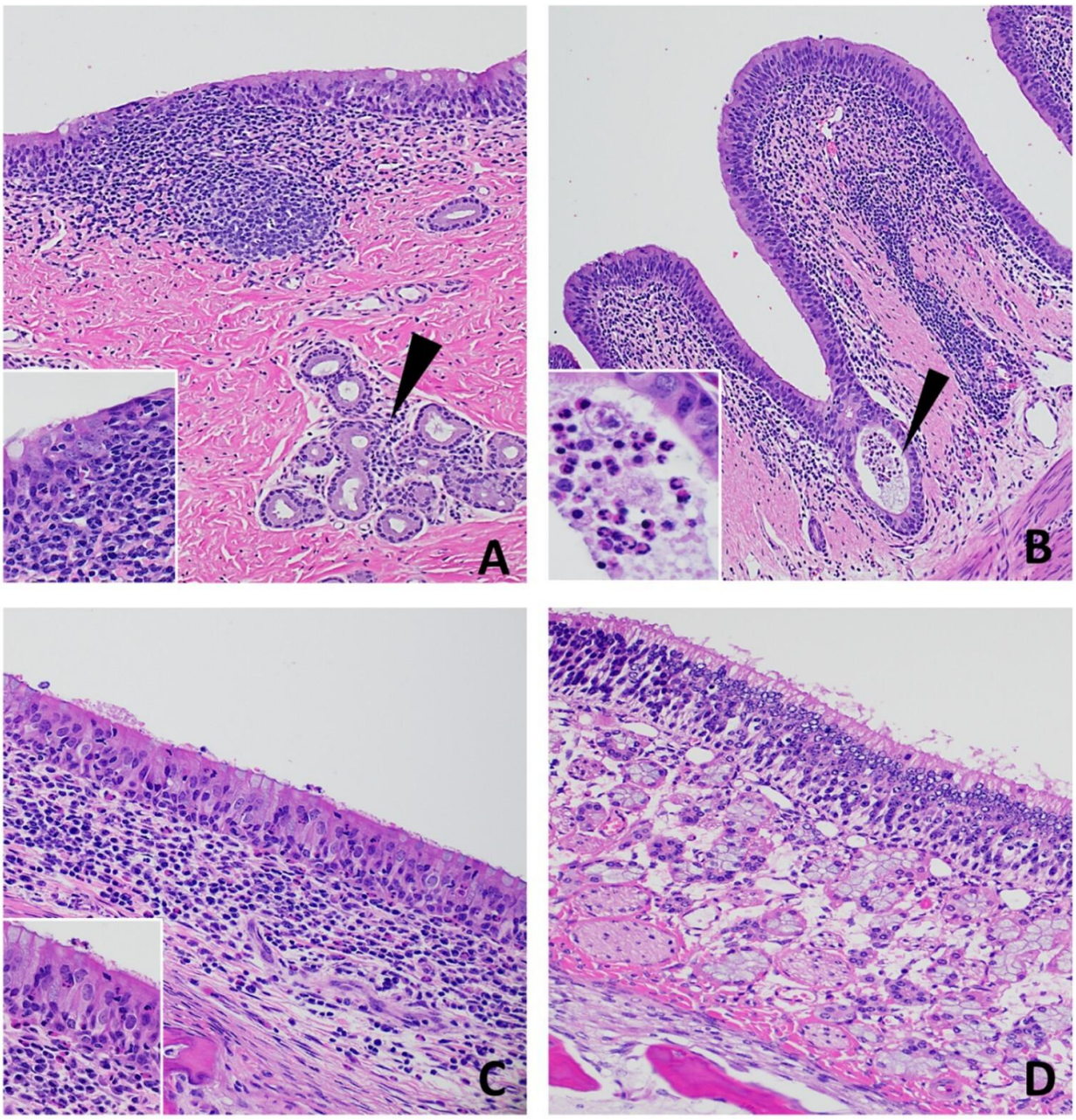

Figure 4.6 Histopathology of 7 DPC respiratory tissues from calf 673

Histopathology of 7 DPC respiratory tissues from calf 673. (A) There was moderate, segmental attenuation and disorganization of the respiratory epithelium with loss of cilia, moderate lymphocyte and/or neutrophil transmigration and individual cellular degeneration and necrosis (Insert). Mononuclear inflammatory cells expanded the lamina propria and were arranged in dense follicular aggregates. Inflammatory cells (lymphocytes and plasma cells) also infiltrated the interstitium between submucosal glands (arrowhead). (B) Mild segmental attenuation of the respiratory epithelium in the bronchi with infrequent cellular degeneration/necrosis. Cellular debris and degenerate neutrophils sporadically accumulated in the lumen or on the epithelial surface (arrowhead and insert). Lymphocytes, plasma cells, macrophages, and lesser numbers of

neutrophils expanded the submucosa and extended between submucosal glands. (C) The rostral turbinates had lymphoplasmacytic and neutrophilic infiltrates with epithelial transmigration of inflammatory cells onto the epithelial surface with segmental loss of cilia (Insert). Loose and dense sheets of mixed lymphocytes, histiocytes, and neutrophils infiltrated the subjacent lamina propria and between glands. (D) The olfactory mucosa of the ethmoturbinates was normal. H&E, 40-400× total magnification.

Inflammation in primary and secondary bronchi was most pronounced at 3 DPC and was characterized by loose infiltrates of lymphocytes, macrophages and plasma cells in the submucosa that was markedly expanded by multifocal to coalescing lymphoid follicles (follicular hyperplasia), similar to the changes seen in the trachea. Occasional clusters of or individual neutrophils were observed scattered within the epithelium and submucosa. Loose, less severe inflammation was observed in the submucosa, accompanied by mild follicular hyperplasia at 7 DPC (**Figure 4.6**) and 20 DPC (**Supplementary Figure 4.2**).

By 20 DPC, the microscopic alterations were most consistent with lymphoid hyperplasia with minimal epithelial changes (**Supplementary Figure 4.2**). IHC and ISH performed on selected tissue sections with lesions (turbinates, trachea, nasopharynx, lung and lymph nodes) from cattle at 3, 7 and 20 DPC failed to identify viral antigen or viral RNA in the lesions despite these tissues being RT-qPCR positive for viral RNA and some being positive by virus isolation.

Lung histology

At 3 DPC, histological evaluation of calf HT1 lung sections with gross evidence of consolidation revealed compressed and congested alveoli (atelectasis). Lung sections from calf HT8 demonstrated several areas of atelectasis in the right cranial lung lobe. As mentioned above, IHC for viral antigen was negative. Lung sections from calf 678 from the right middle and caudal lung lobes had multiple regions of chronic-active, purulent broncho-interstitial pneumonia with abscess formation and intralesional coccobacillary bacteria. These regions were

characterized by central foci of necrosis, mineralization, and large numbers of degenerate inflammatory cells bordered by highly vascularized granulation tissue which in turn was bordered by dense layers of fibrosis (abscess); adjacent lobules were compressed and had alveoli filled with fibrin and mixed inflammatory cell infiltrates; in some regions small coccobacilli occurred in alveolar spaces. IHC for viral antigen was negative as was RT-qPCR. Lung lesions were most consistent with a chronic-active bacterial infection.

Aside from the inflammatory changes described in bronchi (see above and **Figure 6 and Supplementary Figure 4.2**), no significant lesions were seen in the lungs of cattle at 7 and 20 DPC.

Discussion

Cattle are an important source for global food security and economic stability for a large fraction of the world's population. Humans have a long history of dependency on cattle and this close relationship creates opportunities for zoonotic spillover. Human coronavirus OC43, a Betacoronavirus which accounts for 10-30% of common colds in humans, is believed to have spilled over from cattle to humans relatively recently (12, 202). Interestingly, a high seroprevalence of influenza D virus (IDV) amongst cattle workers has been reported which is suggestive of extensive exposure of these workers to IDV from cattle (203). The evidence of previous cross-species viral transmission between cattle and humans and the close interaction between these two species provides the rationale for continued evaluation of cattle for their susceptibility to SARS-CoV-2.

In the present study, we evaluated the susceptibility and transmission of two SARS-CoV-2 variants of concern, Delta and Omicron BA.2, in 4-month-old male Holstein calves. During the 20-day study period, clinical samples were collected, and tissues were harvested from principal

and sentinel calves which were euthanized at 3 (n=3 principal infected), 7 (n=2 principal infected), and 20 DPC (n=5; three principal infected, two sentinels). The results of this study indicate that calves have low susceptibility to the SARS-CoV-2 Delta VOC, which outcompeted the Omicron BA.2 VOC; these data could also suggest that calves are non-permissive to Omicron VOC BA.2. Evidence for this is provided by next-generation sequencing (NGS) data, which revealed the presence of only SARS-CoV-2 Delta VOC in nasal swabs and tissues. Additionally, neutralizing antibodies were generated against SARS-CoV-2 Delta VOC, but not the Omicron BA.2 VOC. Virus isolated from tracheal and lymphoid tissues from two calves at 3 DPC confirmed the presence of an active infection with the Delta VOC.

Previous SARS-CoV-2 challenge studies in cattle, which used Wuhan-like SARS-CoV-2 isolates, including the TGR1/NY/20 isolate, with a similar administration route and dose range as in our study, resulted in very limited infections and only transient serological responses (29, 79, 138). Several findings from our challenge study with the Delta and Omicron BA.2 VOCs are distinct from those previous experiments. First, SARS-CoV-2 RNA was detected in nasal and/or oral swabs in our study from the majority of principal infected animals (six of the eight challenged calves, i.e. 75%) within the first 2 DPC, compared to only 33% of calves in each of the other reported studies (29, 79, 138). Second, we observed that out of the 31 fresh tissue samples which were collected during postmortem examination at 3 DPC from principal-infected calves, 12 tissues (36%) were positive for SARS-CoV-2 RNA. Infectious virus was also isolated from the rostral trachea section of one calf and the mandibular lymph node of another one at 3 DPC. Furthermore, at 7 DPC, SARS-CoV-2 RNA was still detectable in 8/26 tissues (31%) collected from two principal-infected calves. SARS-CoV-2 RNA was also detected in 3/26 tissues (12%) which were collected at 20 DPC from the remaining principal-infected calves.

Conversely, Falkenberg et al. reported detection of SARS-CoV-2 RNA only in the tracheobronchial lymph node of one calf at 9 DPC and did not isolate any virus from swabs or tissues during the study; however, SARS-CoV-2 RNA was detected via *ISH*. Bosco-Lauth et al. also isolated SARS-CoV-2 from the trachea of 1/3 challenged cattle at 3 DPC, although 9 other tissues, including those of the respiratory tract, systemic organs and lymph nodes, were negative for infectious virus and SARS-CoV-2 RNA. Previous studies also reported only transient serological responses in SARS-CoV-2 challenged cattle. In contrast, one calf in our study seroconverted and maintained neutralizing antibody titers until the study's termination on 20 DPC. Overall, our study resulted in a greater proportion of calves shedding SARS-CoV-2 RNA and harboring viral RNA in tissues, with one of the three principal-infected calves remaining after 7 DPC maintaining a neutralizing antibody response. These findings may indicate that cattle are more susceptible to SARS-CoV-2 Delta VOC than the Wuhan-like SARS-CoV-2 isolates which have been used for cattle infection previously (29, 79, 138).

Similar to the study by Ulrich et al. (2020), all calves admitted to our study had varied levels of neutralizing antibody titers against bovine coronavirus (BCV), although we did not detect any BCV RNA in nasal swabs collected prior to challenge, suggesting there was no active BCV infection in the calves enrolled in the study. Consistent with what has been previously reported by Ulrich and colleagues, we did not see any cross-protection provided from prior BCV infection (138). One calf (HT9) in our study had clinical symptoms consistent with mild Bovine Respiratory Disease (BRD) complex prior to SARS-CoV-2 challenge. Interestingly, this calf was the only animal that seroconverted and had low levels of SARS-CoV-2 RNA present in upper respiratory tissues at 20 DPC. This may suggest that the health and immune status of this animal at the time of SARS-CoV-2 challenge might have influenced the course of disease. Previous

studies have determined that health status can affect expression and distribution of host ACE2 receptors (204, 205); this may have contributed to different disease progression in this calf. Additionally, all calves were found to have an underlying infection with influenza D virus (IDV), evident by positive RT-qPCR from nasal swabs collected pre-challenge. Influenza D virus (IDV) is a newly described virus of cattle, not commonly associated with BRD complex but was included in this diagnostic panel as IDV has recently been detected in approximately 12% of clinical samples submitted for BRD testing at KSVDL. Further testing revealed the presence of IDV RNA and SARS-CoV-2 RNA in the same respiratory and lymphoid tissues collected at 3 DPC (**Supplementary Table 2**). IDV can be an incidental finding in cattle or occasionally may present as tracheitis (206, 207). Histological evidence of acute inflammation in the turbinates, trachea and bronchi at 3 DPC with continuation and maturation of the inflammation and lymphoid hyperplasia at 7 DPC and 20 DPC in these animals are consistent with previous SARS-CoV-2 lesions in permissive species as well as those that are less permissive (26, 189). Although attempts were made to localize SARS-CoV-2 antigen or viral RNA within tissues, this testing was negative; however, RT-qPCR did confirm the presence of SARS-CoV-2 RNA in the tissues with lesions. The discrepancy in these results may be attributed to variability in sampling of tissue that was collected for formalin fixation and fresh tissue processing, where a low number of cells were infected and not present in both sample types. Infections with SARS-CoV-2 and IDV have similar target tissues and would be histologically indistinguishable without confirmatory antigen/viral RNA detection within the lesion (26, 207). At this moment, it is not clear whether the presence of IDV infection increases, reduces or if it is neutral for the susceptibility to SARS-CoV-2 infection.

Currently, there is no evidence that cattle serve as a primary reservoir or amplifying host for SARS-CoV-2. This is supported by the results of our study and others, in which low levels of SARS-CoV-2 shedding are present only for a short period after infection; and under experimental conditions, there is no onward transmission to sentinel calves. However, there is now serological evidence of naturally infected cattle in Germany and Italy, where sampling periods coincided with the Delta VOC wave of transmission in humans (48, 77). In Germany, Wernike et al. reported that 11/1,000 cattle were antibody-positive in 83 farms sampled, suggesting these were individual spillover events, likely from infected humans. However, in Italy, Fiorito et al. reported 13/24 lactating cattle which were sampled on a single farm had neutralizing antibodies against SARS-CoV-2; the latter data are suggestive of transmission occurring within the herd. Interestingly, SARS-CoV-2 RNA was isolated from nasal and/or rectal swabs collected from cattle during the Delta VOC wave of transmission in both India and Nigeria, suggesting recent exposure (63, 196). Together, these data support the conclusion that during the Delta VOC wave of transmission in humans, there were instances of spillover of SARS-CoV-2 from humans into cattle. It is conceivable that spillover had also occurred earlier in the pandemic, however cattle were not included in surveillance efforts at that time. Epidemiological evidence of cattle infections only became apparent when enhanced surveillance efforts were put into place as the SARS-CoV-2 pandemic continued and when more focus was placed on surveillance in animals. Most importantly, the findings of our study in conjunction with evidence of naturally infected cattle during the Delta VOC surge in humans, support the conclusion that cattle are more susceptible to SARS-CoV-2 Delta VOC than the previously used Wuhan-like SARS-CoV-2 lineages. Several studies have provided clear evidence that SARS-

CoV-2 VOCs have expanded their host range due to key amino acid substitutions in the RBD of the Spike protein which alter the binding affinity with host ACE2 receptors (190, 191, 193).

While human to human transmission continues to be the main driver for SARS-CoV-2 transmission, it has become apparent throughout the pandemic that *One Health* measures must be implemented for comprehensive monitoring of SARS-CoV-2 spillover transmissions. Infection of SARS-CoV-2 in cattle, other ruminant species, or the diverse range of mammalian species on the susceptible animal species list (WHO) provide opportunities for viral evolution via adaptive mutations and possibly recombination with other SARS-CoV-2 strains or related geno- and pathotypes with the potential to impact both animal and public health. Although cattle do not seem to be highly susceptible to currently circulating strains of SARS-CoV-2, there is potential for this to change with future emerging virus variants. Therefore, it is critical that agriculturally important species which have close contact with humans, such as cattle and other domestic and wild ruminants, are included in national and international surveillance efforts and are evaluated for their susceptibility to newly emergent SARS-CoV-2 VOCs when sufficient evidence is provided (16).

Acknowledgments

We thank the staff of KSU Biosecurity Research Institute, the histology laboratory at the Kansas State Veterinary Diagnostic Laboratory (KSVDL), members of the Histology and Immunohistochemistry sections at the Louisiana Animal Disease Diagnostic Laboratory (LADDL), the Comparative Medicine Group staff at Kansas State University and technical support from Yonghai Li and Baolin Wang, and of KSU. We also thank Kyeong-Ok Chang for the Vero E6/TMPRSS2 cells used in these studies, Roman Pogranichniy for providing the bovine coronavirus antibodies. The SARS-CoV-2/Delta (hCoV-19/USA/NYMSHPSP-PV29995/2021;

lineage B.1.617.2, clade GK) strain was obtained from Viviana Simon (Mount Sinai Pathogen Surveillance program) via Michael Schotsaert (Icahn School of Medicine at Mount Sinai), and the SARS-CoV-2 Omicron BA.2 strain (was acquired from BEI Resources (NR-56520; Manassas, VA, USA).

Disclosure statement

The J.A.R. laboratory received support from Tonix Pharmaceuticals, Xing Technologies and Zoetis, outside of the reported work. J.A.R. is inventor on patents and patent applications on the use of antivirals and vaccines for the treatment and prevention of virus infections, owned by Kansas State University, Manhattan, KS, USA. The M.S. laboratory has received unrelated research funding in sponsored research agreements from ArgenX BV, Moderna, 7Hills Pharma and Phio Pharmaceuticals, which has no competing interest with this work. The A.G.-S. laboratory has received research support from GSK, Pfizer, Senhwa Biosciences, Kenall Manufacturing, Blade Therapeutics, Avimex, Johnson & Johnson, Dynavax, 7Hills Pharma, Pharmamar, ImmunityBio, Accurius, Nanocomposix, Hexamer, N-fold LLC, Model Medicines, Atea Pharma, Applied Biological Laboratories and Merck, outside of the reported work. A.G.-S. has consulting agreements for the following companies involving cash and/or stock: Castlevax, Amovir, Vivaldi Biosciences, Contrafect, 7Hills Pharma, Avimex, Pagoda, Accurius, Esperovax, Farmak, Applied Biological Laboratories, Pharmamar, CureLab Oncology, CureLab Veterinary, Synairgen, Paratus and Pfizer, outside of the reported work. A.G.-S. has been an invited speaker in meeting events organized by Seqirus, Janssen, Abbott and Astrazeneca. A.G.-S. is inventor on patents and patent applications on the use of antivirals and vaccines for the treatment and prevention of virus infections and cancer, owned by the Icahn School of Medicine at Mount Sinai, New York, outside of the reported work. Mention of trade names or commercial products

in this publication is solely for the purpose of providing specific information and does not imply recommendation or endorsement by the U.S. Department of Agriculture. The conclusions in this report are those of the authors and do not necessarily represent the views of the USDA. USDA is an equal opportunity provider and employer.

Funding

Funding for this study was partially provided through grants from the National Bio and Agro-Defense Facility (NBAF) Transition Fund from the State of Kansas (JAR), the AMP Core of the Center of Emerging and Zoonotic Infectious Diseases (CEZID) from National Institute of General Medical Sciences (NIGMS) under award number P20GM130448 (JAR, IM), the NIAID Centers of Excellence for Influenza Research and Surveillance under contract number HHSN 272201400006C (JAR), the United States Department of Agriculture (USDA)-NIFA (A1711 Program) under award number 2020-67015-33157, the German Federal Ministry of Health (BMG) COVID-19 Research and development funding to WHO R&D Blueprint (JAR), the NIAID supported Centers of Excellence for Influenza Research and Response (CEIRR, contract number 75N93021C00016 to JAR), and the USDA Animal Plant Health Inspection Service's National Bio- and Agro-defense Facility Scientist Training Program (KC, CM). This study was also partially supported by a subproject award to M. Carossino from the Center for Lung Biology and Disease (CLBD), Center of Biomedical Research Excellence, an Institutional Development Award (IDeA) from the National Institute of General Medical Sciences of the National Institutes of Health under grant number P20GM130555, start-up funds from the Louisiana State University, School of Veterinary Medicine under award number PG 009641 (MC) and self-generated funds from UBRB and MC (PG008671), the USDA-Agricultural Research Service (WCW), and the Center for Research for Influenza Pathogenesis and Transmission (CRIPT), a

NIAID supported Centers of Excellence for Influenza Research and Response (CEIRR, contract # 75N93019R00028 to AG-S), and by the generous support of the JPB Foundation, the Open Philanthropy Project (research grant 2020-215611 [5384]) and anonymous donors to AG-S. SARS-CoV-2 work in the M.S. laboratory is supported by NIH/NIAID R01AI160706 and NIH/NIDDK R01DK130425.

Supplemental material

Supplemental information can be accessed at:

https://doi.org/10.6084/m9.figshare.24525863.v2

Chapter 5 - H5N1 clade 2.3.4.4b dynamics in experimentally infected calves and cows[6]

Abstract

In March 2024, highly pathogenic avian influenza virus (HPAIV) clade 2.3.4.4b H5N1 infections were reported in dairy cows in Texas, USA (208). Rapid dissemination to more than 380 farms in 14 states followed (11). Here we provide results of two independent clade 2.3.4.4b experimental infection studies evaluating the oronasal susceptibility to and transmission of a US H5N1 bovine isolate, genotype B3.13 (H5N1 B3.13), in calves, and the susceptibility of lactating cows following direct mammary gland inoculation of either H5N1 B3.13 or a current EU H5N1 wild bird isolate, genotype euDG (H5N1 euDG). Inoculation of the calves resulted in moderate nasal replication and shedding with no severe clinical signs or transmission to sentinel calves. In dairy cows, infection resulted in no nasal shedding, but severe acute infection of the mammary gland with necrotizing mastitis and high fever was observed for both H5N1 isolates. Milk production was rapidly and markedly reduced and the physical condition of the cows was severely compromised. Virus titres in milk rapidly peaked at 10^9 50% tissue culture infectious dose ($TCID_{50}$) per ml, but systemic infection did not ensue. Notably, the adaptive mutation E627K emerged in the viral polymerase basic protein 2 (PB2) after intramammary replication of H5N1 euDG. Our data suggest that in addition to H5N1 B3.13, other HPAIV H5N1 strains have

---

- [6] Reprinted with permission from " H5N1 clade 2.3.4.4b dynamics in experimentally infected calves and cows" by Halwe, N.J.*, Cool, K*. *et al., 2025. Nature 637, 903-912.* https://doi.org/10.1038/s41586-024-08063-y *Copyright © 2024,* Halwe, N.J.*, Cool, K*. *et al* . Published by Springer Nature. This article is available under the Creative Commons CC-BY-NC-ND license.

the potential to replicate in the udder of cows and that milk and milking procedures, rather than respiratory spread, are likely to be the primary routes of H5N1 transmission between cattle.

Introduction

Epidemic occurrence of HPAIV of subtype H5 has recently developed into a panzootic disease with dynamic spread into an expansive number of host species (18, 20, 103, 106, 107, 122, 209). In 2021, A/H5N1 clade 2.3.4.4b virus crossed the Atlantic and rapidly spread through wild bird and commercial poultry populations in the Americas (103, 104, 208). Subsequent reports of sporadic mammalian infections have become more frequent, with data suggestive of mammal-to-mammal transmission chains in South American seals since 2023 (100, 105).

Historically, natural infections of cattle with influenza A virus (IAV) are not well documented (210) despite the rare detection of IAV seropositive cattle (23). However, in March 2024, an outbreak of HPAIV H5N1 was reported in dairy cows in Texas, caused by the novel B3.13 genotype, a reassortant of an ancestral European clade 2.3.4.4b virus and North American wild bird AIVs (208). Phylogenetic analyses of whole-genome sequences recovered from wild birds, poultry and mammals suggest a single spillover event into cattle, with the time to the most recent common ancestor indicating that introduction occurred in late 2023 or early 2024 (98, 110). Current epidemiological data suggest that subsequent inter-farm spread is mainly associated with unknowingly transporting infected cows (208). As of 29 October 2024, 388 dairy cattle farms in 14 US states have been affected (11).

In the field, high level H5N1 B3.13 replication has been reported in the mammary gland of infected cows, resulting in high-titre virus shedding in milk accompanied by mastitis, a massive drop in milk production and limited reports of respiratory disease(109, 208). The susceptibility and rapid viral replication of HPAIV in the mammary gland are consistent with the

evidence of highly abundant α2,3-linked sialic acid receptors in the bovine udder(32). A novel PB2 substitution (M631L) accompanied the switch from avian to bovine hosts as a marker mutation(110, 208).

Spillover of bovine-origin B3.13 into several mammalian hosts (such as racoons and cats) has been reported(108, 208), and spillback into domestic and wild avian species with maintenance of bovine adaptations has been sporadically observed(110). Recent human cases of H5N1 have also been directly linked to workers following contact with affected cattle or poultry farms, causing conjunctivitis and conjunctival hemorrhage(211). Accordingly, the current series of outbreaks in US cattle presents several urgent and unanswered questions: (1) Is the B3.13 genotype able to replicate in the bovine respiratory tract with viral shedding capable of onward transmission? (2) At what timepoint after infection do cattle produce IAV-specific neutralizing antibodies? (3) Is the mammary gland also permissive for infection with other H5N1 clade 2.3.4.4b strains? (4) What is the clinical presentation, and what is the duration of virus shedding in milk? And (5) does an H5N1 infection of the mammary gland lead to systemic spread?

Here we performed two independent in vivo experiments to investigate the clinical outcome, pathogenicity, transmission and tissue tropism of H5N1 clade 2.3.4.4b in calves and multiparous lactating cows. Calves ($n = 6$) were oronasally inoculated with H5N1 B3.13^9 and co-housed with sentinel calves ($n = 3$), with additional calves serving as negative controls ($n = 3$). The same virus isolate was used for an intramammary inoculation of lactating cows ($n = 3$). For comparison, three additional lactating cows were inoculated with an EU genotype euDG H5N1 clade 2.3.4.4b wild bird virus isolate (H5N1 euDG). One lactating cow served as a negative control.

Results

Mild clinical presentation in calves

Twelve healthy Holstein calves were enrolled in this study and allocated into three experimental groups: principal-infected calves ($n = 6$; 3 male, 2 female and 1 hermaphrodite); sentinel calves ($n = 3$; 1 male, 2 female); and negative control calves ($n = 3$; 2 male and 1 female). Six principal-infected calves were oronasally inoculated with 1×10^6 50% tissue culture infectious dose ($TCID_{50}$) per calf of a virus suspension of H5N1 B3.13 (A/Cattle/Texas/063224-24-1/2024, GISAID accession number: EPI_ISL_19155861). Two days post infection, sentinel calves were co-mingled with principal-infected calves (Figure 5.1Figure). All calves were monitored daily for clinical signs and clinical samples were collected at regular timepoints (Figure 5.1Figure).

Throughout the 21-day study period, signs of mild respiratory illness were occasionally observed in calves, including nasal mucus secretions (no. 712 at 2 days post infection (dpi); no. 754 at 8 and 9 dpi; and no. 6772 at 2 and 6 dpi) and coughing (no. 6772 at 2 dpi; and no. 754, persistent from 2 dpi until euthanasia). Rectal temperatures generally remained within normal range (Figure 5.2Figure), and no other clinical signs consistent with acute illness or consistent with clinical signs reported in affected dairy cattle in the US were observed. All calves maintained normal appetite (measured by feed intake) and normal activity levels (Figure 5.2)

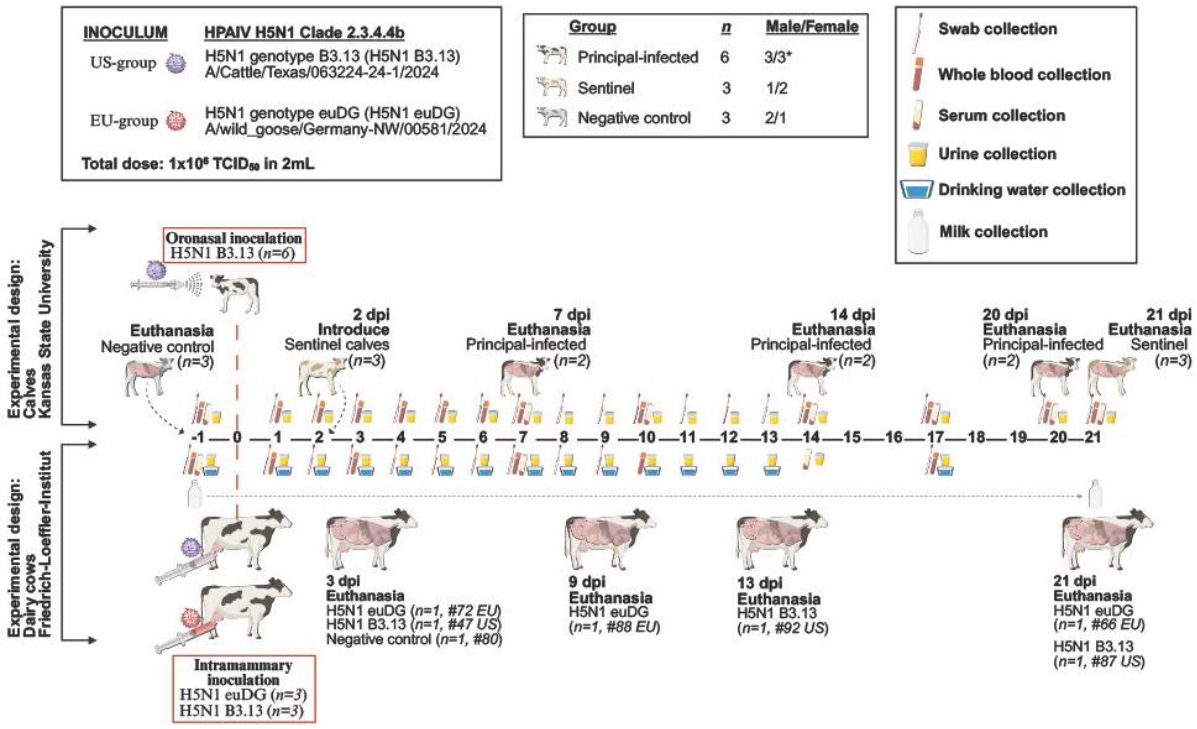

Figure 5.1 Experimental design for infection with HPAIV H5N1 clade 2.3.4.4b isolates

Timeline of the experimental study. Top, 12 Holstein calves of mixed sex (the asterisk indicates that one calf was hermaphroditic) were allocated to three experimental groups: (1) principal-infected (n = 6; 2 female, 3 male, 1 hermaphrodite); (2) sentinel (n = 3; 2 female, 1 male); (3) negative control (n = 3; 1 female, 2 male). Negative control calves were euthanized prior to experimental infection and tissues were collected for baseline comparison. Principal-infected calves were oronasally inoculated with 1 × 106 TCID50 per calf of H5N1 B3.13. Sentinel calves were introduced 48 h post infection. Rectal temperatures and clinical samples, including whole blood and urine, and nasal, oral and rectal swabs, were collected daily for 7 (whole blood) or 14 dpi and every 3 days thereafter. Serum was collected at 0, 7, 10, 14, 17 and 20 or 21 dpi. Postmortem examinations and extensive tissue collections were performed on days 7 (n = 2, principal-infected), 14 (n = 2, principal-infected) and 20 or 21 (n = 2/3, principal-infected/sentinel) post infection. Bottom, 7 Holstein–Friesian multiparous lactating dairy cattle were used in this experiment. Three cows were inoculated in the mammary gland with 105.9 TCID50 per cow of H5N1 B3.13 (A/Cattle/Texas/063224-24-1/2024 (US group), n = 3) and three cows were inoculated in the mammary gland with 106.1 TCID50 per animal of H5N1 euDG (A/wild_goose/Germany-NW/00581/2024 (EU group), n = 3). One cow served as a negative control. Swab samples (nasal, conjunctival and rectal) were taken daily until 9 dpi. EDTA blood samples were taken from individual cattle at 1, 3, 7 and 10 dpi. Urine was taken regularly until 14 dpi. Serum samples were obtained at 7 and 14 dpi and on the day of euthanasia. One cow of each group (no. 47 US and no. 72 EU) reached the humane endpoint at 3 dpi, one further cow reached it at 9 dpi (no. 88 EU) and one additional cow reached it at 13 dpi (no. 92 US); two cows (no. 66 EU and no. 87 US) survived until 21 dpi; All of these were analysed by necropsy. Figure created with BioRender.com under agreement number YH275PUF4T

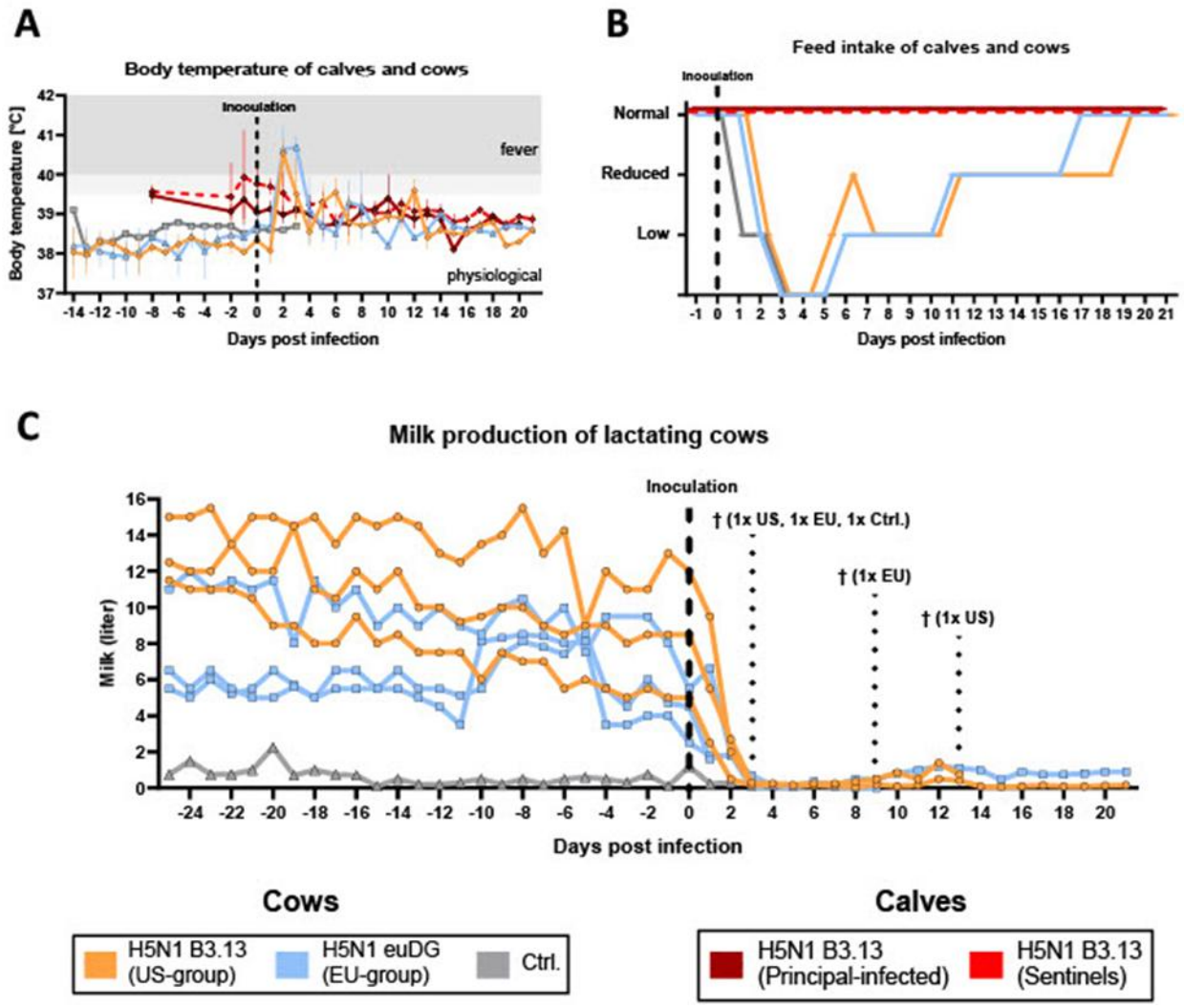

Figure 5.2 Clinical features of calves and lactating cows infected with influenza A/H5N1 clade 2.3.4.4b virus.

a, Rectal temperature of principal-infected (n = 6) and sentinel (n = 3) calves and lactating cows (EU group, n = 3; US group, n = 3; control, n = 1) prior to and following inoculation. Data are shown as mean ± s.d. b, Average feed intake of each group of calves and cows following H5N1 infection. c, Individual milk production of lactating cows prior to and following experimental infection. Milk production of individual cows was tracked daily from −25 dpi until the end of the experiment at 21 dpi. The control animal never produced high amounts of milk. Dotted lines indicate when cows were euthanized.

Severe clinical presentation in lactating cows

Three multiparous Holstein–Friesian cows late in lactation were inoculated by the intramammary route with 2 ml (0.5 ml per teat) of a virus suspension of H5N1 B3.13 (US group), containing $10^{5.9}$ $TCID_{50}$. Three additional cows were similarly inoculated with $10^{6.1}$ $TCID_{50}$ per 2 ml (0.5 ml per teat) of a virus suspension of H5N1 euDG (EU-group)(19). One cow was inoculated with 2 ml NaCl and served as a negative control (Figure 5.1Figure).

Intramammary inoculation induced clinical disease as early as 1 dpi with impaired general condition, postural abnormalities and lethargy. All 6 inoculated cows developed fever (over 40 °C) starting at 2 dpi, further exceeding 40.5 °C in both groups (Figure 5.2aFigure). Moreover, drastically reduced feed intake was observed in both groups of H5N1-infected cows (Figure 5.2bFigure). One cow per group (no. 47 US and no. 72 EU) displayed clinical signs that met criteria for humane euthanasia at 3 dpi. These included postural and motion disorders, refusal of feed and water intake, dehydration and severe lethargy. For direct comparison, the control cow (no. 80) was also euthanized at 3 dpi. Over the next days, one additional cow from each group (no. 88 EU at 9 dpi and no. 92 US 13 dpi) deteriorated into clinical conditions meeting humane endpoint criteria (severe lethargy, postural instability, staggering and signs of respiratory distress).

Prior to infection, daily milk production from individual infected cows ranged from 3 l to 15 l Figure 5.2c Figure). After infection, milk yields rapidly decreased by more than 90%, with only partial recovery observed in the cows remaining at 21 dpi (recovery less than 3% in no. 87 US, and up to a maximum of 25% in no. 66 EU) (Figure 5.2cFigure). Starting at 2 dpi, the milk became mucilaginous and viscous and rapidly separated into a serous and a solid fraction with visible curds (Extended Data Figure.1a,b). Milk yields in the control cow were low prior to

infection, probably owing to drying off of this cow (involution in 3 quarters) (Figure 5.2cFigure). Onset of severe mastitis was confirmed by California mastitis test (CMT) performed daily in both groups (Extended Data Figs. 2, 3 and 4a–c). Clearly positive CMT in infected cows was seen as early as 1 dpi (Extended Data Figs.3a–c and 4a–c).

In conclusion, calves inoculated oronasally presented signs of mild respiratory illness including nasal mucus secretions and coughing, although these cannot be unequivocally associated with outcomes of H5N1 inoculation, whereas intramammary infection of dairy cattle with both clade 2.3.4.4b isolates resulted in severe clinical disease in both groups, requiring early euthanasia in some cases. Severe disease in lactating cows was accompanied by a marked reduction in milk production and obvious changes in milk quality.

Viral shedding dynamics in calves and cows

Shedding of IAV RNA was observed in 5 out of 6 principal-infected calves for a maximum of 8 days, primarily in nasal swabs (Figure 5.3aFigure). Generally, low-to-medium levels of IAV RNA were detected, with peak shedding occurring in nasal swabs between 5–7 dpi in 3 principal-infected calves. IAV RNA was also detected in oral swabs, most frequently at 4–7 dpi, and only seldom detected as suspect-positive (cycle quantification (Cq) ≥ 35, single-replicate positive) in rectal swabs. Vaginal and preputial swabs, conjunctival swabs collected at necropsy, urine and whole blood were negative for IAV RNA throughout the study period. All clinical samples collected from sentinel calves were negative for IAV RNA except for two suspect-positive rectal swabs, attributed to environmental contamination during sample collection, suggesting that no transmission of IAV to sentinel calves occurred throughout the study period. There was no difference observed between male and female calves. Virus isolation and titration were attempted on samples with Cq ≤ 36 (Figure 5.3a Figureand Supplementary Table 1).

Successful recovery of virus was achieved primarily from nasal swabs of 3 different calves at 1, 2, 5 and 7 dpi. (Figure 5.3a) Titres ranged from 4.64×10^1 $TCID_{50}$ ml^{-1} to 1.7×10^3 $TCID_{50}$ ml^{-1}.

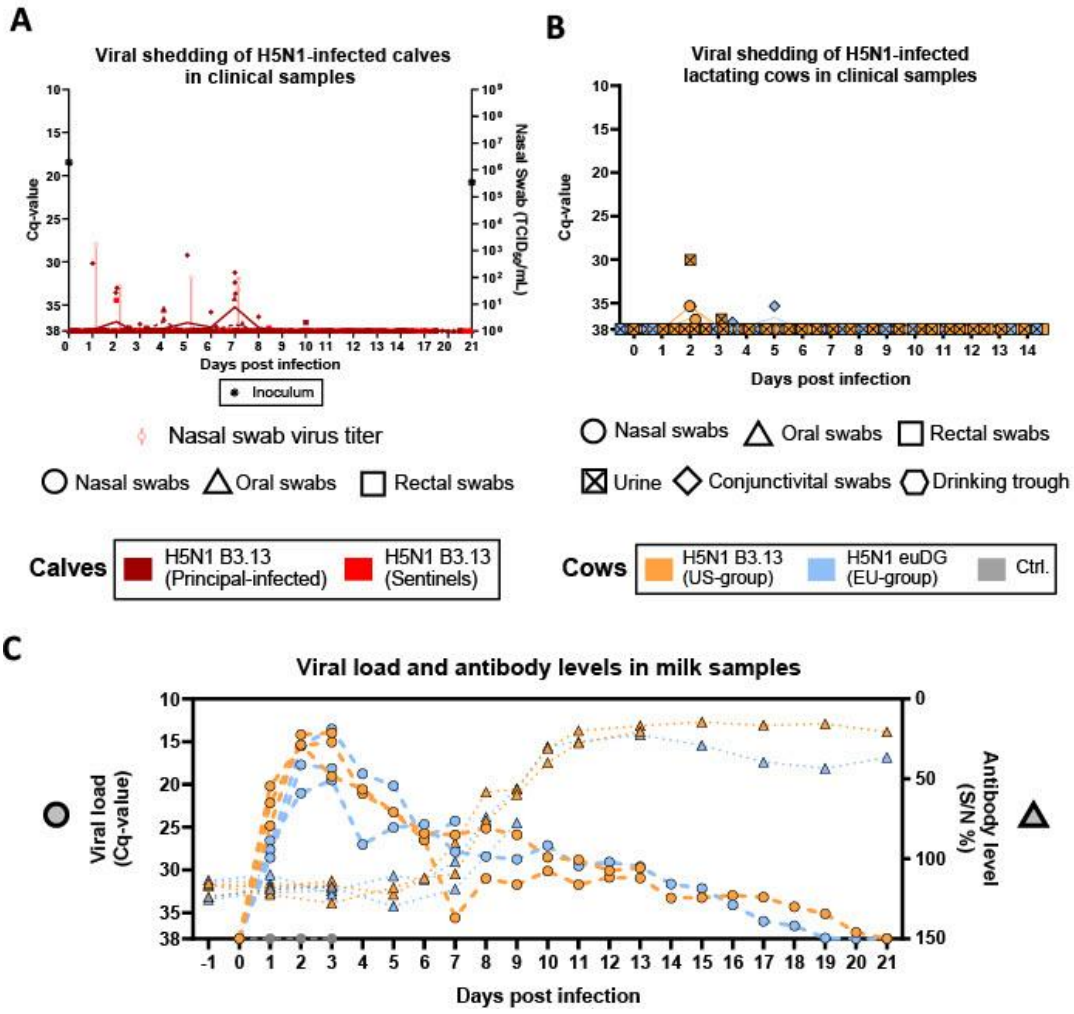

Figure 5.3 Viral shedding of influenza A H5N1 clade 2.3.4.4b virus isolates in experimentally infected calves and lactating cows

a, RT–qPCR was used for the detection of the influenza A M gene (left axis; scatter plot) in nasal, oral and rectal swabs collected from H5N1 B3.13 oronasally infected calves post-inoculation and sentinel calves. Viral titres of nasal swabs (right axis; bars) are represented as the average and standard deviation of positive nasal swabs on each day (n = 3 calves at 7 dpi). The Cq value and titre of the inoculum are shown as asterisks on their respective axes. b, RT–qPCR results from nasal, rectal and conjunctival swabs of lactating cows following intramammary infection with H5N1 B3.13 or H5N1 euDG. c, H5N1 viral genome load (left axis) and corresponding H5-specific antibody titre (right axis) in milk samples over time. All cattle were milked daily and individual pooled milk samples were analysed by RT–qPCR to detect H5N1 viral RNA. Detection of H5-specific antibodies in selected milk samples was achieved using an H5-specific enzyme-linked immunosorbent assay (ELISA) and reported as sample OD450 as a percentage of negative control OD450 (S/N%).

In lactating cows, quantitative PCR with reverse transcription (RT–qPCR) analyses of nasal, conjunctival and rectal swabs and urine samples of cows from the US and EU groups were negative for viral RNA except for 2 nasal swab samples of no. 87 US and no. 92 US (Cq values 35 and 36, respectively) and 2 urine samples of no. 47 US and no. 92 US at 2 and 3 dpi (Cq values of 30 and 36, respectively) (Figure 5.3bFigure). By contrast, milk samples from all cows in both groups tested positive, starting at 1 dpi with peak viral genome loads in milk samples at 3 dpi, revealing Cq values ranging from 13 to 21 (Figure 5.3c Figure). Viral RNA was detectable in milk samples until 20 dpi and by 9 dpi, antibodies directed against the H5 virus were present in milk samples from each cow, increased to a maximum on 11 dpi and stayed at this level until the end of the study period (Figure 5.3c Figureand Extended Data Table 1).

Virus titration from milk samples was performed from 1−13 dpi, but was only successful (that is, infectious virus could be isolated) from 1–8 dpi, with peak titres of greater than 10^9 $TCID_{50}$ ml^{-1} (Figure 5.4aFigure). Owing to the milk composition, it was not possible to determine accurate virus titres from 9 dpi onwards. Virus titration from mammary gland homogenates reached peak titres of around 10^6 $TCID_{50}$ ml^{-1} in cows euthanized at 3 dpi (Figure 5.4bFigure). Nevertheless, infectious virus could still be isolated from the udder of cows euthanized at 9 or 13 dpi (Figure 5.4bFigure). Sequencing of viral RNA from mammary gland tissue and milk samples revealed the emergence of the amino acid substitution E627K in the viral PB2 protein in all three cows after infection with the H5N1 euDG (milk sample of no. 66 EU on day 4, 20% PB2(E627K); milk sample of no. 88 EU on day 4, 83.3% PB2(E627K); udder organ sample of no. 72 on day 3, 89% PB2(E627K)) (Figure 5.4cFigure). Detection of minor variants at this position from samples of milk from day 1 to day 4 post infection showed that this mutation was acquired early after infection, as it was not detected in the inoculum (FigureFigure

5.4c). By contrast, in the H5N1 B3.13-infected cows, the marker mutation PB2(M631L) was maintained and PB2 E627 remained unaltered (Figure 5.4cFigure).

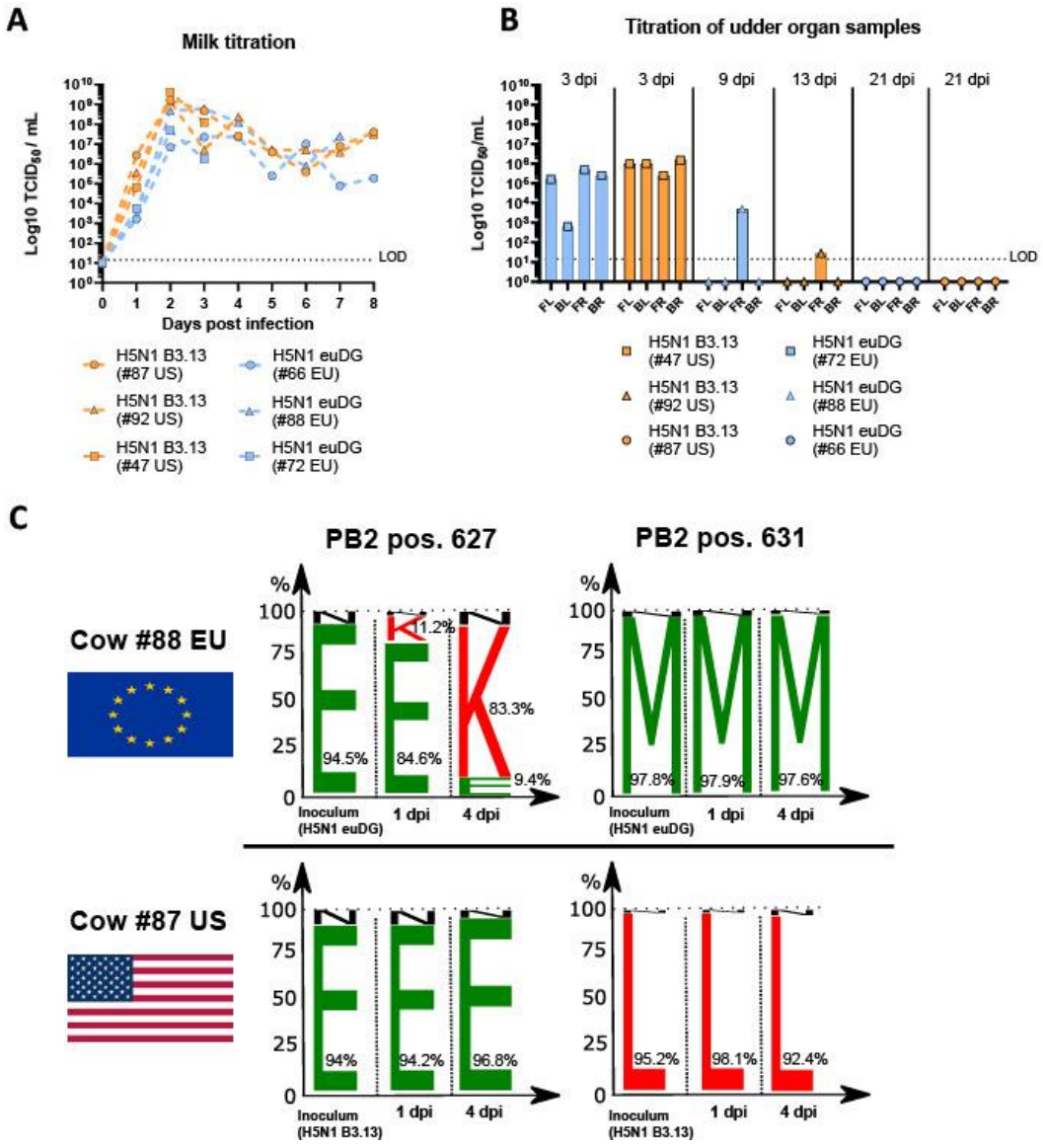

Figure 5.4 Infectious virus yields in milk and udder tissue of H5N1-infected lactating cows and genetic adaptation over time

a, H5N1 viral titres recovered from milk samples of individual H5N1 B3.13- and H5N1 euDG-infected lactating cows. LOD, limit of detection. b, Viral titre of H5N1 infectious viral particles from individual udder quarters (FL, front left; BL, back left; FR, front right; BR, back right) collected at their euthanasia timepoint. c, Genetic adaptation at position 627 and 631 in PB2 of H5N1 B3.13 and H5N1 euDG. The sequence logo plot displays the relative proportion of amino acids present at positions 627 and 631 of PB2 from H5N1 B3.13 and H5N1 euDG in milk sampled from cows no. 88 EU and no. 87 US at indicated timepoints

The high viral loads in milk samples provided an additional opportunity to validate H5-antigen detection using rapid antigen tests (RATs) (Extended Data Figure 5). Two out of three H5N1 B3.13-infected cows (no. 87 US and no. 92 US) tested positive in an AIV-specific RAT at 1 dpi (Extended Data Figure 5a). In RATs, all H5N1-inoculated cows tested positive by 2 dpi (Extended Data Figure 5b,c) and negative at 10 dpi (Extended Data Figure 5d), consistent with increasing antibody levels in milk from 7 dpi onwards (Figure 5.3cFigure).

In summary, oronasal H5N1 B3.13 inoculation in calves resulted in moderate levels of nasal shedding in five out of six principal-infected calves for a maximum of eight days independent of sex, without any evidence for transmission to sentinels. In lactating cows, milk samples obtained from both experimental groups contained high infectious viral loads with viral shedding up to 8 dpi and viral genome detected up to 20 dpi, providing the first evidence for susceptibility of dairy cows to two H5N1 clade 2.3.4.4b viruses belonging to different genotypes from separate continents.

Localized viral replication in calves and cows

Out of nearly 40 organ samples collected from oronasally inoculated calves euthanized at 7, 14 or 20 dpi, IAV RNA was detected only in mucosa-associated lymphoid tissue (retropharyngeal lymph node, palatine tonsil, nasopharyngeal tonsil and suppuration from palatine tonsil) of one principal-infected calf (no. 712) at 7 dpi (Supplementary Table 1). All other liquid, swab and tissue samples (visceral and lymphoid tissues), including lung tissues and bronchoalveolar lavage fluid collected from principal-infected and sentinel calves at 7, 14, 20 and 21 dpi were negative for IAV RNA (Supplementary Table2). Infectious virus was recovered only from the palatine tonsil suppuration collected postmortem at 7 dpi.

RT–qPCR analysis of tissues collected from lactating cows euthanized at 3 dpi revealed peak viral RNA loads in mammary glands, with Cq values of 20 (no. 47 US) and 25 (no. 72 EU) (Extended Data Figure 6a). At 9 (no. 88 EU) and 13 (no. 92 US) dpi, viral genome loads in mammary glands were slightly lower than in mammary gland samples collected at 3 dpi and were undetectable at 21 dpi (no. 66 EU and no. 87 US) (Extended Data Figure 6b and Figure 5.4bFigure). H5N1 viral RNA was also detected at low levels in both groups in neuronal and other tissues at 3 dpi (for example, no. 47 US: spinal cord, Cq = 28; cerebrum, Cq = 36; nervus genitofermoralis Cq = 31; no. 72 EU: nervus genitofermoralis Cq = 34) (Extended Data Figure 6c,d). Organ samples of the respiratory tract were negative in all cows at their euthanasia timepoints (Extended Data Figure 6e). Additionally, there was no IAV RNA detected in whole blood or peripheral blood mononuclear cells collected from oronasally inoculated calves or cows inoculated in the mammary gland.

In summary, low levels of IAV RNA were detected only in mucosa-associated lymphoid tissue of the upper respiratory tract in 1 out of 2 oronasally infected calves at 7 dpi. No IAV RNA was detected in regular ante-mortem whole blood samples or in samples collected post-mortem from major organs, lymphoid tissue, swabs or fluids from principal-infected and sentinel calves, suggesting the absence of a viremic phase of the infection. Similarly, intramammary infection of lactating dairy cattle with two distinct genotypes of clade 2.3.4.4b viruses remained restricted to the mammary gland, and no evidence of systemic spread was observed.

Pathology confirms localized infections

Gross pathology for calves is presented in Extended Data Figure 7. Histological changes in calves oronasally infected with bovine H5N1 at 7 and 14 dpi are depicted in Figure 5Figure. At 7 dpi, there was a suppurative tracheitis in one calf (no. 6760) with degenerate neutrophils filling

the tracheal lumina. The second calf (no. 712) displayed discrete foci of fibrinous interstitial pneumonia with fibrin filling regional alveolar spaces and mild numbers of neutrophils, macrophages and lymphocytes expanding alveolar septa and minimal peribronchiolar inflammatory cells of associated terminal bronchioles at 7 dpi. No viral antigen was detected by immunohistochemistry (IHC) in these samples (Figure 5.5b, dFigure). At 14 dpi, the bronchioles of one calf (no. 754) were lined by hyperplastic epithelium, filled with degenerate neutrophils and partially occluded by papillary projections composed of a core of fibrous connective tissue with few inflammatory cells and lined by bronchiolar epithelium (bronchiolitis obliterans). Bronchioles were also frequently delimited by prominent lymphoid aggregates (bronchus-associated lymphoid tissue (BALT) hyperplasia); however, no viral antigen was detected

(FigureFigure 5.5c).

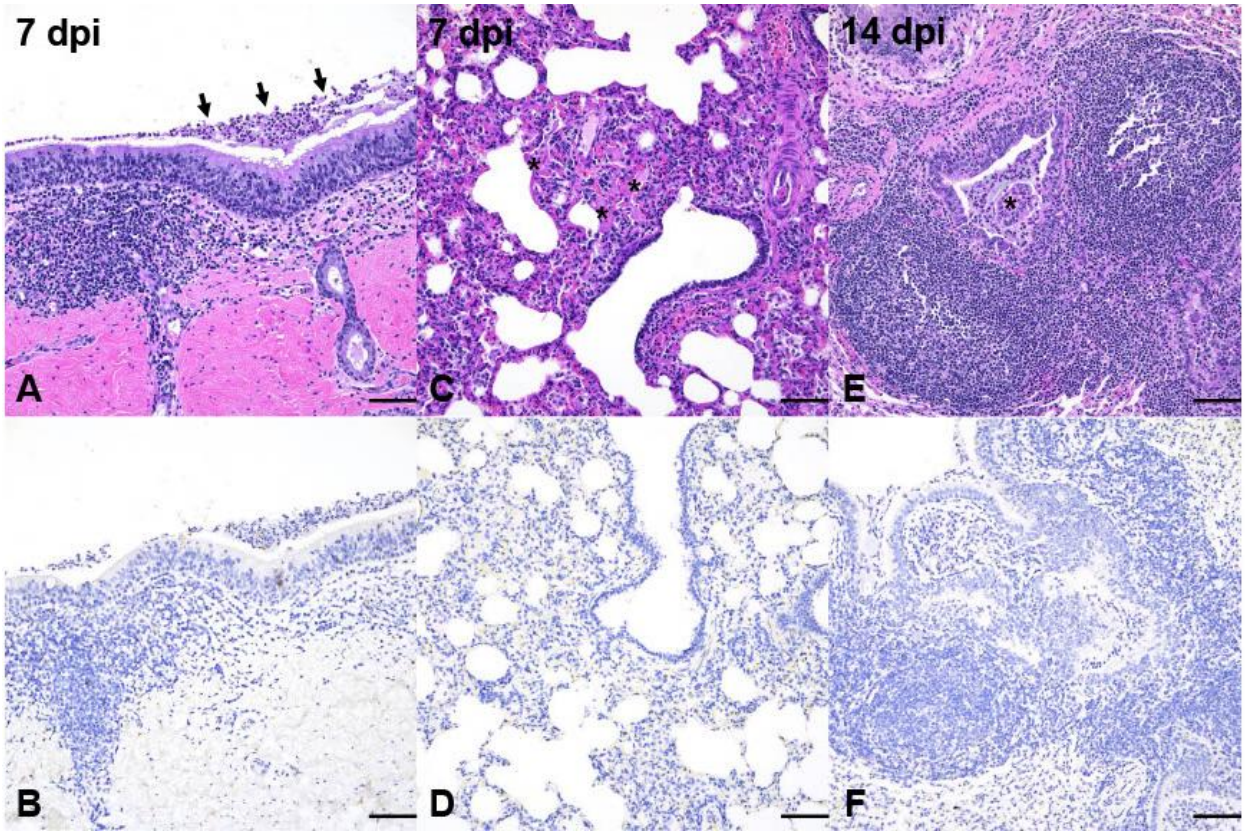

Figure 5.5 Histological changes observed in respiratory tissues of oronasally infected calves

Histological changes in calves oronasally infected with H5N1 B3.13 at 7 dpi (a–d) and 14 dpi (e,f). a,b, Haematoxylin and eosin (H&E) staining (a) shows a segmental region of suppurative tracheitis at 7 dpi (no. 6760). Degenerate neutrophils filled the tracheal lumen (arrows). No viral antigen was detected by IHC (b). c,d, In calf no. 712 (7 dpi), there were multiple small and discrete foci of interstitial pneumonia (c) with fibrin filling regional alveolar spaces (asterisks) and small numbers of neutrophils, macrophages and lymphocytes expanding alveolar septa. No viral antigen was detected (d). e,f, In calf no. 754 (14 dpi), bronchioles were frequently lined by hyperplastic epithelium (e), filled with degenerate neutrophils and partially occluded by papillary projections composed of a core of fibrous connective tissue with few inflammatory cells and lined by bronchiolar epithelium (bronchiolitis obliterans, asterisk). Bronchioles were also frequently delimited by prominent lymphoid aggregates (BALT hyperplasia). No viral antigen was detected (f). Scale bars, 100 μm.

During postmortem examinations of the lactating cows, 45 tissue locations per cow were sampled for histological examination and virus antigen detection (Supplementary Table3). At 3

dpi, H5N1 B3.13 and euDG induced acute mastitis presented with flocculent material in minimal amounts of milk (no. 72, EU and no. 47, US). The character of the histologic changes did not differ between H5N1 B3.13 and euDG. Owing to the small number of cows used, a quantitative comparison of the two isolates with regard to the abundance of the virus antigen was not possible (representative images are shown in Extended Data Figure 8). Up to 90% of the histological sections of secretory alveoli in the mammary gland evaluated showed acute epithelial necrosis with intraluminal cellular debris admixed with many degenerate neutrophils and intralesional antigen detection (FigureFigure 6/ (b). The basal laminae with lining basal–myoepithelial cells remained largely intact (Figure 6c). Intralesional virus antigen was confined to the secretory alveolar epithelium and intraluminal cellular debris (Figure 6d). The teat canal was less prominently affected by necrosis and inflammation, exhibiting IAV nucleoprotein in the remaining lining epithelium (Figure 6e,f) and debris. The enlarged, draining supramammary lymph node exhibited acute lymphadenitis lacking antigen detection. At 9 dpi (no. 88 EU), in addition to the acute necrotic lesions, interstitial, mainly lymphocytic infiltrates were present (Figure 6g) with antigen detection present but limited to up to 50% of the alveoli evaluated histologically, mostly within cellular debris (Figure 6h) as well as single teat canal lining epithelial cells. At 13 dpi (no. 92 US), there was still evidence of acute necrosis (Figure 6i) with scattered antigen detection within cellular debris (Figure 6i). However, the predominant feature observed at this timepoint consisted of regenerative and non-suppurative interstitial inflammatory infiltrates (Figure 6i). Cellular debris in affected mammary alveoli at 21 dpi remained positive for virus antigen (H5N1 B3.13 only; Figure 6k, right). The majority of the examined alveoli were in a regenerative state at 21 dpi (Figure 6l), with mainly lymphoplasmacytic, interstitial infiltrates (Figure 6l). All other tissues tested negative for IAV

antigen, including those identified to contain low levels of viral RNA in individual cows (spinal cord, cerebrum and genitofemoral nerve, cervix, vestibulum vaginae and the urinary bladder; details included in Extended Data Figure 9 a-e). The relevance of the intralobular or interlobular fibrosis of the inflamed mammary tissue to HPAIV infection could not be established, since it was found in varying degrees in the mammary gland, both in the uninfected control cow (no. 80, all quarters) and in individual quarters of all infected cows. In accordance with the clinical findings, a smaller amount of dry, but otherwise normal ingesta was found in the gastrointestinal tract on 3 and 9 dpi, which was interpreted as a sequela of the HPAIV infection. Additional changes were considered as not being associated with infection but were attributed to the age and lactation status of these multiparous cows (details included in Supplementary Table 4).

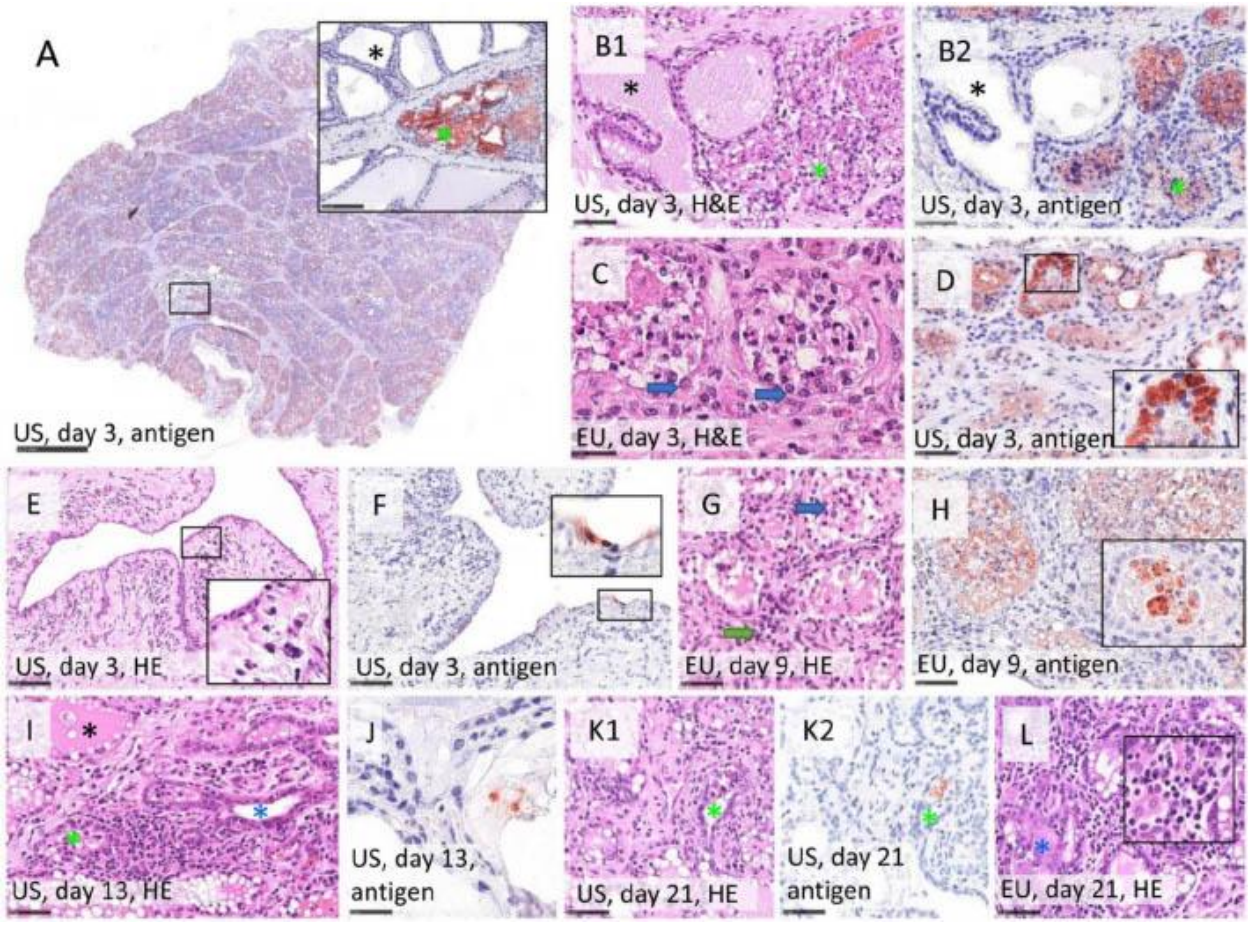

Figure 5.6 Histopathology and IAV NP detection in the mammary gland of multiparous cattle after intramammary infection with H5N1 B3.13 and H5N1 euDG

a, IAV NP detection at 3 dpi. Inset, enlarged view of the outlined region showing juxtaposition of intact, lactating alveoli lacking antigen (black asterisk) and affected areas (green asterisk) in a lobular pattern. IHC using AEC chromogen and Mayer's haematoxylin counterstain. Scale bars: 2.5 mm, main image; 100 µm, inset. b, Full necrosis of the alveolar epithelium, with cellular debris filling the lumen (left) and intralesional detection of IAV antigen (green asterisk) on a consecutive section (right). Some adjacent alveoli remain unaffected (black asterisk). Scale bars, 50 µm. c, Alveoli affected by necrosis with mostly intact basal lamina lined by basal and myoepithelial cells (blue arrows). Scale bar, 25 µm. d, Target cells identified on the basis of morphology following IHC include alveolar secretory epithelium. Scale bar, 50 µm. e, Teat with diffuse degeneration and necrosis of the lining epithelium, subepithelial oedema and mainly neutrophilic infiltrates (inset). Scale bar, 100 µm. f, Target cells identified on the basis of morphology following IHC include teat canal epithelium (inset). Scale bar, 100 µm. g, Necrotic alveoli filled with cellular debris admixed with degenerate neutrophils (blue arrow) in acute lesions and many lymphocytes, and fewer macrophages, neutrophils and plasma cells in the interstitium (green arrow). Scale bar, 50 µm. h, Intralesional IAV NP detection in secretory alveoli, mainly within cellular debris (inset). Scale bar, 50 µm. i, Simultaneous occurrence of intact, lactating alveoli (black asterisk), disruption of alveolar epithelium by necrosis (green asterisk) and beginning of regeneration (blue asterisk). Scale bar, 50 µm. j, Late stage IAV NP

detection is restricted to scattered cellular debris. Scale bar, 25 µm. k, Left, mammary alveolus with intraluminal sloughed epithelium and cellular debris (green asterisk). Right, intralesional detection of IAV antigen on a consecutive slide (green asterisk). Scale bar, 50 µm. l, Regenerating alveoli (blue asterisk) with lack of IAV antigen labelling (not shown). Interstitial immune cell infiltrates include many lymphocytes and plasma cells (inset).Scale bar, 50 µm.

Early detection of antibodies in milk and serum

IAV-specific antibodies in serum collected from oronasally inoculated calves were first evaluated using a NP-specific cELISA. All four principal-infected calves were seropositive by 10 dpi (Table 1). Subsequent evaluation of serum using the H5-subtype-specific cELISA indicated that only 2 calves were seropositive by 14 dpi. However, neutralizing antibodies were detected in 3 out of 4 remaining principal-infected calves at 10 dpi, with all 4 testing positive by 14 dpi (Table 1). Neutralizing titres ranged from 1:5 to 1:80 and were maintained in calves until they were humanely euthanized at 14 or 20 dpi (Table 1). There was no IAV-specific antibody response detected in the sentinel or negative control calves throughout the study period (Extended Data Table 1).

Table 5.1 IAV-specific serological response in calves and lactating cows following inoculation with HPAIV H5N1 clade 2.3.4.4b

			dpi						
Calf ID		**Assay**	**−1**	**7**	**10**	**14**	**17**	**20**	**21**
			H5N1 B3.13 Principal-infected calves						
697	Serum	NP	–	–	+	+	+		+
		$H5_{V3}$	–	–	–	+	–/+		–/+
		VNT_{50}	<5	<5	20	80	80		40
712	Serum	NP	–	–					
		$H5_{V3}$	–	–					
		VNT_{50}	<5	<5					
754	Serum	NP	–	–	+	+			
		$H5_{V3}$	–	–	–	–			
		VNT_{50}	<5	<5	20	20			
6760	Serum	NP	–	–					
		$H5_{V3}$	–	–					
		VNT_{50}	<5	<5					
6768	Serum	NP	–	+	+	+			
		$H5_{V3}$	–	–	–	–			
		VNT_{50}	<5	<5	<5	5			
6772	Serum	NP	–	–	+	+	+	+	
		$H5_{V3}$	–	–	–	–/+	–/+	–/+	
		VNT_{50}	<5	<5	10	20	20	20	
Sentinel	**calves**								
718	Serum	NP	–	–	–	–	–		–
		$H5_{V3}$	–	–	–	–	–		–
		VNT_{50}	<5	<5	<5	<5	<5		<5
748	Serum	NP	–	–	–	–	–		–
		$H5_{V3}$	–	–	–	–	–		–
		VNT_{50}	<5	<5	<5	<5	<5		<5
6770	Serum	NP	–	–	–	–	–		–
		$H5_{V3}$	–	–	–	–	–		–
		VNT_{50}	<5	<5	<5	<5	<5		<5

			dpi					
Cow ID		**Assay**	**0–6**	**7**	**9**	**13**	**14**	**21**
			H5N1 B3.13 lactating cows					
87	Serum	NP	–	+			+	+
		H5	–	–			+	+
		VNT_{100} (B3.13)	<16	<16			406	323
		VNT_{100} (euDG)	<16	<16			645	323
92	Serum	NP	–	+		+		
		H5	–	–		+		
		VNT_{100} (B3.13)	<16	<16		813		
		VNT_{100} (euDG)	<16	<16		813		
47	Serum	NP	–					
		H5	–					
		VNT_{100} (B3.13)	<16					
		VNT_{100} (euDG)	<16					
		H5N1 euDG lactating cows						
66	Serum	NP	–	+			+	+
		H5	–	–			+	+
		VNT_{100} (B3.13)	<16	<16			406	256
		VNT_{100} (euDG)	<16	<16			323	406
88	Serum	NP	–	–	+			
		H5	–	–	+			
		VNT_{100} (B3.13)	<16	<16	<16			
		VNT_{100} (euDG)	<16	<16	25			
72	Serum	NP	–					
		H5	–					
		VNT_{100} (B3.13)	<16					
		VNT_{100} (euDG)	<16					

Nucleoprotein (NP) and hemagglutinin H5-subtype (H5) specific cELISA; positive (+), doubtful (−/+), negative (−); virus neutralization assay (VNT). Serum collected from oronasally inoculated calves (left) and intramammary inoculated lactating cows

(right) was evaluated using commercially available competitive ELISA (cELISA) kits targeting the influenza A virus nucleoprotein (NP) and H5 subtype hemagglutinin protein as well as virus neutralization tests (VNT) against H5N1 B3.13 (calves and cows) and H5N1 euDG (cows). Results of cELISA are calculated as sample OD450/negative control OD450 percentage (S/N%) represented here as positive (+; NP, S/N% ≤ 45%; H5, S/N% ≤ 50%; H5-V3, S/N% ≤ 40%), doubtful (−/+; NP, 45% < S/N% < 50%; H5, 50% < S/N% < 60%; H5-V3, 40% < S/N% < 50%), and negative (–; NP, S/N% ≥ 50%; H5, S/N% > 60%; H5-V3, S/N% ≥ 50%), per manufacturer's instructions. The relative titers of H5N1-specifc neutralizing antibodies are reported as the reciprocal of the final dilution of neutralizing dose 50 (VNT50) or 100 (VNT100) virus neutralization. Serological data for milk samples collected from lactating cows is shown in Extended Data Table 1.

IAV-specific antibodies of infected lactating cows were analyzed by ELISA and VNTs in serum and milk samples throughout the experiment. At 7 dpi, serum samples from 2 out of 2 cows inoculated with H5N1 B3.13 and 1 out of 2 cows inoculated with H5N1 euDG were positive in both the NP-specific and the H5-specific ELISAs (Figure 3c and Table 1). Neutralizing antibodies against H5N1 clade 2.3.4.4b were detectable in milk samples of infected cows from 9 dpi and neutralizing titres ranged from 1:25 to 1:813 (Extended Data Table 1). IAV-specific antibody detection in the milk was delayed by approximately two days in comparison to sera (Table 1 and Extended Data Table 1).

Discussion

H5N1 B3.13 was the first IAV reported to circulate efficiently among dairy cattle, with widespread dissemination between US farms and onward transmission to various avian and mammalian species, including humans (109, 208). This highlights the promiscuous nature of avian influenza viruses, greatly expanding the range of potential hosts and clearly demonstrating their potential to spillover and adapt to new environments. Nevertheless, the capacity for cows to serve as a host supportive of productive HPAIV infection was unexpected, as previous experiments have shown a very low susceptibility of young calves to intranasal inoculation with HPAIV H5N1(210). In this study, we present detailed data on cattle susceptibility to different HPAIV H5N1 genotypes within the broadly circulating clade 2.3.4.4b, providing insights into pathogenesis, potential transmission routes and mammalian adaptation. We demonstrate that high-dose oronasal infection of clinically healthy calves with an early H5N1 B3.13 isolate derived from an infected US dairy cow results in low-to-moderate replication confined to the upper respiratory tract and low-to-moderate oronasal viral shedding, presenting clinically with only mild signs, and IAV-specific antibody production from 7 dpi onwards. However, modest

replication and shedding in principal-infected calves were not sufficient to infect direct contacts despite recovery of live virus from some of these samples up to 7 dpi. Of note, in a previous study using a mammalian H5N1 isolate from 2006, one sentinel calf out of two seroconverted upon H5N1 infection(210). Our results provide evidence that systemic spread or replication in the lower respiratory tract is limited and transmission to sentinels is inefficient following oronasal inoculation of calves under these experimental conditions; H5 A/Goose/Guangdong/1/1996 pathogenicity in male and non-lactating female calves appears to have remained unchanged over the past decades. However, the interaction between suckling calves and cows, and the reciprocal transmission that could occur at this interface were not evaluated here.

Recently, Baker et al.(46) reported results in four heifers inoculated by an aerosol respiratory route. Clinical disease was mild and infection was confirmed by virus detection, lesions and seroconversion, as in the present study. However, transmission was not evaluated in these aerosol-infected heifers, but viral antigen was detected in the lung (46). In our study, pathological alterations in the respiratory tract were limited in calves oronasally infected with H5N1 B3.13. Although the changes noted at 7 dpi and 14 dpi (1 calf each) could be consistent with an acute to late stage of IAV infection, lack of intralesional antigen detection precluded unequivocal confirmation. However, the window for detection of IAV antigen following infection is usually narrow, and antigen could have been present at low abundance in these calves. This probably explains the lack of detection of viral antigen at 7 dpi. The overall histologic alterations and their distributions in both calves are not consistent with bacterial bronchopneumonia associated with the bovine respiratory disease complex despite detection of *Pasteurella multocida*, *Bibersteinia trehalosi* and *Mannheimia haemolytica* by PCR with high

Cq values. The extent to which active or previous infection with influenza D virus (IDV) might influence the course of IAV infection was not evaluated in this study. We believe that prior infection of some calves with IDV did not affect the outcome of the experiment, as there is no known cross-reactivity between IDV and IAV and no difference was found between the IDV-positive and IDV-negative calves.

Drastically different outcomes were observed following direct intramammary inoculation of lactating dairy cows with H5N1 B3.13 or H5N1 euDG. Acute presentation of severe clinical signs including lethargy, fever and impaired general condition were accompanied with abrupt reduction of feed intake and clinical mastitis with immediate and persistent milk losses of more than 90% in all cows, irrespective of the H5N1 virus isolate. Histopathology identified a severe, acute, diffuse, necrotizing mastitis with intralesional virus antigen detection in the secretory epithelium and teat canal lining epithelium, but no evidence of systemic spread of the pathogen. In our study, humane euthanasia of four individual cows was required prior to the initially planned end points owing to the severity of clinical signs (Extended Data Figure 1f). Although there is currently a lack of evidence of increased mortality events in dairy farms across the USA, a recent field observation study demonstrates that two dairy farms reported mortality associated with H5N1 infections (10). Conversely, the severe clinical presentation observed in our study may also be related to the age and late lactation phase of these cattle (4–8 years of age, just before dry-off). It is possible that confounding co-morbidities that are common in older dairy cows contributed to the severity of the disease, and that H5N1-associated disease may be milder in younger, monoparous cows at a different stage of lactation or when individual udder quarters are affected.

It also seems likely that udder manifestation is not a unique feature of genotype B3.13, but rather a particular intrinsic ability of the bovine udder to be readily susceptible to H5N1 clade 2.3.4.4b viruses, as similar tropism and disease were demonstrated in this study with H5N1 euDG. Susceptibility of cattle to IAVs other than H5 is speculative, but there are historic reports of productive intramammary infection in dairy cows by an ancestral human H1N1 (A/PR8) (212-214). Mammary infections of cattle by avian influenza viruses are supported by the recently described expansive expression of α2.3 sialic acid receptors in the udder tissue, but not in the upper respiratory tract of cattle (32). We isolated high levels of infectious virus only from milk and udder samples of H5N1-infected lactating cows, clearly demonstrating that replication of H5N1 clade 2.3.4.4b is restricted to the mammary glands after intramammary inoculation. In addition, RT–qPCR analysis of environmental samples collected daily from a communal water trough, urine samples and nasal, conjunctival and rectal swabs from infected lactating cows revealed only trace amounts of viral RNA, indicating that non-milk-related transmission routes appear to be less relevant; however, modes of transmission in adult cows remain to be evaluated in more detail. Field reports suggest that cow-to-cow transmission is most probably driven by the milking process, and appears to be equipment-related, thus representing a mechanical and anthropogenic event (109, 110, 124, 208). Milk and milking procedures, in this respect, appear to be the central mediator of spread within holdings. This is further supported by recent research showing that raw milk spiked with HPAIV H5N1 remained infectious on milking machines for several hours (120) and can be detected in environmental samples collected from a milking parlor(124). In the field, titres in milk from infected cows can exceed 10^8 $TCID_{50}$ ml^{-1}, about two logs higher than the dose we used for intramammary inoculation. The methods used to inoculate cows (intramammary) may not be a perfect representation of how milking equipment would

infect an udder; however, given the similarity of our virological and clinical results to field reports, they appear to validate the conditions used in our experiment. With respect to oronasal transmission in calves, there is no information on the infectious dose of potential respiratory transmission. If oral transmission occurs by ingestion of contaminated milk, our inoculation dose is probably lower than what calves would be exposed to in the field. If calves are infected by aerosol transmission, the atomization method that we used for infection might not be the appropriate approach and could explain some of the differences that we observed compared with Baker et al.(46). In addition, the extensive cleaning and environmental controls of biosafety level 3 agriculture facilities, where airflow is directional and constantly exchanged, must also be considered, as they do not reflect natural barn conditions and could reduce the opportunity for airborne transmission.

Substitutions in the PB2 gene sequence, such as the M631L mutation in H5N1 B3.13, appear to be very favorable for replication in the mammary gland (110). We found a similar PB2 adaptation, E627K, for H5N1 euDG in our lactating cows, from 1 dpi as a minor variant, with clear presence by 3 dpi. Independent appearance of this substitution in 3 out of 3 cows suggests a strong bottleneck and high evolutionary pressure towards this adaptation. Conclusively, PB2 adaptation to mammalian hosts (at position 627 or 631) seems to be beneficial for replication in the mammary gland, as these genotypes remain stable in any tested milk and udder tissue sample. Notably, H5N1 B3.13 has also acquired the E627K mutation upon replication in a human case (125) and was present as a minor variant (2%) in environmental samples from a dairy farm in Kansas(124). It remains to be determined whether strain and/or host dependencies drive the selection of the two PB2 mutations and whether they resemble similar phenotypes.

Spillback of bovine H5N1 B3.13 into multiple poultry farms has been reported, and this may result in increased environmental contamination in poultry, furthering spillback into wild bird populations and possible zoonotic transmissions. This has recently been demonstrated by an outbreak of H5N1 B3.13 in a large commercial layer hen farm in Colorado, USA, where several farm workers tested positive for H5N1 after culling the infected animals(215). The possibility for non-lactating cattle to serve as a virus source for onward transmission to adult dairy cows, poultry or mammalian species such as cats, should be considered, as we observed nasal shedding of infectious virus for seven days. The same scenario also exists for environments contaminated with milk from H5N1-infected cows.

A tailored surveillance strategy is crucial for effective control. We demonstrate here that in addition to RT–qPCR, AIV-specific RATs might provide a simple testing tool for milk from individual cows and are suitable for the detection of H5N1 clade 2.3.4.4b, including genotype B3.13. Influenza mastitis should be considered as a differential diagnosis whenever milk characteristics change. As antibody levels in milk increase and viral loads decrease, antigens are no longer detected by RATs. Infectious yields in the milk also decrease at this point, owing to the neutralizing activity of secreted antibodies. The unique situation that both viral shedding and neutralizing antibody shedding occur in milk may also present an opportunity to control this epizootic and reduce infectious titres in pooled milk from affected herds. In addition to genomic surveillance, serologic surveillance of pooled milk from individual herds may be appropriate to assess the distribution of IAV among dairy herds and facilitate control efforts.

In conclusion, we demonstrated that: (1) H5N1 B3.13 had only a moderate capacity for respiratory replication in young calves; (2) H5N1 B3.13 was not transmitted to sentinel calves; (3) dairy cattle were readily susceptible to two distinct and geographically separated H5N1 clade

2.3.4.4b isolates of mammalian or wild bird origin following intramammary inoculation; (4) viral replication was localized to the udder with subsequent high-titre shedding in milk; (5) the clinical picture of severe disease in dairy cattle was identical for both strains, with severe mastitis; and (6) high-titre infectious virus was shed in milk for at least 8 days. Finally, the manifestation and main replication site for both tested H5N1 isolates following intramammary inoculation was the mammary gland, and systemic spread and infection of other organ systems, including the respiratory tract, was not observed in lactating cows.

No human-to-human transmission has been reported so far for these strains, supporting the notion that they have not yet overcome critical barriers to enable human-to-human transmission, such as improved receptor binding, pH stability and escape from MxA restriction (121) . The frequent interfaces between humans and affected animals (cattle, poultry and wild birds) provide opportunities for reassortment of the bovine B3.13 with human seasonal influenza viruses or other avian and maybe swine influenza viruses in circulation. Thus, effective mitigation strategies must be urgently outlined and implemented to: (1) prevent continuous replication and spread of this pathogen in cattle; (2) avoid any further mammalian adaptation; and (3) stop spillover and spillback infections to other livestock, wild birds, other mammals and humans. Focused efforts to better characterize transmission pathways and H5N1 ecology in the dairy industry worldwide are critically needed.

Methods

Ethics statement and biosafety

All experiments conducted at Kansas State University were approved and performed under the Kansas State University (KSU) Institutional Biosafety Committee (IBC, protocol no. 1758) and the Institutional Ani- mal Care and Use Committee (IACUC, Protocol no. 4992) in

compliance with the Animal Welfare Act. All animal and laboratory work involving infectious highly pathogenic avian influenza virus were performed in biosafety level 3+ and 3Ag laboratories and facilities in the Biosecurity Research Institute (BRI) at KSU in Manhattan, KS, USA. Further evaluation of inactivated samples was conducted in biosafety level (BSL)-2 laboratories using enhanced biosafety practices. The calf transmission studies mimicked 'natural' transmission events that could happen daily in US dairy operations and are not considered passaging or adaptation experiments, since no further passaging and no forced transmission was attempted.

The lactating dairy cattle experiment was evaluated by the responsible ethics committee of the State Office of Agriculture, Food, Safety, and Fishery in Mecklenburg–Western Pomerania (LALLF M-V) and gained governmental approval under the registration number 7221.3-2-010/23. At the Friedrich-Loeffler-Institut (FLI), the experiments with lactating dairy cattle were performed in the licensed high containment BSL-3 laboratories and BSL-3 large animal facilities of the institute with the required personal protective measures in accordance with the respective permits. The experiments were in compliance with the relevant requirements of the German Infection Protection Act, the Biological Agents Ordinance and the Animal Pathogens Ordinance.

Virus

The European HPAIV isolate A/wild goose/Germany-NW/00581/2024 (H5N1), genotype DE-23-11-N1.3 euDG (H5N1 euDG), was supplied by the German National Reference Laboratory for avian Influenza (T. Harder) at FLI (19). It was propagated in embryonated specific pathogen-free chicken eggs for 5 days at 37 °C, followed by collection of the allantoic fluid, which in turn served as the virus stock. In post-inoculation sterility testing of the original

undiluted H5N1 euDG virus stock, the marginal presence of Enterococcus spp. was confirmed on sheep blood agar. This was confirmed by next-generation sequencing analysis, which revealed a close genetic relationship to *Enterococcus casseliflavus*, a commensal to the normal bacterial flora. There was no evidence that this had any effect on the results obtained in the study.

The North American HPAIV H5N1 isolate A/Cattle/Texas/063224- 24-1/2024, genotype B3.13 (H5N1 B3.13, GISAID accession number: EPI_ISL_19155861) administered to calves and cattle in this study was isolated from the milk of infected dairy cattle in Texas, USA, kindly provided by D. Diel (10). Virus stock was propagated using bovine uterine epithelial cells (CAL-1; in-house) for three passages. A single passage on MDCK cells was used to propagate viral stocks for application in virus neutralization assays. The titres of both virus preparations were determined by endpoint dilution titration on MDCK type II cells.

Cells

FLI Riems: Madin-Darby Canine Kidney (MDCK, RIE-1061) type II cells originating from the Collection of Cell Lines in Veterinary Medicine (CCLV) were used. Cells were incubated at 37 °C under a 5% CO2 atmosphere. Cultivation medium is composed of a mixture of equal volumes of Eagle Minimum Essential Medium (MEM) (Hank's balanced salts solution) and Eagle MEM (Earle's balanced salts solution), 2 mM l-glutamine, nonessential amino acids, adjusted to 850 mg l−1 NaHCO3, 120 mg l−1 sodium pyruvate, pH 7.2 with 10% fetal calf serum (FCS) (Bio & Sell).

Kansas State University: Madin-Darby canine kidney (MDCK) cells were maintained in Dulbecco's Modified Eagle Medium (DMEM; Corning), supplemented with 5% fetal bovine serum (FBS; R&D Systems) and1% antibiotic-antimycotic solution (Gibco). Medium used

during virus cultivation (VNT, virus isolation) was similar, but deprived of FBS and supplemented with 0.3% bovine serum albumin (BSA; Sigma-Aldrich) and 1% minimum essential medium vitamin solution (Gibco), in addition to 1 μg ml^{-1} of TPCK-treated trypsin.

Experimental design for calf study

Twelve Holstein calves (5–6 months of age) of mixed sexes were trans- ported from an Iowa livestock operation to Kansas State University College of Veterinary Medicine (KSU-CVM) in Manhattan, Kansas.

Upon arrival, blood and swabs were collected and screened for cur- rent or recent IAV infection as well as various pathogens associated with bovine respiratory disease complex (BRD), including IDV. Calves were negative for any active or recent infections with IAV based on RT–qPCR and IAV NP-specific cELISA results. Results of the RT–qPCR based BRD panel revealed some calves were qPCR positive for common bovine respiratory pathogens (Supplementary Table 3) (216). Calves were semi-randomly (sorted according to sex; one (female) calf determined to be hermaphroditic; then randomized intro groups) allocated into three experimental groups: principal-infected (n = 6; 2 female, 3 male, 1 hermaphrodite); sentinel (n = 3; 2 female, 1 male); negative controls (n = 3; 1 female, 2 male). The control animals were humanely euthanized prior to the day of infection (−2 and −3 dpi). Calves were in good health prior to virus infection based on health examinations conducted by KSU veterinarians.

On the day of virus infection, sentinel calves were physically separated and placed up-current of the room's directional airflow from principal-infected calves. Principal-infected calves were administered a total dose of 1 × 106 TCID50 (5 × 105 TCID50 ml−1) in 2 ml of H5N1 B3.13 applied as follows: 0.5 ml per nostril using an atomization device (MAD Nasal atomization device, Teleflex) to deliver a fine mist of particles 30–100 μm in size and 1 ml orally

using a syringe. Forty-eight hours post infection, sentinel calves were co-mingled with principal-infected calves (Figure 1).

Clinical observations and rectal temperatures were recorded daily (Figure 1). One calf (no. 6770; sentinel) developed a high fever prior to the start of the experiment, which resolved following treatment with florfenicol. Baseline samples, including swabs and blood, were collected from all calves upon arrival (−8 dpi) and again after an acclimation period outdoors (−1 dpi). Clinical samples, including urine (when possible), nasal, oral, rectal, vaginal and preputial swabs (collected in 2 ml of DMEM containing 1% antibiotic/antimycotic solution) were collected at −1, 1–14, 17, 20/21 dpi (Figure 1). Whole blood samples were collected on −1, 1–7, 10, 12, 14, 17, 20/21 dpi (Figure 1). Serum samples were collected on −1, 7, 10, 14, 17, 20/21 dpi (Figure 1). Thorough post-mortem examinations were conducted on days 7 (n = 2; principal-infected), 14 (n = 2; principal-infected), 20 (n = 2; principal-infected) and 21 (n = 3; sentinel) post infection (Figure 1). Apparent gross lesions were documented prior to extensive sampling of tissue as to determine the scope and extent of impacted tissues (tissue tropism) and any correlation with subsequent IAV detected. Lungs were macroscopically evaluated and scored (a report was generated) according to the percent of lung affected (individual lobes and left/right) with gross lesions including congestion with atelectasis or oedema, pneumonia, haemorrhage and plural fibrosis when present (Extended Data Figures 4 and 10) (217).

Experimental design for lactating dairy cows study

Seven female multiparous lactating Holstein–Friesian dairy cattle in an age range between four and eight years, at a state of decreasing milk production, and around 12 months after last calving were obtained from a local dairy farm. The animals were kept in three separate animal rooms (3 × 3 × 1 animals per stable) in the BSL-3 animal facility of the FLI, Greifswald,

Isle of Riems, Germany. During the 25-day acclimatization period, the animals were milked once per day using a can milking system (Minimelker, Melktechnik-Discount) and the amount of milk produced per cow was documented to have a reliable baseline for each individual (Figure 1). Additionally, a CMT was performed on each udder quarter from each cattle daily from −1 dpi onwards until each individual endpoint. In brief, CMT reagent was mixed with an equal amount of raw milk received directly from the respective cow teat on a special CMT plate (Extended Data Figure 1a), followed by gentle swivelling. The CMT was interpreted according to a comparative picture showing either: (1) unchanged color and consistency (negative, −); (2) low mucus formation (altered, +); (3) strong mucus formation (positive, ++); or (4) intense clumpy and gelatinous mucus formation (strongly positive, +++). Milk production percentages were calculated by generating a mean value of −2 to 0 dpi for each individual animal, which was set as 100%. Prior to infection, all animals tested negative for IAV RNA in nasal swabs and milk samples via RT–qPCR, as well as seronegative in an IAV-specific ELISA targeting the viral NP (ID-Vet). Prior to inoculation, the udder epidermis was cleaned, and the teat and teat orifice were disinfected using an alcohol-based disinfectant. A teat drainage cannula was employed to evacuate all residual milk from the cistern and for inoculation into teat a/o gland cistern. Three animals were inoculated in the mammary gland with 105.9 TCID50 per cow by equally administering 0.5 ml per teat (~2 ml total volume, 105.31 TCID50 per teat, all four teats) of H5N1 B3.13, and three animals were inoculated in the mammary gland with 106.1 TCID50 per cow by equally administering 0.5 ml per teat (~ 2 ml total volume, 105.49 TCID50 per teat, all four teats) of H5N1 euDG. One additional animal, kept in a separate unit, served as negative control and received 0.5 ml sodium chloride solution per teat. The infectious virus titres of both inocula were determined by back-titration on MDCKII cells. Cattle were milked daily, and nasal

swab samples as well as samples from the drinking trough of the animals were taken daily until 9 dpi (Figure 1). Swab samples from conjunctiva and rectal swabs were taken from 4 dpi until 9 dpi (Figure 1). Urine was collected until 14 dpi. EDTA blood samples were taken at 1, 3, 7, 10 and 17 dpi (Figure 1). Serum samples were generated before inoculation, 7, 14 dpi, and at the day of euthanasia (Figure 1). The control cow had a bacterial infection, most probably in the uterus, prior to the start of the experiment. This necessitated the use of antibiotics, which partially resolved the clinical conditions. In addition, this animal did not produce large amounts of milk as it was very close to dry-off. It was therefore chosen as a control. The reduction in feed intake and the low milk yield of this cow was therefore most likely due to these overall conditions.

RNA extraction and RT–qPCR analysis for calf study

To document the presence of H5N1 infection, clinical samples (swabs, EDTA blood) and clarified 10% (weight:volume) tissue homogenates were combined with equal volumes of RLT lysis buffer (Qiagen) prior to total nucleic acid extraction using an automated magnetic bead-based extraction system (Taco Mini, GeneReach; BioSprint 96, Qiagen) in com- bination with associated reagents (GeneReach), according to previously established protocols (124). Subsequently, samples were run in duplicate reactions using a one-step RT–qPCR assay targeting the matrix gene segment of IAV employing a modified M + 64 probe and qScript XLT 1-Step RT–qPCR ToughMix (QuantaBio) on the Bio-Rad CFX96 Optics Module C1000 Touch (Bio-Rad) to determine the quantity of IAV RNA, with thermocycling conditions as described previously (124). A positive Cq cut-off of 38 cycles was established for samples where both wells were positive.

Sample collection, RNA extraction and RT–qPCR analysis for lactating dairy cows study

Raw milk samples were collected individually per quarter and directly used for RNA extraction. In addition, bulk milk samples generated via milking machine were also collected and analysed. Swabs were taken using rayon swabs (DRYSWAB Standard Tips, MWE) and were immediately transferred into 2 ml of cell culture medium containing 1% Baytril (Bayer), 0.5% Lincomycin (WDT) and 0.2% Amphotericin/Gentamycin(Fisher Scientific). Blood samples were taken using the Kabevette G system and disposable needles. Organ samples 2 × 2 × 2 mm in size were transferred into a 2 ml collection tube containing 1 ml of cell culture medium containing 1% penicillin-streptomycin (Biochrome) and one stainless steel bead per sample. Homogenization was established by rough shaking of the samples in a TissueLyser II instrument (Qiagen) for 2 min. at 300 Hz. Viral RNA of all samples was extracted using 100 µl of raw milk or sample medium or supernatant in the NucleoMag Vet-kit (Macherey-Nagel) on a BioSprint 96 platform (Qiagen). Detection of H5N1 B3.13 and H5N1 euDG via RT–qPCR was established as recommended and described (218, 219). Relative quantification was performed using the Bio-Rad CFX Maestro 1.1 Version 4.1.2433.1219 software.

Virus isolation and virus titration for calf study

Clinical samples and tissue homogenates with Ct values < 36 were subjected to virus isolation and virus titration. Viral titration and immuno- fluorescence assays (IFAs) were performed as described previously (217). In brief, tenfold serial dilutions of syringe filtered (0.45 µm) samples, tested in four replicates, were transferred onto 96-well plates containing confluent monolayers of MDCK cells. After infecting cells, 96-well plates were incubated at 37 °C and observed daily (light microscope) to monitor the conditions of the cellular monolayer and

cytopathic effects (CPEs) and cell morphology. After 48 h, plates were washed with PBS prior to fixation with ice-cold 100% methanol for 10 min at −20 °C; then cells were washed with 1× PBS and incubated for 1 h with influenza A-specific H16-L10-4R5 primary antibody (ATCC HB-65 undiluted) at room temperature (220). Subsequent washes with PBS containing 0.05% Tween-20 (PBS-T) were conducted prior to incubation with goat anti-mouse IgG (H + L) secondary antibody (Alexa-488, Fisher Scientific, A11001; 1:1000) and incubation at room temperature for 30 min. Plates were washed and dried prior to observation of fluorescent signal using an EVOS fluorescent microscope (EVOS FL Color, AMEFC4300, Fisher Scientific). Viral titres were calculated using the Reed–Muench method (221) with a limit of detect at 46 TCID50 ml−1.

In parallel, attempts for virus isolation were conducted utilizing 25 cm2 flasks (T-25) of confluent MDCK cells. Cells were first washed with 1× PBS to remove any residual FBS and subsequently incubated with 500 µl diluted (1:10) sample and 2 ml of infection medium for 2 h, gently rocked every 15 min, prior to addition of 2.5 ml of infection medium. After two-three days of incubation at 37 °C, supernatants were collected from T-25 flasks. Flasks were then subjected to IFA protocols as described above and reported as positive or negative for viral presence based on fluorescent signal.

Virus isolation and virus titration for lactating dairy cows study Virus titres of selected milk and udder organ samples were determined by a TCID50 endpoint dilution assay on MDCKII cells. In brief, tenfold serial dilutions of respective samples were prepared and transferred onto 96-well plates containing confluent monolayers of MDCKII cells (duplicates). Plates were incubated for 72 h at 37 °C. Virus titre was evaluated by the presence of a specific CPE and was calculated according to the measure of infectious dose in specific infections (midSIN) method (222).

Serology and host immune responses for calf study

Serum, collected from all calves upon arrival (−8 dpi), prior to infection (−1 dpi), and at defined timepoints (7, 10, 14, 17, 20/21 dpi) throughout the study, were evaluated for the presence of influenza A-specific anti- bodies using several methods.

Neutralizing antibody titres were determined according to previously established protocols (223) with slight modifications. In brief, heat-inactivated serum was combined with an equal volume of H5N1 B3.13 stock virus (propagated additionally once on MDCK cells), diluted to 100 TCID50 per 50 µl, in duplicate wells on 96-well plates and incubated at 37 °C for 1 h. Subsequently, the serum/virus mixture was transferred to 96-well plates containing confluent monolayers of MDCK cells. After 48 h of incubation, IFA was preformed (similar to described above for virus titration and isolation) and neutralizing antibody titres were recorded as 50% inhibition of virus growth per well. Additionally, commercially available enzyme-linked immunosorbent assay (ELISA) kits, validated for application with bovine-origin serum, targeting: (1) the conserved IAV nucleoprotein (NP-ELISA; ID Screen Influenza A Antibody Competition Multi-species, Innovative Diagnostics); and (2) the H5-specific haemagglutinin protein (H5-ELISA; ID Screen Influenza H5 multi-species competitive ELISA V3, Innovative Diagnostics) were used according to manufacturer's instructions on a Varioskan LUX (Thermo Scientific, N16044). Results were extracted from Thermo Scientific SkanIt Software for Microplate Readers (version 6.0, N16243) and further analysed using Microsoft Excel 2016 (version 16.0.5188.1000).

Serology for lactating dairy cows study

Serological analysis of blood samples or milk samples from all animals was performed by using a commercial IAV-specific enzyme-linked immunosorbent assay (ELISA) detecting

NP- and H5-specific antibodies (ID-Vet) according to the manufacturer's instructions. Results were quantified via the Tecan i-control 2014 1.11 software and analysed via Microsoft Excel 2016 (version 16.0.5188.1000). Heat-inactivated serum was used for serum samples, but not for milk samples. There was no indication for any non-specific neutralization or reactivity with the milk samples. The recommended cut-off values in the test kit were used for both serum and milk samples. It is noteworthy at this point, that the cut-off values are not fully validated for milk samples yet.

Virus-neutralizing antibodies were investigated via a VNT100 on MDCKII cells. In brief, serum samples of respective timepoints were serially diluted in DMEM on a 96-well plate (log2 steps) and mixed with 100 TCID50 of H5N1 B3.13 or H5N1 euDG followed by incubation for 1 h at 37 °C. Subsequently, 100 µl of MDCKII cells were added to each well, followed by another incubation period for 72 h at 37 °C. Neutralizing antibodies were evaluated and recognized by light microscopy in the absence of a CPE. The last serum dilution with intact cells and no visible CPE was considered as neutralization titre against the respective virus.

Macroscopic and microscopic pathology for calf study

Postmortem examinations were conducted at 7, 14 and 20/21 dpi. Macroscopic pathology was determined and scored in toto and the percent- age of lung lesions were reported (Supplementary Table 5), based on previously published protocols (217). Tissue samples were fixed in 10% neutral buffered formalin for a minimum of 7 days and subsequently transferred to 70% ethanol and processed using standard histological techniques, and stained with H&E. Collections included paired collections (fresh tissue and formalin-fixed) of representative sections (and lesions) obtained from respiratory, gastrointestinal, and reproductive tract, lymphoid tissue including spleen, various lymph nodes and mucosa-associated lymphoid tissue,

brain, eyes and eye lids, and other tissues including adrenal gland, heart and pancreas. Bronchoalveolar lavage fluid was collected from the right side of the lung. Fluids collected included aqueous humour, cerebral spinal fluid and bile. Transudates from the pericardial sac, thoracic cavity and abdominal cavity and urine were also collected when present. Conjunctival swabs and swabs from the reproductive tract were also collected at necropsy. Selection of animals for necropsy was based on sex to ensure representative samples from each sex, as well as on data that was available regarding viral RNA shedding in nasal and oral swabs. Four-micrometre sections from the lower respiratory tract tissues were stained with routine H&E staining after standard automated processing and paraffin embedding. Routine H&E staining and IHC for the calf study was performed at the Louisiana Animal Disease Diagnostic Laboratory (LADDL), an AAVLD-accredited and National Animal Health Laboratory Network level 1 veterinary diagnostic laboratory that operates with highly standardized procedures and meets high quality standards. Routine H&E staining and IHC were performed using fully automated stainers that yield consistent staining results. For H&E staining, tissue blocks from the study were stained in three independent runs, with comparable staining results. For IHC, the primary antibody was first tested and antibody dilution and antigen retrieval optimized following standardized procedures at LADDL and using influenza virus A H5N1-infected tissues from a recent study (217) IHC was performed on selected respiratory tract and lymphoid tissues of infected calves in 3 independent staining runs, all of which included a positive control tissue slide that yielded consistent results. All evaluations and interpretations were performed by a double board-certified veterinary pathologist and virologist.

IAV-specific IHC for calf study

IHC for detection of IAV H5N1 NP antigen was performed on the auto- mated BOND RXm platform and the Polymer Refine Red Detection kit (Leica Biosystems). Following automated deparaffinization, 4-µm formalin-fixed, paraffin-embedded tissue sections on positively charged Superfrost Plus slides (VWR) were subjected to automated heat-induced epitope retrieval (HIER) using a ready-to-use EDTA-based retrieval solution (pH 9.0, Leica Biosystems) at 100 °C for 20 min. Subsequently, tissue sections were incubated with the primary antibody (rabbit monoclonal anti-IAV NP (Cell Signaling Technology, 99797/ F8L6X) diluted 1:1,200 in Primary Antibody diluent (Leica Biosystems)) for 30 min at ambient temperature followed by a ready-to-use (pre-diluted) polymer-labelled goat anti-rabbit IgG coupled with alkaline phosphatase (30 min). Fast Red was used as the chromogen (15 min), and counterstaining was performed with haematoxylin for 5 min. Slides were dried in a 60 °C oven for 30 min and mounted with a permanent mounting medium (Micromount, Leica Biosystems). Lung sections from a pig experimentally infected with swine influenza virus A/swine/Texas/4199-2/1998 H3N2 and mink-derived clade 2.3.4.4b H5N1 isolate, A/Mink/Spain/3691-8_22VIR10586−10/2022 were used as positive assay controls (Extended Data Figure 10).

Pathology for lactating dairy cows study

Full autopsy was performed on all animals under BSL-3 conditions and macroscopic diagnoses were recorded. In total, 45 samples (Supplementary Table 3) were fixed in 10% neutral buffered formalin. Tissues were paraffin-embedded and 2- to 4-µm-thick sections were stained with H&E. Consecutive slides were processed for IHC according to standardized procedures of avidin-biotin-peroxidase complex-method as described (224). The primary

antibody against the IAV nucleoprotein was applied overnight at 4 °C (ATCC clone HB-64, 1:200), the secondary biotinylated goat anti-mouse antibody was applied for 30 min at room temperature (Vector Laboratories, 1:200). Colour was developed by incubating the slides with avidin-biotin-peroxidase complex solution (Vectastain Elite ABC Kit; Vector Laboratories), followed by exposure to 3-amino-9-ethylcarbazole substrate (AEC, Dako). The sections were counterstained with Mayer's haematoxylin and cover- slipped. As negative control, the non-infected cow was tested with the primary antibody, and consecutive sections of infected animals were labelled with an irrelevant antibody (anti Sars clone 4F3C4, 1:45) (60). A positive control slide from an IAV infected chicken was included in each run (details included in Extended Data Figure 9f–h). All sides were scanned using a Hamamatsu S60 scanner, evaluation was done using the NDPview.2 plus software (Version 2.8.24, Hamamatsu Photonics) by a trained pathologist (T.B.) and a board-certified pathologist (A.B.). H&E-stained sections were evaluated and described. Following IHC the distribution of virus antigen was graded on an ordinal scale with scores as follows: 0, no antigen; 1, focal, affected cells/tissue <5% or up to 3 foci per tissue; 2, multifocal, 6%–40% affected; 3, coalescing, 41%–80% affected; 4, diffuse, >80% affected. The target cell was identified based on the morphology. Routine staining (H&E) was performed in six independent runs, yielding comparable staining results. For virus antigen detection, IHC was performed on up to 45 tissues per cattle (n = 3 per group; Supplementary Table 3). Five independent IHC runs gave com- parable results for the negative and positive controls. Evaluation and interpretation were performed by a board-certified pathologist with more than 17 years of experience.

Next-generation sequencing for calf study

Samples with high quality RNA extracts were subjected to previously established next-generation sequencing methods in order to evaluate the presence/frequency of genomic variants and their potential relation to host-adaptation (in reference to/changes compared to inoculum) (217). The whole-genome sequence of the cattle -derived clade 2.3.4.4b H5N1 virus was determined using the Illumina NextSeq sequencing platform (Illumina). In brief, viral RNA was extracted from the infection inoculum and virus-positive clinical samples (inactivated in RLT lysis buffer; Qiagen) using the QIAamp viral RNA mini kit (Qiagen). Viral gene segments for infection inoculum and clinical samples were amplified using SuperScript III One-Step RT-PCR System with Plati- num Taq DNA Polymerase (Thermo Fisher Scientific) with a universal influenza primer set (40, 102) All samples were normalized to 20 ng µl−1 (100–300 ng) prior to library preparations. Sequencing libraries were prepared using the Illumina DNA Prep kit (Illumina). Libraries were sequenced using pair-end chemistry on the Illumina NextSeq 550 (Illumina, SY-415-1002) platform with the NextSeq 500/550 Mid Output Kit v2.5 (300 cycles). Sequencing reads were demultiplexed and parsed into individual FASTQ files and imported into CLC Genomics Workbench version 23.0.5 (Qiagen) for analysis. Reads were trimmed to remove primer sequences and filtered to remove low quality and short reads. The trimmed reads were mapped to the reference sequence (A/Cattle/Texas/063224-24-1/2024; GISAID: EPI_ISL_19155861).

Following read mapping, all samples were run through the low frequency variant caller module within CLC Genomic Workbench with a frequency cut-off greater than 2%.

MinION sequencing for lactating dairy cows study

MinION-based sequencing of avian influenza positive samples with Cq values < 28 was carried out as described (39, 225). In brief, the RNA was transcribed into DNA using Superscript 60 III One-Step and Platinum Taq (12574026, Thermo Fisher Scientific) Kit with influenza-specific primers (Pan-IVA-1F_BsmF (26mer wobbel) TATTCGTCTCAGG GAGCRAAAGCAGG; Pan-IVA-1R_BsmR (26mer wobbel) ATATCGTCTCGTATTAGTAGAAACAAGG). DNA amplificants were purified with Agencourt AMPure XP beads (A63881, Beckmann Coulter) magnetic beads using DNA LoBind Tubes (0030108051, Eppendorf). Approximately 200 ng of DNA per sample was used for sequencing by a transposase-based library preparation approach with Rapid Barcoding (SQK-RBK114.24, Oxford Nanopore Technologies) and a PromethION Flow Cell (FLO-PRO114M) on a PromethION 2 solo device with MinKNOW Software Core (v5.9.12). Live high accuracy base calling of the raw data with Dorado (v7.3.11, Oxford Nanopore Technologies) was followed by demultiplexing, a quality check and a trimming step to remove low quality, primer and short (<20 bp) sequences. For ana- lysing, the bioinformatic software suite Geneious Prime (Biomatters, version 2024.0.5) was used. The sequences were trimmed, to remove the primer sequences. Consensus sequences were obtained with an iterative map-to-reference approach with Minimap2 (vs 2.24). The H5N1 B3.13 or the H5N1 euDG isolate sequence was used as a reference. Polishing of the final genome sequences and annotation was done manually after consensus generation (threshold matching 60% of bases of total adjusted quality). A total amount of n = 53 samples from the animal experiment as well as both virus stocks were sequenced. For the majority (42 samples) only partial assemblies were achieved. The remaining samples were screened for amino acid exchanges. For major variants A threshold of 55% was used to search

for specific mutations in the consensus sequences within the sequences. For adaptive mutations(PB2 E627K) also minor variants were determined. Sequence analysis was completed using the Geneious Prime 2024.0.5.

IAV-specific RAT evaluation

Milk samples from the animal experiment served as samples for validation of this assay with application to bovine milk origin samples. Serial samples of infected animals were analysed in the AIV-specific Megacor test. In brief, the provided swab was dipped into the respective milk sample and afterwards transferred into the assay buffer and mixed according to the manufacturer's protocol. Afterwards, the test strip provided in the kit was dipped into the assay buffer according to manufacturer's instructions. Results were read after 15 min of incubation.

Open Access

Reporting summary

Further information on research design is available in the Nature Port- folio Reporting Summary linked to this article.

Data availability

Consensus sequences of both isolates used for inoculation are avail- able in the International Nucleotide Sequence Database Collaboration under accession PQ241097–PQ241104 (calves) and under PQ106994– PQ107009 (cows; H5N1 B3.13: PQ106994–PQ107001; H5N1 euDG:PQ107002–PQ107009). Raw data were filed to the Sequence Read Archive under project number PRJNA1141392. Source data are pro- vided with this paper.

Acknowledgements

This work was supported by USDA NACA 58-3022-3-004, National Bio and Agro-Defense Facility (NBAF) Transition Fund from the State of Kansas, the USDA Animal Plant Health Inspection Service's NBAF Scientist Training Program, the AMP and MCB Cores of the Center on Emerging and Zoonotic Infectious Diseases (CEZID) of the National Institutes of General Medical Sciences under award number P20GM130448, and the NIAID supported Centers of Excellence for Influenza Research and Response (CEIRR, contract number 75N93021C00016). This work was further funded by the DURABLE project, co-funded by the European Union, under the EU4Health Programme (EU4H), project no. 101102733, and the Kappa-Flu project, under the Horizon Europe Programme (grant agreement KAPPA-FLU no. 101084171) and the German Federal Ministry of Education and Research within the project 'PREPMEDVET' grant no. 13N15449. Invaluable contributions that supported the success of this work were made by the professional and technical associates/staff of KSU-CEEZAD/ CEZID personnel (not limited to) G. Vediyappan, E. L. Lyoo, S. Elango, S. Ghimire, P. Assato,

D. Madden, Y. Li, I. Fitz and Z. Kohl. Additional support was provided by KSU-VDL molecular diagnostic and histopathology section laboratory personnel (oversight by J. Retallick, G. Hazlicek and L. Knoll), personnel of the histology and IHC sections of Louisiana Animal Disease Diagnostic Laboratory at Louisiana State University and the coordination and oversight provided by the animal care, lab coordinators and biosafety staff of the Biosecurity Research Institute (BRI) at Kansas State University. The authors also thank M. Grawe, S. Schuparis and R. Brandt for technical assistance; F. Klipp, S. Kiepert, C. Lipinski, F. Zimak, R. Siewert, R. Henkel, R. Redmer, M. Beerbohm and A. Bath for their invaluable and dedicated animal care; T. Harder for editorial remarks on the text; L. Mundhenk and C. Grund for scientific advice; and Innovative Diagnostics for providing the H5-ELISA kits

Additional information

Supplementary information: The online version contains supplementary material available at https://doi.org/10.1038/s41586-024-08063-y. Correspondence and requests for materials should be addressed to Martin Beer or Juergen A. Richt.

Chapter 6 - Concluding remarks

Taken together, the outcome of these studies provide new insight into the susceptibility of ruminant livestock to two of the most consequential zoonotic viruses of the 21st century. The outcome of experimental infection of these ruminant species with HPAIV H5N1 and SARS-CoV-2 demonstrated the variable degrees of susceptibility, but none totally refractory to infection under these experimental conditions, the evidence of limited infection, particularly in calves and sheep, suggests that they could someday play in the ecology of these viruses in nature. The detection of viral RNA in clinical samples, broad tissue tropism in most animals through the acute phase of infection, and seroconversion in a subset of animals demonstrates that exposure can lead to subclinical infection outcomes, which are always concerning during outbreaks as they exist as an unrealized source of infection.

For H5N1, the presence of virus in dairy cattle in the field and clear evidence of cow to cow transmission necessitated urgent response and basic research to understand how such high titer virus could be a sooner or later mplifying in a host that had been on the sideline. While the outbreak of H5N1 in dairy cows seems to be slowing down, there is still evidence being reported of sustained transmission of SARS-CoV-2 in white-tailed deer, and occasionally low-level seropositivity in other domestic ruminants. These differences highlight how viral ecology is shaped not just by host receptor compatibility, but by broader ecological and anthropogenic factors—housing, density, interspecies contact, and biosecurity practices.

The message is clear: we cannot afford to make assumptions about host susceptibility based solely on observations in the field or though in-silico or in vitro based evidence.. The pace of viral evolution, the scale of global livestock production, and the increasing frequency of wildlife-livestock-human interfaces mean that susceptibility is no longer stochastic, this is a

rapidly changing (dynamic) ecological system that demands attention. A virus that replicates inefficiently today may be virulent tomorrow. A species that appears unaffected in the lab may serve as a steppingstone in the field.

This is especially true for ruminants. Their global numbers, economic value, and proximity to both humans and wildlife make them critical conduits in the future of zoonotic disease emergence. Ignoring their potential role in viral ecology—whether due to assumptions about receptor usage or historical precedence—risks leaving blind spots in our preparedness strategies. Surveillance, experimental modeling, and risk assessment must include these species not as exceptions, but as integral parts of the system.

This work does not provide all the answers. But it establishes a foundation, offers tools for future research, and reinforces a simple idea: the more we understand about how these viruses behave in livestock, the better chance we have to detect, contain, and prevent the next outbreak—before it crosses the species line.

Despite these advances, critical research gaps remain. Most notably, the duration of viral shedding, potential for subclinical transmission, and the risk of co-infection with other endemic livestock pathogens remain poorly defined. This is particularly relevant for reassortment-prone viruses like influenza A, where simultaneous infection with multiple strains in a permissive host could facilitate genetic exchange and the emergence of novel variants. Comprehensive molecular and field surveillance is needed, with integration of virological, serological, and metagenomic tools. These data should inform both experimental design and policy frameworks aimed at preempting cross-species transmission events in high intensity agricultural systems

Chapter 7 - References

1. Rando Halie M, MacLean Adam L, Lee Alexandra J, Lordan R, Ray S, Bansal V, et al. Pathogenesis, Symptomatology, and Transmission of SARS-CoV-2 through Analysis of Viral Genomics and Structure. mSystems. 2021;6(5):10.1128/msystems.00095-21.

2. Jones KE, Patel NG, Levy MA, Storeygard A, Balk D, Gittleman JL, et al. Global trends in emerging infectious diseases. Nature. 2008;451(7181):990-3.

3. Gov.UK. Emerging infections: How and Why they Arise 2023 [Available from: https://www.gov.uk/government/publications/emerging-infections-characteristics-epidemiology-and-global-distribution/emerging-infections-how-and-why-they-arise.

4. Drexler JF, Corman VM, Drosten C. Ecology, evolution and classification of bat coronaviruses in the aftermath of SARS. Antiviral Res. 2014;101:45-56.

5. Graham RL, Baric RS. Recombination, reservoirs, and the modular spike: mechanisms of coronavirus cross-species transmission. J Virol. 2010;84(7):3134-46.

6. Leifels M, Khalilur Rahman O, Sam IC, Cheng D, Chua FJD, Nainani D, et al. The one health perspective to improve environmental surveillance of zoonotic viruses: lessons from COVID-19 and outlook beyond. ISME Commun. 2022;2(1):107.

7. de Wit E, van Doremalen N, Falzarano D, Munster VJ. SARS and MERS: recent insights into emerging coronaviruses. Nat Rev Microbiol. 2016;14(8):523-34.

8. Otte J, Pica-Ciamarra U. Emerging infectious zoonotic diseases: The neglected role of food animals. One health (Amsterdam, Netherlands). 2021;13:100323.

9. Shang Y, Li H, Zhang R. Effects of Pandemic Outbreak on Economies: Evidence From Business History Context. Frontiers in Public Health. 2021;9(146).

10. Caserta LC, Frye EA, Butt SL, Laverack M, Nooruzzaman M, Covaleda LM, et al. Spillover of highly pathogenic avian influenza H5N1 virus to dairy cattle. Nature. 2024.

11. USDA. HPAI Confirmed Cases in Livestock 2024 [Available from: https://www.aphis.usda.gov/livestock-poultry-disease/avian/avian-influenza/hpai-detections/hpai-confirmed-cases-livestock.

12. Vijgen L, Keyaerts E, Moës E, Thoelen I, Wollants E, Lemey P, et al. Complete genomic sequence of human coronavirus OC43: molecular clock analysis suggests a relatively recent zoonotic coronavirus transmission event. J Virol. 2005;79(3):1595-604.

13. Harvey WT, Carabelli AM, Jackson B, Gupta RK, Thomson EC, Harrison EM, et al. SARS-CoV-2 variants, spike mutations and immune escape. Nature Reviews Microbiology. 2021;19(7):409-24.

14. Prince T, Smith SL, Radford AD, Solomon T, Hughes GL, Patterson EI. SARS-CoV-2 Infections in Animals: Reservoirs for Reverse Zoonosis and Models for Study. Viruses. 2021;13(3).

15. Meekins DA, Gaudreault NN, Richt JA. Natural and Experimental SARS-CoV-2 Infection in Domestic and Wild Animals. Viruses. 2021;13(10).

16. McNamara T, Richt JA, Glickman L. A Critical Needs Assessment for Research in Companion Animals and Livestock Following the Pandemic of COVID-19 in Humans. Vector Borne Zoonotic Dis. 2020;20(6):393-405.

17. Lu L, Sikkema RS, Velkers FC, Nieuwenhuijse DF, Fischer EAJ, Meijer PA, et al. Adaptation, spread and transmission of SARS-CoV-2 in farmed minks and associated humans in the Netherlands. Nature Communications. 2021;12(1).

18. Aguero M, Monne I, Sanchez A, Zecchin B, Fusaro A, Ruano MJ, et al. Highly pathogenic avian influenza A(H5N1) virus infection in farmed minks, Spain, October 2022. Euro Surveill. 2023;28(3).

19. Ahrens AK, Pohlmann A, Grund C, Harder T, Beer M. Novel Genotypes of Highly Pathogenic Avian Influenza H5N1 Clade 2.3.4.4b Viruses, Germany, November 2023. Emerg Infect Dis. 2024;30(8):1737-9.

20. Puryear W, Sawatzki K, Hill N, Foss A, Stone JJ, Doughty L, et al. Highly Pathogenic Avian Influenza A(H5N1) Virus Outbreak in New England Seals, United States. Emerg Infect Dis. 2023;29(4):786-91.

21. Conceicao C, Thakur N, Human S, Kelly JT, Logan L, Bialy D, et al. The SARS-CoV-2 Spike protein has a broad tropism for mammalian ACE2 proteins. PLoS Biol. 2020;18(12):e3001016.

22. Shuai H, Chan JF-W, Yuen TT-T, Yoon C, Hu J-C, Wen L, et al. Emerging SARS-CoV-2 variants expand species tropism to murines. EBioMedicine. 2021;73:103643.

23. Sreenivasan CC, Thomas M, Kaushik RS, Wang D, Li F. Influenza A in Bovine Species: A Narrative Literature Review. Viruses. 2019;11(6).

24. Ardalan M, Cool K, Gaudreault NN, Bold D, Mannix A, Hanzlicek GA, et al. Cattle, sheep, and goat humoral immune responses against SARS-CoV-2. Veterinary and Animal Science. 2024;26:100408.

25. Bosco-Lauth A, Root JJ, Porter S, Walker A, Guilbert L, Hawvermale D, et al. Peridomestic Mammal Susceptibility to Severe Acute Respiratory Syndrome Coronavirus 2 Infection. Emerging Infectious Disease journal. 2021;27(8):2073.

26. Cool K, Gaudreault NN, Morozov I, Trujillo JD, Meekins DA, McDowell C, et al. Infection and transmission of ancestral SARS-CoV-2 and its alpha variant in pregnant white-tailed deer. Emerg Microbes Infect. 2022;11(1):95-112.

27. Damas J, Hughes GM, Keough KC, Painter CA, Persky NS, Corbo M, et al. Broad host range of SARS-CoV-2 predicted by comparative and structural analysis of ACE2 in vertebrates. Proc Natl Acad Sci U S A. 2020;117(36):22311-22.

28. Di Teodoro G, Valleriani F, Puglia I, Monaco F, Di Pancrazio C, Luciani M, et al. SARS-CoV-2 replicates in respiratory ex vivo organ cultures of domestic ruminant species. Vet Microbiol. 2021;252:108933.

29. Falkenberg S, Buckley A, Laverack M, Martins M, Palmer MV, Lager K, et al. Experimental Inoculation of Young Calves with SARS-CoV-2. Viruses. 2021;13(3).

30. Hamdy ME, El Deeb AH, Hagag NM, Shahein MA, Alaidi O, Hussein HA. Interspecies transmission of SARS CoV-2 with special emphasis on viral mutations and ACE-2 receptor homology roles. International Journal of Veterinary Science and Medicine. 2023;11(1):55-86.

31. Brown B, Gravier T, Fricke I, Al-Sheboul SA, Carp T-N, Leow CY, et al. Immunopathogenesis of Nipah Virus Infection and Associated Immune Responses. Immuno. 2023;3(2):160-81.

32. Kristensen C, Jensen HE, Trebbien R, Webby RJ, Larsen LE. Avian and Human Influenza A Virus Receptors in Bovine Mammary Gland. Emerg Infect Dis. 2024;30(9).

33. Keusch GT, Amuasi JH, Anderson DE, Daszak P, Eckerle I, Field H, et al. Pandemic origins and a One Health approach to preparedness and prevention: Solutions based on SARS-CoV-2 and other RNA viruses. Proc Natl Acad Sci U S A. 2022;119(42):e2202871119.

34. Li W, Shi Z, Yu M, Ren W, Smith C, Epstein JH, et al. Bats Are Natural Reservoirs of SARS-Like Coronaviruses. Science. 2005;310(5748):676-9.

35. Rulli MC, D'Odorico P, Galli N, Hayman DTS. Land-use change and the livestock revolution increase the risk of zoonotic coronavirus transmission from rhinolophid bats. Nature Food. 2021;2(6):409-16.

36. Sanchez CA, Li H, Phelps KL, Zambrana-Torrelio C, Wang LF, Zhou P, et al. A strategy to assess spillover risk of bat SARS-related coronaviruses in Southeast Asia. Nat Commun. 2022;13(1):4380.

37. Drexler JF, Corman VM, Drosten C. Ecology, evolution and classification of bat coronaviruses in the aftermath of SARS. Antiviral Res. 2014;101:45-56.

38. Latinne A, Hu B, Olival KJ, Zhu G, Zhang L-B, Li H, et al. Origin and cross-species transmission of bat coronaviruses in China. Nature Communications. 2024;15(1).

39. King J, Harder T, Globig A, Stacker L, Gunther A, Grund C, et al. Highly pathogenic avian influenza virus incursions of subtype H5N8, H5N5, H5N1, H5N4, and H5N3 in Germany during 2020-21. Virus Evol. 2022;8(1):veac035.

40. Zhou B, Wentworth DE. Influenza A virus molecular virology techniques. Methods Mol Biol. 2012;865:175-92.

41. Bosco-Lauth AM, Walker A, Guilbert L, Porter S, Hartwig A, McVicker E, et al. Susceptibility of livestock to SARS-CoV-2 infection. Emerging Microbes & Infections. 2021:1-7.

42. Gaudreault NN, Cool K, Trujillo JD, Morozov I, Meekins DA, McDowell C, et al. Susceptibility of sheep to experimental co-infection with the ancestral lineage of SARS-CoV-2 and its alpha variant. bioRxiv. 2021.

43. Gaudreault NN, Trujillo JD, Carossino M, Meekins DA, Morozov I, Madden DW, et al. SARS-CoV-2 infection, disease and transmission in domestic cats. Emerg Microbes Infect. 2020;9(1):2322-32.

44. Goldberg AR, Langwig KE, Marano J, Rai P, Sharp AK, Brown KL, et al. Wildlife exposure to SARS-CoV-2 across a human use gradient. 2022.

45. Hale VL, Dennis PM, McBride DS, Nolting JM, Madden C, Huey D, et al. SARS-CoV-2 infection in free-ranging white-tailed deer. Nature. 2022;602(7897):481-6.

46. Baker AL, Arruda B, Palmer MV, Boggiatto P, Sarlo Davila K, Buckley A, et al. Experimental reproduction of viral replication and disease in dairy calves and lactating cows inoculated with highly pathogenic avian influenza H5N1 clade 2.3.4.4b. bioRxiv. 2024:2024.07.12.603337.

47. Peña-Mosca F, Frye EA, Maclachlan M, Rebelo AR, De Oliveira PSB, Nooruzzaman M, et al. The impact of influenza A H5N1 virus infection in dairy cows. 2025.

48. Wernike K, Böttcher J, Amelung S, Albrecht K, Gärtner T, Donat K, et al. Antibodies against SARS-CoV-2 Suggestive of Single Events of Spillover to Cattle, Germany. Emerg Infect Dis. 2022;28(9):1916-8.

49. Beaudette F, Hudson C. Cultivation of the Virus of Infectious Bronchitis. Journal of the American Veterinary Medical Association. 1937;90:51–60.

50. Zaki AM, Van Boheemen S, Bestebroer TM, Osterhaus ADME, Fouchier RAM. Isolation of a Novel Coronavirus from a Man with Pneumonia in Saudi Arabia. New England Journal of Medicine. 2012;367(19):1814-20.

51. WHO. Cumulative Number of Reported Cases (SARS). 2003 26 March.

52. CDC CfDC. Severe acute respiratory syndrome--Singapore, 2003. MMWR Morbidity and mortality weekly report: Center for Disease Control; 2003. p. 405-11.

53. De Wit E, Van Doremalen N, Falzarano D, Munster VJ. SARS and MERS: recent insights into emerging coronaviruses. Nature Reviews Microbiology. 2016;14(8):523-34.

54. Reusken CB, Haagmans BL, Müller MA, Gutierrez C, Godeke G-J, Meyer B, et al. Middle East respiratory syndrome coronavirus neutralising serum antibodies in dromedary camels: a comparative serological study. The Lancet Infectious Diseases. 2013;13(10):859-66.

55. Zhong N, Zheng B, Li Y, Poon L, Xie Z, Chan K, et al. Epidemiology and cause of severe acute respiratory syndrome (SARS) in Guangdong, People's Republic of China, in February, 2003. The Lancet. 2003;362(9393):1353-8.

56. Gao G, Liu W, Liu P, Lei W, Jia Z, He X, et al. Surveillance of SARS-CoV-2 in the environment and animal samples of the Huanan Seafood Market. 2022.

57. Crits-Christoph A, Levy JI, Pekar JE, Goldstein SA, Singh R, Hensel Z, et al. Genetic tracing of market wildlife and viruses at the epicenter of the COVID-19 pandemic. Cell. 2024;187(19):5468-82.e11.

58. Sit THC, Brackman CJ, Ip SM, Tam KWS, Law PYT, To EMW, et al. Infection of dogs with SARS-CoV-2. Nature. 2020;586(7831):776-8.

59. Damas J, Hughes GM, Keough KC, Painter CA, Persky NS, Corbo M, et al. Broad host range of SARS-CoV-2 predicted by comparative and structural analysis of ACE2 in vertebrates. Proceedings of the National Academy of Sciences. 2020;117(36):22311-22.

60. Bussmann BM, Reiche S, Jacob LH, Braun JM, Jassoy C. Antigenic and cellular localisation analysis of the severe acute respiratory syndrome coronavirus nucleocapsid protein using monoclonal antibodies. Virus Res. 2006;122(1-2):119-26.

61. Hoffmann M, Kleine-Weber H, Schroeder S, Kruger N, Herrler T, Erichsen S, et al. SARS-CoV-2 Cell Entry Depends on ACE2 and TMPRSS2 and Is Blocked by a Clinically Proven Protease Inhibitor. Cell. 2020;181(2):271-80 e8.

62. WHO. WHO Coronavirus (COVID-19) dashboard data.who.int: World Health Organization 2023 [updated 26/10/2025. Epidemological]. Available from: https://data.who.int/dashboards/covid19/more-resources.

63. Happi AN, Ayinla AO, Ogunsanya OA, Sijuwola AE, Saibu FM, Akano K, et al. Detection of SARS-CoV-2 in Terrestrial Animals in Southern Nigeria: Potential Cases of Reverse Zoonosis. Viruses. 2023;15(5):1187.

64. Goraichuk IV, Arefiev V, Stegniy BT, Gerilovych AP. Zoonotic and Reverse Zoonotic Transmissibility of SARS-CoV-2. Virus research. 2021;302:198473.

65. U.S. Department of Agriculture A, Plant Health Inspection S. SARS-CoV-2 in Animals. 2025.

66. WAHIS P. SARS-ANI VIS: A Global Open Access Dataset of Reported SARS-CoV-2 Events in Animals. 2025.

67. Agnelli S, Capua I. Pandemic or Panzootic—A Reflection on Terminology for SARS-CoV-2 Infection. Emerging Infectious Diseases. 2022;28(12):2552-5.

68. Oude Munnink BB, Sikkema RS, Nieuwenhuijse DF, Molenaar RJ, Munger E, Molenkamp R, et al. Transmission of SARS-CoV-2 on mink farms between humans and mink and back to humans. Science. 2021;371(6525):172-7.

69. Pickering B, Lung O, Maguire F, Kruczkiewicz P, Kotwa JD, Buchanan T, et al. Divergent SARS-CoV-2 variant emerges in white-tailed deer with deer-to-human transmission. Nature Microbiology. 2022;7(12):2011-24.

70. Yen H-L, Sit THC, Brackman CJ, Chuk SSY, Gu H, Tam KWS, et al. Transmission of SARS-CoV-2 delta variant (AY.127) from pet hamsters to humans, leading to onward human-to-human transmission: a case study. The Lancet. 2022;399(10329):1070-8.

71. Zhao J, Wan W, Yu K, Lemey P, Pettersson JHO, Bi Y, et al. Farmed fur animals harbour viruses with zoonotic spillover potential. Nature. 2024.

72. Feng A, Bevins S, Chandler J, Deliberto TJ, Ghai R, Lantz K, et al. Transmission of SARS-CoV-2 in free-ranging white-tailed deer in the United States. Nature Communications. 2023;14(1).

73. Caserta LC, Martins M, Butt SL, Hollingshead NA, Covaleda LM, Ahmed S, et al. White-tailed deer (Odocoileus virginianus) may serve as a wildlife reservoir for nearly extinct SARS-CoV-2 variants of concern. Proceedings of the National Academy of Sciences. 2023;120(6).

74. Kuchipudi SV, Surendran-Nair M, Ruden RM, Yon M, Nissly RH, Vandegrift KJ, et al. Multiple spillovers from humans and onward transmission of SARS-CoV-2 in white-tailed deer. Proceedings of the National Academy of Sciences. 2022;119(6):e2121644119.

75. Hewitt J, Wilson-Henjum G, Collins D, Linder T, Lenoch J, Heale J, et al. Landscape-scale Epidemiological Dynamics of SARS-CoV-2 in White-tailed Deer. 2024.

76. Ardalan M, Cool K, Gaudreault NN, Bold D, Rojas C, Mannix A, et al. Bison, Elk, and Other Captive Wildlife Species Humoral Immune Responses against SARS-CoV-2. Animals. 2024;14(19):2829.

77. Fiorito F, Iovane V, Pagnini U, Cerracchio C, Brandi S, Levante M, et al. First Description of Serological Evidence for SARS-CoV-2 in Lactating Cows. Animals : an open access journal from MDPI. 2022;12(11).

78. Kumar A, Panwar A, Batra K, De S, Maan S. In-silico Analysis of Angiotensin-converting Enzyme 2 (ACE2) of Livestock, Pet and Poultry Animals to Determine its Susceptibility to SARS-CoV- 2 Infection. Comb Chem High Throughput Screen. 2021;24(10):1769-83.

79. Bosco-Lauth AM, Walker A, Guilbert L, Porter S, Hartwig A, McVicker E, et al. Susceptibility of livestock to SARS-CoV-2 infection. Emerg Microbes Infect. 2021;10(1):2199-201.

80. Cool K, Gaudreault NN, Morozov I, Trujillo JD, Meekins DA, McDowell C, et al. Infection and transmission of ancestral SARS-CoV-2 and its alpha variant in pregnant white-tailed deer. Emerging Microbes & Infections. 2022;11(1):95-112.

81. Goldberg AR, Langwig KE, Brown KL, Marano JM, Rai P, King KM, et al. Widespread exposure to SARS-CoV-2 in wildlife communities. Nat Commun. 2024;15(1):6210.

82. Fusco G, Cardillo L, Levante M, Brandi S, Picazio G, Napoletano M, et al. First serological evidence of SARS-CoV-2 natural infection in small ruminants. Vet Res Commun. 2023;47(3):1741-8.

83. Cool K, Gaudreault NN, Trujillo JD, Morozov I, McDowell CD, Bold D, et al. Experimental co-infection of calves with SARS-CoV-2 Delta and Omicron variants of concern. Emerging Microbes & Infections. 2024;13(1).

84. Di Guardo G. Transmission of SARS-CoV-2 from a cat to a person. Vet Rec. 2022;191(2):81.

85. Fuentealba NA, More G, Bravi ME, Unzaga JM, De Felice L, Salina M, et al. First detection and molecular analysis of SARS-CoV-2 from a naturally infected cat from Argentina. Vet Microbiol. 2021;260:109179.

86. Animal USDoA, Plant Health Inspection S. Interim SARS-CoV-2 Guidance and Recommendations for Farmed Mink. 2021.

87. Centers for Disease C, Prevention. Guidance for Safely Importing and Handling Mink and Mink Products — Bringing an Animal into the United States. 2021.

88. Food, Agriculture Organization of the United N. FAO publication (bitstream 04d7e4bb-329c-41e2-80c3-5f8f43472407). 2021.

89. World Organisation for Animal H. Guidance on working with farmed animals of species susceptible to SARS-CoV-2 (Version 2.1). 2021.

90. Hadfield J, Megill C, Bell SM, Huddleston J, Potter B, Callender C, et al. Nextstrain: real-time tracking of pathogen evolution. Bioinformatics. 2018;34(23):4121-3.

91. Data GGIoSAI. Submission Tracker Global. 2025.

92. Data GGIoSAI. hCoV-19 Variants Dashboard. 2025.

93. Morozov I, Gaudreault NN, Trujillo JD, Indran SV, Cool K, Kwon T, et al. Preliminary Study on the Efficacy of a Recombinant, Subunit SARS-CoV-2 Animal Vaccine against Virulent SARS-CoV-2 Challenge in Cats. Vaccines. 2023;11(12):1831.

94. Gaudreault NN, Trujillo JD, Carossino M, Meekins DA, Morozov I, Madden DW, et al. SARS-CoV-2 infection, disease and transmission in domestic cats. Emerging Microbes & Infections. 2020;9(1):2322-32.

95. Gaudreault NN, Carossino M, Morozov I, Trujillo JD, Meekins DA, Madden DW, et al. Experimental re-infected cats do not transmit SARS-CoV-2. Emerging Microbes & Infections. 2021;10(1):638-50.

96. Lopez Bernal J, Andrews N, Gower C, Gallagher E, Simmons R, Thelwall S, et al. Effectiveness of Covid-19 Vaccines against the B.1.617.2 (Delta) Variant. New England Journal of Medicine. 2021;385(7):585-94.

97. Kustin T, Harel N, Finkel U, Perchik S, Harari S, Tahor M, et al. Evidence for increased breakthrough rates of SARS-CoV-2 variants of concern in BNT162b2-mRNA-vaccinated individuals. Nature Medicine. 2021;27(8):1379-84.

98. Abdelwhab EM, Beer M. Panzootic HPAIV H5 and risks to novel mammalian hosts. npj Viruses. 2024;2(1):22.

99. Holmes EC, Krammer F, Goodrum FD. Virology—The next fifty years. Cell. 2024;187(19):5128-45.

100. Leguia M, Garcia-Glaessner A, Munoz-Saavedra B, Juarez D, Barrera P, Calvo-Mac C, et al. Highly pathogenic avian influenza A (H5N1) in marine mammals and seabirds in Peru. Nat Commun. 2023;14(1):5489.

101. Grange ZL, Goldstein T, Johnson CK, Anthony S, Gilardi K, Daszak P, et al. Ranking the risk of animal-to-human spillover for newly discovered viruses. Proc Natl Acad Sci U S A. 2021;118(15).

102. Lee DH. Complete Genome Sequencing of Influenza A Viruses Using Next-Generation Sequencing. Methods Mol Biol. 2020;2123:69-79.

103. Bevins SN, Shriner SA, Cumbee JC, Jr., Dilione KE, Douglass KE, Ellis JW, et al. Intercontinental Movement of Highly Pathogenic Avian Influenza A(H5N1) Clade 2.3.4.4 Virus to the United States, 2021. Emerg Infect Dis. 2022;28(5):1006-11.

104. Caliendo V, Lewis NS, Pohlmann A, Baillie SR, Banyard AC, Beer M, et al. Transatlantic spread of highly pathogenic avian influenza H5N1 by wild birds from Europe to North America in 2021. Sci Rep. 2022;12(1):11729.

105. Uhart M, Vanstreels RET, Nelson MI, Olivera V, Campagna J, Zavattieri V, et al. Massive outbreak of Influenza A H5N1 in elephant seals at Península Valdés, Argentina: increased evidence for mammal-to-mammal transmission. bioRxiv. 2024:2024.05.31.596774.

106. (WHO) WHO. The panzootic spread of highly pathogenic avian influenza H5N1 sublineage 2.3.4.4b: a critical appraisal of One Health preparedness and prevention 2023

[Available from: https://www.who.int/publications/m/item/the-panzootic-spread-of-highly-pathogenic-avian-influenza-h5n1-sublineage-2.3.4.4b--a-critical-appraisal-of-one-health-preparedness-and-prevention.

107. Baechlein C, Kleinschmidt S, Hartmann D, Kammeyer P, Wohlke A, Warmann T, et al. Neurotropic Highly Pathogenic Avian Influenza A(H5N1) Virus in Red Foxes, Northern Germany. Emerg Infect Dis. 2023;29(12):2509-12.

108. Burrough ER, Magstadt DR, Petersen B, Timmermans SJ, Gauger PC, Zhang J, et al. Highly Pathogenic Avian Influenza A(H5N1) Clade 2.3.4.4b Virus Infection in Domestic Dairy Cattle and Cats, United States, 2024. Emerg Infect Dis. 2024;30(7):1335-43.

109. Hu X, Saxena A, Magstadt DR, Gauger PC, Burrough E, Zhang J, et al. Highly Pathogenic Avian Influenza A (H5N1) clade 2.3.4.4b Virus detected in dairy cattle. bioRxiv. 2024:2024.04.16.588916.

110. Nguyen T-Q, Hutter C, Markin A, Thomas M, Lantz K, Killian ML, et al. Emergence and interstate spread of highly pathogenic avian influenza A(H5N1) in dairy cattle. bioRxiv. 2024:2024.05.01.591751.

111. Halwe NJ, Cool K, Breithaupt A, Schön J, Trujillo JD, Nooruzzaman M, et al. H5N1 clade 2.3.4.4b dynamics in experimentally infected calves and cows. Nature. 2024.

112. Baker AL, Arruda B, Palmer MV, Boggiatto P, Sarlo Davila K, Buckley A, et al. Dairy cows inoculated with highly pathogenic avian influenza virus H5N1. Nature. 2025;637(8047):913-20.

113. Kirk NM, Liang Y, Ly H. Comparative Pathology of Animal Models for Influenza A Virus Infection. Pathogens [Internet]. 2024; 13(1).

114. Chopra P, Ray SD, Page CK, Shepard JD, Kandeil A, Jeevan T, et al. Receptor-binding specificity of a bovine influenza A virus. Nature. 2025;640(8059):E21-E7.

115. Matrosovich M, Stech J, Klenk HD. Influenza receptors, polymerase and host range. Rev Sci Tech. 2009;28(1):203-17.

116. Weber M, Sediri H, Felgenhauer U, Binzen I, Banfer S, Jacob R, et al. Influenza virus adaptation PB2-627K modulates nucleocapsid inhibition by the pathogen sensor RIG-I. Cell Host Microbe. 2015;17(3):309-19.

117. Sediri H, Schwalm F, Gabriel G, Klenk HD. Adaptive mutation PB2 D701N promotes nuclear import of influenza vRNPs in mammalian cells. Eur J Cell Biol. 2015;94(7-9):368-74.

118. Matrosovich M, Herrler G, Klenk HD. Sialic Acid Receptors of Viruses. Top Curr Chem. 2015;367:1-28.

119. Ganti K, Bagga A, Carnaccini S, Ferreri LM, Geiger G, Joaquin Caceres C, et al. Influenza A virus reassortment in mammals gives rise to genetically distinct within-host subpopulations. Nat Commun. 2022;13(1):6846.

120. Le Sage V, Campbell AJ, Reed DS, Duprex WP, Lakdawala SS. Persistence of Influenza H5N1 and H1N1 Viruses in Unpasteurized Milk on Milking Unit Surfaces. Emerg Infect Dis. 2024;30(8):1721-3.

121. Ciminski K, Chase G, Schwemmle M, Beer M. Advocating a watch-and-prepare approach with avian influenza. Nat Microbiol. 2023;8(9):1603-5.

122. Plaza PI, Gamarra-Toledo V, Rodriguez Eugui J, Rosciano N, Lambertucci SA. Pacific and Atlantic sea lion mortality caused by highly pathogenic Avian Influenza A(H5N1) in South America. Travel Med Infect Dis. 2024;59:102712.

123. Agüero B, Berrios F, Pardo-Roa C, Ariyama N, Bennett B, Medina R, et al. First detection of Omicron variant BA.4.1 lineage in dogs, Chile. Veterinary Quarterly. 2024;44(1):1-10.

124. Singh G, Trujillo JD, McDowell CD, Matias-Ferreyra F, Kafle S, Kwon T, et al. Detection and characterization of H5N1 HPAIV in environmental samples from a dairy farm. Virus Genes. 2024.

125. Uyeki TM, Milton S, Abdul Hamid C, Reinoso Webb C, Presley SM, Shetty V, et al. Highly Pathogenic Avian Influenza A(H5N1) Virus Infection in a Dairy Farm Worker. N Engl J Med. 2024;390(21):2028-9.

126. World Health O. Global Influenza Surveillance and Response System (GISRS). 2025.

127. Rosenblatt E, Cook JD, DiRenzo GV, Grant EHC, Arce F, Pepin KM, et al. Epidemiological modeling of SARS-CoV-2 in white-tailed deer (Odocoileus virginianus) reveals conditions for introduction and widespread transmission. PLoS Comput Biol. 2024;20(7):e1012263.

128. Oude Munnink BB, Sikkema RS, Nieuwenhuijse DF, Molenaar RJ, Munger E, Molenkamp R, et al. Transmission of SARS-CoV-2 on mink farms between humans and mink and back to humans. Science. 2020.

129. Shi J, Wen Z, Zhong G, Yang H, Wang C, Huang B, et al. Susceptibility of ferrets, cats, dogs, and other domesticated animals to SARS-coronavirus 2. Science. 2020;368(6494):1016-20.

130. Halfmann PJ, Hatta M, Chiba S, Maemura T, Fan S, Takeda M, et al. Transmission of SARS-CoV-2 in Domestic Cats. N Engl J Med. 2020;383(6):592-4.

131. Kim YI, Kim SG, Kim SM, Kim EH, Park SJ, Yu KM, et al. Infection and Rapid Transmission of SARS-CoV-2 in Ferrets. Cell Host Microbe. 2020;27(5):704-9 e2.

132. Imai M, Iwatsuki-Horimoto K, Hatta M, Loeber S, Halfmann PJ, Nakajima N, et al. Syrian hamsters as a small animal model for SARS-CoV-2 infection and countermeasure development. Proc Natl Acad Sci U S A. 2020;117(28):16587-95.

133. Singh DK, Singh B, Ganatra SR, Gazi M, Cole J, Thippeshappa R, et al. Responses to acute infection with SARS-CoV-2 in the lungs of rhesus macaques, baboons and marmosets. Nat Microbiol. 2021;6(1):73-86.

134. Griffin BD, Chan M, Tailor N, Mendoza EJ, Leung A, Warner BM, et al. SARS-CoV-2 infection and transmission in the North American deer mouse. Nature Communications. 2021;12(1):3612.

135. Shuai L, Zhong G, Yuan Q, Wen Z, Wang C, He X, et al. Replication, pathogenicity, and transmission of SARS-CoV-2 in minks. National Science Review. 2020;8(3).

136. Zhao Y, Wang J, Kuang D, Xu J, Yang M, Ma C, et al. Susceptibility of tree shrew to SARS-CoV-2 infection. Sci Rep. 2020;10(1):16007.

137. Bosco-Lauth AM, Hartwig AE, Porter SM, Gordy PW, Nehring M, Byas AD, et al. Experimental infection of domestic dogs and cats with SARS-CoV-2: Pathogenesis, transmission, and response to reexposure in cats. Proc Natl Acad Sci U S A. 2020;117(42):26382-8.

138. Ulrich L, Wernike K, Hoffmann D, Mettenleiter TC, Beer M. Experimental Infection of Cattle with SARS-CoV-2. Emerg Infect Dis. 2020;26(12):2979-81.

139. Schlottau K, Rissmann M, Graaf A, Schön J, Sehl J, Wylezich C, et al. SARS-CoV-2 in fruit bats, ferrets, pigs, and chickens: an experimental transmission study. The Lancet Microbe. 2020;1(5):e218-e25.

140. Meekins DA, Morozov I, Trujillo JD, Gaudreault NN, Bold D, Carossino M, et al. Susceptibility of swine cells and domestic pigs to SARS-CoV-2. Emerg Microbes Infect. 2020;9(1):2278-88.

141. Zhou B, Thao TTN, Hoffmann D, Taddeo A, Ebert N, Labroussaa F, et al. SARS-CoV-2 spike D614G change enhances replication and transmission. Nature. 2021;592(7852):122-7.

142. Palmer MV, Martins M, Falkenberg S, Buckley A, Caserta LC, Mitchell PK, et al. Susceptibility of white-tailed deer (Odocoileus virginianus) to SARS-CoV-2. J Virol. 2021.

143. Chandler JC, Bevins SN, Ellis JW, Linder TJ, Tell RM, Jenkins-Moore M, et al. SARS-CoV-2 exposure in wild white-tailed deer (Odocoileus virginianus). bioRxiv. 2021:2021.07.29.454326.

144. Matsuyama S, Nao N, Shirato K, Kawase M, Saito S, Takayama I, et al. Enhanced isolation of SARS-CoV-2 by TMPRSS2-expressing cells. Proc Natl Acad Sci U S A. 2020;117(13):7001-3.

145. Hierholzer JC, Killington RA. 2 - Virus isolation and quantitation A2 - Mahy, Brian WJ. In: Kangro HO, editor. Virology Methods Manual. London: Academic Press; 1996. p. 25-46.

146. Sunwoo SY, Noronha LE, Morozov I, Trujillo JD, Kim IJ, Schirtzinger EE, et al. Evaluation of A Baculovirus-Expressed VP2 Subunit Vaccine for the Protection of White-Tailed Deer (Odocoileus virginianus) from Epizootic Hemorrhagic Disease. Vaccines. 2020;8:1bh+.

147. Carossino M, Ip HS, Richt JA, Shultz K, Harper K, Loynachan AT, et al. Detection of SARS-CoV-2 by RNAscope(®) in situ hybridization and immunohistochemistry techniques. Archives of virology. 2020;165(10):2373-7.

148. Tillett RL, Sevinsky JR, Hartley PD, Kerwin H, Crawford N, Gorzalski A, et al. Genomic evidence for reinfection with SARS-CoV-2: a case study. Lancet Infect Dis. 2020.

149. Goldman JD, Wang K, Roltgen K, Nielsen SCA, Roach JC, Naccache SN, et al. Reinfection with SARS-CoV-2 and Failure of Humoral Immunity: a case report. medRxiv. 2020.

150. Harrington D, Kele B, Pereira S, Couto-Parada X, Riddell A, Forbes S, et al. Confirmed Reinfection with SARS-CoV-2 Variant VOC-202012/01. Clinical infectious diseases : an official publication of the Infectious Diseases Society of America. 2021.

151. Palmer MV, Cox RJ, Waters WR, Thacker TC, Whipple DL. Using White-tailed Deer (Odocoileus virginianus) in Infectious Disease Research. J Am Assoc Lab Anim Sci. 2017;56(4):350-60.

152. Thorne LG, Bouhaddou M, Reuschl AK, Zuliani-Alvarez L, Polacco B, Pelin A, et al. Evolution of enhanced innate immune evasion by the SARS-CoV-2 B.1.1.7 UK variant. bioRxiv. 2021.

153. Parker MD, Lindsey BB, Shah DR, Hsu S, Keeley AJ, Partridge DG, et al. Altered Subgenomic RNA Expression in SARS-CoV-2 B.1.1.7 Infections. bioRxiv. 2021:2021.03.02.433156.

154. Alekseev KP, Vlasova AN, Jung K, Hasoksuz M, Zhang X, Halpin R, et al. Bovine-like coronaviruses isolated from four species of captive wild ruminants are homologous to bovine coronaviruses, based on complete genomic sequences. J Virol. 2008;82(24):12422-31.

155. Hou YJ, Chiba S, Halfmann P, Ehre C, Kuroda M, Dinnon KH, 3rd, et al. SARS-CoV-2 D614G variant exhibits efficient replication ex vivo and transmission in vivo. Science. 2020;370(6523):1464-8.

156. Yurkovetskiy L, Wang X, Pascal KE, Tomkins-Tinch C, Nyalile T, Wang Y, et al. SARS-CoV-2 Spike protein variant D614G increases infectivity and retains sensitivity to antibodies that target the receptor binding domain. bioRxiv. 2020.

157. Yurkovetskiy L, Wang X, Pascal KE, Tomkins-Tinch C, Nyalile TP, Wang Y, et al. Structural and Functional Analysis of the D614G SARS-CoV-2 Spike Protein Variant. Cell. 2020;183(3):739-51 e8.

158. Liu Y, Liu J, Plante KS, Plante JA, Xie X, Zhang X, et al. The N501Y spike substitution enhances SARS-CoV-2 transmission. bioRxiv. 2021.

159. Clark MA. Bovine coronavirus. Br Vet J. 1993;149(1):51-70.

160. Vlasova AN, Saif LJ. Bovine Coronavirus and the Associated Diseases. Front Vet Sci. 2021;8:643220.

161. Verstegen J, Dhaliwal G, Verstegen-Onclin K. Canine and feline pregnancy loss due to viral and non-infectious causes: a review. Theriogenology. 2008;70(3):304-19.

162. Zambrano LI, Fuentes-Barahona IC, Bejarano-Torres DA, Bustillo C, Gonzales G, Vallecillo-Chinchilla G, et al. A pregnant woman with COVID-19 in Central America. Travel Med Infect Dis. 2020;36:101639.

163. Allotey J, Stallings E, Bonet M, Yap M, Chatterjee S, Kew T, et al. Clinical manifestations, risk factors, and maternal and perinatal outcomes of coronavirus disease 2019 in pregnancy: living systematic review and meta-analysis. BMJ. 2020;370:m3320.

164. Galang RR, Newton SM, Woodworth KR, Griffin I, Oduyebo T, Sancken CL, et al. Risk Factors for Illness Severity Among Pregnant Women With Confirmed Severe Acute Respiratory Syndrome Coronavirus 2 Infection—Surveillance for Emerging Threats to Mothers and Babies Network, 22 State, Local, and Territorial Health Departments, 29 March 2020–5 March 2021. Clinical Infectious Diseases. 2021;73(Supplement_1):S17-S23.

165. Ko JY, DeSisto CL, Simeone RM, Ellington S, Galang RR, Oduyebo T, et al. Adverse Pregnancy Outcomes, Maternal Complications, and Severe Illness Among US Delivery Hospitalizations With and Without a Coronavirus Disease 2019 (COVID-19) Diagnosis. Clinical infectious diseases : an official publication of the Infectious Diseases Society of America. 2021;73(Suppl 1):S24-s31.

166. Woodworth KR, Olsen EO, Neelam V, Lewis EL, Galang RR, Oduyebo T, et al. Birth and Infant Outcomes Following Laboratory-Confirmed SARS-CoV-2 Infection in Pregnancy - SET-NET, 16 Jurisdictions, March 29-October 14, 2020. MMWR Morbidity and mortality weekly report. 2020;69(44):1635-40.

167. Edlow AG, Li JZ, Collier AY, Atyeo C, James KE, Boatin AA, et al. Assessment of Maternal and Neonatal SARS-CoV-2 Viral Load, Transplacental Antibody Transfer, and

Placental Pathology in Pregnancies During the COVID-19 Pandemic. JAMA Netw Open. 2020;3(12):e2030455.

168. Fenizia C, Biasin M, Cetin I, Vergani P, Mileto D, Spinillo A, et al. Analysis of SARS-CoV-2 vertical transmission during pregnancy. Nature Communications. 2020;11(1):5128.

169. Rabalski L, Kosinski M, Mazur-Panasiuk N, Szewczyk B, Bienkowska-Szewczyk K, Kant R, et al. Zoonotic spillover of SARS-CoV-2: mink-adapted virus in humans. bioRxiv. 2021:2021.03.05.433713.

170. Chakraborty C, Sharma AR, Bhattacharya M, Agoramoorthy G, Lee SS. Evolution, Mode of Transmission, and Mutational Landscape of Newly Emerging SARS-CoV-2 Variants. Mbio. 2021;12(4).

171. Munster VJ, Feldmann F, Williamson BN, van Doremalen N, Perez-Perez L, Schulz J, et al. Respiratory disease in rhesus macaques inoculated with SARS-CoV-2. Nature. 2020;585(7824):268-72.

172. Cool K, Gaudreault NN, Morozov I, Trujillo JD, Meekins DA, McDowell C, et al. Infection and transmission of SARS-CoV-2 and its alpha variant in pregnant white-tailed deer. bioRxiv. 2021.

173. Suarez DL, Pantin-Jackwood MJ, Swayne DE, Lee SA, DeBlois SM, Spackman E. Lack of Susceptibility to SARS-CoV-2 and MERS-CoV in Poultry. Emerg Infect Dis. 2020;26(12):3074-6.

174. Mykytyn AZ, Lamers MM, Okba NMA, Breugem TI, Schipper D, van den Doel PB, et al. Susceptibility of rabbits to SARS-CoV-2. Emerging Microbes & Infections. 2021;10(1):1-7.

175. Freuling CM, Breithaupt A, Muller T, Sehl J, Balkema-Buschmann A, Rissmann M, et al. Susceptibility of Raccoon Dogs for Experimental SARS-CoV-2 Infection. Emerg Infect Dis. 2020;26(12):2982-5.

176. Niu Z, Zhang Z, Gao X, Du P, Lu J, Yan B, et al. N501Y mutation imparts cross-species transmission of SARS-CoV-2 to mice by enhancing receptor binding. Signal Transduction and Targeted Therapy. 2021;6(1):284.

177. Imai M, Halfmann PJ, Yamayoshi S, Iwatsuki-Horimoto K, Chiba S, Watanabe T, et al. Characterization of a new SARS-CoV-2 variant that emerged in Brazil. Proc Natl Acad Sci U S A. 2021;118(27).

178. Hammer AS, Quaade ML, Rasmussen TB, Fonager J, Rasmussen M, Mundbjerg K, et al. SARS-CoV-2 Transmission between Mink (Neovison vison) and Humans, Denmark. Emerg Infect Dis. 2020;27(2).

179. Villanueva-Saz S, Giner J, Fernández A, Lacasta D, Ortín A, Ramos JJ, et al. Absence of SARS-CoV-2 Antibodies in Natural Environment Exposure in Sheep in Close Contact with Humans. Animals : an open access journal from MDPI. 2021;11(7).

180. Li H, Mendelsohn E, Zong C, Zhang W, Hagan E, Wang N, et al. Human-animal interactions and bat coronavirus spillover potential among rural residents in Southern China. Biosafety and Health. 2019;1(2):84-90.

181. Tan CCS, Lam SD, Richard D, Owen CJ, Berchtold D, Orengo C, et al. Transmission of SARS-CoV-2 from humans to animals and potential host adaptation. Nature Communications. 2022;13(1).

182. Goldberg AR, Langwig KE, Marano J, Sharp AK, Brown KL, Ceci A, et al. Wildlife exposure to SARS-CoV-2 across a human use gradient. 2022.

183. Braun KM, Moreno GK, Halfmann PJ, Hodcroft EB, Baker DA, Boehm EC, et al. Transmission of SARS-CoV-2 in domestic cats imposes a narrow bottleneck. PLOS Pathogens. 2021;17(2):e1009373.

184. Yen HL, Sit THC, Brackman CJ, Chuk SSY, Gu H, Tam KWS, et al. Transmission of SARS-CoV-2 delta variant (AY.127) from pet hamsters to humans, leading to onward human-to-human transmission: a case study. Lancet. 2022;399(10329):1070-8.

185. WOAH. SARS-CoV-2 in Animals - Situation Report 20. https://www.woah.org/en/document/sars-cov-2-in-animals-situation-report-20/; 2022 12/31/2022. Report No.: 20.

186. Meekins DA, Morozov I, Trujillo JD, Gaudreault NN, Bold D, Carossino M, et al. Susceptibility of swine cells and domestic pigs to SARS-CoV-2. Emerging Microbes & Infections. 2020;9(1):2278-88.

187. Luan J, Jin X, Lu Y, Zhang L. SARS-CoV-2 spike protein favors ACE2 from Bovidae and Cricetidae. J Med Virol. 2020;92(9):1649-56.

188. Lean FZX, Núñez A, Spiro S, Priestnall SL, Vreman S, Bailey D, et al. Differential susceptibility of SARS-CoV-2 in animals: Evidence of ACE2 host receptor distribution in companion animals, livestock and wildlife by immunohistochemical characterisation. Transbound Emerg Dis. 2022;69(4):2275-86.

189. Gaudreault NN, Cool K, Trujillo JD, Morozov I, Meekins DA, McDowell C, et al. Susceptibility of sheep to experimental co-infection with the ancestral lineage of SARS-CoV-2 and its alpha variant. Emerging Microbes & Infections. 2022;11(1):662-75.

190. Thakur N, Gallo G, Newman J, Peacock TP, Biasetti L, Hall CN, et al. SARS-CoV-2 variants of concern alpha, beta, gamma and delta have extended ACE2 receptor host ranges. Journal of General Virology. 2022;103(4).

191. Kim Y, Gaudreault NN, Meekins DA, Perera KD, Bold D, Trujillo JD, et al. Effects of Spike Mutations in SARS-CoV-2 Variants of Concern on Human or Animal ACE2-Mediated Virus Entry and Neutralization. Microbiol Spectr. 2022;10(3):e0178921.

192. Kant R, Kareinen L, Smura T, Freitag TL, Jha SK, Alitalo K, et al. Common Laboratory Mice Are Susceptible to Infection with the SARS-CoV-2 Beta Variant. Viruses. 2021;13(11):2263.

193. Escalera A, Gonzalez-Reiche AS, Aslam S, Mena I, Laporte M, Pearl RL, et al. Mutations in SARS-CoV-2 variants of concern link to increased spike cleavage and virus transmission. Cell Host Microbe. 2022;30(3):373-87.e7.

194. Shuai HP, Chan JFW, Yuen TTT, Yoon C, Hu JC, Wen L, et al. Emerging SARS-CoV-2 variants expand species tropism to murines. EBioMedicine. 2021;73:12.

195. Low-Gan J, Huang R, Kelley A, Jenkins GW, McGregor D, Smider VV. Diversity of ACE2 and its interaction with SARS-CoV-2 receptor binding domain. Biochemical Journal. 2021;478(19):3671-84.

196. Kumar D, Antiya SP, Patel SS, Pandit R, Joshi M, Mishra AK, et al. Surveillance and Molecular Characterization of SARS-CoV-2 Infection in Non-Human Hosts in Gujarat, India. Int J Environ Res Public Health. 2022;19(21).

197. Matsuyama S, Nao N, Shirato K, Kawase M, Saito S, Takayama I, et al. Enhanced isolation of SARS-CoV-2 by TMPRSS2-expressing cells. Proceedings of the National Academy of Sciences. 2020;117(13):7001-3.

198. Hierholzer JC, Killington RA. 2 - Virus isolation and quantitation. In: Mahy BWJ, Kangro HO, editors. Virology Methods Manual. London: Academic Press; 1996. p. 25-46.

199. Schroeder ME, Bounpheng MA, Rodgers S, Baker RJ, Black W, Naikare H, et al. Development and performance evaluation of calf diarrhea pathogen nucleic acid purification and detection workflow. J Vet Diagn Invest. 2012;24(5):945-53.

200. Liao H, Cai D, Sun Y. VirStrain: a strain identification tool for RNA viruses. Genome Biology. 2022;23(1).

201. Bold D, Roman-Sosa G, Gaudreault NN, Zayat B, Pogranichniy RM, Richt JA. Development of an Indirect ELISA for the Detection of SARS-CoV-2 Antibodies in Cats. Front Vet Sci. 2022;9:11.

202. Kenney SP, Wang Q, Vlasova A, Jung K, Saif L. Naturally Occurring Animal Coronaviruses as Models for Studying Highly Pathogenic Human Coronaviral Disease. Vet Pathol. 2021;58(3):438-52.

203. White SK, Ma W, McDaniel CJ, Gray GC, Lednicky JA. Serologic evidence of exposure to influenza D virus among persons with occupational contact with cattle. Journal of Clinical Virology. 2016;81:31-3.

204. Pinto BGG, Oliveira AER, Singh Y, Jimenez L, Gonçalves ANA, Ogava RLT, et al. ACE2 Expression Is Increased in the Lungs of Patients With Comorbidities Associated With Severe COVID-19. The Journal of Infectious Diseases. 2020;222(4):556-63.

205. Kaur N, Oskotsky B, Butte AJ, Hu Z. Systematic identification of ACE2 expression modulators reveals cardiomyopathy as a risk factor for mortality in COVID-19 patients. Genome Biology. 2022;23(1).

206. Ferguson L, Olivier AK, Genova S, Epperson WB, Smith DR, Schneider L, et al. Pathogenesis of Influenza D Virus in Cattle. Journal of Virology. 2016;90(12):5636-42.

207. Ruiz M, Puig A, Bassols M, Fraile L, Armengol R. Influenza D Virus: A Review and Update of Its Role in Bovine Respiratory Syndrome. Viruses. 2022;14(12):2717.

208. Caserta LC, Frye EA, Butt SL, Laverack M, Nooruzzaman M, Covaleda LM, et al. Spillover of highly pathogenic avian influenza H5N1 virus to dairy cattle. Nature. 2024.

209. (CDC) CfDCaP. Technical Report: June 2023 Highly Pathogenic Avian Influenza A(H5N1) Viruses 2023 [Available from: https://www.cdc.gov/bird-flu/php/technical-report/h5n1-070723.html?CDC_AAref_Val=https://www.cdc.gov/flu/avianflu/spotlights/2022-2023/h5n1-technical-report_june.htm.

210. Kalthoff D, Hoffmann B, Harder T, Durban M, Beer M. Experimental infection of cattle with highly pathogenic avian influenza virus (H5N1). Emerg Infect Dis. 2008;14(7):1132-4.

211. (CDC) CfDCaP. CDC A(H5N1) Bird Flu Response Update, July 19, 2024 2024 [Available from: https://www.cdc.gov/bird-flu/spotlights/h5n1-response-07192024.html.

212. Mitchell CA, Walker RV, Bannister GL. Preliminary Experiments Relating to the Propagation of Viruses in the Bovine Mammary Gland. Can J Comp Med Vet Sci. 1953;17(3):97-104.

213. Mitchell CA, Walker RV, Bannister GL. Further Experiments Relating to the Propagation of Virus in the Bovine Mammary Gland. Can J Comp Med Vet Sci. 1953;17(5):218-22.

214. Mitchell CA, Nordland O, Walker RV. Myxoviruses And Their Propagation In The Mammary Gland Of Ruminants. Can J Comp Med Vet Sci. 1958;22(5):154-6.

215. (CDC) CfDCaP. CDC Confirms Human Cases of H5 Bird Flu Among Colorado Poultry Workers 2024 [Available from: https://www.cdc.gov/media/releases/2024/p-0715-confirm-h5.html.

216. Henritzi D, Hoffmann B, Wacheck S, Pesch S, Herrler G, Beer M, et al. A newly developed tetraplex real-time RT-PCR for simultaneous screening of influenza virus types A, B, C and D. Influenza Other Respir Viruses. 2019;13(1):71-82.

217. Kwon T, Trujillo JD, Carossino M, Lyoo EL, McDowell CD, Cool K, et al. Pigs are highly susceptible to but do not transmit mink-derived highly pathogenic avian influenza virus H5N1 clade 2.3.4.4b. Emerg Microbes Infect. 2024;13(1):2353292.

218. Laconi A, Fortin A, Bedendo G, Shibata A, Sakoda Y, Awuni JA, et al. Detection of avian influenza virus: a comparative study of the in silico and in vitro performances of current RT-qPCR assays. Sci Rep. 2020;10(1):8441.

219. Disease ERLfIaN. Detection of Type A Avian Influenza Virus by Real-time RT-PCR [Available from: ww.izsvenezie.com/documents/reference-laboratories/avian-influenza/diagnostic-protocols/sop-vir-018.pdf.

220. Ma W, Belisle SE, Mosier D, Li X, Stigger-Rosser E, Liu Q, et al. 2009 pandemic H1N1 influenza virus causes disease and upregulation of genes related to inflammatory and immune responses, cell death, and lipid metabolism in pigs. J Virol. 2011;85(22):11626-37.

221. Reed L, Muench H. A simple method of estimating fifty percent endpoint512. American Journal of Epidemiology. 1938;27(3):493-7.

222. Cresta D, Warren DC, Quirouette C, Smith AP, Lane LC, Smith AM, et al. Time to revisit the endpoint dilution assay and to replace the TCID50 as a measure of a virus sample's infection concentration. PLoS Comput Biol. 2021;17(10):e1009480.

223. Gauger PC, Vincent AL. Serum Virus Neutralization Assay for Detection and Quantitation of Serum Neutralizing Antibodies to Influenza A Virus in Swine. Methods Mol Biol. 2020;2123:321-33.

224. Graaf A, Ulrich R, Maksimov P, Scheibner D, Koethe S, Abdelwhab EM, et al. A viral race for primacy: co-infection of a natural pair of low and highly pathogenic H7N7 avian influenza viruses in chickens and embryonated chicken eggs. Emerg Microbes Infect. 2018;7(1):204.

225. King J, Harder T, Beer M, Pohlmann A. Rapid multiplex MinION nanopore sequencing workflow for Influenza A viruses. BMC Infect Dis. 2020;20(1):648.